CRANFIELD UNIVERSITY

Judith Ugbeh-Johnson

Effects of Particulate Contamination and Jet Fuel Chemistry on the Nucleation of Water and Ice in Aircraft Fuel Systems

Cranfield Defence and Security

PhD
Academic Year: 2021 - 2022

Supervisor: Mark Carpenter
Associate Supervisors: Nathalie Mai and Mike Williams

April 2022

CRANFIELD UNIVERSITY

Cranfield Defence and Security

PhD

Academic Year 2021 - 2022

Judith Ugbeh-Johnson

Effects of Particulate Contamination and Jet Fuel Chemistry on the Nucleation of Water and Ice in Aircraft Fuel Systems

Supervisor: Mark Carpenter
Associate Supervisors: Nathalie Mai and Mike Williams

April 2022

This thesis is submitted in partial fulfilment of the requirements for the degree of PhD

© Cranfield University 2021. All rights reserved. No part of this publication may be reproduced without the written permission of the copyright owner.

ABSTRACT

The aviation industry is currently facing increasing environmental and energy challenges regarding its fuel use. Research is therefore currently under way to develop new sustainable aviation fuels. Understanding the properties of these fuels (along with the changing properties of existing fuel types) is required to understand their impact on aircraft fuel systems. Water solubility, water settling and ice formation in fuel are such properties of interest. The presence of water in jet fuel/fuel systems has been a long-standing issue in the aviation industry. Therefore, it is important to precisely identify the conditions and features that may exacerbate this phenomenon, understanding how fuel composition, temperature, water droplet sizes, flowrate and pipe surface affect ice formation and water solubility. Currently, there is relatively limited data regarding water solubility/settling rate and ice formation in sustainable fuels, specifically those specified in ASTM D7566.

This work gives a comprehensive account of the recent advances and technologies in the literature indicating conditions that might lead to the nucleation of water and ice in aircraft fuel systems. These conditions have then been applied to characterizing dispersed water droplets in alternative fuels and conventional Jet A-1. Subsequently, the requirements have been applied to the design, set up, and effectiveness of an ice test rig to understand the types and amounts of ice that can be produced from different sustainable aviation fuel blends. In doing so, this work has helped shed light on the role of fuel composition in ice accretion and whether ice accumulation on a pump inlet strainer may impact pump performance.

Furthermore, the results from this work will serve as a basis for design guidelines to minimise ice formation within an aircraft fuel system and help identify some potential/sustainable jet fuel candidates for ASTM D7566 certified jet fuels.

Keywords: Jet fuel, sustainable fuel, water-solubility, ice formation, ice accretion, fuel systems, aviation.

ACKNOWLEDGEMENTS

Foremost, the completion of this work would not have been possible without the grace of God. I wish to express my profound gratitude to God almighty. I would also like to express my sincere gratitude to my amazing supervisor Mark Carpenter, for his continuous guidance and support since the very day I started. I have learnt so much from him and will not have asked for a better supervisor. Grateful to God I completed this under his guidance. Also, to the funding bodies EPSRC-UKRI and the entire Airbus operations team for their relentless support and for providing access to their test area and equipment.

I also acknowledge and extend recognition to my entire family members for the moral, financial, and mental support- Emmanuel Jay, my mom (I love and miss you so much), my dad and siblings, friends, Dr Colleen Williams, Dr Mike Williams, Dr Nathalie Mai, Dr Jeff Pons, and Dr Nonso Okeke.

TABLE OF CONTENTS

ABSTRACT iii
ACKNOWLEDGEMENTS v
LIST OF FIGURES ix
LIST OF TABLES xiv
LIST OF ABBREVIATIONS xvi
1 Chapter 1 Introduction 1
1.1 Background 1
1.2 Research Development 2
1.3 Aims and Objectives 10
1.4 Thesis Plan 10
2 Chapter 2 Complexities Associated with Nucleation of Water and Ice from Jet fuel in Aircraft Fuel Systems: A Critical Review 16
2.1 Introduction 17
2.1.1 Overview of Jet Fuel 19
2.2 Water and its behaviour in Jet Fuel 21
2.2.1 Water Solubility/Settling in Jet Fuel 22
2.3 Water Content Determination 29
2.3.1 Karl Fischer Analysis 34
2.4 Complexities Associated with Water in Jet Fuel at High Altitude 37
2.5 Ice and its Behaviour in Jet Fuel 42
2.6 Effect of Material/ Surfaces on Nucleation of Ice 46
2.7 Conceptual problems and knowledge gaps identified from the literature 54
2.8 Conclusion 56
3 Chapter 3 Assessment of HEFA, ATJ, GTL-S8 & Farnesane as Alternative Jet Fuels Based on their Water Shedding Characteristics 59
3.1 Introduction 60
3.1.1 Alternative Fuels 60
3.2 Research Target and Objectives 64
3.2.1 The water settling rate test 64
3.3 Experimental Section 67
3.3.1 Material and method 67
3.3.2 Procedure for water settling rate 68
3.4 Results and Discussion 70
3.4.1 Comparative Study of water settling rate in conventional jet fuel and alternative blends 70
3.5 Conclusions and Recommendations 73
4 Chapter 4 Characterization of water droplets size distribution in aviation turbine fuel: Ultrasonic homogeniser vs High shear speed mixer 75

4.1 Background of study 76
4.1.1 Experimental procedure 77
4.2 Results and discussion 81
4.2.1 Effects of shearing conditions 81
4.2.2 Effects of total water content 87
4.3 Water droplets- free and hindered settling velocity 92
4.4 Conclusions and Recommendations 95
5 Chapter 5 Investigation of Water Droplet Size Distribution in Conventional and Sustainable Aviation Fuels 97
5.1 Introduction 97
5.2 Experimental Section 100
5.2.1 Jet fuel characterization 100
5.2.2 Droplet size measurement using the Jorin Visual Process Analyser (ViPA) 103
5.3 Results and Discussion 109
5.3.1 ViPA data analysis 109
5.4 Conclusions and Recommendations 122
6 Chapter 6 How will sustainable aviation fuels impact ice formation and pump performance in aircraft fuel lines? 124
6.1 Background to study 125
6.2 Materials and Method 126
6.2.1 Rig Overview 126
6.2.2 Description of Test Equipment and Instruments 129
6.2.3 Rig Materials and Features 131
6.2.4 Fuels 132
6.3 Results 137
6.3.1 Influence of stirring effect and fuel flow velocity 138
6.3.2 Influence of SAF blends 139
6.4 Discussion 143
6.5 Conclusion and recommendation 149
7 Chapter 7 Overall Discussion: Implementation of the work 151
8 Chapter 8 Conclusions and Future Work 153
8.1 Conclusion 153
8.2 Future work 154
REFERENCES 157
APPENDICES 182
Appendix A Assessment of HEFA, ATJ, GTL-S8 & Farnesane as Alternative Jet Fuels Based on their Water Shedding Characteristics 182
Appendix B Characterization of water droplets size distribution in aviation turbine fuel: Ultrasonic homogeniser vs High shear speed mixer 196

Appendix C Investigation of Water Droplet Size Distribution in Conventional and Sustainable Aviation Turbine Fuels..... 198
Appendix D How will sustainable aviation fuels impact ice formation and pump performance in aircraft fuel lines? 202

LIST OF FIGURES

Figure 1.1 Schematic representation of the connection between papers and objectives..... 14

Figure 1.2 Schematic representation between chapters 15

Figure 2.1 Photos from an ice accumulation testing of jet fuel through cold fuel feed pipes showing that more ice accumulated at the critical icing temperatures (-12 ℃) 18

Figure 2.2 Compilation of results from the literature on the water solubility versus temperature profile for various jet fuels..... 22

Figure 2.3 Effects of temperature/chemical composition on the water solubility of jet fuel showing; water solubility increasing with a) an increase in temperature and b) an increase in aromatic content..... 23

Figure 2.4 Graph of water solubility vs temperature a) results by Charro et al., fitting a third-degree polynomial trend for synthesised fuels, whereas conventional fuels fit an exponential trend b) result by West et al., fitting an exponential trend, and no form of limit was noticed above 30 °C 25

Figure 2.5 Graph of water solubility vs temperature; result by Zherebtsov and Peganova showing that the water solubility data fits an exponential trend [22] 26

Figure 2.6 Average water settling rates for a) 1000 ppm and b) 10,000 ppm nominal water addition [25][103]..... 28

Figure 2.7 Water droplet formation from Jet A-1 fuel with dissolved water a) at -3.8 ºC b) at -34 ºC. Ice crystals seen in b), on holding the temperature of the fuel at -34 ºC [23]..... 43

Figure 2.8 The trend of average ice thickness on an aluminium surface blasted with glass beads against time on cooling from 0 ºC to -18 ºC [20]..... 46

Figure 2.9 a) Column chart showing the effect of surface wettability on contact angles b) Comparative compilation of data from the literature, showing the effect of surfaces on the nature of ice formed..... 48

Figure 2.10 Pipe configuration variations showing that stainless steel accumulates more ice than scratched aluminium [19] 49

Figure 2.11 a) Schematic showing that off-surface ice growth (OSG) does not adhere firmly to the surface and can be dislodged easily. Along-surface ice growth (ASG) remains bonded to the surface; therefore, it cannot be displaced readily by fluid flow; b) Test panels cooled to − 20.2 °C prepared with adjacent coatings; with a water-repelling surface (of high contact angle of 156.6°) and water-loving surface (low contact angle of 2.9°) to illustrate

that water-repelling surfaces ease the removal of ice after blowing with a gust of wind [149] 52

Figure 3.1 Theoretical settling velocity data of water droplets in neat fuels..... 66

Figure 3.2 Schematic of settling column extraction point..... 68

Figure 3.3 Experimental setup for the water settling experiment..... 69

Figure 3.4 a) Water settling rate for the fuel blending ratios in comparison to neat fuels. b) best curve fit water settling rate for the fuel blending ratios 72

Figure 3.5 Water settling rates for blends of farnesane/Conv. Jet A-1 and farnesane/GTL S-8 73

Figure 3.6 Average of triplicate tests conducted for 10,000 ppm nominal water addition..... 73

Figure 4.1 Instruments used for water dispersion a) X 620 high shear mixer: b) UP200S Ultrasonic processor..... 79

Figure 4.2 ViPA analysis unit experimental set up 81

Figure 4.3 Image captured of the dispersed water droplet on mixing Jet A-1 fuel with the high shear mixer and ultrasonic horn 82

Figure 4.4 a) and b); DSD (with smoothened kernels for case b.1 to b.4). The blue vertical bar is the average diameter of the droplet. The green vertical bar is the average WVA; c) and d); comparison and evidence of repeatability for all shearing experiments 83

Figure 4.5 Water droplet count a) settling profile for jet fuel/500 ppm dispersed water mixture produced with HSM and ultrasonically; b) settling profile for jet fuel/1,000 ppm dispersed water mixture produced with HSM and ultrasonically; c) shearing effect on droplet size; d) shearing effect on the weighted volume average (volume of droplets) 85

Figure 4.6 Cumulative frequency DSD for the different shearing experiments showing a higher frequency of larger droplets in the HSM case in comparison to that of the ultrasonic 86

Figure 4.7 Estimated average droplet count of added water 88

Figure 4.8 The a) weighted volume average data against time; b) Mean droplet size against time for test cases c.1 to case c.6..... 89

Figure 4.9 Captured ViPA images at the start (~2 minutes) and end (~60 minutes) of the experiment..... 91

Figure 4.10 Comparative analysis of the frequency distribution for the total water content explored for this work (phase 2 experiments) 92

Figure 4.11 Relationship between droplet diameter, WVA and concentration.. 94

Figure 5.1 Instruments used for water dispersion, X 620 high shear mixer 108

Figure 5.2 Experimental setup used for suspended water droplet size analysis 109

Figure 5.3 Water droplet count with error margin a) settling profile for case a.1 to a.6; b) average droplet count histogram data for case a.1 to a.6; c) Repeatability droplet counts data for case a.1 and a.6 113

Figure 5.4 Water droplet size population with respect to time for each fuel cases a.1 to a.6..... 115

Figure 5.5 Shows the a) weighted volume average data against time; b) Arithmetic mean droplet size against time for test cases a.1 to case a.6; c) repeatability data for arithmetic mean droplet size against time for test cases a.2; d) repeatability data for arithmetic mean droplet size against time for test cases a.6 117

Figure 5.6a Frequency distribution of water droplet sizes for aviation fuels explored in this work (Cases a.1 to a.6)..... 118

Figure 5.7 The images captured from the ViPA software at the start of experiment time at 2 minutes are the unprimed labels at the left (a.1 to a.6); and at approximately time at 60 minutes are the primed labels at the centre (a.1'-a.6'). The double primed labels at the right plot (a.1''-a.6'') show the water droplet size distribution's smoothened kernels 120

Figure 6.1 Cold fuel test rig schematic 127

Figure 6.2 Cold fuel test rig with fuel tank in the environmental chamber..... 127

Figure 6.3 Strainer section in flowing fuel at; a) Room temperature and; b) After an icing experiment; c) Strainer section removed after an icing experiment; d) After an icing experiment (inside view); e) After an icing experiment, removable mesh and outer support cone; f) Fuel sample point 128

Figure 6.4 a) Mettler Toledo C30 Karl Fischer Titrators with associated solution exchange. coulometer on left; b) Branson 1510 ultrasonic bath used for homogenising fuel/water mixtures 130

Figure 6.5 Temperature profile for flowing fuel; see Figure 6.1 for temperature points..... 134

Figure 6.6 a) Typical form of pressure measurement data, showing measurement scatter, for pressures across the strainer with temperature; Pressure_1 was the upstream pressure, Pressure_2 the downstream pressure. Jet A-1 containing 260 ppm water. b) The RH curve illustrates the best fit curve of the pressure difference. 138

Figure 6.7 a) Jet A-1 containing 260 ppm water. a) ∆P against T with and without stirrer, N and NS respectively; b) ∆P against T for Jet A-1 fuel at different flow velocity..... 139

Figure 6.8 Repeat tests of ∆P against T for a) 100% Jet A-1; b) and 100% SPK. 140

Figure 6.9 Repeat tests of ∆P against T for a) 100% HEFA; and b) 100% ATJ. Screenshot of mesh section after an icing experiment in; a*) 100% HEFA fuel and; b*) 100% ATJ fuel..... 141

Figure 6.10 Comparative plots of ∆P against T for a) 100% SAF and 100% Jet A-1; and b) 25% SAF and 100% Jet A-1 c) 50% S.AF and 100% Jet A-1... 142

Figure 6.11 a) Average ∆P at -6 °C: SAF and Jet A-1 fuels; b) Average ∆P at -16 °C: for 100%, 75%, 25% bends of SAF and conventional Jet A-1 fuel 143

Appendices

Figure A-1 Settling profile at 1000 ppm and 500 ppm nominal water cases... 191

Figure A-2 Water settling rate for GTL S-8 & Conv. Jet A-1 (10,000 ppm nominal water addition)..... 192

Figure A-3 Water settling rate with data points for neat fuels/fuel blends..... 194

Figure A-4 Average of duplicate tests conducted for 1000 ppm nominal water level..... 195

Figure B-1 KF experimental data for neat fuels with 1,000 ppm nominal water addition..... 198

Figure C-1 Frequency distribution of the different size water droplets after 100 minutes settling for the six aviation fuels explored in this work..... 200

Figure C-2 Water droplet size population represented against time for test cases a.1 to a.6; a.1' to a.6'shows an indication that coalescence occurred 201

Figure D-1 Unfiltered data for conventional Jet A-1 fuel..... 202

Figure D-2 Comparative analysis: Separate plots of SPK blends, HEFA blends and ATJ blends with 100% Jet A-1..... 203

Figure D-3 Repeat tests for SAF blends explored..... 204

Figure D-4 Fitted curve formula for individual experimental runs 205

LIST OF TABLES

Table 1.1 Properties of the current alternative aviation fuels against Jet A-1 3

Table 1.2 Advantages and Disadvantages of promising Alternative Fuels/technology 7

Table 1.3 Thesis structure and publication status 12

Table 2.1 Overview of the available methods for the determination of water content 31

Table 2.2 Summary of key elements discussed in section 2: Water in Jet Fuel 40

Table 2.3 Ice in jet fuel summary table 44

Table 2.4 Summary of Substrates Explored in the literature for Contact angle between ice crystals and different substrates 53

Table 3.1 Prominent alternative fuel feedstocks and their final products 62

Table 3.2 Properties of alternative aviation fuels against ASTM D1655 63

Table 3.3 Fuel blends used for water-shedding and water solubility experiments 67

Table 3.4 Calculated equations for the water settling rate measurements for fuels/fuel blends with 1000 ppm water addition 70

Table 4.1 Test conditions using conventional Jet A-1 fuel 80

Table 4.2 Result data summary for shearing experiments explored for this work and hexanol 87

Table 4.3 Semi-empirical correlations that account for water concentration in a hindered settling 95

Table 5.1 Summary of the characteristics of fuels used for these tests 103

Table 5.2 Summary of ‘case a’ test fuels. In each case, 0.1% water addition was made; the water was dispersed with a high shear mixer 107

Table 5.3 Result data summary for test cases a.1 to a.6 110

Table 5.4 Kurtosis and skewness data for case a.1 to case a.6 121

Table 6.1 Phase 1: initial set of test conditions cooling from 20 ℃ to -18 ℃ ... 135

Table 6.2 Phase 2: influence of fuel composition and flow rate on cooling from 20 ℃ to -18 ℃ 136

Table 6.3 Peak ΔP measurements for all fuel types explored for this work ... 147

Appendices

Table A-1 KF results for neat fuels with 500 ppm nominal water addition 182

Table A-2 KF results for neat fuels with 1,000 ppm nominal water addition ... 185

Table A-3 KF results for fuel blends with 1,000 ppm nominal water addition . 188

Table C-1 KF experimental data for neat fuels with 1,000 ppm nominal water addition 198

LIST OF ABBREVIATIONS

AAIB	Air Accidents Investigation Branch
AFS	Aircraft fuel systems
AFQRJOS	Aviation Fuel Quality Requirements for Jointly Operated Systems
ASTM	American Society for Testing and Materials
ASG	Along-surface growth
ATJ	Alcohol to jet fuel
ATEX	Abbreviation for two European Directives for controlling safety in potentially explosive atmospheres
AVCAT	Aviation carrier turbine fuel
AVTUR	Aviation turbine fuel
BDT	Biomass U.S. dry ton
CCD	Charge-coupled device
CERA	Cambridge Energy Research Associates
CH	Catalytic hydrothermolysis
CRC	Coordinating Research Council
cSt	Centistoke
DSD	Droplet size distribution
EE	Explosive environment
GGE	Gallon of gasoline equivalent (US gallon)
GHG	Greenhouse gas
FAST	Fuel Architecture & Systems Technology
FSII	Fuel systems icing inhibitor
FT	Fischer-Tropsch (synthetic fuels)
GC	Gas chromatography
GTL	Gas to liquid fuel
HC	Hydrocarbons
HDCJ	Hydrotreated depolymerized cellulosic jet fuel
HEFA	Hydroprocessed esters and fatty acids
HRJ	Hydroprocessed renewable jet
HSM	High shear mixer
IATA	International Air Transport Association
IR	Infrared spectroscopy
JIG	Joint Inspection Group
KF	Karl Fischer
KFR	Karl Fischer reagent
LabVIEW	Laboratory Virtual Instrumentation Engineering Workbench
MIE	Minimum ignition energy
MSEP	Microseparometer
NMR	Nuclear magnetic resonance spectroscopy

NumPy	Numerical Python
OPEC	Organization of the Petroleum Exporting Countries
OSG	Off-surface growth
PELV	Protective extra-low voltage
ppm	Parts per million
RO	Research objectives
RPM	Revolutions per minute
RTV	Room temperature vulcanizing
SAF	Sustainable aviation fuel
SASOL	**S**uid-**A**frikaanse **S**teenkool-, **Ol**ie- en Gasmaatskappy - South African Synthetic Oil
SDA	Static dissipator additive
SPK	Synthetic paraffinic kerosene
TBAF	Tetrabutylammonium fluoride
UK	United Kingdom
UPs	Ultrasonic processor
UKERC	UK Energy Research Centre
USA	United States of America
V	Terminal velocity
VAC	Volts alternating current
ViPA	Visual Process Analyser
WVA	Weighted volume average
ΔP	Pressure differential

Standards

ASTM D1655	Standard Specification for Aviation Turbine Fuels
ASTM D3240	Standard Test Method for Undissolved Water in Aviation Turbine Fuels
ASTM D4176	Standard Test Method for Free Water and Particulate Contamination in Distillate Fuels (Visual Inspection Procedures)
ASTM D6304	Standard Test Method for Determination of Water in Petroleum Products, Lubricating Oils, and Additives by Coulometric Karl Fischer Titration
ASTM D7566	Standard Specification for Aviation Turbine Fuel Containing Synthesized Hydrocarbons

ASTM D7619	Standard Test Method for Sizing and Counting Particles in Light and Middle Distillate Fuels, by Automatic Particle Counter
ASTM D8166	Standard Test Method for Sizing and Counting Particulates in Middle Distillate Fuels and Biodiesel Blend (B6 to B20) Using Continuous Flow and Bottle Sampler Automatic Particle Condition Monitors

1 Chapter 1 Introduction

1.1 Background

Water is undoubtedly a dominant and ubiquitous natural resource [1]. Accurate water determination in jet fuel can be very difficult because of its complex nature and the huge varieties of hydrocarbons. The ability of a fuel to attract water vapour from air depends on its chemical composition and properties [2]. Water is virtually insoluble in hydrocarbons and the two do not mix. Extensive hydrogen bonding is one of the distinctive attributes of water molecules that impacts mutual solubility. Therefore, breaking of the hydrogen bond is an important effect when considering the phase equilibrium between water, hydrocarbons, and other chemicals [3]. Pure saturated hydrocarbons (alkanes, which are the main blend component found in jet fuel) are non-polar, and bound only by weak van der Waals forces. The strong intermolecular force present in water is non-existent in hydrocarbons.

Water can get into fuel in so many ways; during fuel distribution, mishandling and equipment failure. However, the most common means by which water can enter fuel or a fuel tank is from condensation in the ullage (vapour headspace in the fuel tank) especially in high humidity regions [4][5]. Ice formation will occur when an aircraft is at a high altitude for a prolonged period [6–10]. This occurrence results from micro droplets of water in jet fuel which can pose a significant threat to aircraft safety as it can degrade fuel quality, promote microbiological growth (‘microbes’), cause rust/corrosion of fuel system parts and freeze to form ice particles [11–15]. This issue with water contamination can cause inlet pressure reduction due to a blockage to the fuel lines and feed pumps.

As a result, extensive research has been performed on investigating water interactions and ice formation in conventional Jet A-1 fuel [16–20]. As an antecedent to this work, Airbus UK, Dayton Research Institute in the USA, and other research bodies have extensively studied water interactions like water

solubility in some sustainable aviation fuels [21–24]. This was done because an understanding of the properties of these sustainable fuels, along with the changing properties of existing fuel types, is required to understand their impact on aircraft fuel systems. Water solubility, settling rate, droplet size distribution, ice formation and accretion on surfaces are some of the properties of interest as it is a known problem within the aviation industry. From previous studies, it was revealed that water solubility and ice formation in jet fuel mainly depends on the temperature and composition of the fuel [16][21][23] [25]. A study by the Dayton Research Institute, United States concluded that water settling is a function of the water droplet size, which agrees with Stokes law [24]. Yet, no available data shows how alternative jet fuels will affect the ice formation/accretion on a surface and the size/frequency distribution of dispersed water droplets in aircraft fuel systems. This explains why the focus of this thesis was to investigate the influence of these new fuel compositions (sustainable fuels) on the above-listed properties in aircraft fuel systems. The project employed the use of sustainable fuels currently approved for use (as per ASTM D7566). Various blend ratios were assessed against a conventional Jet A-1 fuel for comparison purposes. From this thesis, it became apparent that fuel composition impacts the measure of pressure drop across the pump mesh as a result of ice accumulation. The data set from this work also revealed that water droplet size/count distribution can be influenced by fuel composition, shearing, and total water content of the fuel. Therefore, this work will provide the industry with better insight into the behaviour of dispersed water droplets in various commercially available certified alternative jet fuels.

1.2 Research Development

This work was presented as part of the Airbus green fuels project, which in turn is part of a wider package of work called FAST (Fuels Architecture & Systems Technology). FAST is partially subsidised by the UK government (Innovate UK), and, as such, strict milestones and targets are in place to receive funding. Water contamination and ice formation in aircraft fuel systems have been a long-standing problem in the aviation industry. It can promote micro-biological growth and corrosion, impact fuel gauging and lead to ice formation. Ice formation can

result in blockage to the fuel lines, which can affect engine operation. Extensive testing of ice formation has therefore been performed at Airbus with conventional Jet A-1 fuel. However, there is limited data regarding alternative fuels, specifically those specified in ASTM D7566. These fuels are derived from renewable sources or biomass so can therefore reduce the contribution of GHG emission to the global climate. Alternate jet fuels could be adopted in order to reduce the impact of aviation industry on air quality [26] [27][28] [29] [30]. The D7566 that focuses on alternative jet fuels is an expansion of D1655. It is the standard specification for aviation turbine fuel containing synthesized hydrocarbons (HC). The alternative fuels must meet international specification or at least be a 99.999% replacement for the conventionally refined fuels. Table 1.1 shows the properties of the alternative aviation fuels investigated against those specified in ASTM D1655.

Table 1.1 Properties of the current alternative aviation fuels against Jet A-1 Compiled from: [32] [33] [34] [35] [23] [36]

Property	ASTM D1655-21	Sasol SPK	Shell GTL	HEFA	ATJ	S-8	Farnesane
Total sulphur (wt. %)	0.3, maximum	<0.001	<0.001	<0.001	<0.01	<0.001	0.05
Aromatics (wt. %)	25, maximum	<0.5	<0.2	<0.2	0	<0.1	-
Initial boiling point (°C)	-	149	146	174	174	182	247
10% recovered (°C)	205, maximum	166	162	201	178	195	-
50% recovered (°C)	-	170	180	267	182	228	-

Property	ASTM D1655-21	Sasol SPK	Shell GTL	HEFA	ATJ	S-8	Farnesane
90% recovered (°C)	-	180	208	288	-	-	-
Final boiling point (°C)	300, maximum	228	228	293	262	280	-
Flash point (°C)	38, minimum	44	44	3	50	49	107.5
Freezing point (°C)	−40[a], -47[b] max	<-78	-54	<-77	-81	-59	<-80
Density @ 15 °C (kg/m^3)	775–840	762	737	751	800	757	773
Viscosity @ −20 °C (cSt)	Maximum -47	3.6	2.6	3.3	5.1	4.6	14.6
Net heat of combustion (MJ/kg)	42.8, minimum	44	44.2	44.3	-	44.1	-
Smoke point (mm)	25, minimum	>40	40	50	50	>43	-
Derived Cetane Number [31]		31.28	64.69	60.70	--	58.7	-

a Freezing point for Jet A

b Freezing point for Jet A-1

ATJ fuels are viable alternative fuels that are produced from alcohol (ethanol, iso-butanol) and processed through dehydration, oligomerization, hydrogenation and fractionation [37]. ATJ produced from iso-butanol mainly comprises of highly branched iso-alkanes of 8, 12, or 16 carbons [38]. According to the life-cycle assessment by Wang et al, the production process focuses on feedstocks, bio

refinery process and enzyme [35]. An intensive study on the Brooks et al shows that the conversion process to ATJ demands an excessive usage of water and fossil energy [39].

HEFA or HRJ is among the most commercially available alternative jet fuels with renewable feedstocks. In comparison to the conventionally refined jet fuel, HEFA has a higher cetane number, lower aromatic, and sulphur content the production process involves a hydrogenation, decarboxylation/hydro deoxygenation, hydro-isomerization, and hydrocracking.

The gas to liquid pathway converts natural gas or syngas into biodegradable jet fuel. The conversion process involves either the Fischer-Tropsch biomass to liquid technology or the gas fermentation process [40]. The Fischer-Tropsch technology is an indirect conversion/liquefaction process that involves the catalytic conversion of syngas to liquid hydrocarbons [35] [34]. However, the biomass to liquid type of F-T fuels is non-synthetic FT fuels while the synthetic FT fuels are known as the synthetic paraffinic kerosene (SPK). In the gas fermentation process, syngas is fermented to liquid alternative jet fuels. The gas fermentation process has a higher energy efficiency of 57% compared to F-T process which has an energy efficiency of 47% [38]. Sasol IPK is an iso-paraffinic kerosene that comprises mostly of branched chain paraffin's. IPK are produced from light Fischer-Tropsch alkenes (C_3 to C_5). The steps involved are oligomerization, hydrocracking, naphtha reforming, aromatic alkylation, and hydrogenation. Sasol synthetic fuels are known to have properties like that of the conventionally refined jet fuels. The Sasol synthetic fuels are a mixture of five different hydro processed streams: IPK, heavy F-T and heavy coal tar naphtha, light F-T and light creosote distillate [40].

HEFA and FT alternative fuels have the tendency of completely replacing the conventionally refined jet fuel [27][30][38]. Additionally, recent study conducted by some scientists [41] [15] concluded that there is a huge potential for the hydrothermal liquefaction (HTL) technology of algae to produce a drop in replacement for Jet A-1 fuel. Furthermore, another group of scientists [41] lay

emphasis on the challenges facing HTL technology currently and further proposes potential solutions. The solutions proposed are recycling from by-product and reducing large-scale pumpability risk [41].

Unlike other SAF, Farnesane (synthesized isoparaffins - SIP) is mono-constituent hydrogenated sesquiterpene produced commercially from hydro processed fermentation of sugarcane [38][42]. The resulting SIP fuel could contain traces of olefins and other by-products [38].

The revolution of alternative jet fuels seems like a very promising technology for the aviation industry. The feedstock price, availability and energy intensity of the production process are significant barriers that cannot be overlooked.

In summary, the development of alternative fuels is both advantageous and disadvantageous to the aviation industry. This is summarized in Table 1.2

Table 1.2 Advantages and Disadvantages of promising Alternative Fuels/technology

Alternative Fuels/ Process	Advantage	Weaknesses
FT Fuels	Cleaner burn producing app 2.4% less CO_2	Higher GHG emission during the production process
	Low Aromatic content	Shrinkage and hardening of engine seals O-rings.
	Low GHG emissions	Competition for farmland
	Low in sulphur content	Decreases fuel lubricity
	Low fuel price	Energy intensive
	Abundant reserves for feedstocks	Only large-scale production can be cost effective
	Carbon neutral (carbon absorbed during the growing process of the feedstock offsets the carbon emitted during its burn).	Poor high-temperature thermal stability

HEFA/HRJ	Efficient process with a high oil yield	Low energy density
	Low temperature properties	Storage instability
	High thermal stability	Time consuming
ATJ	Low in aromatics	High sulphur content
	High energy density (ethanol to jet pathway)	
	80% reduction in carbon emissions (ethanol to jet)	
Pyrolysis	Fast process	Oil produced tends to have a low heating value, high amount of oxygen and water content.
Transesterification to bio-jet fuel	Involves the use of lower temperatures compared to other process like the hydrocracking that requires high temperatures	Expensive

		Higher GHG emission during the production process
Centia^{TM}	High oil yields and high energy density	Higher GHG emission during the production process

Compiled from: [15] [39] [35] [34]

As these emerging fuels are entering the market, it is deemed necessary to understand the types and amounts of ice that can be produced in different fuel blends. As such, this research was developed to investigate the influence of new fuel composition on the behaviour of water and ice in aircraft fuel systems. Various blend ratios were assessed against a conventional Jet A-1 fuel for comparison purposes. Also, it was desirable to determine whether ice accumulation on a pump mesh may result in a measurable pressure drop across it (as this has the potential to affect pump performance).

1.3 Aims and Objectives

The overall aim of the research work was to examine jet fuel constituents & the influence of new fuel composition on the behaviour of water and ice in aircraft fuel systems. Accordingly, the following objectives were set to achieve this aim;

Objective 1. A critical review of the key complexities associated with jet fuel and nucleation of water and ice in aircraft fuel systems

Objective 2. Investigation of the effects of hygroscopicity/water-shedding and corresponding water droplet size distribution for various fuel blends

Objective 3. Critical analysis of the effects of fuel constituents on the water droplet size distribution in different fuel blends

Objective 4. Test campaign to investigate ice formation with various fuel blends - create empirical models of ice formation and pressure drops across strainer mesh

1.4 Thesis Plan

This thesis is structured into a series of chapters presented in a journal paper format. All papers were written by the primary author, Judith Ugbeh-Johnson and emended by my supervisor (Mark Carpenter) and co-supervisor (Nathalie Mai). All experimental work was conducted by Judith Ugbeh-Johnson at Cranfield university-Shrivenham campus and the Airbus Filton site. Chapters 5 and 6 come

from an eight months industrial placement at Airbus with all experiments conducted by Judith Ugbeh-Johnson. The Airbus team provided support in building the ice test rig used for the work, providing the different test fuels consumables and also making their test facility available.

Figure 1.1 and Figure 1.2 and Table 1.3 illustrates links between each objective and chapters in this work. Firstly, chapter 2 presents a comprehensive literature review highlighting the recent advances/technologies that exist and identifying the conditions that might lead to the nucleation of ice in aircraft fuel systems. The review provides significant knowledge gaps highlighting that the availability of data showing the influence of jet fuel composition on some associated properties/characteristics of water contamination is still deficient. As such, further research was carried forward in chapter 3, paper 2, on the assessment of alternative jet fuels based on their water-shedding/settling characteristics. The outcome of chapter 3 informed the decision to establish the particle size distribution of water droplets in jet fuels at a given period. This further research led to chapter 4, paper 3, which explores the characterization of dispersed water droplets in aviation turbine fuel using an ultrasonic homogeniser and a high shear speed mixer. Observations from this work helped determine the requisite shearing method for producing a less stable emulsion for a more quantifiable set of data in investigating sustainable alternative fuels (that conform with ASTM D7566) under dynamic conditions. The investigation of droplet size distribution in sustainable fuels is detailed in chapter 5, paper 4. Findings reveal that water droplet frequency and size distribution are sensitive to changes in fuel composition, shearing conditions, and water content.

Furthermore, chapter 6 (paper 5) optimises the outcome from previous chapters (chapters 2,3,4 and 5) and employs the selected fuel candidates for ice nucleation/accretion analysis. Chapter 6 shows the influence of alternative fuels on ice accretion, ice formation and build-up across a pump strainer in a simulated aircraft fuel system.

Chapter 7 is a general discussion on the correlation of all chapters and the implications of water contamination and its associated properties/characteristics in alternative jet fuel.

Finally, chapter 8 summarises the key findings and recommends research work that requires future development.

Table 1.3 Thesis structure and publication status

Chapter	Objective addressed	Paper	Paper Title	Journal	Status
2	1,2,4	1	Complexities associated with nucleation of water and ice from jet fuel in aircraft fuel systems: A Critical Review	Elsevier-Fuels	Published
3	2	2	Assessment of HEFA, ATJ, GTL-S8 & Farnesane as alternative jet fuels based on their water-shedding characteristics	IASH conference proceedings	Published
4	2	3	Characterization of water droplets size distribution in aviation turbine fuel: Ultrasonic homogeniser vs High shear speed mixer	Elsevier - Fuels	Published
5	3,4	4	Investigation of water droplet size distribution in petroleum-derived and sustainable aviation fuels	SAE- Fuels & lubricants	Published
6	3,4	5	How do sustainable aviation fuels impact ice formation and pump	The Aeronautical journal	Accepted

			performance in aircraft fuel lines?		
7	1,2,3,4	--	Overall Discussion: Implementation of the work	--	--
8	--	--	Conclusions and Future Work	--	--

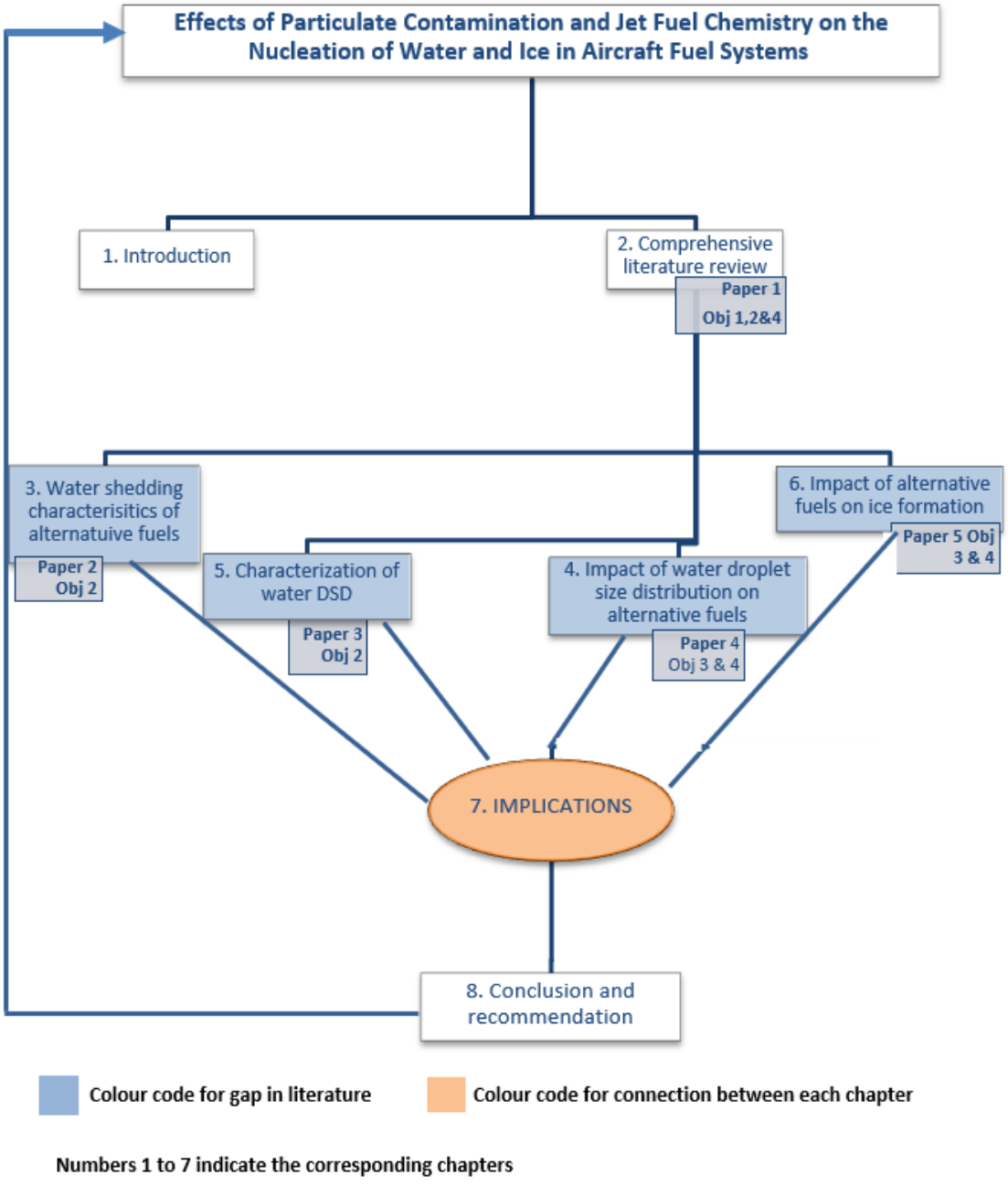

Figure 1.1 Schematic representation of the connection between papers and objectives

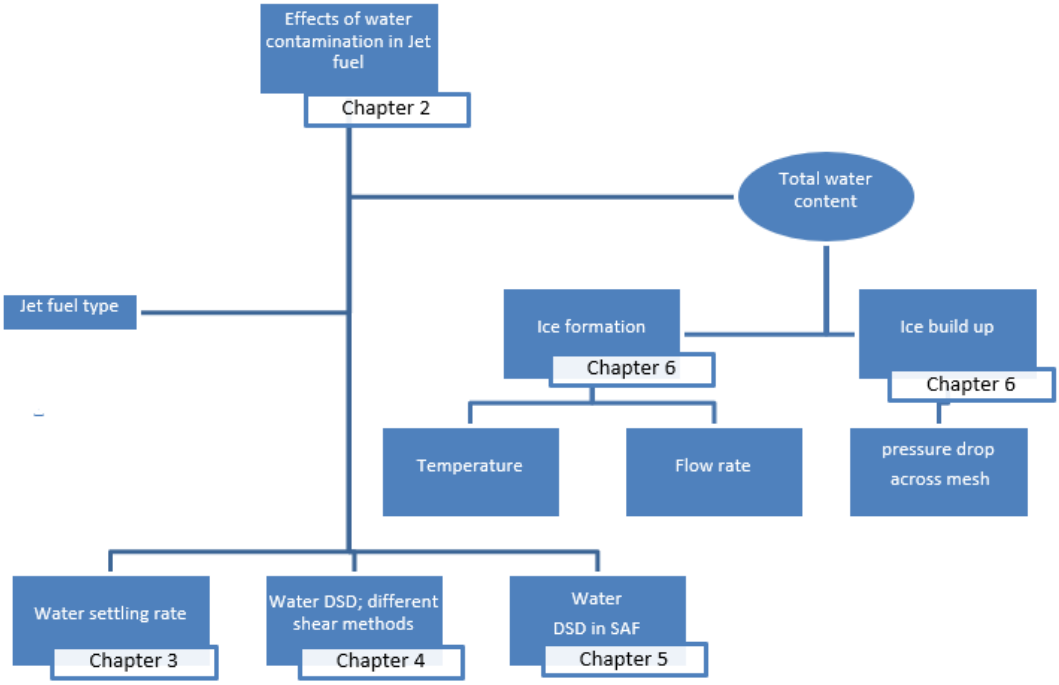

Figure 1.2 Schematic representation between chapters

2 Chapter 2 Complexities Associated with Nucleation of Water and Ice from Jet fuel in Aircraft Fuel Systems: A Critical Review

Abstract

The contamination and behaviour of water in aircraft fuel systems remains a significant global research interest following several aircraft incidents. To engineer a solution to the problem of icing in jet fuel, it is crucial to precisely identify the conditions and features that may exacerbate this phenomenon. This review will aid prospective researchers to identify work that has been done and work that is yet to be available for future study. In this review, conclusive data integrating a wide range of literature and providing an in-depth description of the factors that influence the behaviour of trace water ice formation in jet fuels was carefully summarised. On investigational studies, it was discovered that no work is available that studies the impact of sustainable jet fuel and its blends on ice formation, size and frequency distribution of dispersed water droplets in aircraft fuel systems. Findings from comparative studies also reveal that surfaces will have an essential role in the growth pattern of ice in aircraft fuel systems. Furthermore, results show that supercooled water droplets with sizes greater than or equal 5 μm can induce ice accretion. This review identified a common problem with the main methods of reporting results as a graphically fitted plot. Subsequently, it proposed that authors of any original technical work provide raw data as supplementary information to allow comprehensibility. The study further offers a system that could help manage the nature of ice in aircraft fuel tank systems—making it readily available and accessible.

Keywords: Ice accretion, Fuel systems, Aviation fuel, alternative fuel, water-solubility, sustainable aviation fuel, synthetic aviation fuel

2.1 Introduction

The issue of water and particulate contamination in jet fuel has long been recognised for the associated problems affecting an aircraft fuel system and causing maintenance downtime. It is accepted that the presence of water in jet fuel is undesirable and potentially hazardous [17][43][44]. The presence of free water can assist the growth of microbiologic cultures, which have the potential to form biofilms in aircraft fuel tanks [11][12]. Thus, the free water content has to be maintained below a certain level, typically below 15 ppm at the time of fuelling [13]. Coalescing technology is employed to keep the amount of free water to a minimum value. At about 21 °C, a saturated fuel usually contains about 40 to 80 parts per million (ppm) of dissolved water [45]. In icy conditions, dissolved water may precipitate from the solution; this free water in the fuel can form ice. Also, ice crystals can form in the presence of particulates at temperatures below 0 ºC in the cooler parts of the wing tank [8]. For example, the observation from the investigation conducted by the Air Accidents Investigation Branch (AAIB) indicated that ice accumulation in fuel systems is often inconsistent, as shown in Figure 2.1[1][9]. From figure 1, critical icing temperatures (temperature in which more ice are like to form peak pressure differences) were identified as being between -9 ℃ and -11 ℃ [1]. At these critical icing temperatures, ice crystal agglomeration occurs, which can potentially lead to blockage or restrictions in the fuel feed system, particularly if accreted ice is dislodged or released in a snow shower or transient ice event. However, on reducing the temperature below -18 ℃, the ice crystals tend to stick to themselves and not the surfaces. Therefore, becoming larger in size. From this study, the sticky range (range of temperature where ice sticks more to its surroundings rather than itself) was identified to be between -5 ℃ and -20 ℃.

The behaviour of water and ice has been studied from different angles, as summarised in Table 2.2 and Table 2.3[18][19][46]. Also, studies have emphasised that the growth of ice on surfaces depends on the hydrophobic or hydrophilic nature of those surfaces [46][47][48][49][50]. Therefore, it can be

concluded that surfaces play an important role in the nature and degree of ice formation.

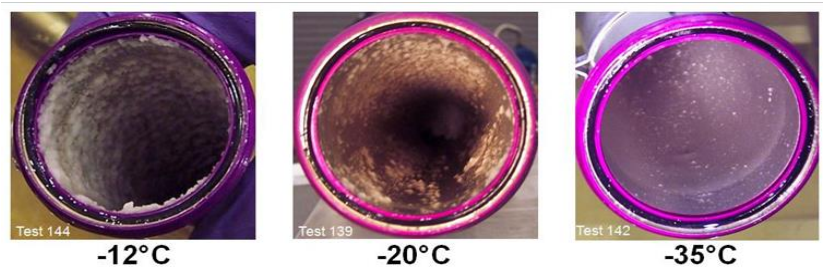

Figure 2.1 Photos from an ice accumulation testing of jet fuel through cold fuel feed pipes showing that more ice accumulated at the critical icing temperatures (-12 ℃)

Trace contaminants may be present in jet fuel from many sources, for example, from the crude oil or synthetic feedstock, manufacturing process or entrained during distribution. Trace water is inherently present and has safety implications on how it affects aircraft fuel systems. However, the most recent reviewed paper related to this topic was by Baena in 2013, but the review focuses on the behaviour of water in conventional jet fuel only and nothing on synthesised aviation fuel and its effect on ice formation in aircraft fuel systems dissolved [2]. Understanding the properties of this synthetic aviation fuel, along with the changing properties of existing fuel types, is required to understand their impact on aircraft fuel systems. Water solubility, settling rate, and droplet size distribution ice formation/accretion, amongst others, is one such property of interest as it is a known problem within the aviation industry. Even though understanding the properties of these sustainable fuels and the changing properties of existing fuel types is required to understand their impact on aircraft fuel systems, there is very limited data available in the literature related to this topic. Unfortunately, most of the data available are related to ice formation in conventional jet fuel pipes only. A large body of work on adhesion testing on ice does not demonstrate how sustainable aviation fuel may affect it. Despite this, no research experiment has been conducted to fill these knowledge gaps. This could be because of the

difficulty for potential researchers trying to identify work that has been done and work that is yet to be available.

The purpose of this review is to collect a great amount of data and compare and analyse the recent advances and technologies in the literature on this subject. This review paper also describes some complexities associated with jet fuel chemistry, knowledge gaps, systematic hypothesis, and recommendation for future development. The study further proposes a system that could possibly help manage the nature in which ice forms in aircraft fuel tank systems. Making it readily available and accessible to those wanting to obtain data in this area. Over one hundred and twenty articles from scientific papers have been examined. The sources came from journals, books, and conference proceedings, to cover a broad range of studies and views regarding the water and icing phenomenon. Data were collected from several papers and plotted in a scatter graph or bar chart for the purpose of comparison. Most of the key information extracted from the literature was discussed, making it easier to find and comprehend.

2.1.1 Overview of Jet Fuel

Jet fuels are intended to power gas-turbine engines for aviation purposes. The two major classes of jet fuel are the civil grades (Jet A, Jet A-1 and similar specifications) and military grades (JP-5, JP-8, AVTUR/FSII, AVCAT, F-24, and similar specifications). The military grades differ from the civil grades based on the type of additives used [1][51]. Jet fuel does not have a particular chemical composition but is a complex mixture that is mainly specified by physical characterisation [22][30,34,52–58]. Studies have shown that jet fuel is based on numerous constituents, which contribute towards providing appropriate thermal output, clean combustion characteristics, and oxidation stability [1][29,39,59–61]. Blends of over a hundred species exist in jet fuel, and the blends or mixtures are mainly hydrocarbons with the number of carbon molecules ranging from eight to sixteen. The major categories of hydrocarbon found in jet fuel are alkanes (also referred to as paraffin), cycloalkanes (also referred to as naphthenes), and aromatics [62][63]. The main difference between the different categories is the

connection of the carbon atoms and their bonds Paraffins and naphthenes are the dominant components found in jet fuel. In comparison to naphthenes, paraffin has a high hydrogen-to-carbon ratio, high heat release per unit of mass and a cleaner burn characteristic. In comparison, naphthenes have a slightly lower hydrogen-to-carbon ratio, which consequently lowers the heat released per unit of mass but increases the fuel's density [39]. Aromatic hydrocarbons are good energy sources; however, their maximum acceptable levels in jet fuels are restricted to about 20-25%. Lack of aromatics yield fuels that are below minimum density and can also lead to shrinkage of elastomers; however, when in excess can lead to swelling of the elastomers, more soot production as a result of incomplete combustion and so must be restricted [64]. Finally, alkenes also known as olefins are unsaturated hydrocarbons with lower hydrogen to carbon ratios. The maximum acceptable levels are restricted to less than 1% by volume [1][65]. Traces of other elements like sulphur and sulphur compounds can also be found in aviation fuels. Their presence in aviation fuel can be beneficial in some aspects (good lubricating abilities) and not beneficial to others (environmental impacts) [66][67]. Furthermore, jet fuel may contain additives that are determined by the specific uses of the fuel [68][69]. These additives may be added to the fuel to help improve its performance.

Jet fuel has specialised features, properties and characteristics, which make it different from other fuels [23]. Some of these features are its low freezing point temperature (-40 °C for Jet A and -47 °C for Jet A-1), good combustion efficiency with low carbon monoxide/pollutant emission measurements, high specific energy, density, and thermal stability.

In order to maintain a uniform supply of jet fuel worldwide, a group of companies formed the Joint Inspection Group (JIG) and proposed the Aviation Fuel Quality Requirements for Jointly Operated Systems (AFQRJOS) [70–72]. The checklist contains the most rigorously binding requirements from the defence standards and the ASTM international specifications for jet fuels [14][1][26,28,35,73]. Although conventional fuel still accounts for a vast majority of aviation fuels, sole dependency on petroleum-derived fuels poses an increase in environmental

concerns and price fluctuations [74][75]. Due to the rapid increase in global energy demand and large consumption of oil by the aviation sector, novel technologies to help optimize sustainable aviation fuel sources are now a significant area of global research interest. This is because the use of SAF is featured to have the potential to decrease the life-cycle of greenhouse-gas emissions [54][30][55][76–78]. These fuels are derived from renewable sources or biomass, so they can therefore reduce the contribution of GHG emissions to the global climate. According to several authors, alternate jet fuels could be adopted in order to reduce the impact of the aviation industry on air quality [26][27]. It is important to note that a certified fuel must meet the basic aviation fuel criteria for safety purposes [27][60][79]. Currently, the D7566 focuses is the standard specification for aviation turbine fuel containing synthesized hydrocarbons (HC) [60].

2.2 Water and its behaviour in Jet Fuel

Water in jet fuel has been a significant area of research following several notable aircraft incidents [43,80,81]. One such scenario is the case of a British Airways Boeing 777-200ER engine that faced an un-commanded thrust as a result of ice blocking the face of the fuel-oil heat exchanger. Water in jet fuel is undesirable and may be hazardous because it can lead to corrosion problems, microbiological growth, and may precipitate out as ice [13–15][72]. These problems are significant and can increase aircraft operating/maintenance costs. However, water is always present and cannot be eliminated. Therefore, the water content should be kept to a minimal level [24]. Typically, a water-saturated fuel contains between 40 and 80 ppm dissolved water at ambient temperature (about 21 °C) [82].

Water may exist in fuel in the form of dissolved water, suspended/entrained water and free water [12][17][25][83–85]. Water may be introduced into fuel by various causes during fuel distribution, condensation, and equipment failure. However, a fuel's ability to attract water vapour from the air depends largely on the chemical composition and temperature [2]. Carpenter et al. conducted research on how

water behaves in aviation fuels at low temperatures [83]. In this work, Carpenter et al. explored three different model hydrocarbon types, including aromatics, alkanes, and cycloalkanes. Their results showed that on cooling to about -44 °C, visible ice crystals were formed in the aromatic model fuel. However, no ice crystals were observed in the model alkane and cycloalkane fuels, even at temperatures as low as -44 °C [83].

2.2.1 Water Solubility/Settling in Jet Fuel

Different authors have suggested that water solubility in jet fuel predominantly depends on the temperature and composition of the fuel [4][23][84][86]. When an aircraft is cruising at a high altitude, the fuel in the wing tank becomes cold, causing water to separate into a second phase. This has the appearance of a cloud or fog in the fuel [24][87][88]. As seen in Figure 2.2, previous studies on this topic found that the solubility of water in hydrocarbons increases with an increase in temperature [4][21][23][24][25][83][2,86–89].

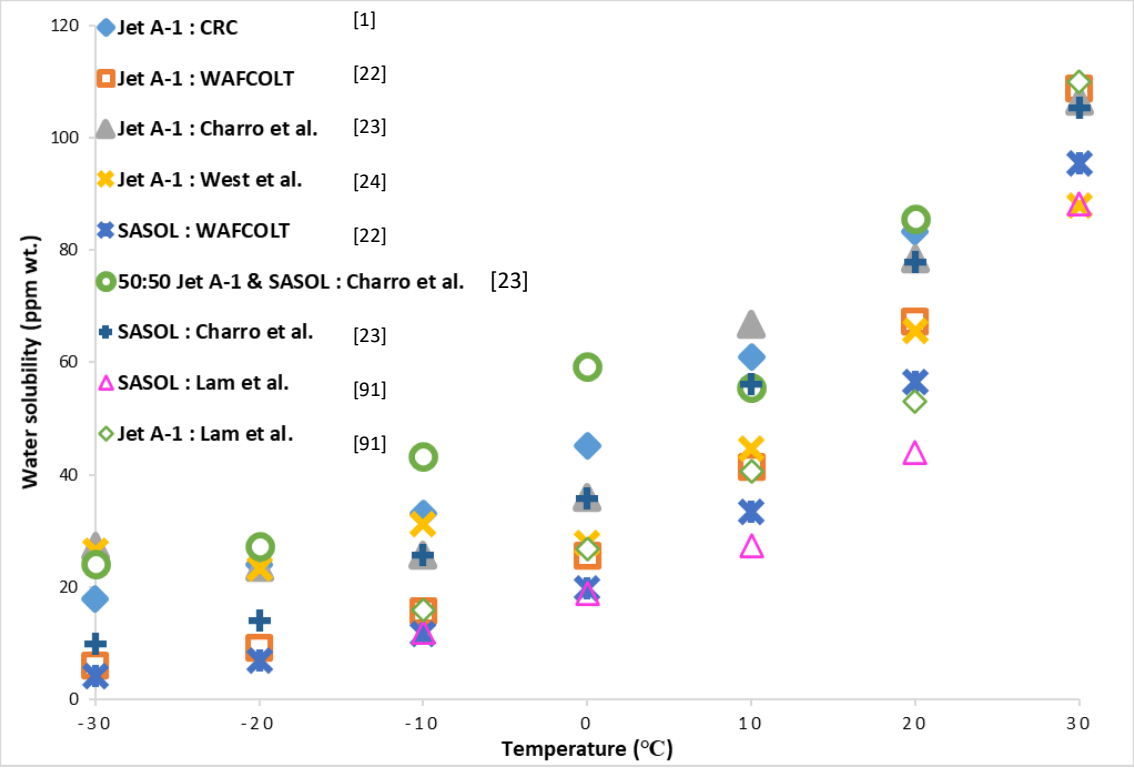

Figure 2.2 Compilation of results from the literature on the water solubility versus temperature profile for various jet fuels

An experiment analysing how the concentration of anti-icing agents, temperature and aromatic content will affect the water content of China No.3 jet fuel was conducted [90]. It was concluded that anti-icing agent has no effect on the water content of jet fuel; however, temperature and aromaticity play a key role in fuel water solubility. Temperature has a great effect on the fuel water solubility. As can be seen on Figure 2.3 a, the fuel water solubility augments steadily with increasing fuel temperature. Aromaticity is another factor affecting the solubility of water in fuel. Pure aromatic fuels like toluene, have a higher affinity for water and could contain seven times more dissolved water than fuels with similar carbon contents but containing only alkanes or cycloalkanes [83]. A study by Carpenter et al. shows that as the aromatic content in the fuel increases, the water solubility increases (Figure 2.3 b) [2]. This is because aromatics have extended delocalised π electron clouds that are capable of forming hydrogen bonds with water [2][91].

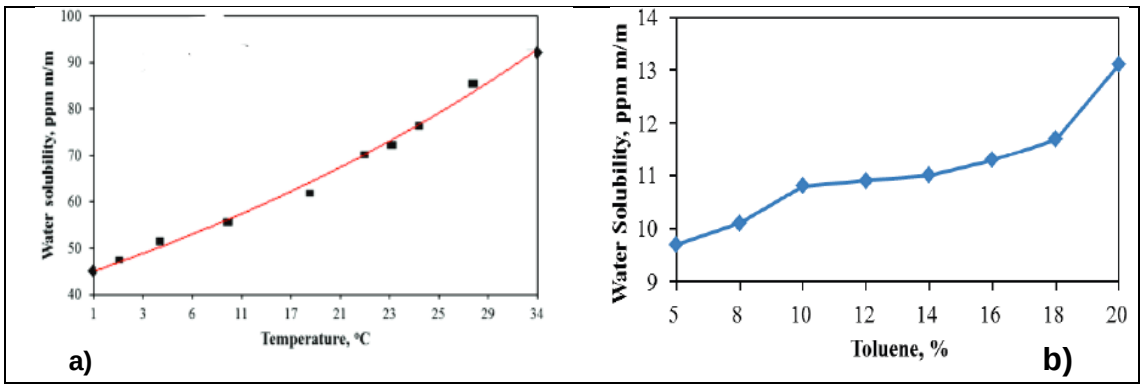

Figure 2.3 Effects of temperature/chemical composition on the water solubility of jet fuel showing; water solubility increasing with a) an increase in temperature and b) an increase in aromatic content

Lam et al. evaluated five different kerosene fuels and one wide-cut fuel at temperatures between -5 °C and 25 °C. The work conducted by Lam et al. proposed an exponential function that can predict the water solubility of fuels with a known flashpoint and aromatic content [91]. The results of the evaluation indicated that icing problems might be greatest in fuels with high aromatic contents as a result of their high affinity for water. The results from work by Lam

et al. is in good agreement with work carried out by Marche et al., Wu et al., and Carpenter et al. that showed high aromatic content in jet fuel governing the increase in water solubility. For this reason, it can be concluded that the higher the amount of water that is likely to precipitate out of the solution, the more ice is likely to form. Furthermore, experiments that involved additives shows that it can play a key role in water uptake. For example, a study that explores the effects of static dissipator additive (SDA) suggested that it was likely to increase water uptake in fuels [92]. Also, according to Repetto et al., a fuel dehydrating icing inhibitor can help protect jet fuels against water contamination [93]. Repetto et al. proposed a dual-action strategy using a fuel-soluble water scavenger that mitigates against the effects of water crystallisation [93]. Although additives can play a key role in water uptake, the result of another experiment conducted by Carpenter et al. established this claim but noticed no significant difference in the water content in the presence or absence of the SDA [83].

Zherebtsov et al. carried out a study on naphthenic-based kerosene fuel and concluded that oxidation of jet fuel plays a key role in the solubility of water in fuels [94][95]. Goebel et al. suggested that an increase in water solubility could be attributed to the increase in natural surfactant-oxidation products, which in turn increases the number of polar molecules [94].

Marche et al. developed an apparatus that measures the mutual solubility of water and hydrocarbons for toluene and some alkyl cyclohexanes. Their results show that water solubility increases with the number of carbons in the alkyl cyclohexane and, as expected, an increase with temperature (ranging from 30 °C to 180 °C) [25]. The data reported by Marche et al. agrees with other literature published to date [25][84][86]. Even though Jet fuel composition varies considerably, depending on the production process, parent source, or physical characterization, minimal data is available in the literature for synthetic jet fuels. An extensive assessment of the water solubility characteristics of six drop-ins/synthesised jet fuel blends was conducted by Charro et al. [23]. This study suggested that the water solubility of SAF/synthetic fuels behaves differently from that of conventional jet fuels. A graph of water solubility ppm weight by

weight (ppm w/w) versus temperature (°C) fits a third-degree polynomial trend for SAF/synthetic fuels, whereas conventional fuels fit an exponential trend. This effect is unphysical as it is unlikely to have a decrease in solubility at higher temperatures. Another drawback of the study carried out by Charro et al. was that the experiments were not replicated, and conclusions were drawn from a set of single experiments; therefore, they are likely to not be physical [23]. Replicating the experiments for each temperature explored will provide a more precise judgment by either refuting or corroborating the trends from the experiment. A major comparative study by West et al. further analysed the water solubility trends with respect to temperature for thirty-six drop-in aviation fuel and model solvents samples (conventionally refined and synthetic aviation fuels) [24]. This work indicated that two out of thirty-six samples analysed had high water solubility because of their high aromatic content. Figure 2.4 shows the water solubility versus temperature graphs for two different sets of experiments conducted by West et al. and Charro et al. for comparison.

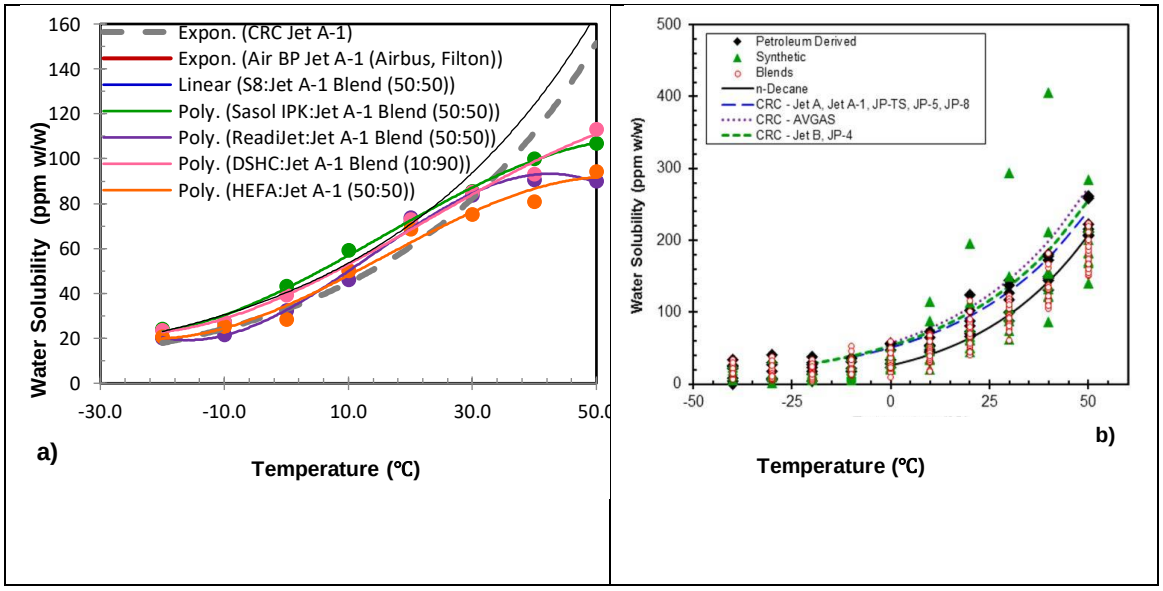

Figure 2.4 Graph of water solubility vs temperature a) results by Charro et al., fitting a third-degree polynomial trend for synthesised fuels, whereas conventional fuels fit an exponential trend b) result by West et al., fitting an exponential trend, and no form of limit was noticed above 30 °C

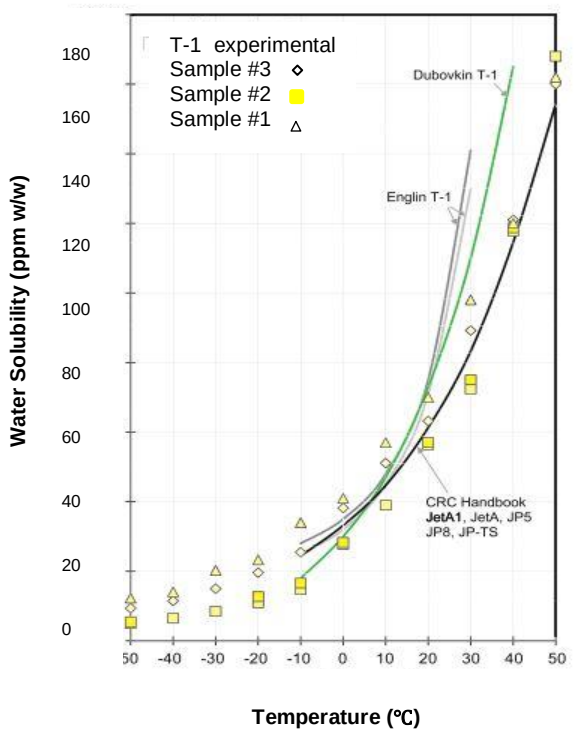

Figure 2.5 Graph of water solubility vs temperature; result by Zherebtsov and Peganova showing that the water solubility data fits an exponential trend [21]

It is unsure if the difference observed by Charro et al. is as a result of the water content level used, and fuel composition or merely because conclusions were drawn from the set of experiments conducted [23]. For this reason, it will be advantageous to replicate the set of experiments conducted by Charro et al. for result verification. Zherebtsov and Peganova experimented on water contamination in three different batches of Russian fuel TS-1. They reported that the linear regression for the logarithm of water solubility versus the inverse of temperature has a different inclination, and this was attributed to the slight differences in fuel batches [21]. However, the reason for this discrepancy may be due to the experimental technique adopted by the authors. A note of caution is due here since all the authors used Karl Fischer's analysis for the water content determination. In observational studies from the literature, there is still a potential for bias regarding the most widely used method for water content determination; several authors have also concluded that the Karl Fischer analysis is not a completely reliable technique [64][67][96][98][99]. Kang et al. showed that even

after using a glove box for the Karl Fischer experiment, ambient moisture was still absorbed, limiting the accuracy and yielding high results [100]. Although the glove boxes are not hermetically sealed, the differences in results from work in this area cannot be ignored. Unfortunately, due to many of such differences, these findings are rather difficult to interpret. This explains the need to benchmark this procedure to see if there is any consistent offset to set a correction factor in place. This leads to the need to validate the trends observed by West et al., Zherebtsov et al. and Charro et al. This can simply be done by using a single experimental technique to explore the trends for conventional and synthesised fuels at different test conditions (e.g., different water content levels) with repeat tests.

The water settling rates in conventional and alternative fuels has been investigated by West et al. and Ugbeh-Johnson et al. employing the Karl Fischer coulometer for water determination [24][101]. Whilst Ugbeh-Johnson et al. focused on 1000 ppm by volume (ppmv) and a longer time interval. West et al. presented results for 10,000 ppmv, a relatively high concentration unlikely to represent an aircraft fuel system scenario. This concentration is not representative because, in a real scenario, the water content must be kept within a tolerable limit, typically below 90 to 260 ppmv for normal and emergency system operations [102]. Also, a fuel containing 10,000 ppm of water will likely appear cloudy and will probably fail the clear and bright test required before fuel can be used in an aircraft. Nonetheless, the results of both experiments followed a similar pattern, as shown in Figure 2.6. It was concluded that the rate of free water settlement, assuming droplets are perfectly spherical, is a function of the droplet size in accordance with Stokes law (however, this is only true for perfectly spherical droplets) [24][101]. According to Ugbeh-Johnson et al., the governing Stokes law equation, as seen in Equation 2-1, is mainly based on the size of a water droplet and the viscosity of the fuel. According to the author, water droplets will fall through jet fuel under the effect of gravity since water has a higher density than jet fuel.

$$\mathbf{V} = \frac{\mathbf{g}\cdot\mathbf{D}^{\mathbf{2}}(\boldsymbol{\rho}_{\mathbf{w}}-\boldsymbol{\rho}_{\mathbf{f}})}{\mathbf{18}\cdot\boldsymbol{\eta}_{\mathbf{f}}\cdot\boldsymbol{\rho}_{\mathbf{f}}}$$

Equation 2-1

Where:

$\boldsymbol{\rho}_{\mathbf{w}}$ = density of water (kg/m^3)

$\boldsymbol{\rho}_{\mathbf{f}}$ = density of fuel (kg/m^3)

$\mathbf{g}$ = acceleration due to gravity (m/s^2)

$\boldsymbol{\eta}_{\mathbf{f}}$ = kinematic viscosity of the fuel (m^2/s)

$\mathbf{V}$ = terminal velocity of the water droplet (m)

$\mathbf{D}$ = Water droplet diameter (m)

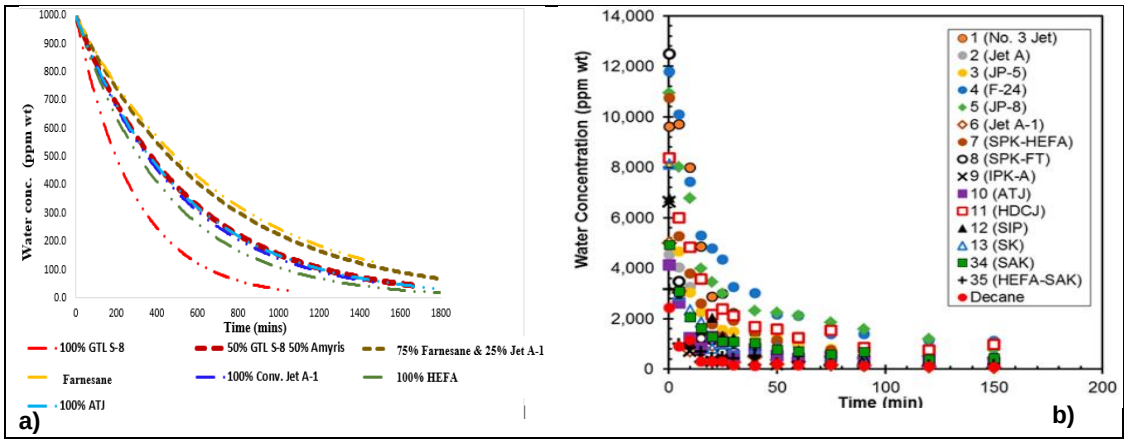

Figure 2.6 Average water settling rates for a) 1000 ppm and b) 10,000 ppm nominal water addition [24][101]

Literature has established that the water droplet in fuel is dependent on the form in which the water is present in the fuel. For example, dissolved water droplets are often regarded as a constituent of jet fuel as they are very tiny droplets that are naked to the eye [2]. Lam et al. reported suspended water droplets to be between 5 to 13 µm, with the latter dropping out as free water, whilst Clarke et al. reported free water droplet diameter to be within a range of 20 to 30 µm [22][12]. However, it is essential to note that sizes below 30 µm could negatively affect performance by impeding flow through filters and causing other safety issues [20][24].

2.3 Water Content Determination

Traditionally, water is detected by taking a fuel sample and looking to see if it is clear and bright. However, this method can detect only high-water concentrations and many operating conditions need to be considered, like the operators' interpretation, quality of vision and sunlight. Meanwhile, a clear and bright test (appearance test) is still considered the most basic test carried out to check for water in fuels. Additionally, different industries employ several techniques for the determination of water content in samples. There are many physical, drying, separation, radiochemical and chemical methods available [103–105]. Water is a significant contaminant in fuel, and this explains why water monitoring techniques must be accurate, repeatable, and reproducible so that any increase in water content can be rectified [106].

Water in fuel has been one of the significant issues facing the aviation industry [9]. Its presence can be potentially detrimental and lead to fatal consequences. It has been reiterated by several authors [2][100] that keeping the jet fuel free from water contamination is important, as its inclusion can negatively affect its performance. An overview of the methods for the determination of water content is tabulated in

Table **2.1**.

Table 2.1 Overview of the available methods for the determination of water content

Method	Principle	Disadvantage	Measurement Range	Measurement Accuracy
Infrared & Halogen Drying	Uses direct infrared, halogen radiation and absorbed energy causes the heating of the sample	Water and some other volatile substances might vaporize	0.5-99%	0.1-0.5%
	Differential weighing	It might not be suitable for samples with a small amount of moisture		
Karl Fischer Titration	This method involves the oxidation of Sulphur-di-oxide (SO_2) by iodine (I_2) in methanol.	Can form side reactions if the analyte contains species that interacts with the KFR	0.0001 – 1%	-
	Coulometric titration involves the electrochemical oxidation of iodide until it detects a trace of unreacted iodine	Variables can affect the endpoint (Temperature, lightning and atmospheric variations)		
		Contamination of sample/syringe during introduction into the KF cell		
		Its pH sensitivity might affect the endpoint. (Optimum pH value for water determination is between 5 & 8)		

Method	Principle	Disadvantage	Measurement Range	Measurement Accuracy
		Additional water might form if the pH does not fall within the range of accepted values. This can be attributed to side reactions as reactions tend to proceed at a faster or slower rate (Except the sample is buffered)		
Nuclear Magnetic Resonance Spectroscopy (NMR)	The spin of a proton (hydrogen atom) determines the number of water nuclei in the sample.	NMR determines all nuclear properties of the H-atoms in samples. Rather than the properties of the water molecule itself	0-15%	0.1%
IR- Infrared Spectroscopy	Irradiation of a sample with Infrared beam through an optical fibre transmitting energy at a particular wavelength (0.7 to 2.4 µm for water)	Variations in temperature can affect the result Band for water is not precise	1-80%	0.3-1%
Headspace Gas Chromatography	GC involves the use of a high polarity ionic liquid-based GC column and a pressurized loop headspace injection system. This technique is believed not to be affected by side reactions or other volatile constituents/contaminants	Adsorption on the stationary phase is seen as poor peak shapes due to its consistent exposure to water. Therefore, producing unpredictable results	0.1-1%	0.01%

Method	Principle	Disadvantage	Measurement Range	Measurement Accuracy
		On direct injection, volatile compounds tend to interfere with water peaks. This can lead to column deterioration.		

Compiled from: [97–100][105–110]

2.3.1 Karl Fischer Analysis

Karl Fischer analysis is a method that helps to numerically measure the content of moisture in the matter, which is in the form of liquid or solid [103]. Karl Fischer analysis is an analytical method that involves an oxidation reaction where the iodine oxidises sulphur dioxide with the consumption of water [109]. Volumetric and coulometric analyses are the two different Karl Fischer titration techniques employed to determine water content in a particular sample. The selection of a suitable approach depends on the measured water content required for sampling [108]. The volumetric Karl Fischer titration is ideal for samples where water is present as a major component (0.01% to 100%) [109][111]. In contrast, coulometric analysis is suitable for trace water determination levels, usually from 0.0001% to 5% [112]. This explains why the coulometric Karl Fischer titration is often employed for water content determination in jet fuels, as it contains typically 40 to 80 ppm of water at room temperature [45].

Karl Fischer reagent (KFR) usually contains sulphur dioxide and iodine [113]. The iodine is ionized, and due to the presence of this iodide ion, current flow begins [108]. Based on stoichiometry, the amount of water in a particular sample is equivalent to the amount of current flow or iodine used up. There will be no more usage of the current flow only when the entire water content in the sample has completely reacted with the iodine. The coulometric Karl Fischer cell has two separate compartments known as the cathode and the anode. The anodic compartment is where the iodine is coulometrically generated, and based on stoichiometry, 1 ml of iodine reacts with 1 mol of water. Thus, the endpoint of the coulometric titration is determined as soon as the current detect unreacted iodine [114]. Various experimentalists using the Karl Fischer method have determined water content in fuels. However, a group of authors revealed that the Karl Fischer analysis method was not as effective as the thermometric titration method [115]. According to this author, the thermometric titration method provides more accuracy, rapidity, automation, convenience and applicability [115]. Another group of authors suggested the thermometric titration method be divided into two

different groups [116]. The authors suggested water content be determined by using Karl Fischer analysis firstly and secondly by the exothermic heat of reaction measuring temperature pulse caused by the reaction of water and the KFR using a thermistor Wheatstone bridge system [116]. The total amount of water capable of reacting with the KFR represents the temperature increment. Thermometric titration is an analytical method that measures the content of a particular substance because of an enthalpy change [117]. In this method, the titrant is added continuously into the reactant. The maximum temperature reached signifies the endpoint of the titration. In other work, the water content is based on an endothermic reaction between the titrant and the water [115].

A method of water content determination that a group of scientists claim is more sensitive, rapid, and convenient than coulometric KF is the F-NMR (with a combination of reagents like anhydrous fluoride salts (like tetrabutylammonium fluoride (TBAF) and iodobenzene diacetate ($PhI(OAc)_2$)) [106]. The authors stated that handling errors were larger in the Karl Fischer analysis than that in the F-NMR because the sample preparation for the NMR method could be done in a glovebox [106].

2.3.1.1 Limitations to Accuracy for Use of Karl Fischer

As depicted in

Table **2.1**, using Karl Fischer Coulometer creates hurdles in the evaluation of water content because some samples undergo side reactions, and acidic samples can influence the pH value during the water content determination. The presence of sulphur can lead to the acidity of jet fuels [118]. In the same way, variables can affect the endpoint (temperature, sunlight and humidity variations). Also, possible contamination of the sample/syringe during introduction into the KF cell can affect the result. The limitation to the accuracy of using the KF cell was elaborated in

Table **2.1**.

2.4 Complexities Associated with Water in Jet Fuel at High Altitude

Aircraft are equipped with vents that allow air into the tank and allow for changes in atmospheric temperature and pressure [4][5]. This explains why factors like relative humidity, temperature and altitude are considered in the level of water gain/loss in aviation fuels. It has been hypothesised by Goertz et al. that temperature influences the formation of ice in hydrocarbon fuels like diesel [119]. Similarly, a study on the morphogenesis of ice by Libbrecht et al. shows that temperature and supersaturation (humidity) influences ice growth [6]. The research by Libbrecht et al. reviewed earlier studies on ice growth and concluded that ice grows into different shapes and sizes. Therefore, this shows that the appearance, shape and morphology of the ice that is likely to form in fuel sensitively depend on the level of supersaturation and temperature of the fuel. This theory can also be related to work carried out by the AAIB that indicated the ice sticky range temperature to be between -10 ºC to -20 ºC.

According to the Coordinating Research Council (CRC) handbook for aviation fuels, extensive studies conducted by both Boeing in the 1950s showed that fuel tank temperatures could reduce to -40 °C when cruising at a low speed after about 4 hours while the tank temperature drops to -29 °C at a speed of Mach 0.82 [1]. The conclusion from these studies suggested that fuels with a maximum freezing point of -50 °C would be beneficial for civil aviation purposes to manage risks of wax formation. At such low temperatures, it should be noted that fuel viscosity will also increase, promoting entrainment of the wax and free water crystals formed, perpetuating hazards of filter blockage and engine fuel starvation. As discussed, work to investigate the behaviour of water in jet fuel has been done; however, it has been mainly based on conventionally refined fuel, and very few SAF and synthetic aviation fuels have been tested. Several authors also reported that the CRC handbook for aviation fuels contains data for only petroleum-derived fuel [1][23][120].

Carpenter et al. experimented on the behaviour of water uptake in three batches of jet fuels and model hydrocarbons at temperatures above -60 ºC [83]. The fast/slow heating and cooling method of testing was employed for the analysis, and from the result of the analysis, there was no evidence of ice crystals even at −44 ºC for some of the fuels explored [83]. This disagrees with other reports that supercooled tiny water droplets (≥50 μm) freeze homogenously in fuel at temperatures between -32 ºC to -44 ºC [8][10]. However, the results of all these experiments were obtained through laboratory-based experiments only. According to Tascón et al., 'even though experimental results are in good agreement with simulation results, simulations can help to easily perform an in-depth and a ''what if'' analysis that is unexpected and beyond limits of applicability' [121]. Also, a recent study by Fitzner et al. suggested that although computational efficiency has some limitations, it can help conceive a large breadth of study with sufficient data diversity [122]. Consequently, it is highly recommended that due to the complexity of this analysis, an advanced and reliable data analytics computer-based tool capable of capturing fuel-related effects be employed for future work to accurately reflect the randomness and interdependence present in real-world systems.

Research is currently ongoing by the jet fuel screening and optimisation platform (JETSCREEN) design tool that is capable of predicting jet fuel properties using a machine-learning algorithm "Gaussian process regressor'' (GauProReg) [123][124]. So far, the result from works has suggested that the GauProReg is probably fit for predicting traditional jet fuel properties but lacks clarity for new fuels with unfamiliar compositions. It is recommended that the future models from this work be tested and validated on experimental measurements. Additionally, it is essential to note that fuel/air temperature will vary depending on weather conditions [2]. The effectiveness of the experiment related to the water in jet fuel mentioned by Zherebtsov and Peganova argued that the relationship between water solubility and temperature behaves differently at temperatures below and above 0 °C [21]. Zherebtsov and Peganova attributed this to discontinuous and continuous change in enthalpy and entropy during the phase separation of

water/ice. A discontinuity in the water solubility line is possible if there is a discontinuity in entropy during the transition through 0 °C. Several authors suggested that at higher altitudes, as the aircraft meets lower pressure (extreme cold conditions), the fuel in the aircraft wing tanks becomes cold [7][10]; this decrease in temperature is likely to decrease fuel water solubility. Lao et al. explored the behaviour of water in a simulated fuel tank. The result of the analysis found that water solubility in the fuel decreases as the temperature decreases, thereby leading to a fog regime (dissolved water that appears in the form of a cloud of fine water droplets) [16]. Lao et al. further revealed that at temperatures below -10 ºC, a hexagonal type of ice crystal would form in areas with sharp surfaces like edges growing at the expense of ice of the cubic of ice crystal [83][16][125]. The lowest temperature simulated by Lao et al. was -17.3 ºC. In a comparative study by West et al., conditions that more closely replicate actual aircraft system operation (temperature of -47 °C) were simulated. However, the study concentrated on the quantification of equilibrium partitioning of fuel system icing inhibitor (FSII) [126]. Furthermore, from work carried out by the AAIB, a fuel temperature of -35 ºC was estimated with water content between 35 and 40 ppm [43]. However, the results experienced were unusual. This study observed that the rate of ice accumulation increased at the critical icing temperature (-5 ºC to -20 ºC) and reduced as soon as the temperature dropped from -20 ºC to -34 ºC. This suggests the need to run experiments exploring sub-zero temperatures to ambient temperatures and vice versa whilst varying the added water content level. The trends from the result of this analysis will give a better understanding of the growth of ice in aviation fuel. Lam et al. took a step further by studying the ice growth in jet fuels [120]. From this work, some hexagonal ice crystals were observed. However, it was noticed that the larger ice crystals tend to grow at the expense of metastable ice particles near them. This is similar to results obtained from more recent studies by Moon et al. that metastable ice crystals help with the growth of a hexagonal type of ice crystals [127]. Moon et al. further classified shapes of ice crystals obtained in a fluid static condition into three different types (plate/spherical shapes, columnar shapes, and irregular shapes) [127].

A study conducted by the AAIB observed that ice crystals tend to stick to surface surroundings and other ice crystals near them at the critical icing temperature (also called the 'sticky' range) between -5 ºC and -20 ºC [43]. This scenario can be attributed to the Ostwald ripening process [67]. Jiao et al. further explain that the rate of the ripening process can differ depending on the composition of the fuel/nature of surfactant present [128–130]. The uncertainty as to how water behaves in jet fuel is still a challenge faced by the aviation industry to date. Several authors state that water will remain in its supercooled state and will not form ice even below its freezing point as long as it is a homogenous mixture [10][7][131]. Furthermore, freezing occurs in the presence of particulates for a heterogeneous mixture [132].

Soria et al. emphasised that ice formation in jet fuel is an important issue that cannot be overlooked as it is capable of leading to fatal consequences [133]. Thus, it is rather difficult to determine the severity of atmospheric temperature so that excessive formation of ice and its accumulation could be prevented. Campbell et al. argued that researchers must have sufficient information on the chemical compositions of jet fuel. However, due to its complexity, it is difficult to develop a theory about the behaviour of ice in fuel [134]. To date, the behaviour of ice has been studied through different angles, whereas no study in the literature has provided a complete description of all the factors that influence the behaviour of ice in jet fuels. Table 2.2 summarises some key information discussed in this section.

Table 2.2 Summary of key elements discussed in section 2: Water in Jet Fuel

Topic	Analysis/Comment	References
Water Solubility	Depending on the temperature and composition of the fuel - water solubility decreases with a decrease in temperature An increase in water solubility could be attributed to an increase in natural surfactant-oxidation products	[4][16][21][23][25][84] [86] [94]
Fuel Aromaticity	The higher the aromatic content, the higher the water solubility and dissolved water concentration	[2][18][24][83][91][90]

Topic	Analysis/Comment	References
	Lack of aromatics yield fuels that is below minimum density and can also lead to shrinkage of elastomers; however, when in excess, can lead to swelling of the elastomers, more soot production as a result of incomplete combustion and so must be restricted	[64]
Water Shedding	The rate of free water settling is a function of the water droplet size following Stokes law	[1][24] [101]
Surfactants	An increase in water solubility could be attributed to an increase in natural surfactant	[94][95]
	Ostwald ripening rate reduces with increasing surfactant concentration	[128][130][135]
	Surfactants can reduce water droplet size and consequently, reduce its settling velocity	[18][135]
Additives	Anti-icing agents: Water content may increase with an increase in the concentration of anti-icing agents	[90]
	Static dissipator additive is likely to increase water uptake	[83][92]
Homogenous Mixture	Water may remain in its liquid state even below its freezing point	[7][8][10][131]
Heterogeneous Mixture	At cold temperatures, freezing occurs in the presence of particulates	[8][132]
Karl Fischer Analysis (KFA)	As with all measurement techniques, a consensus has it that the limit to the accuracy of using the KFA is the tendency of forming side reaction	[64][96][98][99]

Topic	Analysis/Comment	References

2.5 Ice and its Behaviour in Jet Fuel

Gibbs's free energy (energy associated with a chemical reaction that is available to do useful work) must be overcome for ice to be formed from water. Hence nucleation is simply the birth of a new thermodynamic phase (crystal in this case) [136][137]. Water content, droplet size, surface type and ambient conditions have been identified as having an influence on the process of ice formation in jet fuel [28]. One of the most important factors impacting the ice formation in jet fuel is the presence of supercooled water droplets [138]. According to Schmitz et al., ice formation is a result of fine water droplets that have precipitated out and solidified into ice crystals [19]. Also, Baena et al. state that the ratio or extent of supercooled water droplets influences the rate of accretion or growth of the ice [44]. Furthermore, the accretion of ice on a subcooled surface that is immersed in fuels was examined by Lam et al. [22]. The strength of the accreted ice was evaluated. It was deduced that the amount of ice accretion (which is a process in which a film of ice forms/builds upon a solid surface exposed to freezing precipitation) increased subcooled surface temperature was lowered [22]. Similarly, previous work conducted by Baena et al. suggests that low temperature dispersed water can lead to ice crystals within the aircraft fuel systems [17]. The results of the experiment conducted show that the amount of ice accretion increases with higher cooling rates.

Analysis of the formation of ice in fuels contaminated with particulates was conducted by Murray et al. [8]. Their experiments observed that ice is more likely to form when the fuel is contaminated with particulates. Water tends to remain in its supercooled liquid state as long as there is no contact with any particulates until it gets to its homogenous freezing point of about -36 ºC [8]. However, particulates are always present in jet fuel, so an ideal situation is impossible. Lam et al. carried out an experimental study on ice growth in fuels; a visual representation can be seen in Figure 2.7 [22]. In this study, they observed that

ice formed homogenously and was detected between -32 ºC and -36 ºC, which compares well with the temperature of -36 ºC that has been observed by Murray et al. as the homogenous freezing point [7][8].

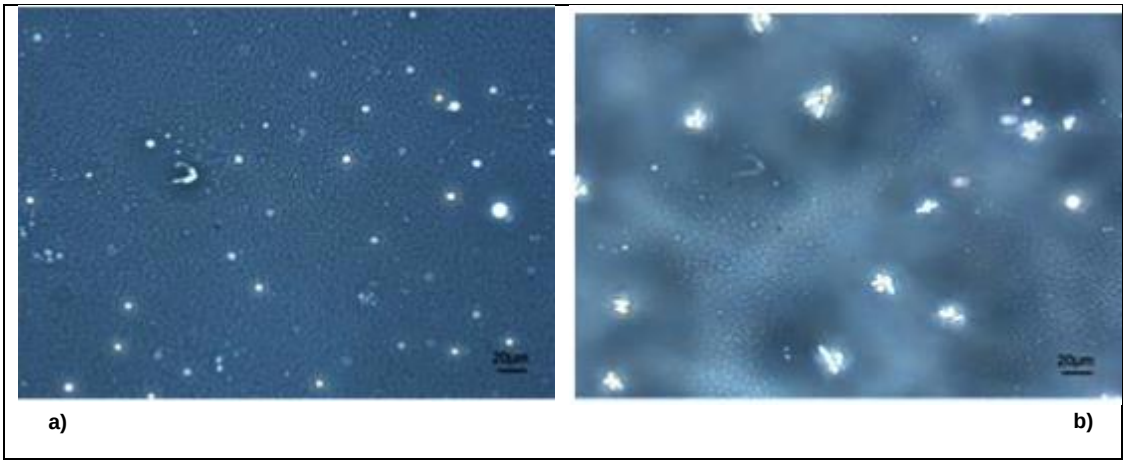

Figure 2.7 Water droplet formation from Jet A-1 fuel with dissolved water a) at -3.8 ºC b) at -34 ºC. Ice crystals seen in b), on holding the temperature of the fuel at -34 ºC [22]

In addition to that, several authors have acknowledged that ice nucleation rates are size-dependent [139]. Supercooled water droplets with sizes greater than or equal to 5 µm can induce the accretion of ice [22][138][49,140,141]. At temperatures below 0 ºC, water droplets can exist in a supercooled metastable state depending on its size [9]. Other authors carried out experiments using micro and nanometre-size droplets to investigate ice nucleation [142][143]. One of the studies by Laksmono et al. on micrometre-sized (microsize) water droplets showed a slower nucleation rate increase as the temperature decreases. The authors also observed that microsize droplets (between 3−12 µm diameter) do not form ice crystals at temperatures below -41 ºC [143]. Baena et al. took a step further to analyse the effects of these ice crystals on a mesh strainer [44]. They designed a test rig, and experiments were conducted at -12 °C and -15 ° C. From the experiments, it was concluded that both the amount of water in fuel and the temperature of the fuel play vital roles in the thickness of ice layers on mesh strainers. They concluded that the amount of ice accretion in the fuel is related to the quantity of water in the fuel. A summary table of ice in jet fuel is shown in Table 2.3.

Table 2.3 Ice in jet fuel summary table

Topic	Analysis/Comment	References
Ice Nucleation	The contact angle is an essential factor that governs ice nucleation	[18]
	Gibbs free energy has to be overcome for ice (the critical nucleus) to form from the liquid	[136][137] [143]
Ice Accretion	Ice accretion increases with a decrease in temperature (until it reaches the critical icing temperature between -5 °C to -20 °C) and an increase in nucleation sites.	[17–19][22]
	Size of supercooled water droplets greater than or equal to 5 µm can induce the accretion of ice	
	Ice accretion is dependent on the amount of water in the fuel and the temperature of the fuel	[22] [138][49,140,141]
	Fuel flow rates of between 0.2 and 0.6 m/s favour ice accretion	[136]
	Ice accumulation can be quantified by differential pressure measurements that occur as a result of fuel flow restriction	[43]
		[18]
Sticky Range	Ice crystals tend to adhere to surface surroundings and other ice crystals near them	[43][99]

Topic	Analysis/Comment	References
Additives	According to Zabarnick et al., cold flow improving additives: Alters the ice crystal structure/size in jet fuel at low temperature A strategy that involved the use of fuel dehydrating icing inhibitor (FDII) alongside a fuel-soluble water scavenger to aid in protecting jet fuel against the effects of water contamination was predicted by Repetto et al Although di-ethylene glycol monomethyl ether aids in preventing water solidification at low temperatures, it is less efficient than FDII when used in low concentrations	[144] [93][145] [93]
Ice Adhesion	The strength oice adhesion to a surface decreases with an increase in hydrophobicity Ice adhesion depends on the nature of the surface Key parameters affecting ice adhesion are temperature and roughness of a surface	[18][16][146–148] [48–50] [146][151–154] [50][148]
Nature of Ice	Soft, fluffy and snowflake-like ice with high porosity and little adhesion strength (Ice formed from dissolved water) Hard ice with more adhesion strength (Ice formed from free water) Crystalline, spherical ice particles of cubic and hexagonal habit (Ice formed from dissolved water)	[18][19][43][83] [46] [18]

Topic	Analysis/Comment	References
		[8][16][22]
High Altitudes	A decrease in temperature is likely to decrease water solubility	[6][7][10]

2.6 Effect of Material/ Surfaces on Nucleation of Ice

Aluminium is the most widely used material in the aviation industry, from the fuselage to main engine components; however, just like other metals, it is susceptible to corrosion under adverse conditions and biofilm contamination in the presence of microbial growths [16][153][154]. Figure 2.8 shows the trend of ice growth with time on an aluminium surface blasted with glass beads on cooling from 0 ºC to -18 ºC [19]. Schmitz et al. evaluated the effect of surface roughness and surface types on ice accretion in flowing fuel to help understand the ice accretion process in flowing fuel. As seen from the result in Figure 2.8, the ice thickness increases steadily with time [19].

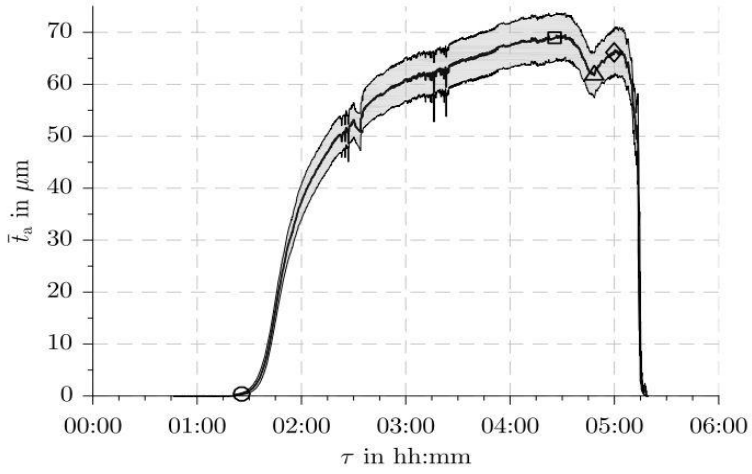

Figure 2.8 The trend of average ice thickness on an aluminium surface blasted with glass beads against time on cooling from 0 ºC to -18 ºC [19]

The dip seen at time 04:26 in Figure 2.8 is due to the gradual increase of the volume flow rate by the authors Schmitz et al., thereby making part of the

accreted ice shed off then reducing its thickness [19]. The effect of wettability (a measure of the water contact angle and sliding angle) and roughness on hydrophobic, hydrophilic, and superhydrophobic surfaces has been explored by Bharathidasan et al. [146]. This work deduced that silicone-based hydrophobic surfaces manifested an ice adhesion strength that is approximately forty-three times lower than the adhesion strength of bare aluminium alloy [146]. This was followed up in 2018 by Zhang et al. fabricating a superhydrophobic surface (with a water contact angle >150 º) on an aluminium surface to enhance its application [48]. Figure 2.9 compares the result of experiments conducted by several authors on this topic.

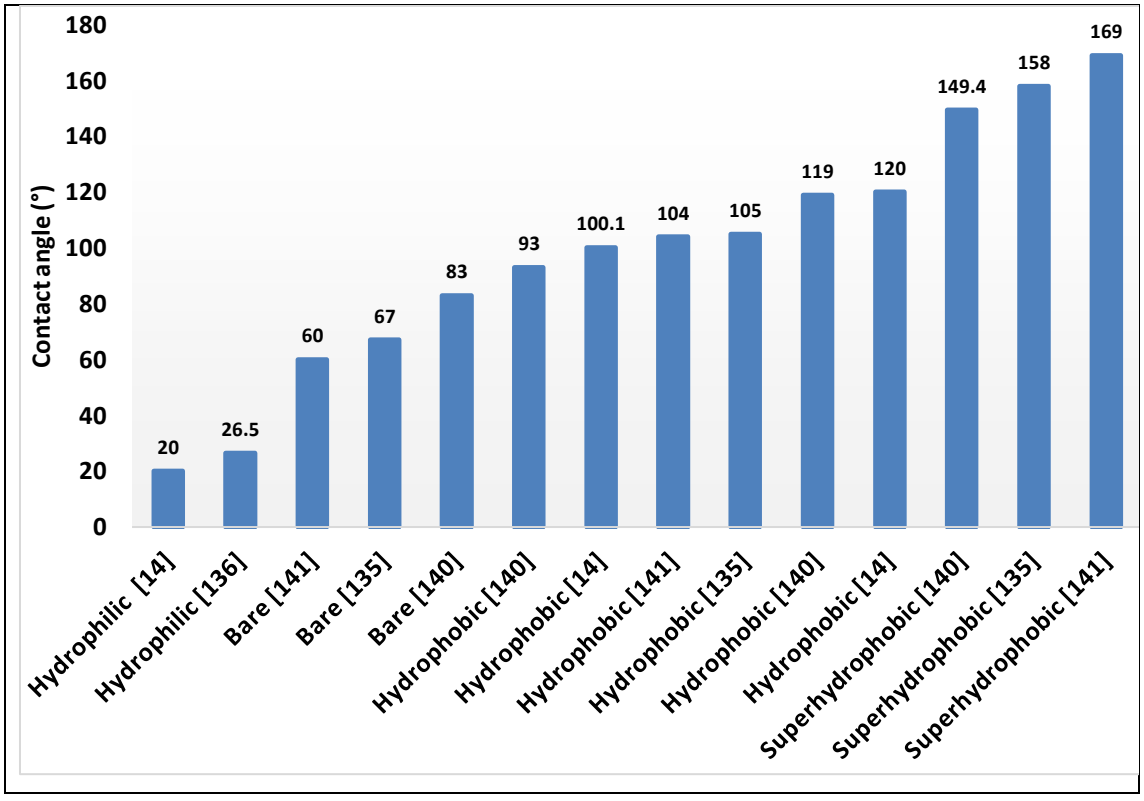

a)

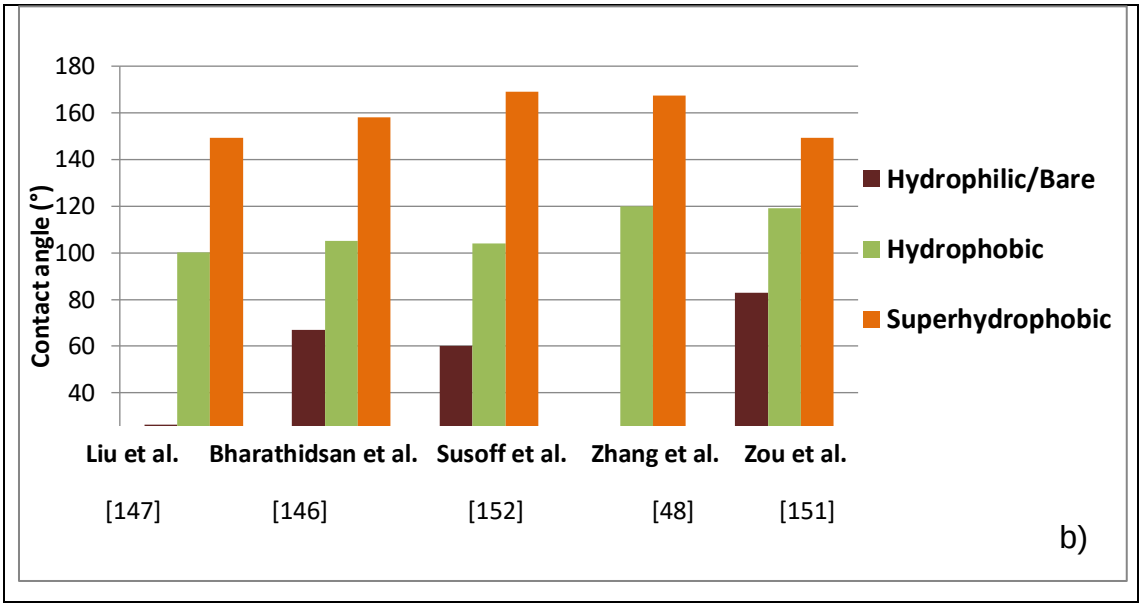

Figure 2.9 a) Column chart showing the effect of surface wettability on contact angles b) Comparative compilation of data from the literature, showing the effect of surfaces on the nature of ice formed

Figure 2.9 shows the impact of a surface's wettability on the contact angle; the contact angle between a hydrophobic surface and ice crystals, formed in-situ, is larger than the contact angle for ice crystals that grow on hydrophilic surfaces. Table 2.4 summarises the different substrates evaluated in reported contact angle experiments.

The nature and morphology of ice can be very dynamic [6]. Experiments on the behaviour of interfacial shear strength of accreted ice on subcooled surfaces immersed in jet fuels showed the accreted ice formed to be soft and fluffy [16][46][155]. No differences in adhesive strength were noted between the ice deposits formed on three different surface materials (aluminium, painted aluminium and carbon fibre) that were explored by Lam et al. [46]. On the other hand, a study carried out by Maloney et al. showed that a given material surface is not only influenced by the size and quantity of supercooled water droplets but it is also affected by the flow rate, Reynolds number (a dimensionless quantity that is a function of the flow velocity, pipe diameter and fluid viscosity), quality and nature of the material used [18][20]. Maloney et al. explained that stainless steel accumulated more ice than roughened aluminium and Teflon, as seen in Figure 2.10 [18]. Similarly, a recent study by Airbus on the ice accretion/release test in a large scale flowing fuel system indicated the non-uniformity of ice

thickness and porosity and suggested that it results from the water injection/mixing method [156]. Therefore, it can be concluded that the variation in reported data throughout the literature can be attributed to different testing conditions and experimental techniques.

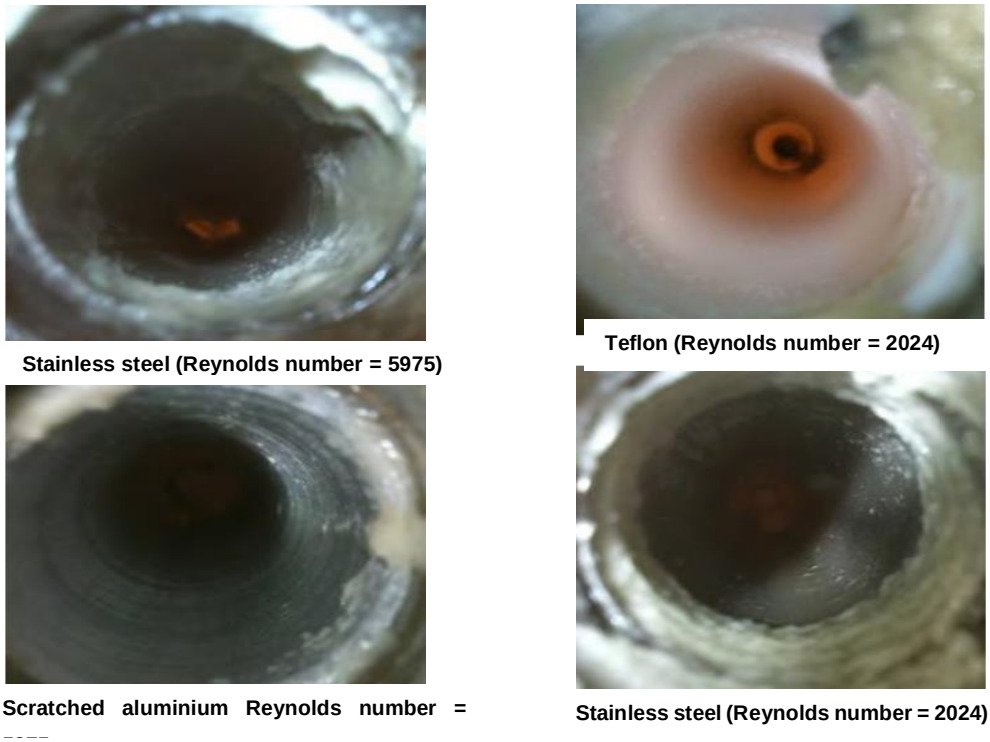

Figure 2.10 Pipe configuration variations showing that stainless steel accumulates more ice than scratched aluminium [18]

Maloney et al. assessed the ice accumulation along the test pipes by employing detachable test pipe sections for easy examination and measuring the pressure drop across the pipes [18][20]. As shown in Figure 2.10, the layer of ice accumulation decreases with an increase in Reynolds number and an increase in hydrophobicity. In this line, a study by Cox et al. stated that an efficient nucleating agent should not bind water too strongly, while a strongly adsorbing surface is detrimental to ice nucleation as a result of a higher water coverage [10]. Experiments conducted on different surfaces (silicon, mica, and glass) showed that water drops freeze near the homogeneous temperature limit. This homogenous temperature limit was said to be unaffected by roughening the

surface with diamond powders of different size distributions [134]. This is further supported by Elliott et al., emphasising that the growth of ice on surfaces solely depends on the hydrophobic or hydrophilic nature of the surface [49]. Additionally, an earlier study conducted by Antonini et al. suggested that alongside a de-icing strategy, a hydrophobic/superhydrophobic coating strategy should also be implemented for anti-icing systems [47]. Fitzner suggested that ice crystals are birthed from the mobility of water molecules adopting their lattice position [157]. Then, Thompson et al. postulated that fuel tank systems coated with hydrophobic substances reduce the size of water droplets and simultaneously increase the migration speed of the water droplets to the sump once in motion [158]. This system might help manage how ice forms or accumulates in aircraft fuel tank systems because the amount of ice accretion is related to the quantity of water in the fuel, as stated in section 2.2 [44].

A relationship between ice adhesion and surface roughness has been recently developed [146][48,50,149–152]. Elliott et al. explored a liquid droplet's behaviour on rough/smooth surfaces, and the results showed that the roughness of a surface influences ice formation [49]. Elliott et al. stated that the reason for this rapid liquid adhesion on a rough solid surface is the number of potential nucleation sites for bonding [49]. This is because the rough surface has stronger surface energy than the surface tension of water; therefore, the surface energy will overpower the surface tension of water, leading to a lower contact angle. Hence, roughness increases the probability of interaction between water droplets and the surface, leading to a faster nucleation rate. Susoff et al. screened different coatings and the influence roughness has on the surfaces; they observed that surface roughness increases the ice adhesion strength and [93]. Also, Zou et al. investigated the effects of surface roughness on the ice adhesion strength and found that a decrease in the ice adhesion strength on surfaces with similar roughness was related to the water contact angle [151]. A comprehensive study by Work et al. compared data in the literature and concluded that the key parameters affecting ice adhesion to a solid substrate are temperature and

roughness [50][159][160]. A nearly linear increase in adhesion strength with decreasing temperature from 0 to -20 was noticed. Other studies by Liu et al. and Alizadeh et al. illustrated that water-repelling surfaces ease the removal of ice [147][148]. Ice crystals appear to grow at right angles on a hydrophobic surface and grow across a hydrophilic surface, as seen in Figure 2.11. The important questions are: is it better to have a multitude of ice crystals floating in the fuel tank? Or a large thickness of ice in the wall of the fuel tank? This is difficult to measure because either scenario can potentially have safety implications. For example, ice might not accumulate in the fuel tank but will adhere to the inner walls of the aircraft fuel distribution pipework. The second scenario is that the multitude of ice crystals could form a big snowball and potentially block the fuel distribution pipework. These questions will need to be answered as the ice crystals from both scenarios can potentially block the fuel distribution pipework. The reason for this, as per the first scenario, is that the large thickness of ice that adheres to the inner walls might eventually slide (where there is a slight increase in temperature) and still lead to potential blockage. To answer these questions, experiments must be conducted in a simulated aircraft wing tank comparing the behaviour of ice when the pipe's inner walls are made of a superhydrophobic or hydrophilic material.

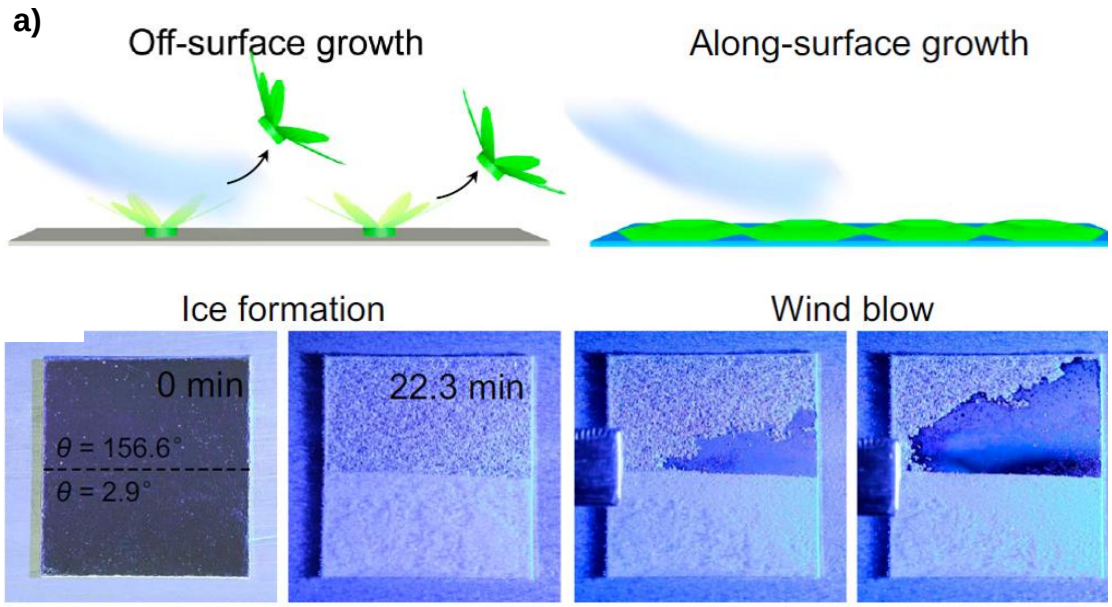

Figure 2.11 a) Schematic showing that off-surface ice growth (OSG) does not adhere firmly to the surface and can be dislodged easily. Along-surface ice growth (ASG) remains bonded to the surface; therefore, it cannot be displaced readily by fluid flow; b) Test panels cooled to -20.2 °C prepared with adjacent coatings; with a water-repelling surface (of high contact angle of 156.6°) and water-loving surface (low contact angle of 2.9°) to illustrate that water-repelling surfaces ease the removal of ice after blowing with a gust of wind [147]

Zhang et al. took a step further to analyse supercooled droplets of water on different superhydrophobic surfaces [48]. They suggested that at a high/low speed, smooth superhydrophobic surfaces with microscale and nanoscale roughness repel supercooled water droplets better than a rough superhydrophobic surface [48]. Mohammed et al., Zhang et al., and Chan et al. supported this work amongst many other authors that emphasised that superhydrophobic surfaces show high water repellence with both rough and smooth surfaces [146][48][149][158][161–163]. Also, a superhydrophobic surface tends to have a remarkable ice-phobicity (the high repellence ability of a solid surface), but its repellence on a rough surface can be controversial [131][48][160][163]. In comparison, a hydrophobic surface can repel impacting water droplets before ice nucleation occurs, but superhydrophobic surfaces were found effective in preventing ice formation instead of fighting its build-up [48][162].

Findings from different studies in the literature also reveal in Table 2.4 that surfaces will have an important role to play in the growth pattern of ice in aircraft fuel systems; it is not yet known if having a multitude of ice crystals floating is better than having a large thickness of ice in the wall of the fuel tank. Yet, no work has been carried out to evaluate the effect of surface types on ice accretion in synthetic aviation fuels for the basis of comparison with conventional jet fuel.

Table 2.4 Summary of Substrates Explored in the literature for Contact angle between ice crystals and different substrates

Author	Surface	Substrate	θ (°)
Liu et al. 2017 [147]	Hydrophilic Surface	Aluminium Surface	26.5 ± 1.2
	Hydrophobic Surface	1H,1H,2H,2H-Perfluoromethyldecyltrimethoxysilane	100.1 ± 1.0
Zhang et al. 2018 [48]	Super-hydrophobic Surface	Nano Silicon	149.4 ± 1.2
		P_4S_3[a]	156.8 ± 1.6
		SHS-Al[b]	167.4 ± 1.4
Bharathidsan et al. 2014 [146]	Hydrophilic	Bare Aluminium Alloy	67.0 ± 2
	Hydrophobic	RTV 11[c]	105 ± 1.5
	Super-hydrophobic	RTV11-EH5[d]	158
Upadhyay et al. [164]	Amphiphilic	Amphiphilic siloxane polyurethane (AmSiPU) coatings	90 - 110
Susoff et al. [152]	Super-hydrophobic	Sol-gel fluorinated Aerosil,	169
	Hydrophilic	Sol-Gel PEG	10-60
	Hydrophobic	Siloxane modified polysiloxane	104

a. Phosphorus sesquisulfide; superhydrophobic surfaces with micrometre-scale and submillimetre-scale posts fabricated on the solid surface using photolithography and etching of inductively coupled plasma on silicon surfaces.

b. Super-hydrophobic coating sprayed uniformly on an Aluminium surface (multi-surface aerosol, Rust-oleum Corporation).

c. RTV 11- Vulcanised silicone rubber hydrophobic coating (Cured at room temperature).

d. RTV11-EH5- a mixture of RTV 11 and toluene with ultrasonically dispersed CAB-O-SIL EH5 and silica resin.

2.7 Conceptual problems and knowledge gaps identified from the literature

Many problems have been identified in the literature. With authors adopting different experimental techniques and conditions for testing, there exist some prominent methods that have emerged as favourites. One of which is the use of the Karl Fischer analysis, which is the most widely used method for water content determination. The second will be the water introduction method that involves adopting an equilibrium jacketed cell to achieve the saturation limit of water maintained at a 100% relative humidity vapour space in a test fluid. A classic example is an investigation of water solubility in jet fuels by three different authors [21][23][24]. Even though all three authors adopted the same water introduction and water analysis method, the trend observed by West et al. agrees only with that observed by Zherebtsov and Peganova [21][24]. It is unsure if the difference observed by Charro et al. is because conclusions were drawn merely from a set of single experiments or as a result of the experimental technique adopted by the authors**.** Although it is not possible to make a direct comparison as a result of the large number of variables that may exist, it may be possible that replicating the experiments for each temperature explored by Charro et al. will provide a more precise judgment by either refuting or corroborating the trends observed from the experiment [23]. Bias trends in the data could also be a result of the water content determination test employed. Therefore, it is recommended that authors provide raw data as part of the supplementary information rather than just graphical plots with fitted curves. Curve fits can be obscure as the integrity of the result is usually unknown.

A primary problem that has been identified by several authors in the literature is that the Karl Fischer analysis is not a completely reliable technique as it has the potential to form side reactions and some other limitations to accuracy [64][67][96][98][99]. To reconcile these differences, the authors suggest benchmarking this procedure to see if there is any consistent offset to set a correction factor in place. Also, the authors suggest that a good homogenisation

method be used for introducing water into the fuel, and also, water should be introduced at room temperature to achieve reliable conditioning of the fuel. This is because the KF analysis is only accurate for measuring dissolved water, and unfortunately, free water never has a homogenous distribution[163].

The complexity of how water and ice behave in jet fuel is still extremely problematic, making it difficult to reach a definitive agreement. For example, comparing results from a study by Carpenter et al. on ice formation in aviation jet fuel, it was observed from this study that ice formed homogenously at -44 ºC. However, this is a much lower temperature than the -36 ºC observed by Murray et al. as the homogenous freezing point [7][8]. Again, this may be due to the selected jet fuel composition, experimental technique or conditions adopted by the authors. Furthermore, findings from different studies in the literature reveal that surfaces have an important role in the growth pattern of ice in aircraft fuel systems. Yet, no work has been carried out to evaluate the effect of surface types on ice accretion in SAF/synthesised fuels for the basis of comparison with conventional jet fuel. Hence, it may be important to run tests investigating the role surface may play on ice accretion in flowing synthetic aviation fuel. An open question has been identified from section 3 in the discussion on ice crystals growing at right angles of a hydrophobic/superhydrophobic surface and growing across a hydrophilic surface. The important questions are: Is it better to have many ice crystals floating in the fuel tank? Or a large thickness of ice in the wall of the fuel tank? As discussed, this will be difficult to measure because either scenario can potentially have safety implications; for example, ice might not accumulate in the fuel tank but will adhere to the aircraft fuel distribution pipework's inner walls. The second scenario is that the multitude of ice crystals could form a giant snowball and potentially block the fuel distribution pipework. These questions will need to be answered as the ice crystals can potentially clog the fuel distribution pipework from both scenarios. The only way these questions can be answered is by conducting experiments comparing both scenarios at the same test conditions and variables.

It is noteworthy that minimal data exist in the literature on investigating some of the properties of existing synthetic aviation fuels and their impact on aircraft fuel systems. The bulk of data in the literature is from work done on conventionally refined jet fuel. However, available data in the literature focusing on this type of synthesised fuels explores the effect of water solubility and water settling rate only.

The majority of this is on water solubility investigation, and only one paper by West et al. exists on the effect of water settling rate in synthetic aviation fuels [24]. Unfortunately, the trends obtained will require verification as the results presented are for 10,000 ppmv which is unrealistic and a relatively high concentration unlikely to represent in-flight conditions.

2.8 Conclusion

This study has identified knowledge gaps in the literature that require to be filled in order to engineer a lasting solution to the problem of ice formation in jet fuel. To gain a better understanding and identify precisely the conditions and features that may exacerbate free water drop-out, ice accretion and formation in flowing fuel, a number of questions must be answered: Can the Karl Fischer analysis for water content determination be benchmarked? How will surface type on ice accretion be affected by synthetic aviation fuels in comparison to conventional jet fuel? How will jet fuel composition affect the frequency size distribution of dispersed water droplets? Does the theoretical assumption about droplet size/frequency distribution in jet fuel being governed by shearing conditions agree with experimental data? How will jet fuel composition influence the rate of water-shedding under realistic and representative test conditions? How will an increased blending portion with conventional jet fuel on the synthesised fuels approved by ASTM D7566 affect this water-shedding rate? Is it better to have a multitude of ice crystals floating in the fuel tank? Or a large thickness of ice in the wall of the fuel tank? Currently, there is very little to no information on any of the questions listed above. Therefore, further work is required to establish the

viability of these experiments as this might help proffer a better understanding and help manage the nature in which ice forms in aircraft fuel tank systems. This study proposes implementing a hydrophobic/superhydrophobic coating strategy alongside a de-icing strategy in future aircraft fuel systems design. Thereby serving as a basis for design guidelines to minimise ice formation within an aircraft fuel system and finally suggest possible solutions to prevent future occurrence.

This review investigated over 150 papers and collected a significant amount of information for the basis of comparison and analysis with the recent advances and technologies in the literature. This study provides conclusive data providing a detailed description of the factors that influence the behaviour of water and ice in jet fuels. Furthermore, the study presents a detailed account of some complexities associated with jet fuel chemistry, knowledge gaps, systematic hypothesis, and future development recommendation. The authors of this work identified significant problems with the way results are reported and recommended that authors provide raw data rather than just graphically fitted plots as curve fits can be obscure due to the unknown veracity of the result.

The literature summarises that the study of the behaviour of water and ice in jet fuel is rather complicated. Hence a computer-based tool for multivariable analysis and modelling is required to reflect the randomness and interdependence present in reality adequately. Furthermore, it is advised to make laboratory tests more representative by attempting to correlate this observation with what happens in in-service aircraft fuel tanks. Hence, in this work, it is proposed to develop a metric from an experiment that involves exploring sub-zero temperatures to ambient temperatures and vice versa.

In observational studies from the literature, there is still a potential for bias regarding the most widely used water content determination method. Several authors have concluded that Karl Fischer's analysis is not entirely a reliable

technique. Unfortunately, due to many discrepancies, there is a need to benchmark this procedure to see if there is any consistent offset to set a correction factor in place.

3 Chapter 3 Assessment of HEFA, ATJ, GTL-S8 & Farnesane as Alternative Jet Fuels Based on their Water Shedding Characteristics

Abstract

Previous studies have shown that impurities like surfactants in jet fuel have impacted the performance of coalescer filters. Therefore, aircraft maintenance schedules require an additional operation which is commonly known as water sumping. Normally after bulk fuel transfers, fuels are allowed to settle in tanks and sumping is carried out to remove free water.

Water settling tests can indirectly measure surfactants in jet fuels, yet there is no reliable data that focuses on the water settling rate of alternative jet fuels that comply with or are very similar to the Jet A-1 specification. Additionally, the influence of the jet fuel composition on the rate of water-shedding is still unknown. Therefore, there is a need for a reliable study to fill this lack of knowledge.

In this work, the water settling rate of five different jet fuels made to different national standards in comparison to conventional Jet A-1 fuel was evaluated. GTL S-8, HEFA and ATJ has been identified as potential/alternative candidates for ASTM D7566 certified jet fuels.

3.1 Introduction

The presence of water and particulates in jet fuel is undesirable and can promote biological growth that can be potentially detrimental, leading to fatal consequences [11][12]. Thus, according to the Air Transport Association (ATA) specification 103, water content has to be maintained below 15 ppm at the time of fuelling [165][13]. Coalescing filter technology is employed to keep the amount of free water to a minimum value. However, previous studies have shown that traces of surfactant in fuel have impacted the coalescing performance of fuel filters. Sumping is one of the operational practices adopted to remove free water that has settled in the base of fuel tanks. Fuel in bulk storage tanks is usually allowed to stand for some time after bulk fuel transfers with subsequent sumping. The water settling rate can indirectly measure surfactants, as a high-water settling rate indicates the fuel has little or no surfactant and vice versa.

However, it is important to determine if water settles at similar or different rates in alternative aviation fuels. There is a need for reliable data for future use of different alternative fuels/blends and to generate new data where this is believed to be lacking. This work was designed to critically analyse the rates of water settling from various jet fuel blends. The target for this work is to select the best fuel/blend candidate to run further chemical/physical tests for future ASTM validation.

3.1.1 Alternative Fuels

Dependency on petroleum-derived fuels poses an increase in environmental concerns and price fluctuations [74][75]. However, conventional fuel still accounts for the vast majority of aviation fuels [70]. A study by Nygren et al. showed that conventional fuels are still the largest energy providers in the transportation sector [77]. Additionally, a study by the Cambridge Energy Research Associates (CERA) and the UK energy research centre (UKERC) indicated that a peak in conventional supply is likely before the year 2030 [166][167]. Further indications by the organization of petroleum exporting countries (OPEC) are that jet/kerosene is the fastest-growing fuel in the outlook and has estimated the oil

demand in the aviation sector to rise due to rising income levels fostering the demand for air travel services [168]. However, to reduce GHG emissions, the use of, the use of alternative aviation fuels is featured to have the potential to decrease the life-cycle of greenhouse gas (GHG) emissions [77][76][26].

These fuels are derived from renewable sources or biomass, so they can reduce GHG emissions' contribution to the global climate. According to several authors, the introduction of alternative aviation fuels has the potential to reduce soot particulates as they have a low aromatic content [29][30].

Although alternative fuels seem like a promising technology for the aviation industry, some alternative fuels (including oxygenated alternative fuels) are low in Sulphur, low in aromatics and have a high water solubility [77][27][30]. These can expose the fuels to the risk of low lubricity, elastomer (seal) shrinkage and increased water contamination [30][169]. The introduction of alternative fuels suggests these will compete with food production land space and subsequently lead to deforestation [30][27][170][171]. The development of alternative fuels is both advantageous and disadvantageous to the aviation industry. Some of these are the low aromatic content, low sulphur content and good low-temperature properties [34]. On that account, several authors suggested the exploitation of renewable non-food energy crops with high oil content [74][30][27][172][173]. These feedstocks are known as second-generation fuel sources as they require low-quality land and high water usage compared to third-generation sources [174]. Second generation feedstock includes jatropha, camelina, halophytes, and sewage waste [173][175].

Table 3.1 Prominent alternative fuel feedstocks and their final products

	Feedstock	Final Product	Intermediate-Yield GGE/BDT[4]	Jet Fuel Yield GGE/BDT[4]	Specific Energy MJ/kg
	2nd Generation				
Oil to Jet	Jatropha	HRJ[1]	92	59.9/67.7	Up to 38
	Jatropha	CH[2]	56	8.9/10.1	Up to 38
	Camelina	HRJ[1]	85.9	47.2/53.3	Up to 38
	Camelina	HRJ[1]	121.4	66.2/74.8	Up to 38
	3rd Generation				
	Algae	HRJ[1]	61.9	44.3/50	Up to 23
	Algae	HDCJ[3]	29.9	15.2/17.2	Up to 23

Compiled from [176]-[178]

1 **HRJ** Hydro processed renewable jet

2 **CH** Catalytic hydrothermolysis

3 **HDCJ** Hydrotreated depolymerized cellulosic jet fuel

4 **GGE/BDT** GGE- Gallon of Gasoline Equivalent, BDT-Biomass U.S. Dry Ton

Currently, alternative fuels can only be used once blended with a certain percentage of conventionally refined jet fuel [27][30][60][79][91]. Aviation fuels must meet strict criteria to be admissible to civil aviation authorities. Several specifications like ASTM D1655, DEF Stan 91-91 and ASTM D7566 exists for jet fuel certification. ASTM D7566 is the standard specification for aviation turbine fuel containing synthesized hydrocarbons (HC), focusing on alternative jet fuels and is an expansion of ASTM D1655. The alternative fuels must demonstrate compliance with the relevant product specification. Table 3.2 shows the properties of some potential alternative aviation fuels against ASTM D1655.

Several organizations and research institutions are exploring two prospective processes, known as pyrolysis and catalytic hydro-thermolysis (CH) [35][179]. The pyrolysis pathway is also called hydro-treated depolymerized cellulosic jet (HDCJ). Additionally, a process known as CentiaTM is a patented development at North Carolina University in the USA. This process reuses oil from different feedstocks to produce bio-jet fuels [15].

Table 3.2 Properties of alternative aviation fuels against ASTM D1655

Property	ASTM D1655-19	Air BP Jet A-1 (Conventional)	Shell GTL	Hydro-processed ester and fatty acid (HEFA - camelina)	Alcohol-to-jet (ATJ) fuel	Syntroleum Fischer-Tropsch Gas-to-Liquid (GTL S-8)
Total sulphur (wt. %)	<0.3	0.02	<0.001	<0.001	<0.01	<0.001
Aromatics (wt. %)	<25	19.5	<0.2	<0.2	0	<0.1
Initial boiling point (°C)	Report (D86)	156	146	151	174	182
10% recovered (°C)	<205	167	162	161	178	195
Final boiling point (°C)	<300	258	228	259	262	280
Flash point (°C)	≥38 min	42	44	39	50	49
Freezing point (°C)	< −40[a] <−47[b]	-50	-54	<-77	-81	-59
Density at 15 °C (kg/m^3)	775–840	804	737	751	800	757
Viscosity at −20 °C (cSt)	< 8	3.5	2.6	3.3	5.1	4.6
Net heat of combustion (MJ/kg)	≥ 42.8 min	43.5	44.2	44.3		44.1
Smoke point (mm)	≥ 25 min	25	40	50	35	>43

a. Freezing point for Jet A

b. Freezing point for Jet A-1

Compiled from [34][23] [36]

The properties detailed in Table 3.2 cover the jet fuels studied for this work compared to ASTM D1655. Previous studies have shown that the aromatic component influences the water uptake and release of water, and the aromaticity effect is likely to be masked by natural surfactants in a fuel [83]. The alternative fuels mostly meet the ASTM specification but are low in aromatics and tend to have a lower density.

3.2 Research Target and Objectives

Because of the compositional difference between conventional and alternative jet fuels, it is important to analyse the different rates of water from various jet fuel blends. The objectives for this work are as stated below:

- Investigation of water settling from various fuel blends.
- Effects of increased blending portion on water settling in comparison to the currently permitted blend percentage.
- Comparison between the blendstocks and conventional jet fuel.
- Selection of the best fuel/blend candidate to run further chemical/physical tests for future certification.

3.2.1 The water settling rate test

The water-shedding experiment rates the ability of a fuel to shed emulsified or entrained water.

It is important to know if water separates from alternative fuel blends in the same manner as conventionally refined jet fuel.

The test indirectly measures the presence of trace surfactants in jet fuels. Surfactants may compromise the filtering efficiency of filter separators by coating the filter fibres. This may inhibit the free water separation characteristics of the filter, potentially allowing free water to pass through the filter; a secondary consequence is that it will alter the size distribution of the water droplets. Surface active agents have the potential to lower the interfacial tension between two fluids. Therefore, fuel that contains trace surfactant is likely to contain less water droplet count and more dissolved water. A high-water settling rate indicates the water is easily coalesced, implying that the fuel is relatively free of surfactant materials and has lower water solubility.

Theoretical water settling rate calculations have been based on Stokes' law (**Equation 3-1**); this is an expression that describes the resisting force on a spherical particle falling through a liquid under the effect of gravity. Although Stokes' law was derived for solid particles falling through a fluid, it is reasonable for water droplets falling through jet fuel. Since the cohesive forces of water molecules will tend to minimize volume and surface area, i.e., they tend toward spheres, a low water settling rate will indicate that the water molecules will resist distorting forces.

$$\mathbf{V} = \frac{\mathbf{g} \cdot \mathbf{D^2}(\boldsymbol{\rho}_\mathbf{w} - \boldsymbol{\rho}_\mathbf{f})}{\mathbf{18} \cdot \boldsymbol{\eta}_\mathbf{f} \cdot \boldsymbol{\rho}_\mathbf{f}}$$ **Equation 3-1**

Where:

$\boldsymbol{\rho}_\mathbf{w}$ = density of water (kg/m^3)
$\boldsymbol{\rho}_\mathbf{f}$ = density of fuel (kg/m^3)
$\mathbf{g}$ = acceleration due to gravity (m/s^2)
$\boldsymbol{\eta}_\mathbf{f}$ = kinematic viscosity of the fuel (m^2/s)
V = terminal velocity of the water droplet (m)
D = Water droplet diameter (m)

Stoke's law is based on the size of a water droplet, density and viscosity of the fuel. Assuming there are no interactions between the fluid and the sphere, the settling rate of water droplets relates to the density of the fuel. Since water has a higher density (997 kg/m3 at 25 °C) than jet fuel (795 kg/m3), water droplets will fall through jet fuel under the effect of gravity. Depending on the viscosity of the fuel, it will resist the force at different rates. Larger water droplets are expected to have a high settling rate. Presumably, water droplets below 3 µm may not settle

since these are micro convection cells within a large body of fuel, which will tend to help keep them in suspension.

The theoretical settling velocity of water droplets in neat fuels available for this work was calculated. A graphical representation of calculated terminal velocity against water particle diameter for different fuels is as shown in Figure 3.1. For future work, the terminal velocity should be recalculated, assuming the water droplet is undergoing free settling or hindered settling. Also, a visual process analyser (ViPA) is recommended for establishing the particle size distribution and water count frequency analysis on the various jet fuels explored for this work. The ViPA can continuously monitor the physical characteristics of a laboratory sample, so this will help give real-time results.

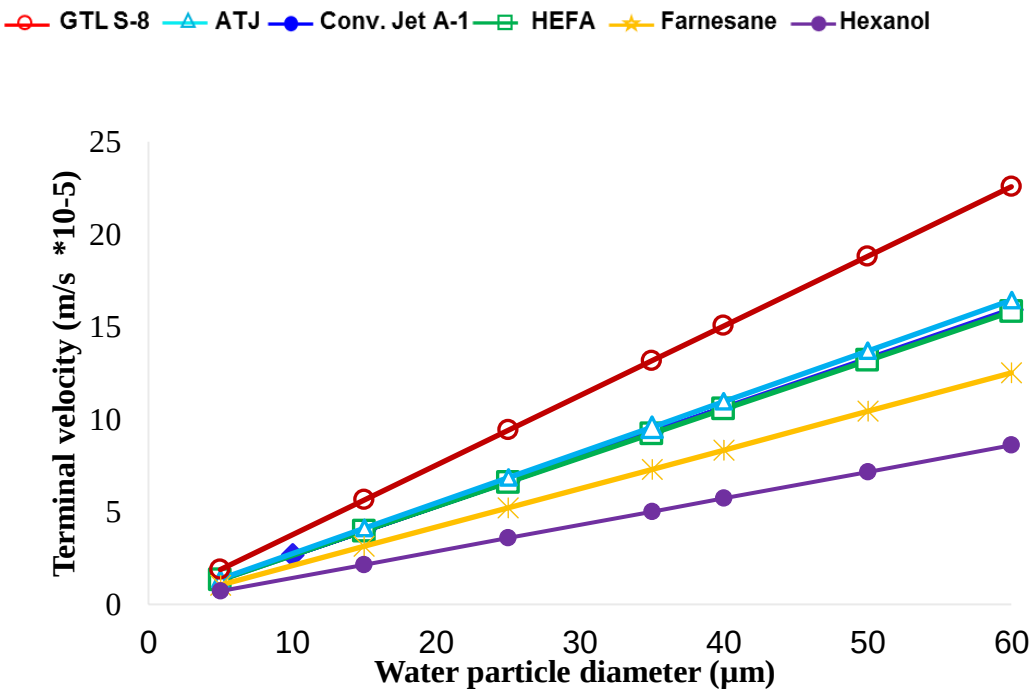

Figure 3.1 Theoretical settling velocity data of water droplets in neat fuels

Differences between the fuels are driven by viscosity and density, as will be apparent from Equation 3-1. This provides context for the empirical data in the results section and gives a correlation between theoretical data and experimental

data. It can be seen from Figure 3.1 that the gas to liquid fuel (GTL S-8) is predicted to release water faster in comparison to the other fuels explored. This will be expatiated on in the results section.

3.3 Experimental Section

3.3.1 Material and method

Airbus Filton, Bristol, procured the fuels used for this work. The percentages of the fuel blends employed for this work are as shown in Table 3.3 below. The water settling tests were carried out at an ambient temperature of about 23 °C.

Table 3.3 Fuel blends used for water-shedding and water solubility experiments

Conventional fuel % Blend	**Syntroleum (S-8 FT-GTL)**	**HEFA**	**Farnesane (Amyris SIP)**	**ATJ**	**Hexanol**
0%	100%	100%	100%	100%	
15%	85%	85%	85%	85%	
50%	50%	50%	50%	50%	
85%	15%	15%	15%	15%	
100%	0%	0%	0%	0%	
-	85%	-	-	-	15%

The standard test method for determining water separation/shedding characteristics of aviation turbine fuels is by use of a portable separometer (MSEP test) in accordance with ASTM D3948. ASTM D3948 was developed to measure the presence of surfactants in fuel; however, certain additives can have an adverse effect on the ratings. The MSEP test has a numerical measurement range of 50 to 100. Any value outside these limits is undefined; therefore, low results can be obtained with some fuels that do not affect the performance of a coalescing filter. ASTM D7224 was introduced to improve the precision of ASTM D3948.

Test D7224 was developed using representative materials currently used in commercial filter separators. It is important to note that a filter coalescer can only remove free or suspended water but will not remove dissolved water. This is why Karl Fischer's (KF) analysis was adopted for analysing the total water contents of the different fuel blends. A Metrohm KF 831 coulometer was used; the working cell was filled with Sigma Aldrich Hydranal AG-H anolyte and the generator electrode with CG catholyte

3.3.2 Procedure for water settling rate

Fuel/water mixtures were prepared in a 100 mL measuring cylinder to give the following nominal water concentrations: 500 ppm, 1000 ppm, and 10,000 ppm. For 500 ppm water concentration, 0.05 mL of water was mixed with 100 ml of fuel using an X 620 high shear mixer. The fuel/water solution (emulsion) was mixed for at least 2 minutes at 11,000 revolutions per minute. The fuel/water mixture was then allowed to stand for 2 minutes. Emulsion samples were taken at a depth of 120 mm max from the settling column (260 mm high) using a clean 1 ml glass syringe fitted with a 170 mm long fine needle. The dimensions are as shown in Figure 3.2.

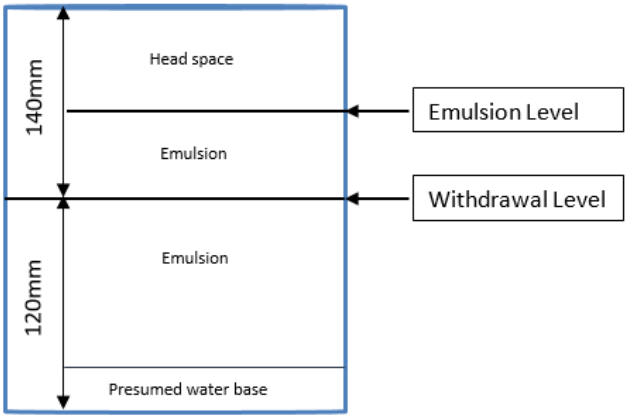

Figure 3.2 Schematic of settling column extraction point

As there is a settling column of sizable water droplets, there is the possibility that a large droplet might be siphoned out when taking aliquots hence the inconsistency in the early stage of the experiments as shown in the results

tabulated in Appendix A in Table A-1 and Table A-3. An ultrasonic bath/probe is recommended for the mixing process to improve this test for future work. In the proposed test, the emulsion created by an ultrasonic bath should be compared to the emulsion produced using the high shear mixer.

For this work, samples were evaluated using a Metrohm KF 831 coulometer, following the technique described in ASTM D6304. The experimental setup for this work is as illustrated in Figure 3.3. Tests were repeated at least five times for each batch of fuel. The results are as given in Figure A-4.

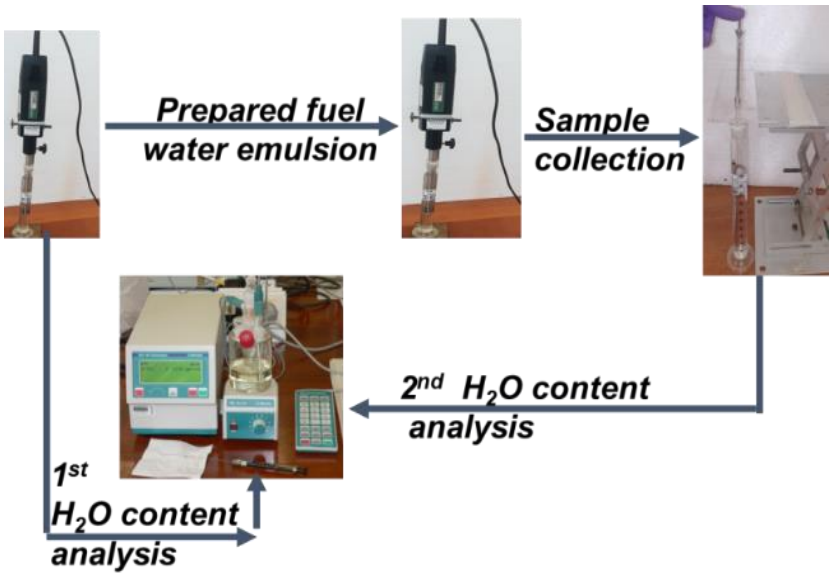

Figure 3.3 Experimental setup for the water settling experiment

To optimise the KF for an accurate and quick water determination analysis, minimum sample mass and volume were based on the recommended 50 µg minimum water injection per determination. This helped to ensure that the KF cell was not swamped with excess water and that the KF reagent was not over-diluted with jet fuel. In this work, the added water concentrations were 500, 1000 and 10,000 ppm, so the recommended fuel sample mass/ volume ratios were 0.1 g/0.13 ml, 0.05 g/0.06 ml, and 0.01 g/0.01 ml, respectively.

3.4 Results and Discussion

The calculated water droplet terminal velocity has provided context for experimental data. Triplicates of all tests on the different fuels explored were conducted, and the mean was plotted in Figure 3.4 to Figure 3.6. According to the coordinating research council (CRC) handbook, the water settling rate in aviation fuel is a function of particle size. From Table A-1 to Table A-3, it can be seen that there is no consistency in the water settling results at the beginning of the experiment. This can be attributed to the settling column of big water droplets at the start of the experiment (approximately 10 minutes), with the fine dispersion settling over time.

3.4.1 Comparative Study of water settling rate in conventional jet fuel and alternative blends

The results of the water settling rate experiments are displayed graphically in Figure 3.4 to Figure 3.6; trendlines have been fitted to the series of data points. Exponential curves seemed to give the best curve fit, as seen in Figure 3.4b. The water exhibited the fastest settling rate in GTL S-8, hydro processed ester & fatty acid (HEFA) & alcohol to jet (ATJ) fuels which were predicted by Stokes' law calculations. Exponential growth shows how a quantity (an exponential function of time) may increase or decrease over time. From Table 1.3, the constant of proportionality is negative, which implies an exponential decay with time.

Table 3.4 Calculated equations for the water settling rate measurements for fuels/fuel blends with 1000 ppm water addition

Fuels	Equation
75% GTL, 25% Hexanol	$y=1006.7e^{-0.002x}$
100% Farnesane	$y=1173.9e^{-0.002x}$
100% Conv. Jet A-1	$y=1020.7e^{-0.006x}$
50% Conv. Jet A-1 & 50% Farnesane	$y=1443.5e^{-0.009x}$
50% GTL S-8 50% Conv. Jet A-1	$y=1169.4e^{-0.01x}$
100% ATJ	$y=976.41e^{-0.011x}$
100% HEFA	$y=937.7e^{-0.01x}$
100% GTL S-8	$y=843.3e^{-0.008x}$

From Figure 3.4a, water exhibited the slowest settling rate in 75% GTL S-8 and 25% hexanol blend with 564 ppm after 1744 minutes. The next slowest fuel to settle was Farnesane at 158 ppm in 1,269 minutes. Water exhibited the fastest settling rate in neat GTL S-8 at approximately 55 ppm after 1,000 minutes. Water settling rates follows an exponential equation and are summarised in

Table 3.4.

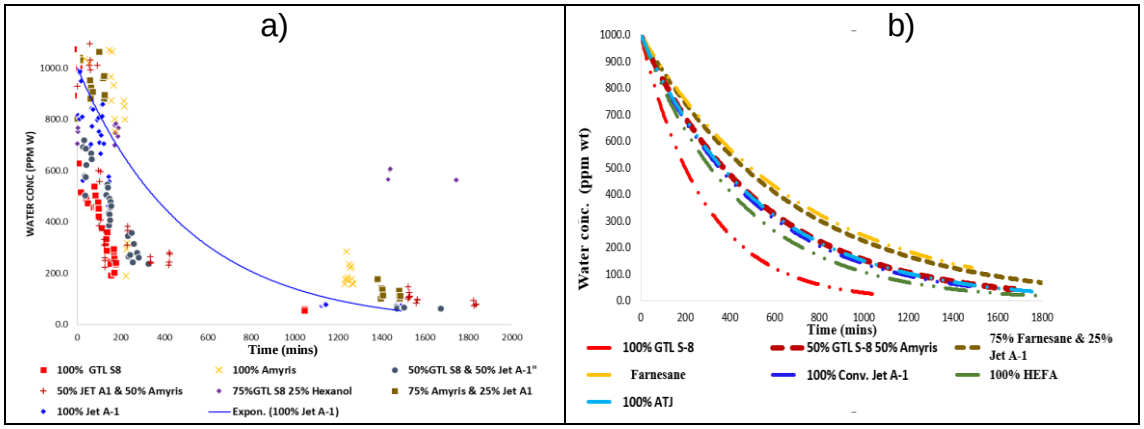

Figure 3.4 a) Water settling rate for the fuel blending ratios in comparison to neat fuels. b) best curve fit water settling rate for the fuel blending ratios

It can also be deduced from Figure 3.4a and b that various blending ratios have a notable impact on the settling rate of water in jet fuel. As the 75 % farnesane 25 % GTL S-8 blend has a lower settling rate than the 50% conventional Jet A-1 fuel 50 % GTL S-8 blend. It can be seen that there is more driving force for the water to come out of suspension in the GTL S-8 blend with farnesane in comparison to the conventional Jet A-1 fuel with farnesane fuel. As predicted by Stokes' law calculation, Farnesane has a significant tendency to take up and hold water in solution because it has the highest kinematic viscosity and density (2.52 cSt and 830 kg/m3, respectively) in comparison to the other fuels explored for this work. Therefore, the terminal velocity is expected to be lower as there is a greater resisting force on the water droplets. The fuel will appear to clarify at the top first as bigger droplets fall out quickly. However, after mixing with GTL S-8, it had a noticeable effect on the settling rate, as shown in Figure 3.5. As this can be indirectly related to the fuel's surfactant level of the fuel, it can be concluded that the GTL S-8 has fewer surfactants than conventional Jet A-1. (Note that in this work, it is assumed that dispersion of water droplets in a fuel column will settle at rates predicted by Stokes' law.

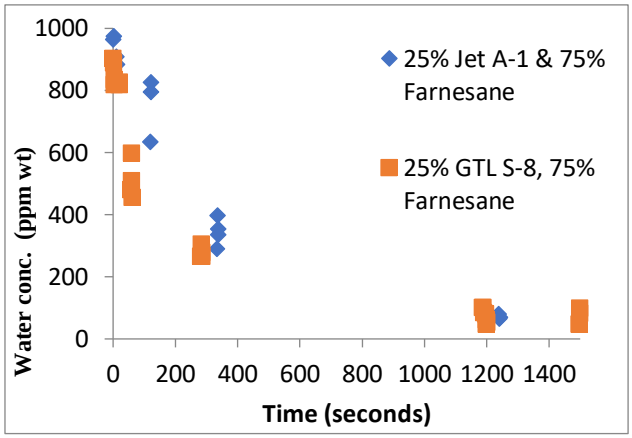

Figure 3.5 Water settling rates for blends of farnesane/Conv. Jet A-1 and farnesane/GTL S-8

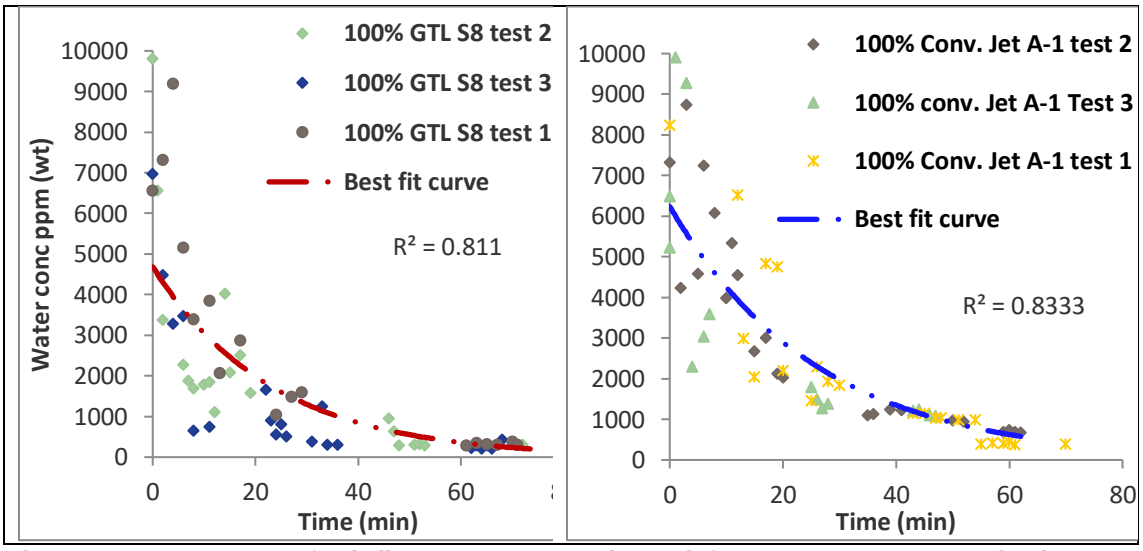

Figure 3.6 Average of triplicate tests conducted for 10,000 ppm nominal water addition

It can be seen from Figure 3.6 that water settles out faster from GTL S-8 than conventional jet fuel. Therefore, GTL S-8 has proven to be a good candidate for an increased blending portion with the conventionally refined jet fuel in comparison to other alternative fuels explored for this study.

3.5 Conclusions and Recommendations

In addition to the variables from Stoke's law (radius, density and viscosity), an intermolecular factor should be considered. This is directly linked to the presence of surfactants. Thus, a high-water settling rate indicates that water droplets may

have easily coalesced. Previous studies have shown that the presence of surfactants can have an adverse effect on filter separators since it may affect the water separation characteristics. From this study, it can be deduced that the water settling experiment indirectly measures the presence of surfactants in jet fuels. In terms of water droplet rejection from suspension, GTL S-8, HEFA and ATJ has proven to be good candidates for increased blending portion with conventional fuel.

It is recommended that MSEP tests be conducted on the fuels explored for this study for the basis of comparison. Also, it would be interesting to see if the water droplets tend to grow after a given period before dropping out. Hence a more representative experiment is proposed to establish the particle size distribution of water droplets in jet fuels at a given period. Then, input the particle diameter at a particular time to get a settling rate curve and compare the result with different fuels. Recalculate terminal velocity assuming the water droplet is undergoing free settling or hindered settling after conducting the particle size distribution and counting analysis on the various jet fuels. The visual process analyser (ViPA) is proposed as it can continuously monitor the physical characteristics of a lab sample (Fuel/water mix in this case). Finally, experiments on other physical and chemical tests should be conducted, employing the selected fuel candidates in accordance with the ASTM standard test methods for future validation. Monitoring these properties will help the aircraft maintenance team decide on the proper water management in aviation fuel/fuel systems for optimum process efficiency.

4 Chapter 4 Characterisation of water droplets size distribution in aviation turbine fuel: Ultrasonic homogeniser vs High shear speed mixer

Abstract

Pumps, pressure drops across fittings, and flight operations (such as turning manoeuvres, take-off, and landing) are some of the many sources of turbulence mixing and shearing in aircraft fuel systems, therefore, making it an inevitable condition. Literature established that shearing conditions would influence the droplets and droplets size distribution in oil/water emulsion. So, low-intensity shearing conditions could be beneficial as it promotes droplet coalescence, which could be a driving force for a weak emulsion. However, to date, no experimental data shows the influence of homogenising intensity and total water content on dispersed water droplet size distribution (DSD) in aviation fuel. Therefore, to expand knowledge of improving quantification to the measurements of dispersed water droplets in aviation fuel, this study characterizes dispersed water droplets in aviation turbine fuel, varying available laboratory homogenising gadgets and water content. The results presented show that droplet count increases with water concentration and shearing effect. Furthermore, the kurtosis and skew values were calculated from the extrapolated data and compared with data from a hexanol/water mixture, given that hexanol is likely to form a stable emulsion. Experimental results show that the higher the homogenising intensity, the more stable the emulsion is likely to be with a higher kurtosis and skew value close to that for the hexanol/water mixture.

Keywords: Droplet size, Stokes law, Aviation fuels, Fuel systems, Shedding, Jet fuel, Aircraft

4.1 Background of study

Take-off, landing, turning manoeuvres are some of the many flight operations that contributes to mixing and shearing the fuel in aircraft fuel systems, therefore, making it an inevitable condition. Work by Noor et al. suggested that mild shearing conditions could be beneficial as it promotes droplet coalescence, which could be a driving force for a weak emulsion [135]. Additionally, findings by [180] and [181] established that shearing conditions would have a tremendous effect on the droplet size variation in oil/water emulsion. Consensus has it that the higher the shearing effect (energy input), the greater the fuel/water dispersion and the probability of smaller the water droplets size production [180–182]. It has been established in the literature that ice accretion is dependent on the amount of water in fuel, temperature and size of supercooled water droplets of the fuel [2,13,75,183]. Also, Goodarzi et al. suggested that droplets interact with each other and deform from the original spherical shape at high water concentrations of dispersed phase; the researchers suggested correction factors as a function of the dispersed phase volume fraction to consider the deformation of droplets. The results obtained from work by Goodarzi et al. show that there is a good separation in the water in oil mixture with higher total water content [180]. As a result, the influence of water content on the average droplet size distribution is evaluated to demonstrate the impact of water content and time on the water droplet size and count distribution.

Fuel tanks can be contaminated with water during re-fuelling, normal flight operations and maintenance. Water in aviation fuel has been a long-standing area of concern in the aviation industry [23,140,141,184–187]. There are three different forms in which water could exist in aviation fuel; as dissolved water, dispersed water and free water [2,188]. Water that has dissolved in aviation fuel, exists as molecules that could likely precipitate out of the solution as suspended or free droplets at cold temperatures. Suspended water droplets can be formed when the water solubility limit of the aviation fuel has been exceeded or suspended water can usually be formed by mechanical agitation by a jet pump or during aircraft manoeuvres and or pressure refuelling [45,189]. Suspended

water droplets normally take time to settle out or coalesce but eventually does as free water that settles at the bottom of the tank [13,19,20]. Droplets of a few microns can also be problematic and previous work done in this area has shown that free water has a droplet size range of 20 – 30 µm, whilst suspended water droplets have a droplet size ranges below 5 µm and up to 13 µm [190][12].

Detailed visual droplets counting procedures have been reported in ASTM D7619-17 and ASTM D8166-21a to assist in addressing safety issues and also improve categorisation and quantification of water contamination in fuel [12,191]. Yet, the mechanism of water droplet formation and uptake in aviation fuel is an area that lacks sufficient knowledge in the literature. It is paramount to understand the underlying fundamental properties that could extensively influence the process and behaviour of water in aviation fuel. Previous study on water-in-oil emulsion has demonstrated that the DSD is one such factor that could play a key role in characterising water behaviour in an emulsion [180]. Therefore, this present study is aimed at characterizing the droplet size and frequency distribution by laying emphasis on the following objectives. (a) To demonstrate based on theoretical assumptions that droplet size/frequency in jet fuel distribution is governed by shearing conditions. (b) To demonstrate the impact of water content and time on the water droplet size and count distribution. A notable point is that the choice of added water content was arbitrary for this study; the importance was having a considerable and comparable amount of free water as free water content can be affected by the total water content of the fuel.

4.1.1 Experimental procedure

4.1.1.1 Particle Image analyser, the Jorin Visual Process Analyser (ViPA)

The ViPA was manufactured by Jorin Ltd., Whetstone, Leicester, England. The imaging analysis is a continuous cycle employing a recording microscope that produces visual images and videos. The units size detection limit is a minimum of ~1.5 microns and a maximum of ~300 microns. Continuous experimental information was collected for approximately 3900 s and recorded as counts per 39 s. The ViPA unit allows the user to define parameters that differentiate different

particles based on sizes or shapes. The unit can quantify data on a number of several measured parameters allowing the user to decide at their discretion which parameters are fit for the purpose of the work. In this study, the size and volume parameters were analysed.

The mean droplet size was calculated using the below equation

$$\underline{D}_{[1,0]} = \frac{\sum_{i=0}^{\infty} n_i d_i}{\sum_{i=0}^{\infty} n_i} \qquad \textbf{Equation 4-1}$$

Also, the ‘’De Brouckere mean diameter or weighted volume average(WVA)’’ was employed as it takes into account the mass and volume of a given distribution [192,193]. The equation for the weighted- volume average $\underline{D}_4,3$ can be written as:

$$\underline{D}_{[4,3]} = \frac{\sum_{i=0}^{\infty} n_i d_i^4}{\sum_{i=0}^{\infty} n_i d_i^3} \qquad \textbf{Equation 4-2}$$

Further statistical analysis was conducted by computing the kurtosis and skewness to improve confidence in the experimental data generated [194]. Kurtosis statistically measures the sharpness of the tail on the distribution curve and the combined weight of the data points relative to the mid-section of the distribution curve. Meanwhile, the skew value measures the distortion or asymmetry of the DSD. If a data set is a perfect symmetry, then the skew value is expected to be near zero. The skew parameter can have either a negative or a positive value. A distribution is said to be negatively skewed when the majority of its data points are skewed to the left or, for the purpose of this work, where there exists outliers or peaks at a larger diameter in the distribution (coalescence-Collison of small droplets to form larger ones). The equation for kurtosis and skewness is provided as:

$$Skewness\ (sk) = \frac{n}{(n-1)(n-2)} \sum_{i=1}^{n} \left(\frac{di - \underline{d}}{s.d}\right)^3$$

Equation 4-3

$$Kurtosis\ (k) = \frac{n(n+1)}{(n-1)(n-2)(n-3)} \sum_{i=1}^{n} \left(\frac{di - \underline{d}}{s.d}\right)^4 - 3\frac{(n-1)^2}{(n-2)(n-3)}$$

Equation 4-4

s.d = standard deviation, $\underline{d}$ = mean droplet size diameter

4.1.1.2 The procedure adopted for producing dispersed water in aviation fuel

The fuel-water sample was prepared using a 100 mL measuring cylinder ~32 mm diameter to accommodate the handheld homogeniser and the stirrer. The clean and dry 100 mL measuring cylinder was filled with 100 mL of fuel and 0.1 mL of water or 0.05 mL of water, depending on the case experiment. Blending was done using either a high shear mixer (HSM) or an ultrasonic horn, as seen in Figure 4.1 below.

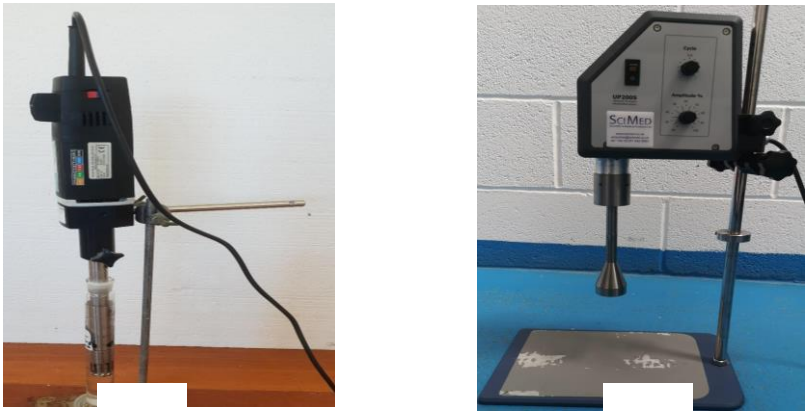

a) b)

Figure 4.1 Instruments used for water dispersion a) X 620 high shear mixer: b) UP200S Ultrasonic processor

The experiments were subjected to different shearing methods for the purpose of comparison. This was done to analyse the shearing effect on the water droplet size distribution and counts. The ultrasonic horn (UP200S model) has a frequency of 24 kHz, a nominal power output of 200 watts, and an amplitude

adjustable from 20-100 %. Table 4.1 summarises sets of test conditions conducted for this study.

Table 4.1 Test conditions using conventional Jet A-1 fuel

S/N	Experiment	Weight % water added	Shearing effect
1	**Phase 1 experiments**	0.05	Ultrasonic horn
2		0.05	High shear mixer
3		0.1	Ultrasonic horn
4		0.1	High shear mixer
5	**Phase 2 experiments**	0.02	High shear mixer
6		0.05	High shear mixer
7		0.1	High shear mixer
8		1	High shear mixer

The ultrasonic processor (UP200S model) converts an electrical signal into a high-frequency vibration, producing high-intensity ultrasonic waves, which form small vacuum bubbles or voids in the liquid that collapse quickly, thereby disrupting the liquid molecules and enhancing the mixing of the water and fuel. For the X 620 HSM, the shearing rate can be changed to increase or reduce the speed of the revolving impeller. For the present study, the shearing rate was set to a constant set speed of 11,000 revolutions per minute (RPM) and allowed to homogenise for 60 s.

As soon as the emulsion had been prepared, the ViPA system was set in place to begin the experimental analysis. Figure 4.2 shows the schematic of the setup.

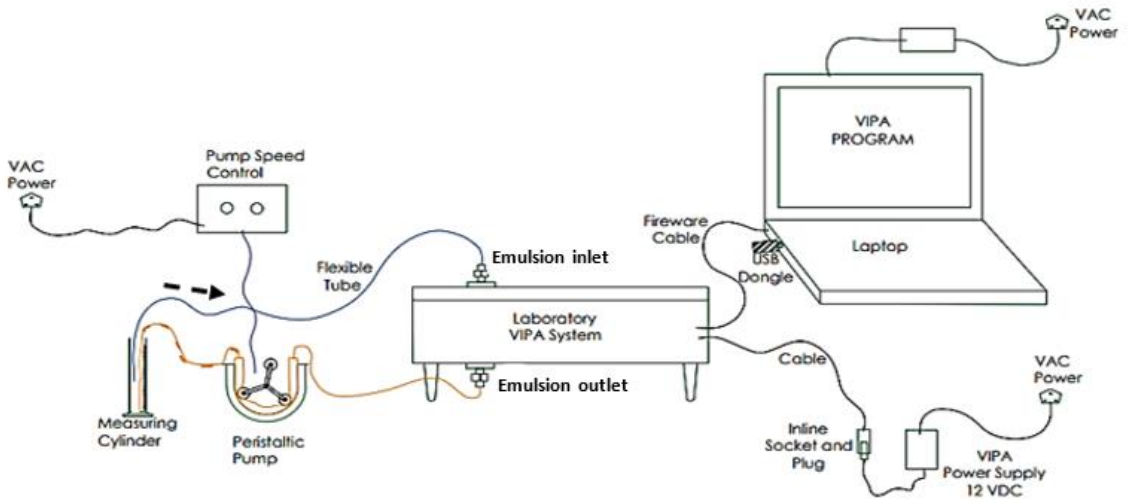

Figure 4.2 ViPA analysis unit experimental set up

As seen in Figure 4.2, the blue flexible passage “inlet’’ was positioned at the centre of the sampling container while the orange flexible passage ‘‘outlet’ was positioned at the bottom of the cylinder. Afterwards, the ViPA system is started, and the experimental analysis begins. Snapshots were taken at the start and finish of the experiment for comparative analysis. Furthermore, the Karl Fischer coulometer was employed for the water content analysis. This analysis was done immediately after the emulsion had been prepared. Experiments were conducted in separate phases. Phase 1 examined the effects of mechanical agitation, and phase 2 examined the effects of total water content. For the phase 2 experiments, a known amount of distilled water (0.1%, 0.02%, 0.05%, 0.1%, and 1%) was added to the fuel and homogenized for 60 s at 11,000 RPM using an X 620 high shear mixer.

4.2 Results and discussion

4.2.1 Effects of shearing conditions

Pumps, pressure drops across fittings, and flight operations (such as turning manoeuvres, take-off and landing) are some of the many sources of turbulence mixing and shearing in aircraft fuel systems, making it an inevitable condition. Work by Noor et al. suggested that mild shearing conditions could be beneficial as it promotes droplet coalescence, which could be a driving force for a weak

emulsion [135]. Additionally, Findings by [180] and [181] established that sheering conditions would have a tremendous effect on the droplet size variation in oil/water emulsion. Consensus has it that the higher the shearing effect (energy input), the greater the fuel/water dispersion and the probability of smaller the water droplets size production [180–182]. To investigate if shear conditions govern droplet size/frequency distribution in jet fuel, water droplets produced by a high shear mixer were compared to those produced by ultrasonic dispersion for this study. The result from this set of experiments is shown in Figure 4.3 and Figure 4.4.

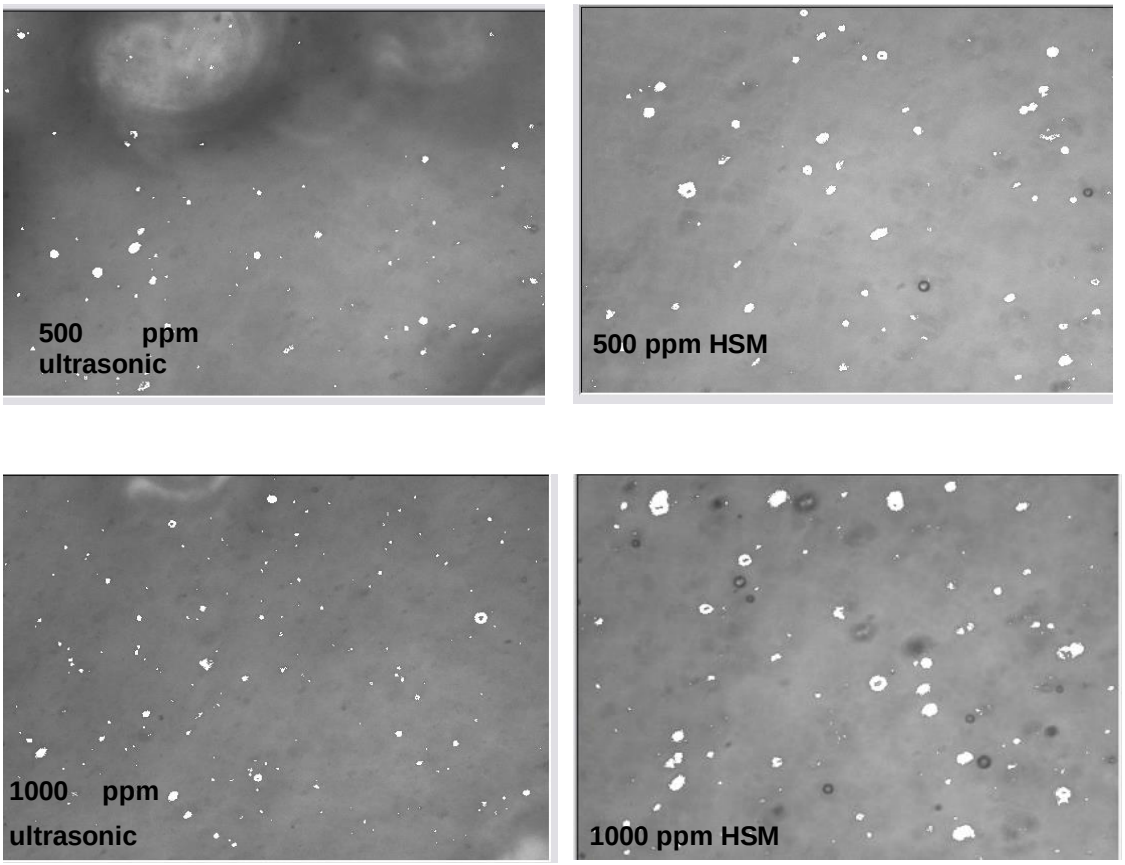

Figure 4.3 Image captured of the dispersed water droplet on mixing Jet A-1 fuel with the high shear mixer and ultrasonic horn

Figure 4.3 shows a visual representation of the ViPA image analyser at the start of the experiment. As shown in Figure 4.3 above, smaller droplets can be visually

formed with the ultrasonic processor compared to the HSM. Furthermore, Figure 4.4 shows the droplets frequency distribution for the ultrasonic and HSM cases explored.

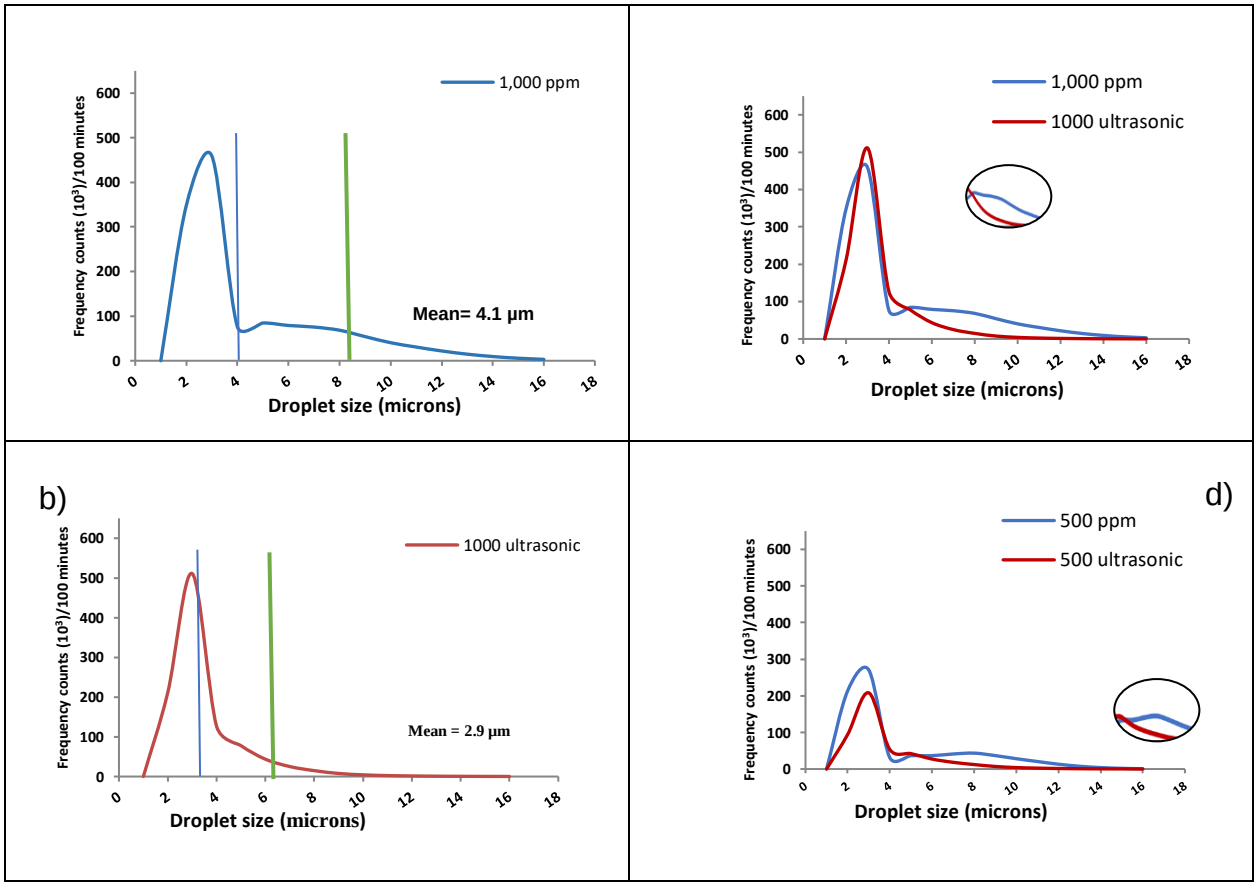

Figure 4.4 a) and b); DSD (with smoothened kernels for case b.1 to b.4). The blue vertical bar is the average diameter of the droplet. The green vertical bar is the average WVA; c) and d); comparison and evidence of repeatability for all shearing experiments

The skew to the right seen in the droplet distribution in Figure 4.4 a and b shows that both shearing conditions exhibit a positive skewness as the right-hand tail is longer than the left. The droplet size distribution for mixtures with higher shear conditions (ultrasonic horn) is characterised by their near monomodal (single peak) distribution and a slightly higher kurtosis value of 13.45. While droplet size distribution for a mixture with a mild shear rate, HSM is characterised by their almost evident second peak and a lower kurtosis value of 7.5. Also, as

anticipated, the skewness value is lower for the high shear mixer distribution (2.86) compared to the ultrasonic horn distribution (3.57).

On mixing with the ultrasonic horn, a high-intensity shearing effect is generated as it introduces a lot of energy into the system. Thereby producing a single mode distribution as seen in Figure 4.4c and d; showing bigger droplets when the high shear mixer was employed compared to when the ultrasonic horn was used. For clarity, Figure 4.4a and b demonstrate the droplet size distribution with smoothened kernels. On shearing with the HSM, a collis46ion of small drops with a diameter of around 2 µm gives rise to larger droplets around 5 µm. Therefore, the distribution observed in Figure 4.4a, with one large peak denoted as centred around 3 µm and small broadband around 6 µm. However, for the emulsion formed using the ultrasonic horn, which in theory introduces more energy into the system (higher shear rate), a monomodal distribution was observed as seen in Figure 4.4b, with one narrow peak around 3 µm. Also, in both cases, the maximum value of volume-weighted mean and mean diameter is reached in the HSM case (green and blue vertical bar, respectively) because of the presence of larger droplets sizes and counts (Figure 4.5). Therefore, it can be concluded that increased shear conditions lead to a decrease in the mean size of droplets (4 to 2.9 in this case) and leads to a narrower droplet size distribution, as seen in Figure 4.4c and d. The plot is shown in Figure 4.5a, and b further elucidates that a lesser droplet count is produced from the ultrasonically dispersed fuel/water mixture.

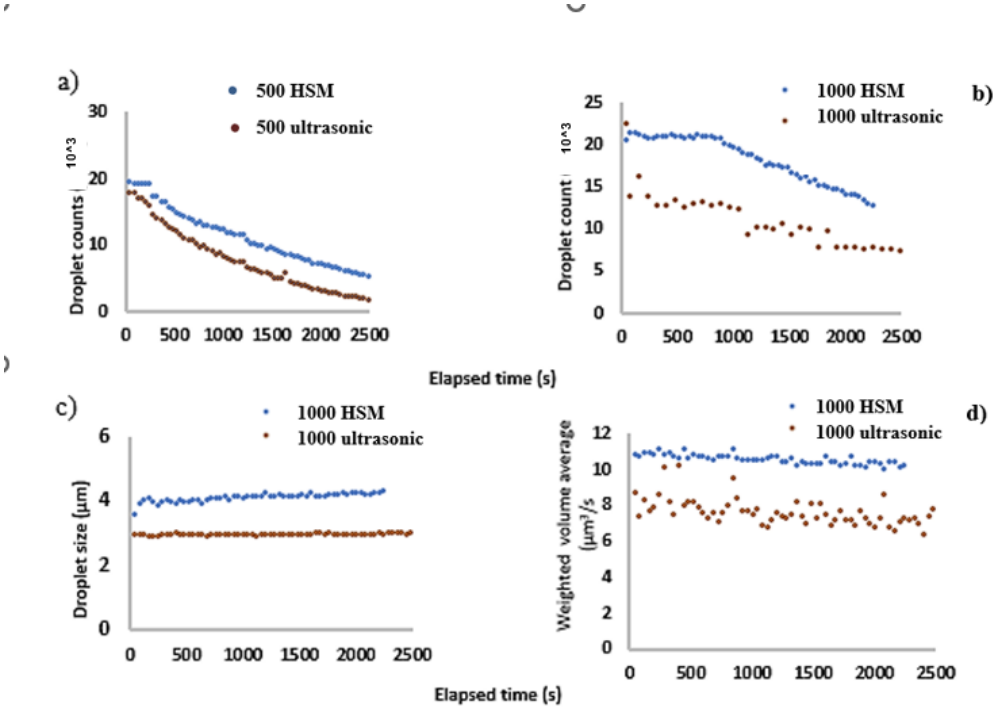

Figure 4.5 Water droplet count a) settling profile for jet fuel/500 ppm dispersed water mixture produced with HSM and ultrasonically; b) settling profile for jet fuel/1,000 ppm dispersed water mixture produced with HSM and ultrasonically; c) shearing effect on droplet size; d) shearing effect on the weighted volume average (volume of droplets)

Additionally, the result obtained for the different shearing experiments shows that there is a decrease in the droplet count over time. However, in this case, the rate of decrease is faster with a mild shearing effect, HSM, compared to the higher shearing effect (ultrasonic horn). In contrast, a slight increase in the average droplet size with time- HSM is noticeable in Figure 4.5c, whilst there is no significant change in the droplet diameter over time with the ultrasonic processor. This increase in droplet size over time could be attributed to the coalescence phenomenon.

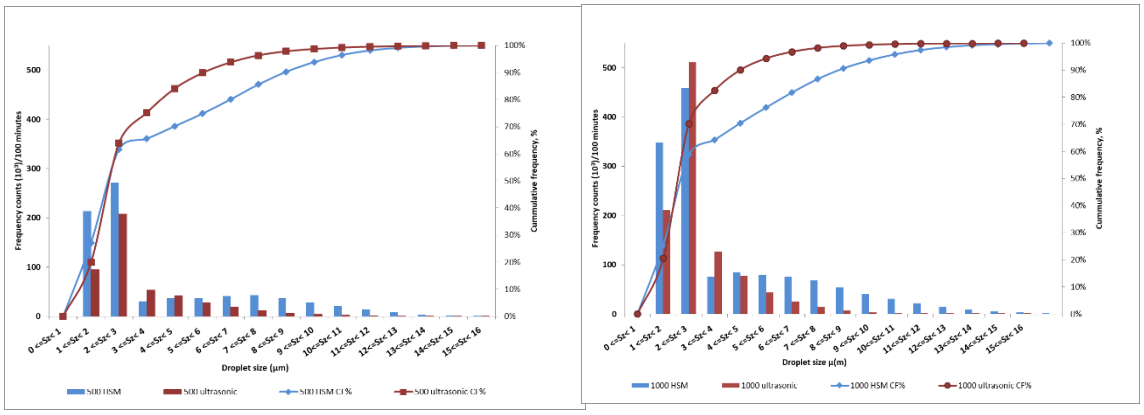

Figure 4.6 Cumulative frequency DSD for the different shearing experiments showing a higher frequency of larger droplets in the HSM case in comparison to that of the ultrasonic

The cumulative frequency (CF) distribution represented in Figure 4.6 shows some similarity in the median diameter (d50, CF of 50%) of both shearing methods in the 500 ppm case. However, very minimal change in the 1000 ppm case was seen. 3-4 micron-sized droplets are seen to have a CF of 80% for the ultrasonic case. However, at the same CF of 80%, 6-7 micron-sized droplets are seen for the HSM case. The DSD shows that there exists a higher frequency of larger droplets in the HSM case in comparison to that of the ultrasonic. This could mean that the ultrasonic case produces a more stable emulsion with a better homogenising effect. A notable point from Figure 4.4, Figure 4.5, and Figure 4.6 are that the highest value of volume-weighted mean and mean diameter is reached on shearing with the high shear mixer.

Table 4.2 Result data summary for shearing experiments explored for this work and hexanol

Shear condition	Kurtosis	Skew	Mean $D_{1,0}$ (µm)	WVA $D_{4,3}$ (µm)	Average drop count
Ultrasonic processor	13.45	3.57	2.9	7.1	15,000
High shear mixer HSM	7.5	2.86	4.1	10.11	21,000
Hexanol Using HSM	34.90	5.07	2.6	6.3	134

From Table 4.2, hexanol, which is likely to form a very stable emulsion, has the highest kurtosis and skew values of 34.90 and 5.07, respectively. This further means that a more stable emulsion was formed using the ultrasonic processor. From a practical point of view, the right choice of emulsification is essential in obtaining a stable emulsion. Therefore, from this work, it can be concluded that mild shearing conditions could be beneficial as it promotes droplet coalescence, leading to a faster/ better separation ability: as an increased level of water, contamination can lead to damage to aircraft fuel systems. The high-intensity shearing conditions lead to a tighter emulsion, resulting in poor water separation.

4.2.2 Effects of total water content

The literature has established that ice accretion depends on the amount of water in fuel, temperature, and size of supercooled water droplets of the fuel [2,13,188]. Also, Goodarzi et al. suggested that droplets interact with each other and deform from the original spherical shape at high water concentrations of dispersed phase; the researchers suggested correction factors as a function of the dispersed phase volume fraction to consider the deformation of droplets. The

results obtained from work by Goodarzi et al. show that there is a good separation in the water and fuel mixture in fuels with higher total water content [180]. As a result, the influence of water content on the average droplet size distribution is evaluated to demonstrate the impact of water content and time on the water droplet size and count distribution. The choice of added water content was arbitrary for this study; the importance was having a considerable and comparable amount of free water as free water content can be affected by the total water content of the fuel. The result illustrated in Figure 4.7 shows the influence of water content on the droplet size and count. The total droplet count data were plotted against the different total water contents explored in Figure 4.7a. The ViPA detected an average count of about 22,079 in the 60 minutes at 10000 ppm and 1087 at 200 ppm. Count data for the added water test cases show a steady decrease in the order of 10000>5000>1000>500>200>fuel as received.

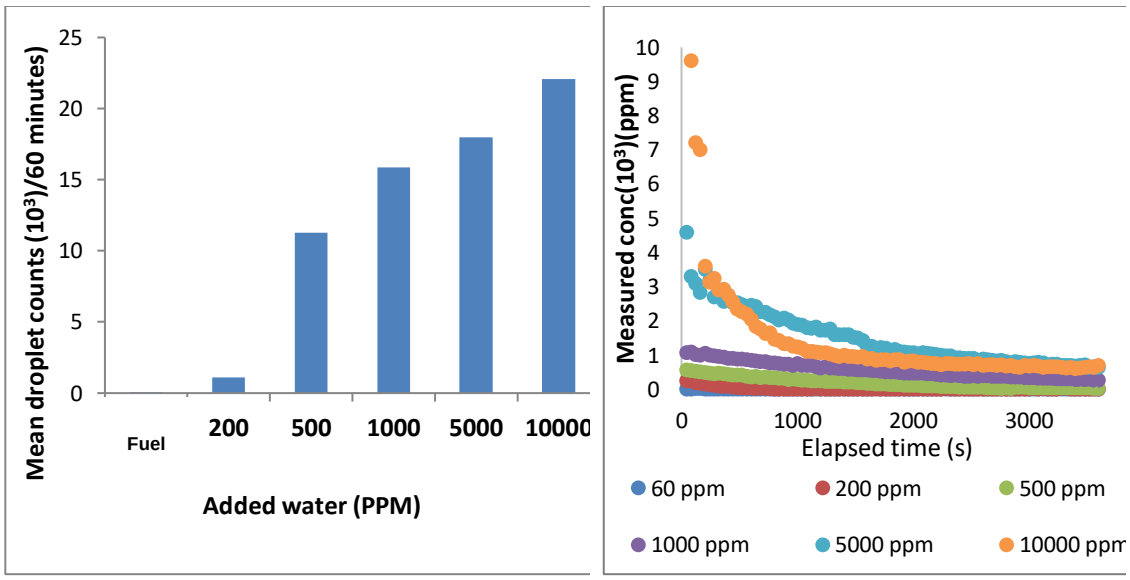

a) b)

Figure 4.7 Estimated average droplet count of added water

Figure 4.7b shows the water settling rate profile for the added water content in aviation fuel. The settling profile illustrates that total added water content could impact water-shedding rates. As seen in Figure 4.7b, there is more driving force for the water to come out of the suspension at a higher nominal water level hence

the steeper curve at 10,000 ppm nominal water level. This result is consistent with the proportionality seen in Figure 4.8a. This is because the rate at which water droplets will fall out of a solution is dependent on the droplet volume concentrations and the square of the diameter. As seen from Figure 4.8a, water droplets fall out at a higher rate in the 10000 ppm case because of the larger droplets compared to other lower total added water cases. This shows that the water droplet data is consistent with theoretically assumptions that droplet size impacts water-shedding rates.

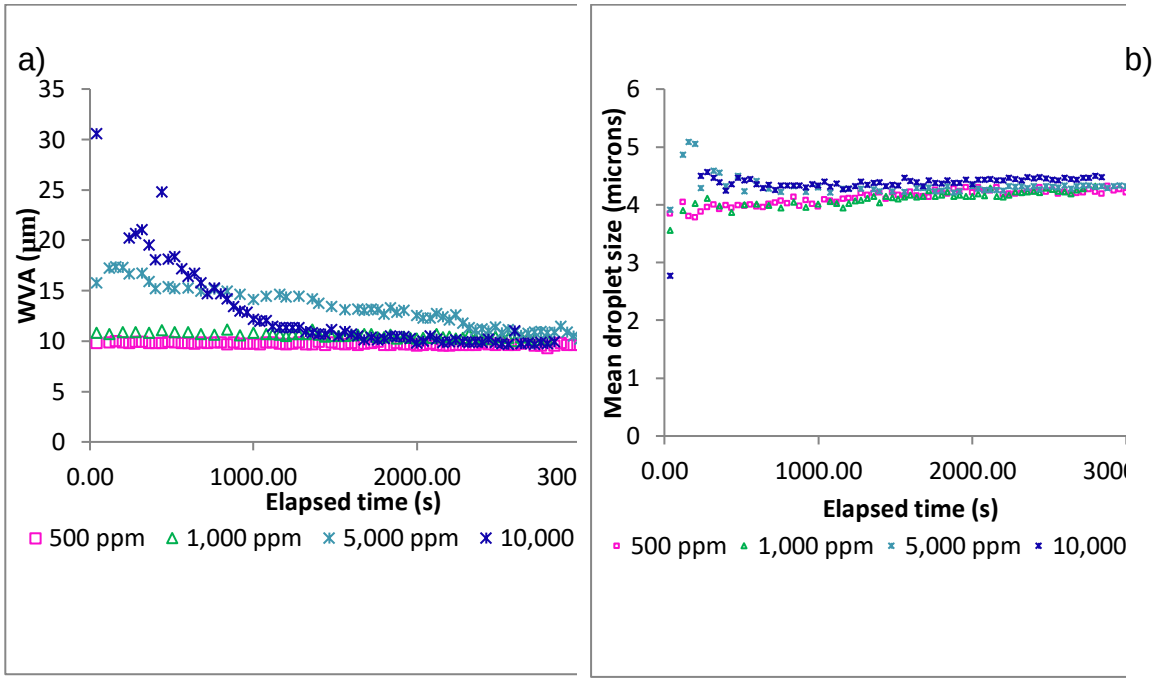

Figure 4.8 a) weighted volume average data against time; b) Mean droplet size against time for test cases c.1 to case c.6

The result observed in Figure 4.8 is consistent with the proportionality shown in Figure 4.7, as the 10000 ppm case has the highest droplet count, WVA and droplet size diameter. Therefore, it is noticeable from Figure 4.7 and Figure 4.8 that larger water droplets and count are formed with a higher total water content level. Furthermore, the detected water droplet sizes for all phase 2 experiments is illustrated in Figure B-1.

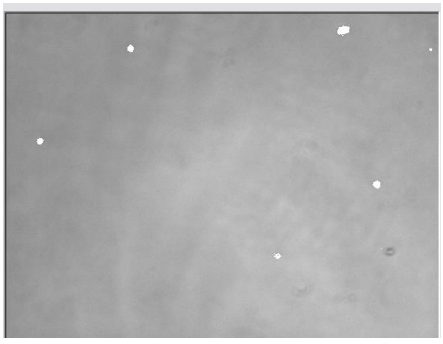

200 ppm at start of experiments

200 ppm after 60 mins

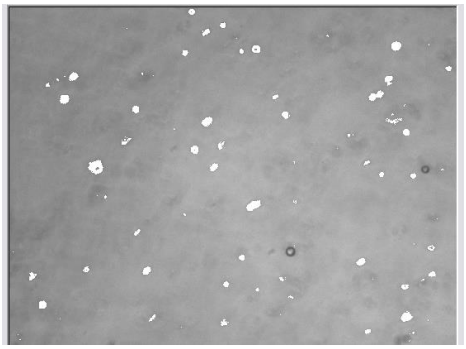

500 ppm at start of experiments

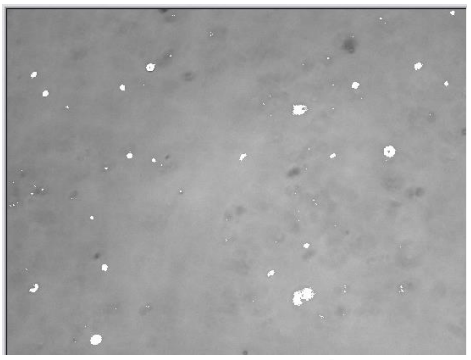

500 ppm after 60 mins

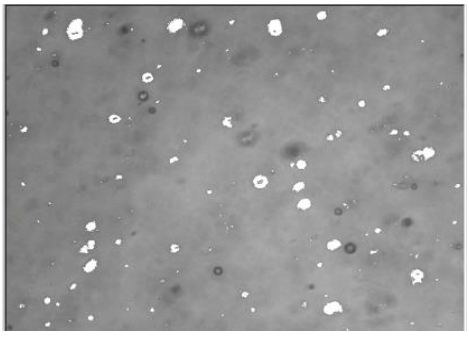

1000 ppm at start of experiments

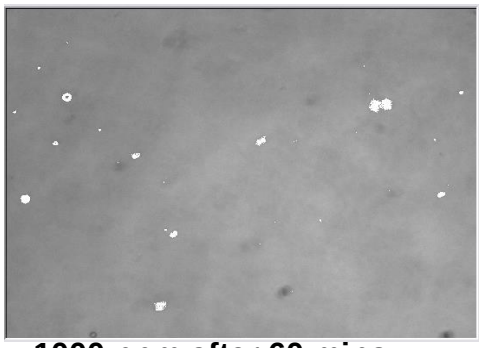

1000 ppm after 60 mins

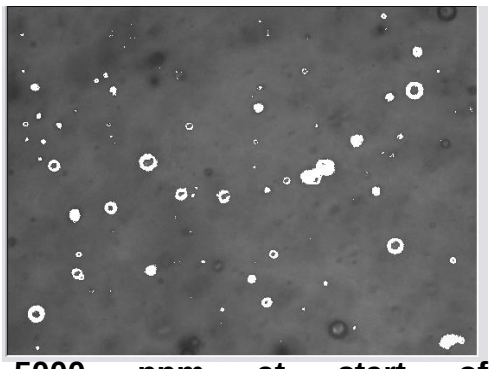

5000 ppm at start of experiments

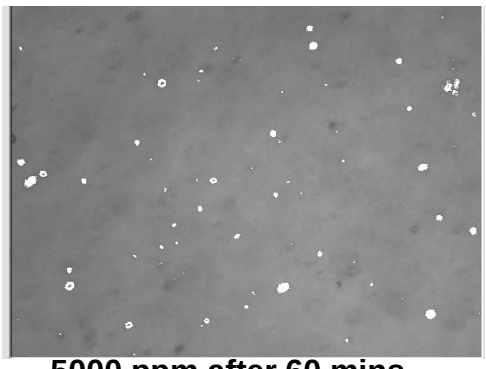

5000 ppm after 60 mins

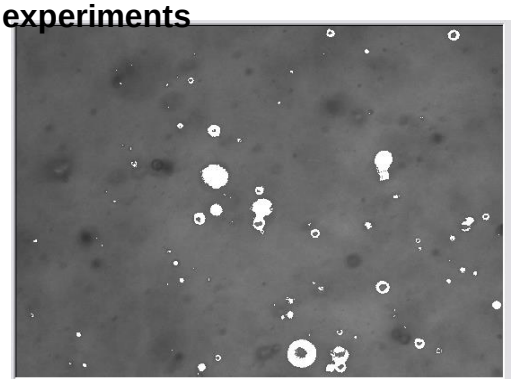

10000 ppm at start of experiments

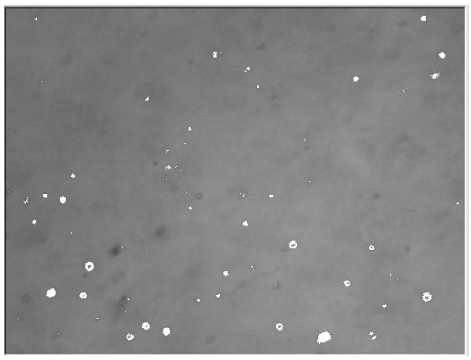

10000 ppm after 60 mins

Figure 4.9 Captured ViPA images at the start (~2 minutes) and end (~60 minutes) of the experiment

Figure 4.9 shows screenshots from the ViPA image analyser, illustrating that droplet size and count reduce over time. The fewer droplet counts over time is because of settling, with a steady decrease of count and water concentration expected as time progresses. Figure 4.10 shows a bar chart that compares the DSD for the total water content explored (0 to 10,000 ppm).

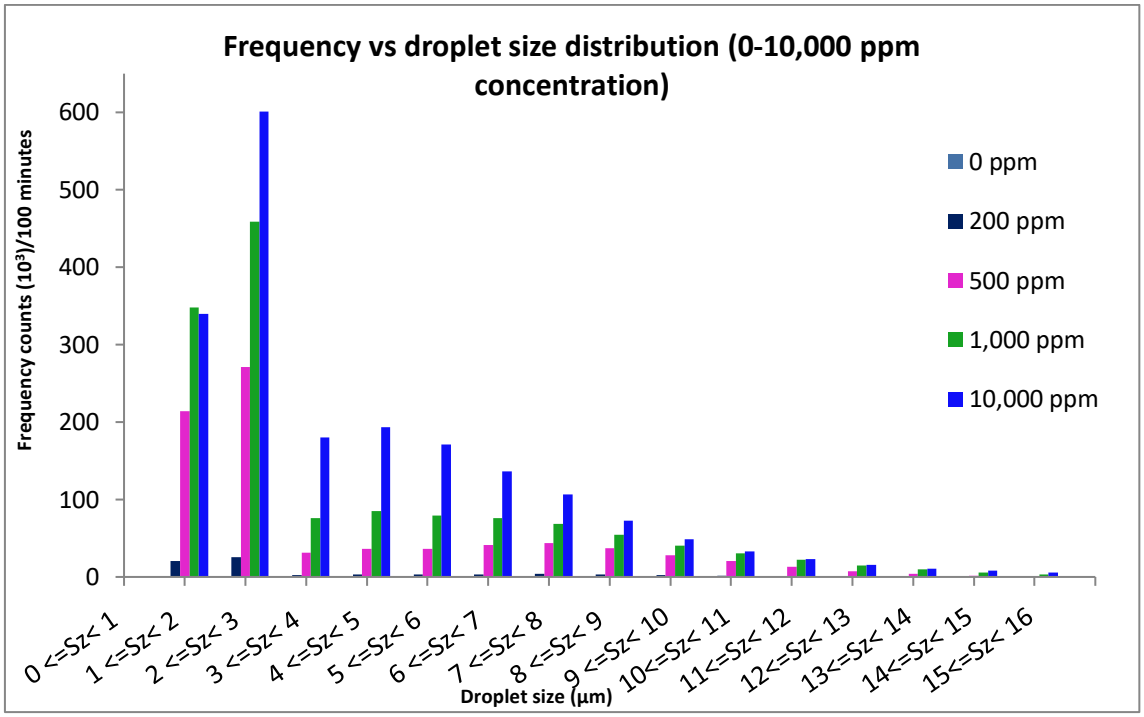

Figure 4.10 Comparative analysis of the frequency distribution for the total water content explored for this work (phase 2 experiments)

As volume concentrations are principally based on the mass equivalent, the 10000 ppm case contains the highest frequency of smaller and larger droplets compared to all other added water cases. The results from this section explain why keeping the water present in jet fuel at a minimal level is highly important to prevent large volumes/sizes of droplets from forming in fuel tanks and potentially causing problems at high altitudes.

4.3 Water droplets- free and hindered settling velocity

The first step towards having an idea of the size of droplets formed is to consider the emulsion as undergoing a free settling process (i.e., only one water droplet is settling through the continuous phase of fuel). A process is termed free settling when a particle is at a sufficient distance from the walls of the container and from other particles so that its fall is not affected by the walls or other particles. The governing Stokes law equation gives an idea of the maximum size of the droplet that can be obtained from the emulsion. For spherical particles settling freely, a droplet of mass 'm' is assumed to fall under gravity and settles out at a constant velocity (terminal velocity). Stokes law is used to calculate the terminal velocity

for a given droplet size. The resulting terminal velocity is proportional to the square of the droplet diameter. Stokes Law is given as follows:

$$v = \frac{g \cdot D^2(\rho_w - \rho_f)}{18 \cdot \eta_f \cdot \rho_f} \qquad \textbf{Equation 4-5}$$

Where:

ρ_w = density of water (kg/m^3)

s = density of fuel (kg/m^3)

g = acceleration due to gravity (m/s^2)

η_f = Viscosity of fuel (m^2/s)

V = Stokes terminal velocity (m/s)

D = Water droplet diameter (m)

For free settling calculation, it was assumed that terminal velocity was reached, i.e., acceleration time is neglected, flow is laminar with a low settling velocity, Reynolds number of Re < 0.2, and those droplet particles are spherical, smooth, and rigid.

For this work, the measured water WVA was used to calculate the terminal velocity, and then a graph that describes the relationship between terminal velocity and the WVA for different water concentrations conducted is s shown in Figure 4.11.

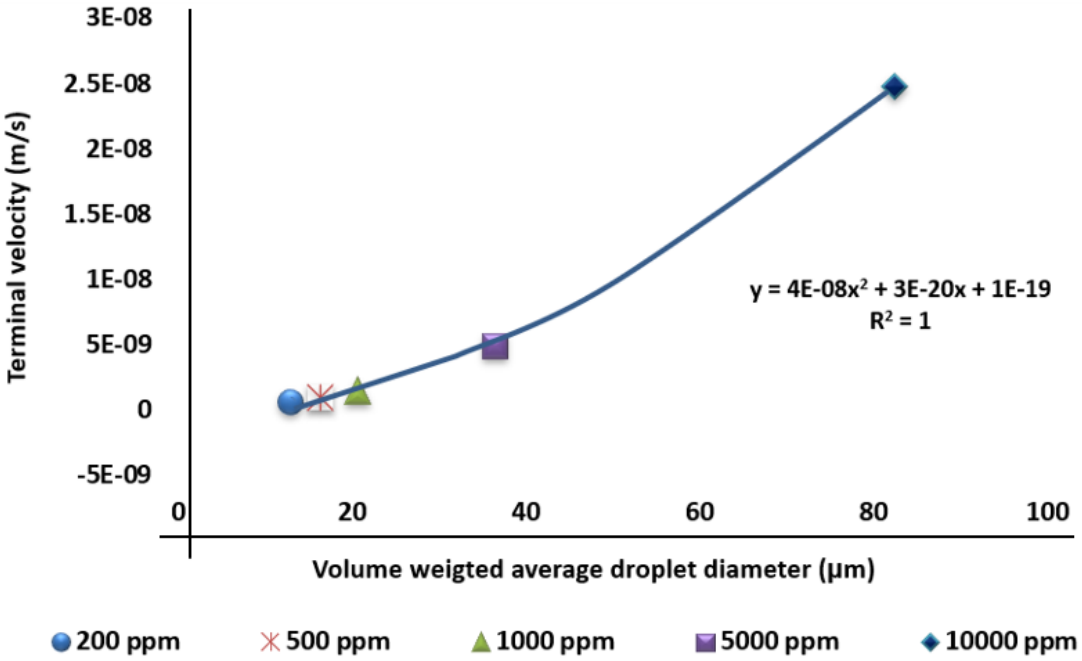

Figure 4.11 Relationship between droplet diameter, WVA and concentration

This relationship was obtained using stokes law. Figure 4.11 above shows how the droplet diameter varies with water concentration. It is evident that the terminal velocity increases with increasing concentration as a result of the increase in WVA. This is because the additional water increases the mass of the fuel/water sample and, therefore, an increased WVA (De Brouckere mean diameter that takes into account the mass and volume of the droplets). This is consistent with work from the literature that suggests that settling velocities are affected by high concentrations [195]. But stokes law accounts for a single perfectly spherical droplet falling freely in a medium, without emphasis on the effect of water concentration in a hindered settling (which is the likely typical scenario). In hindered settling, the settling particles or droplets will have a much lower settling rate or velocity than particles in free settling because of the interactions of the crowded droplets. The droplets tend to hinder the settling velocity of one another. One of the widely accepted semiempirical factors that accommodate the concentration term is given by Richardson and Zaki [196]. This semi-empirical equation for hindered settling is given below:

$$U=V(1-C)^{n}$$

Equation 4-6

Where:

U: Settling velocity, m/s

V: Stokes terminal Velocity, m/s

n: It ranges from 4.65 - 2.4 for increasing particle Reynolds Number

C: Volume Concentration

It is therefore proposed that models that could be used to account for the effect of water concentration and settling be developed. Some proposed suggestions have been listed in Table 4.3 below. It is recommended that more experiments be done to modify the empirical correlations to fit the test with water droplets since the index exponents for some of the experiments are for solid particles.

Table 4.3 Semi-empirical correlations that account for water concentration in a hindered settling

S/N	Reference	Formulated model	n value
1	Richardson and Zaki [196]	$U = V (1 - C)^{n}$	n = 4.65
2	Garside and Al-Dibouni [197]	$U = V (1 - C)^{n}$	n = 5.14
3	Al-Naafa and Sami-Selim [198]	$U = V (1 - C)^{n}$	n = 6.55

4.4 Conclusions and Recommendations

Observed data experimentally reveals that water droplet size/count distribution is influenced by the type of shearing/mechanical agitation method used for the water introduction method. Mild shearing conditions (HSM in this case) could help promote droplet coalescence, leading to a better separation ability. The droplet coalescence phenomenon was evident in the shearing phase 1 experiment with

the high shear mixer (medium energy input in this case). Mild shearing conditions (HSM in this case) promote droplet coalescence, leading to a better separation ability. From a higher energy input to medium energy input, DSD changed significantly in terms of mean values and the higher skewness and kurtosis value.

The present study recommends that provided the correct value of n is implemented, a hindered settling velocity for water droplets could be formulated using the Richardson and Zaki equation. Therefore, further research is carried out to develop a new empirical model to account for water droplets hindered settling a medium. Also, it is suggested that an independent experimental data set be collected to validate the model formulated in this study.

5 Chapter 5 Investigation of Water Droplet Size Distribution in Conventional and Sustainable Aviation Fuels

Abstract

Water droplet size variation has been established in the literature as an important variable that influences the behaviour and characteristics of water in fuel emulsion. However, with the growing demand for sustainable aviation fuels (SAF), no data is available that shows how these fuels will affect dispersed water droplets' size and frequency distribution. To address this lack of knowledge, this study explores and presents experimental results on the characterization of dispersed water droplets in alternative fuels and Jet A-1 fuel under dynamic conditions. The alternative fuels comprised of two fully synthetic fuels, two fuels synthesised from bio-derived materials and one bio-derived fuel. The data and statistics presented reveal that water droplet frequency and size distribution is sensitive to changes in fuel composition. Observations showed an evident transition of the droplet's percentile over time in the cumulative frequency distribution; this could be attributed to droplet coalescence to form larger droplets. Mean droplet diameters between 3 and 6 μm were observed for all the fuels tested. With further analysis based on recommendations proposed in this work, the data may assist in providing insight to filter manufacturers.

Keywords: Sustainable, Turbine fuels, Fuel systems, Aviation, Shedding, Jet fuel, Aircraft

5.1 Introduction

Sole dependency on petroleum-derived fuels poses an increase in environmental concerns and price fluctuations [75,183]. Hence, the revolution of sustainable aviation fuels is featured to have the potential to decrease the life-cycle of greenhouse gas emissions [30,76–78]. These sustainable fuels are derived from renewable sources or biomass and can therefore reduce the contribution of greenhouse gas (GHG) emissions to the global climate. Alternative jet fuels could

be adopted in order to reduce the impact of the aviation industry on air quality [26,27].

Although alternative fuels seem like a promising technology for the aviation industry, some alternative fuels (oxygenated fuels) have high water solubility [199]. The alternative fuels available are low in sulphur and tend to be low in aromatics [44,91,187,200]. Previous work has established that a low aromatics content may lead to a reduced water contamination and elastomer (seal) shrinkage, while a low sulphur content leads to lower lubricity of the fuel [187]. As a result, most sustainable aviation fuels can be used after being blended with a certain percentage of conventionally refined jet fuel [30]. An understanding of the properties of sustainable fuels, along with the chemical properties of existing fuel types, is required to understand their impact on aircraft fuel systems.

Water uptake is one such property of interest as it is a known problem within the aviation industry [2]. An upper limit on water content in conventional fuels is not mandated in ASTM D1655, but the expectation is that the fuel will be maintained in a clean condition and be relatively absent of free water and solid particulates; a qualitative test for free water is described in ASTM D4176 (the ‘Clear and Bright’ test) and ASTM D3240 describes a quantitative test for undissolved water in a flowing fuel stream. The specification for jet fuel containing synthesized components is stricter on water content and requires a maximum of 75 mg/kg total water, as assessed by Karl Fischer coulometry to ASTM D6304.

Water is said to be ubiquitous and has no calorific value. Entrained water droplets in aircraft fuel systems may result in ice formation at low temperatures, with the potential to cause an interruption of fuel flow to engines. Water may enter fuel tanks during normal flight operations like intake of moist air during aircraft descent, re-fuelling, and routine aircraft maintenance. In jet fuel, water could exist as puddles at the bottom of fuel tanks, suspended droplets, and in dissolved form [2,161]. Water is said to be dissolved when it exists in a molecular form and is invisible to the human eye. Dissolved water can gradually dissociate from fuel and become suspended or dispersed as tiny droplets. Dispersed water can exist

in fuel when the total water content exceeds the solubility limit of the fuel at a given temperature. Free water is excess water that settles at the bottom of the fuel tank as a separate layer because water is denser than fuel [13,19,20]. Traditionally, dispersed or free water can be detected by looking to see if a fuel sample is clear and bright, and free from a second phase [45,189]. Operating conditions must be taken into consideration because the smallest possible size the unaided human eye can resolve is between 30 and 40 µm at ~200 mm from the eye. Droplets of the order of a few microns can negatively affect fuel system performance since they can freeze, and accrete to form larger ice crystals, which might impede flow through filters [20]. Work by Lam et al. reported the initial sizes of suspended droplets (below 5 µm) form an emulsion with the fuel whilst droplets with sizes greater than 13 µm could later settle out as free water and collect at the bottom of the fuel tank or stagnation points due to their higher density [190]. Work by Clark et al. reported that free water droplets within fuel can have a diameter within the range of 20 – 30 µm [12]. Free water or dispersed water can be controlled by regularly draining it out from the bottom of the tank after settling [161]. This activity is referred to as ‘sumping’ [158,187]. Sumping is an operational maintenance procedure that is practised to date because of the safety implications of free water in jet fuel. Yet, there is no reliable data that focuses on the quantification of dispersed water droplet sizes in alternative aviation fuels (those that conform to the requirements of ASTM D7566). The study conducted by Clark et al. in 2011 quantified the droplet size and dirt count distribution exclusively in Jet A-1 fuel [12]. Clark et al. conducted experiments at ambient temperature using a process image analyser; the result obtained identified the maximum droplet sizes to be in the range of 20 - 30 µm for fuel free of surfactants and below 10 µm in fuel containing low levels of surfactants. Work sponsored by the European Aviation Safety Agency (EASA) quantified droplet measurement over a temperature range of 10 to -44 °C using cold stage microscopy and a visual process analyser (ViPA) [12]. The water droplet count reported in this work was shown to increase with a decrease in temperature while the sizes detected were in the range of 2 to 5 µm [12].

The literature has identified water solubility, total water content, size of water droplets, particulates, and temperature to predominantly influence the process of ice formation/accretion in aircraft fuel systems [23,140,141,184–187]. So far, the effects of water solubility and temperature in sustainable and conventionally refined jet fuels have been studied from different angles, whilst research activities are still ongoing to develop more efficient ways to tackle the issue of water contamination in fuel. An extensive review by Goodarzi et al. deduced that a fundamental variable that influences water behaviour and characteristics in fuel emulsion is the water droplet size distribution (DSD) [180]. Visual particle counting methods have been introduced in ASTM D7619-17 and ASTM D8166-21a to improve the quantification of water contamination in fuel. However, the availability of data in this research area is deficient. It has been postulated that continuous visual particle analysis will help address safety concerns and increase operational performance by improving classification (organising generated data into relevant categories) [12,191]. Additionally, continuous visual particle monitors may give a better insight, especially to filter manufacturers, with respect to separation processes. This work is aimed at establishing the particle size and frequency distribution of dispersed water in jet fuel by focusing on the following objectives:

- To examine the frequency size variation and count of dispersed water droplets in alternative aviation fuels under dynamic conditions.
- To demonstrate the impact of water content and time on the water droplet size and count distribution.

5.2 Experimental Section

5.2.1 Jet fuel characterization

The fuels were provided by Airbus for this work and were representative of both conventional and alternative jet fuels (to ASTM D7566) commercially available at the time these tests were conducted. Conventional jet fuel is defined as fuel refined principally from crude oil resources. In contrast, alternative jet fuel is identified as any fuel produced from unconventional sources. Unconventional

sources include a range of energy-carrying materials which can be reprocessed either individually or in combination to yield aviation grade fuels. Such materials include a range of hydrogen-carbon containing materials such as biofuel, alcohols, hydrogen, coal-derived liquid fuels, and natural gas. Synthetic fuels are liquid fuels produced from coal, natural gas, or organic feedstocks by a gasification process, followed by Fischer-Tropsch synthesis and then conventional refining processes. Sustainable aviation fuel (SAF) is a subset of alternative jet fuel and is regarded as a fuel produced from organic feedstocks, which have absorbed carbon dioxide during growth, such as purpose-grown crops, biomass, algae, agricultural residue, or waste oils, e.g., used cooking oil and fats. The use of SAF partly mitigates the issue of global warming from aviation with a reduction in new carbon emissions compared to conventional jet fuel.

The five alternative fuels supplied by Airbus were representative of different feedstocks and processing routes that can be used to create alternative fuels; a brief summary of the fuels tested is given in Table 5.1 (compiled from safety data sheet of the individual fuel). These kerosene fuels contain hydrocarbons which are similar to those found in conventional jet fuels, but the range and distribution of hydrocarbon types is limited, due to the different process characteristics. Alternative fuels tend to be light in aromatics and naphthenics, which means the fuels may struggle to meet the minimum Jet A/Jet A-1 specifications for aromatics and density. However, within limits, they can be blended with conventional fuels to yield a product fit for aviation purposes. Owing to compositional differences compared to conventional Jet A-1, the alternative fuels would be expected to have different water solubilisation and hold-up characteristics.

Fully synthetic fuels are produced by a multi-stage process. Firstly, the feedstock must be modified to yield syngas, a mixture of carbon monoxide and hydrogen; solid feedstocks like coal or biomass are gasified, whilst light hydrocarbon gases need to be steam reformed. The second stage is Fischer-Tropsch (FT) synthesis which involves reacting the syngas mixture at an appropriate temperature and pressure in the presence of a FT catalyst to create liquid hydrocarbons; process

conditions and hydrogen to carbon ratio affect the output hydrocarbons. Finally, the product is hydroprocessed, and refined in the usual way [33][34]. The SASOL fuel was derived from coal and the FT process largely yields paraffinic hydrocarbons, i.e., a mixture of n- and iso-alkanes; hence the end product is known as synthetic paraffinic kerosene (SPK). The Syntroleum fuel was derived from natural gas, so the process is known as gas to liquid technology or GTL; like SASOL, the process tends to yield mainly paraffinic hydrocarbons.

Hydroprocessed esters and fatty acids (HEFA) is a fuel derived from fatty or oily materials of vegetable or animal origin. It is one of the most commercially viable alternative jet fuels produced from renewable feedstocks. The precursor molecules are triglycerides - three fatty acids of carbon chain lengths between C8 and C24, linked together by a glycerol backbone. Apart from pre-treatment, the main process step is hydrotreatment to break the glycerol linkage, remove oxygen and open residual double bonds. The fuel can then be refined in the normal way. Like the previous two fuels, HEFA tends to be composed of n-alkanes and iso-alkanes [38][42].

Alcohol-to-jet (ATJ) fuels are viable alternative fuels that are produced from ethanol or iso-butanol and processed by dehydration, oligomerization, hydrogenation and fractionation [37]. ATJ produced from iso-butanol mainly comprises of highly branched iso-alkanes of 8, 12, or 16 carbons [36]. The Gevo ATJ-SPK is produced from iso-butanol, and consists mostly of 2,2,4,6,6-pentamethylheptane ($C_{12}H_{26}$) with a lesser amount of 2,2,4,4,6,8,8-heptamethylnonane ($C_{16}H_{34}$); it does not contain significant aromatics, although it is possible to modify the process route to include an aromatisation step and create a fuel closer to the Jet A/Jet A-1 specification [35].

Unlike other SAF, farnesane (synthesized iso-paraffins or SIP) is a mono-constituent hydrogenated sesquiterpene. It is produced commercially by fermentation of sugarcane using a genetically engineered yeast to yield farnesene, a branched C15 iso-alkene with four double bonds [38][42]. Farnesene is then hydroprocessed to break the double bonds and yield

farnesane; 2,6,10-trimethyldodecane. The resulting SIP fuel could contain traces of olefins and other by-products [38].

Table 5.1 Summary of the characteristics of fuels used for these tests

Fuel type	Category	Hydrocarbon composition	Density @ +15 °C (kgm^{-3})	Viscosity @ -20 °C (mm^2s^{-1})	Aromatic content (% v/v)
Coryton Jet A-1	Conventional fuel	$C_{11.4}H_{22.3}$	796.7	3.559	17.1
SASOL FT SPK	Synthetic fuel	$C_{11.6}H_{23.2}$	761	3.4	2.1
Syntroleum S-8 GTL	Synthetic fuel	$C_{10.8}H_{23.6}$	756*	4.7	0.0
Gevo ATJ-SPK	Synthetic bio-derived fuel	$C_{16}H_{34}$	759	4.8	0.5
Honeywell HEFA-SPK	Synthetic bio-derived fuel	$C_{12}H_{26}$	760	5.1	0.6
Total Amyris farnesane	Bio-derived fuel	$C_{15}H_{32}$	770	14.28	-**

* at 15.6°C
** not specified, but approximately zero since farnesane is a mono-constituent fuel

5.2.2 Droplet size measurement using the Jorin Visual Process Analyser (ViPA)

The Visual Process analyser (ViPA) system selected for this experiment was manufactured by Jorin Ltd., Whetstone, Leicester, England. This unit uses a video microscope that consists of a high-speed digital video camera, a light source, and a lens. Images were analysed in an ongoing sequence from the video system at approximately 20 frames per second; periodic data collection was specified. In this mode, images were collected and then written to memory in brief

bursts, to monitor the size distribution trend in real-time. The flow through the cell was maintained at a constant rate to ensure that droplets were not counted more than once. The continuous data were accumulated for 1 hour and reported as counts per 39 s.

5.2.2.1 ViPA data analysis

The objective of this study was to characterize the effects of water concentration and homogenisation conditions on the droplet size distribution, droplet count, frequency distribution, and estimated volume in different fuels.

A set of user-defined parameters were entered into the ViPA enabling the system to discriminate between various classes of particle (based on shape, size, and opacity). The system can calculate data on several classes of measured parameters, but in the present study, size, shape factor, visible water concentration, and volume were analysed. For the size parameter, the system measures particle diameter in a specified direction between two parallel tangential lines and reports it as the mean of the measured feret diameter (measurement along a specified direction). For each object, the ViPA measures four diameters, which are known as feret diameters, at fixed angular intervals. The average droplet sizing for this work is defined as the summation of the diameter ‘d’ of droplet size from ‘i’ equals zero to ∞ (number of imaged particles) then divided by the summation of the total number of frames or total frequency of occurrence (n).

The flow cell channel is approximately 6 mm wide x 2 mm deep; at a volumetric flow rate of 20 mL/min, this gave a linear flow of 27.8 mm/s. Images were captured at regular intervals (20 frames per second) and sent to the computer for analysis. The image captured by the system is 1024 x 778 pixels with a pixel size of 0.47 µm. This equates to a field of view of 481 x 366 µm; the depth of field is 300 µm, which gives an assessed fluid volume of 52.8×10^6 μm^3. In practical

terms, this means that the smallest particle that can be detected reliably is 1.5 μm and the largest is less than 300 μm.

To determine if a particle is round (spherical water droplet or gas bubble) a minimum of 3 adjacent dark pixels are required in a 3 x 3 grid. When an object is smaller than 1.5 μm, the system cannot determine sphericity and the particle is assumed to be a hard solid. The software interprets what is a valid object and what is not using two parameters: 'Edge strength' and 'Threshold'. The 'Edge strength' is a measure of the object being in focus; an object in focus will appear with well-defined edges. 'Threshold' defines the different tones (256 grey levels) possible on the grey scale. This gives the software the ability to differentiate between objects of interest, which tend to obscure light and therefore appear darker grey, and the background fuel, which appears pale grey. Water droplets in jet fuel generally appear to be circular with a dark perimeter and brighter centre, whilst hard particulates tend to be more angular and will appear to be uniformly dark.

The De Brouckere mean diameter was selected for this work because the distribution calculated takes volume and mass into account [192][193]. The De Brouckere mean diameter is the weighted volume average (WVA) of a particle size distribution. The equation for the average droplet sizing $\underline{D}_{\mathbf{1,0}}$ and weighted-volume average $\underline{D}_{\mathbf{4,3}}$ can be written as:

$$\underline{D}_{[1,0]} = \frac{\sum_{i=0}^{\infty} n_i d_i}{\sum_{i=0}^{\infty} n_i} \qquad \textbf{Equation 5-1}$$

$$\underline{D}_{[4,3]} = \frac{\sum_{i=0}^{\infty} n_i d_i^4}{\sum_{i=0}^{\infty} n_i d_i^3} \qquad \textbf{Equation 5-2}$$

The key parameter that enables the system to discriminate between objects is the shape factor. Mathematically, the shape factor (SF) for any class of object is represented as SF = 4π Area/Perimeter^2. In principle, the SF is inversely proportional to the square of the perimeter; therefore, for a given area, an

increase in the perimeter decreases the shape factor. The system defines a spherical shape factor to be within the range of 0.9 - 1 and a square as 0.75. The visible water concentration in ppm is principally analysed based on the focal volume. Therefore, the concentration assumes that the volume of fluid passing through the flow cell is sufficient that, for every frame captured, a fresh volume of fluid is analysed. Concentrations are not absolute but have been proved to be statistically reliable. However, the visible parts per million (Vppm) has been proved to be a representation of changes to measurements over time [192]. Finally, the estimated volume of water droplets is mathematically represented as the volume of a sphere ($4/3\ \pi r^3$).

Results obtained for size distribution are presented in histograms/distribution curves showing the frequency and size distribution for a given set of test conditions. Another way the droplet size distribution result was presented was by calculating the kurtosis and skewness for all test cases. The kurtosis and skewness provide more statistical evidence [194]. The equations used for calculating skewness and kurtosis are given by

:

$$Skewness\ (sk) = \frac{n}{(n-)(n-2)} \sum_{i=1}^{n} \left(\frac{di - \underline{d}}{s.d}\right)^3 \qquad \textbf{Equation 5-3}$$

$$Kurtosis\ (k) = \frac{n(n+1)}{(n-1)(n-2)(n-3)} \sum_{i=1}^{n} \left(\frac{di - \underline{d}}{s.d}\right)^4 - 3\frac{(n-1)^2}{(n-2)(n-3)} \qquad \textbf{Equation 5-4}$$

Where *s.d* is the standard deviation and $\underline{d}$ the mean droplet size diameter.

Kurtosis relates to the "tailedness" of a real-valued random variable's probability distribution and how the data corresponds to the greater effect of outliers. For a standard normal distribution, the value of kurtosis is three. Statistically, the skewness measures the lack of symmetry of a data set. The skew parameter tends to be negative mostly when a secondary peak at a high diameter is present in the distribution (small droplets colliding to form large droplets can lead to such secondary peaks).

5.2.2.2 Preparation of dispersed water in the jet fuel mixture

100 mL of fuel was prepared in a 100 mL measuring cylinder (approximately 32 mm diameter) to allow a reasonable height for the rate of water settling to be analysed. The emulsion was prepared by adding a measured amount of distilled water (0.1% w/w of water) to the fuel at approximately 19°C and blending with a X 620 high shear mixer.

All water content measurements reported in this paper were conducted by Karl Fischer (KF) coulometry using a Metrohm 831KF coulometer; this unit was fitted with a generator electrode with diaphragm. The titration vessel was filled with Hydranal Coulomat AG-H solution. It is noteworthy that, as received, all fuels were below the maximum specified total water content of 75 ppm (for fuels that comply with ASTM D7566) before the water addition. Table **5.2** summarises the fuel mixtures prepared. The 'case a' tests examined the effects of fuel composition.

Table 5.2 Summary of 'case a' test fuels. In each case, 0.1% water addition was made; the water was dispersed with a high shear mixer

Test cases	**Fuel**	**Fuel type/ Category**
case a.1	Coryton Jet A-1	Conventional fuel
case a.2	SASOL	Synthetic fuel
case a.3	GTL S-8	Synthetic fuel
case a.4	HEFA	Synthetic bioderived fuel
case a.5	ATJ	Synthetic bioderived fuel
case a.6	Farnesane	Bio derived fuel

Figure 5.1 , X 620 high shear mixer used for water dispersion+

The X620 mixer is shown in Figure 5.1. The fluid was sheared by a high-speed revolving impeller; the shearing effect is proportional to the impeller speed. For these tests, the emulsion was homogenised for 60 s at a constant speed of 11,000 RPM.

After preparation of the emulsion, the “inlet” flow line (blue flexible tube in figure 2) was placed in the middle of the measuring cylinder whilst the “outlet” flow line was placed in an empty beaker. At this point, the peristaltic pump was started to allow approximately 2 mL to flush through the system to coat the inside of the flow line and to eliminate any air trapped in the system. Subsequently, software analysis was started, and the open end of the “outlet” flow line was located at the bottom of the measuring cylinder (orange flexible tube in Summary of ‘case a’ test fuels. In each case, 0.1% water addition was made; the water was dispersed with a high shear mixer). This procedure ensured that the emulsion retains the

dispersed water droplets as some fuels tend to shed water fractions quickly depending on their level of hydrophobicity, or presence of polar compounds.

Immediately after starting the ViPA system, a snapshot and a video were taken for visual comparison of the water droplet size at the beginning and end of an experiment run. The experimental setup is shown schematically in Figure 5.2.

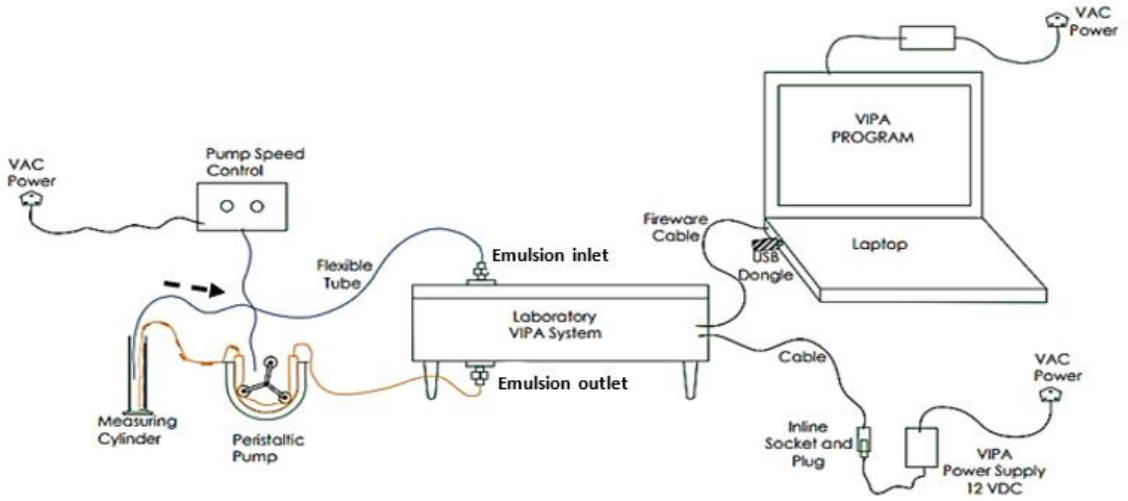

Figure 5.2 Experimental setup used for suspended water droplet size analysis

An initial water content analysis was conducted using KF coulometry a few minutes after mixing the emulsion, and then at intervals through each test (typically every 10 minutes); the KF tests adopted the procedure given in ASTM D6304. The KF results are shown in Table C-1.

5.3 Results and Discussion

5.3.1 ViPA data analysis

Table 5.3 summarises the results from the ViPA data analysis for test cases a.1 to a.6. The shape factor for these test cases was well within the range of 0.9 – 1, indicating that the detected droplets were spherical. The uncertainty of the arithmetic mean diameter is 5% at 95 % confidence level for every measurement.

Table 5.3 Result data summary for test cases a.1 to a.6

Test case	a.1	a.2	a.3	a.4	a.5	a.6
The summary result after 1 hr						
Arithmetic mean diameter- $\underline{D}_{[1,0]}$ (µm)	4.15	3.73	4.36	4.0	3.97	4.20
Weighted-volume average- $\underline{D}_{[4,3]}$ (µm^3)	10.46	10.67	10.86	11.68	12.6	10.36
Average count after 1 hr	15,876	14,365	17,058	12,113	9,285	5,424
Shape factor	0.92	0.92	0.91	0.91	0.92	0.91
Time history of particle characterisation (arithmetic mean size, µm***)***						
39 s	4.02	3.65	4.16	3.82	3.48	4.13
1170s	4.09	3.66	4.37	4.0	3.94	4.13
2340s	4.18	3.76	4.28	3.98	4.08	4.23
Time history of particle characterisation (weighted volume average size, µm^3***)***						
39s	10.85	11.45	12.52	13.55	14.88	9.84
1170s	10.67	10.68	11.32	12.1	13.02	10.36
2340s	10.32	10.54	13.72	11.23	12.27	10.31
Time history of particle characterisation (droplet count)						

39 s	20,000	18,900	16,400	18,000	17,000	9,000
1170s	10,200	14,500	10,500	12,000	8,000	5,000
2340s	7,500	11,000	7,500	9000	6,000	3,300

In use, the video system operates at 20 frames per second. It performs a background calibration of 100 frames and then a burst of 361 frames in image analysis mode. From the frame rate, it can be deduced that the instrument makes measurements for 18.05 s within each imaging cycle. Each particle that is identified by the software is measured and aggregate statistics recorded in spreadsheet form. On completion of an imaging cycle, the data is stored to hard disk drive and the sequence repeated. Each cycle takes 39 s and, for the purposes of this investigation, the instrument was run continuously for 1 hour for each test case.

Table 5.3 shows the average of the chosen parameter (size, shape, and count) for all the images captured at different interval of time. The count for all fuel samples reduces dramatically over time. This is due to recirculation of the liquid stream that creates turbulence that favours the coalescence of water droplets to larger droplets resulting in settling. Also, from Table 5.3, a slight drop in the WVA over time can be seen whilst there is a slight unstable increase in the average droplet diameter with time. However, it is noteworthy that even though case a.6 exhibited the second highest mean diameter of 4.20 µm, it had the lowest average count of 5,400 and lowest WVA of 10.36 μm^3. Also, case a.5 exhibited the lowest mean size of 3.97 µm, yet it had the highest WVA of 12.6 μm^3 and a count of 9,200. This shows that there is a relationship that exists between the water droplet size, count, and droplet volume concentration. The following sections help shed light on these correlations and expatiate on the test results for cases a.1 to a.6.

5.3.1.1 Effects of fuel composition

Jet fuel does not have a particular chemical composition but is a complex mixture that is mainly specified according to physical characterization as investigated and reported by a few studies [201]. So far, it has been established that fuel properties can be directly affected by chemical composition. However, with the growing demand for sustainable aviation fuels, understanding the effect of chemical composition has become a vital topic of interest as it could potentially assist in accelerating the fuel approval process as well as providing information for fuels additive companies and filter manufacturers. Therefore, the water droplet size distribution of sustainable aviation fuels was evaluated in comparison to Jet A-1 fuel in this work. The influence of chemical composition on the rate of droplet count can be seen in Figure 5.3a. The time it takes the dispersed water droplets to drop out of the fuel/water mixture is a measure of the settling rate/profile. Data in Figure 5.3a illustrates the settling profile of the different fuels. Reported recent work compared the settling profile of sustainable aviation fuels and conventional jet fuel, and found the rate to decrease with time [187][202]. Qualitatively, it is anticipated that the water separation ability can be directly influenced by the droplet size and droplet coalescence. From Figure 5.3a, it can be seen that the droplet counts decrease with time and that all fuels tend to exhibit a steady exponential decay over time. This mirrors previous work by West et al. that showed that the water settling rate steadily decayed over time for both conventional and sustainable aviation fuels [200]. In context, the rate of decay of droplet counts may be attributed to droplet coalescence [135]. Evidence that will indicate that droplet coalescence was occurring is in Figure 5.3 and Figure 5.4, shows a plot of water droplet diameter represented by 10%, 20%, 50% to 90%, or d10, d50 and d90.

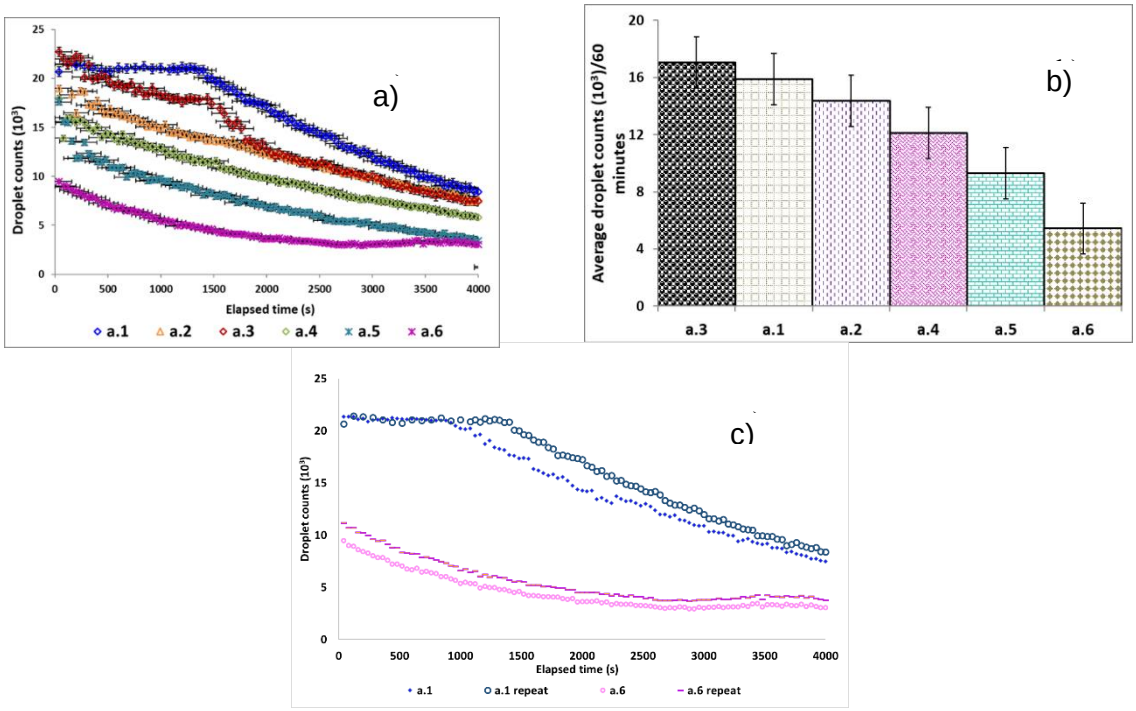

Figure 5.3 Water droplet count with error margin a) settling profile for case a.1 to a.6; b) average droplet count histogram data for case a.1 to a.6; c) Repeatability droplet counts data for case a.1 and a.6

As illustrated in Figure 5.3a, the rates of droplet count decay are different for all the fuels; fuel case a.6 showed the least tendency to form and suspend individual water droplets, and the slowest settling rate of all the fuel/water mixes. However, fuels with higher settling rates and a good separation ability are beneficial to the aviation industry as most aircraft fuelling systems utilise filter coalescers. Since case a.6 exhibits poorer separation ability, it can be concluded that there was good mixing and that most of the water molecules remained in solution. The high-water content in the KF results for case a.6, shown in Table 5.1 suggests there were more than just traces of polar compounds present. To elucidate this point on settling behaviour, the average total droplet count data were plotted for the different fuels in Figure 5.3b. The ViPA detected an average count of about 15,500 after 60 minutes for case a.1 with 1000 ppm water addition. Under the same test conditions as case a.1, the GTL S-8 synthetic fuel employed for case a.3 exhibited similar behaviour; the ViPA system detected an average count of 17,000 after 60 minutes. Count data for cases a.1 to a.6 showed a steady decrease in droplet count, ranked as a.3>a.1>a.2>a.4>a.5>a.6.

The water solubility in jet fuel is predominantly dependent on the fuel composition, aromatics content among other factors. While the water droplet diameter, density, and viscosity can affect the settling rate of precipitated droplets in fuel. Case a.6 showed the slowest settling rate and lowest droplet count; this is a bio-derived fuel with very low aromatics content and the highest viscosity, as noted in table 1. Pathway analysis by Zschocke et al and a GC/MS characterisation by Pires et al suggests that farnesane could contain traces of unsaturated hydrocarbons (olefins) [203][38]. Olefins contain one or more double bonds, that consist of one sigma bond and one pi bond, and therefore may contribute to slightly enhanced uptake of water.

Literature has established that viscosity plays a key role in the behaviour of droplets in a suspension. According to Stokes' law (which is an expression that describes the resisting force on a particle moving through a viscous liquid) the terminal velocity of a water droplet is directly proportional to the square of the droplet diameter and the density difference between fuel and water, and inversely proportional to the dynamic viscosity of the fuel [187]. Figure 5.4 shows the shift in the corresponding water droplet size population against time for cases a.1 to a.6.

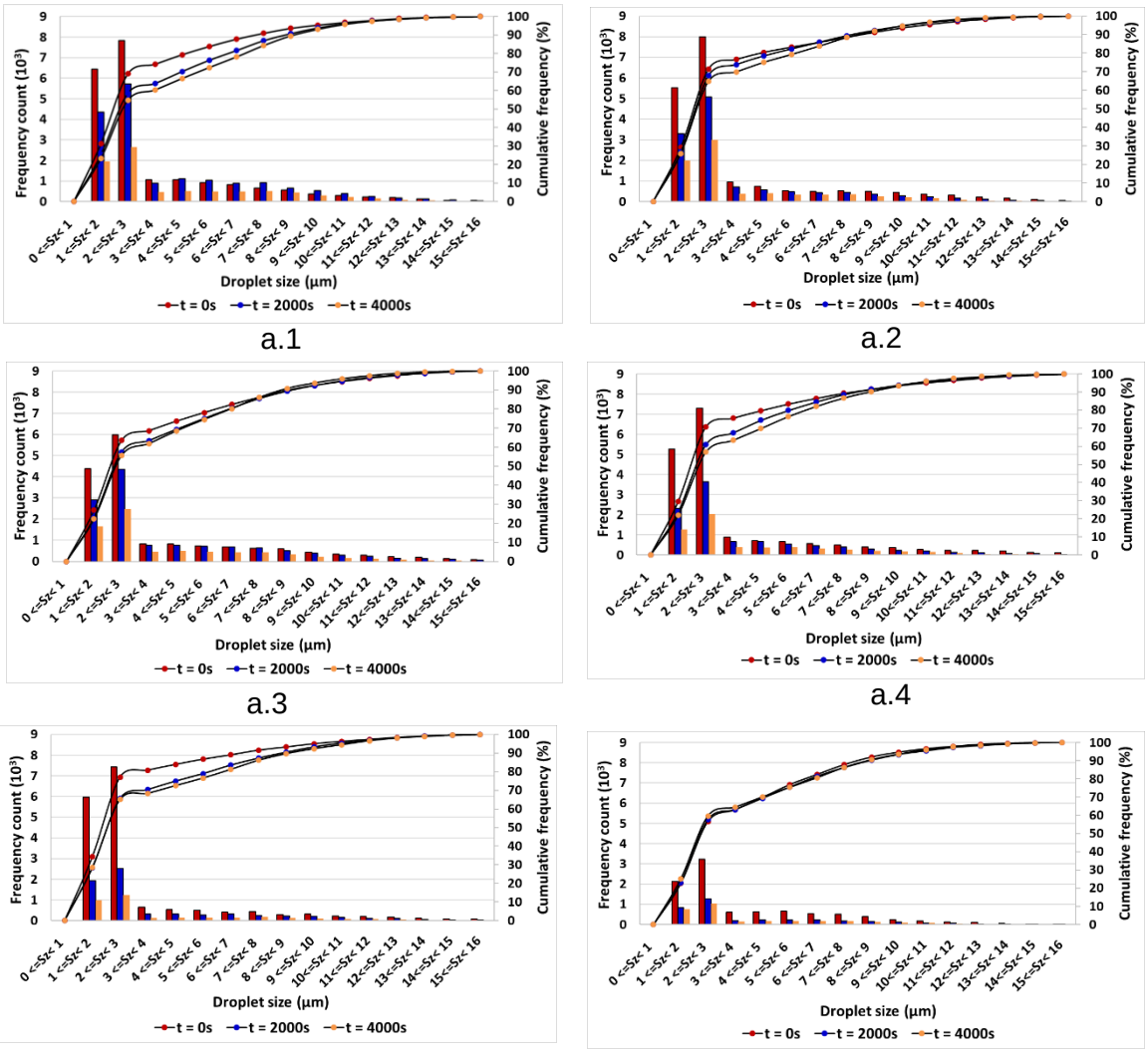

Figure 5.4 Water droplet size population with respect to time for each fuel cases a.1 to a.6

The shift in the cumulative frequency can be used to describe the transition of the percentile of droplets over time (up to t=4000 s). For instance, 10%, 50%, and 90%, or d10, d50, and d90, are represented as water droplet diameters equal to or below the corresponding diameter of that percentile. Water droplet size population represented from d10 to d90 against time for test cases a.1- a.6 is shown in Figure C-2.

It can be seen from Figure 5.4 that the majority of the detected water droplets were between 2 and 4 µm. Droplet counts decrease with time, due to droplet coalescence, which causes an incremental shift of the d70 – d90 populations at

different times. This is consistent with the relationship shown in Figure 5.5 (illustrating the mean droplet size for all fuels with time as a variable). It can also be deduced from the cumulative frequency curve in Figure 5.4 that droplet sizes between d40-10 are likely to remain suspended in the fuel/water mixture as no settling was noticed. No noticeable change was detected with time for case a.6 compared to other test cases.

It can be elucidated from Figure 5.4 that droplet size does not conform to the same pattern as droplet count. To explain this point, case a.6 (farnesane) with the lowest droplet count of all the cases explored (Figure 5.3) maintained the lowest WVA over time (Figure 5.5). However, it exhibited a larger average droplet size over time than cases a.1, a.2, a.4, and a.5 (Figure 5.5b). Case a.3 (GTL S-8) showed the highest average droplet count and droplet sizes over time but did not have the highest droplet volume concentration (WVA). Previous work in this area suggests that the rate at which water droplets will fall out of a solution is dependent on the droplet volume concentrations and the square of the diameter [200]. Figure 5.3 and Figure 5.5 shed light on the relationship that exists between the water droplet size, count, and droplet volume concentration.

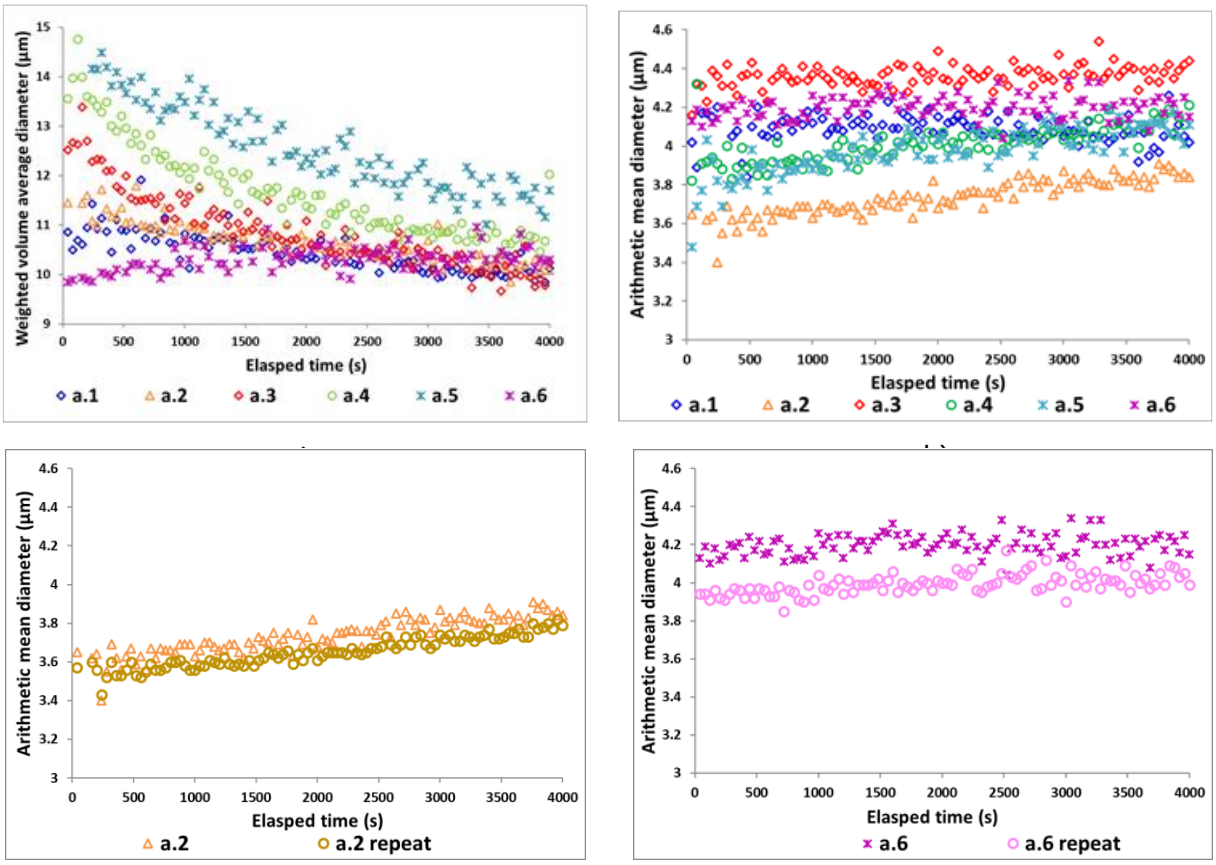

Figure 5.5 Shows the a) weighted volume average data against time; b) Arithmetic mean droplet size against time for test cases a.1 to case a.6; c) repeatability data for arithmetic mean droplet size against time for test cases a.2; d) repeatability data for arithmetic mean droplet size against time for test cases a.6

It is noticeable from Figure 5.5 that the behaviour of water droplets in hydrocarbons is often complex, and random as evidenced by a slight increase in the average droplet size with time (Figure 5.5b).

However, a noticeable drop in the water droplet volume over time can be is seen in Figure 5.5a. This demonstrates that the contribution from larger droplets or high-frequency counts of smaller droplets could all influence the droplet volume. A high droplet count does not necessarily correspond to a high droplet volume and, similarly, a fuel that contains few but larger water droplets does not necessarily signify that the volume will be high. The volume concentration is

principally based on the mass equivalent as there could be a high-water count with small droplet sizes or a low water count with large droplet sizes. For instance, even though case a.6 (farnesane) contained large water droplets, it had the lowest droplet volume. In addition, it had the lowest count of water droplets, whilst case a.5 (ATJ) had a higher WVA because it contained a higher proportion of larger droplets. It is worth noting that cases a.2 (SASOL) and a.1 (Jet A-1) do not have the highest droplet volume (Figure 5.5a) but they both have the highest frequency of smaller droplets compared to all other fuels, as shown in Figure 5.6.

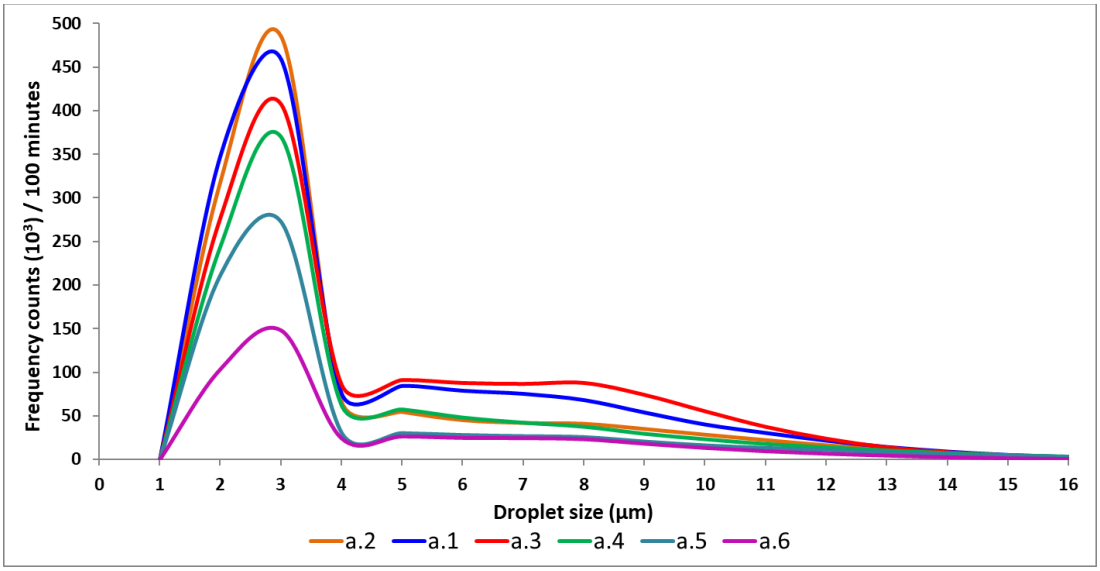

Figure 5.6a Frequency distribution of water droplet sizes for aviation fuels explored in this work (Cases a.1 to a.6)

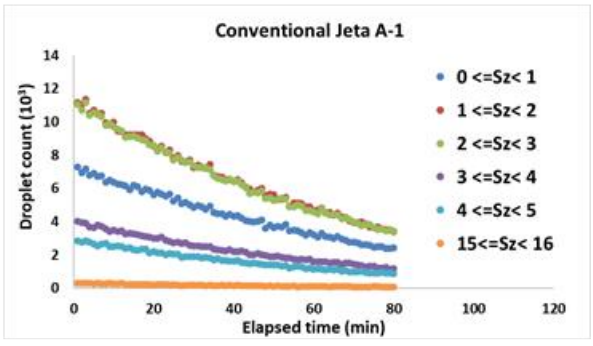

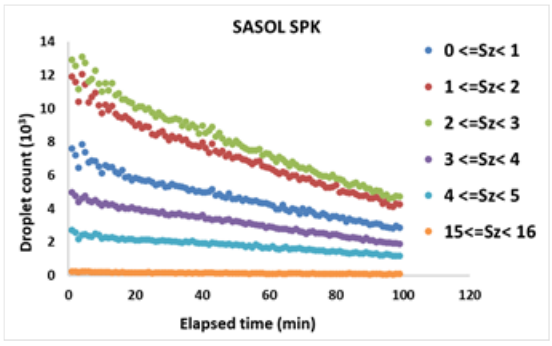

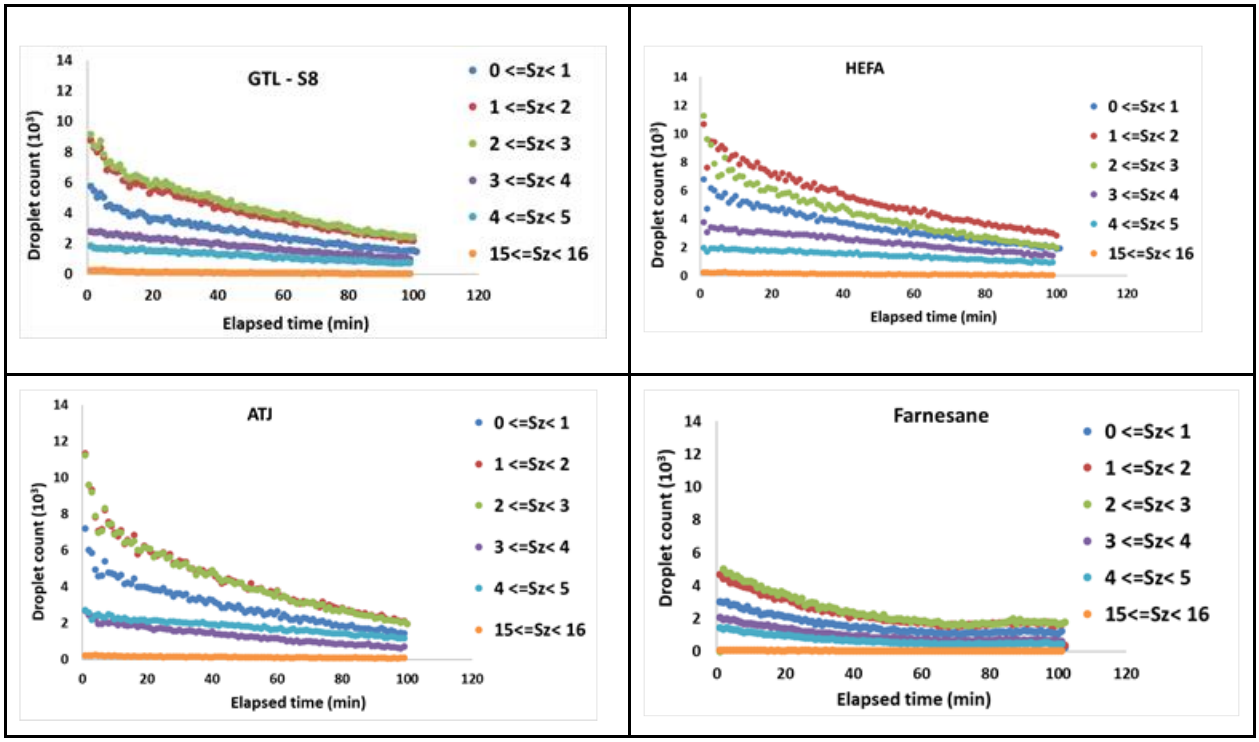

Figure 5.6b. comparative analysis of the frequency distribution between the conventional Jet A-1 fuel and sustainable aviation fuels explored for this work (Case a.1 to a.6)

The frequency distribution for each test in Figure 5.6 presents the droplet counts separated into discrete size intervals between Jet A-1 fuel and the sustainable aviation fuels explored for this work. The height of the distribution peak indicates the total count of water droplets for each size range. Figure 5.6 shows that the mode droplet count frequency for all fuels explored fell within the droplet interval of 2 to 3 µm. Case a.1- Jet A-1 and case a.2- SASOL exhibited the highest frequency of smaller droplets ranging from 1 to 3 µm.

Figure 5.6b shows the droplet count for each class of droplet size over time. Starting with case a.6, the gradual slope for farnesane confirms that the settling rate of droplets is low compared to the other fuels. This implies that the farnesane formed a more stable emulsion relative to the other fuel types. The result correlates with data from a study by Leiva et al. on the expected behaviour of emulsions and the changes in their droplet size distributions [204]. Figure C-1 shows a comparative analysis of the frequency distribution between Jet A-1 fuel

and the sustainable aviation fuels explored for this work.

To illustrate the appearance and distribution of water droplets in different fuels, Figure 5.7 shows typical images captured from the ViPA software near the start and finish of each experimental run. The images help with visualisation of the reduction in water droplet populations seen in the frequency distribution data in Figure 5.6, where water droplets disappear over time due to settling.

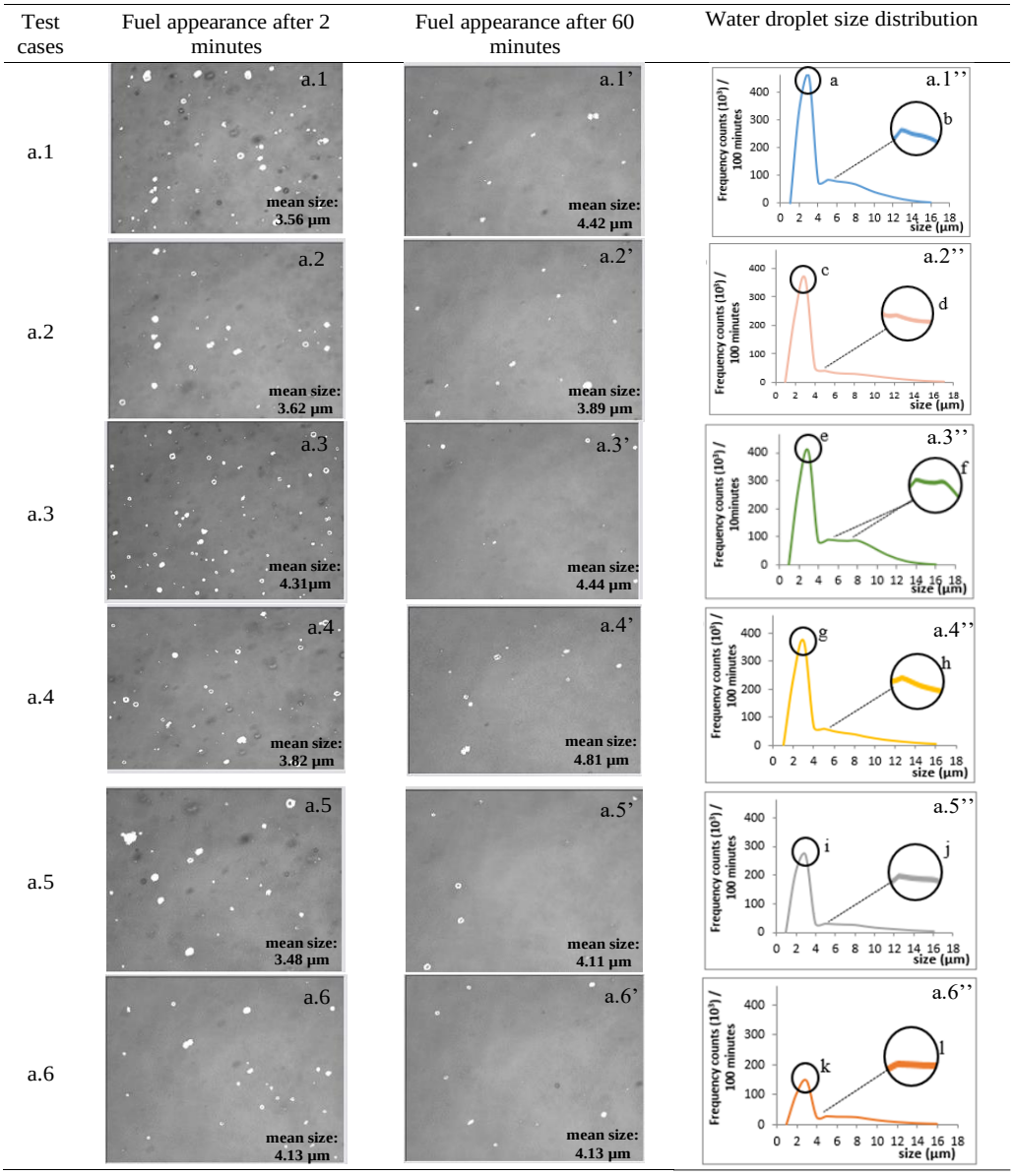

Figure 5.7 The images captured from the ViPA software at the start of experiment time at 2 minutes are the unprimed labels at the left (a.1 to a.6); and at approximately time at 60 minutes are the primed labels at the centre (a.1'-a.6').

The double primed labels at the right plot (a.1''-a.6'') show the water droplet size distribution's smoothened kernels

The size distribution plot in Figure 5.7 a.1''-5.7 a.6''agrees with the data plot in Figure 5.4 a.1'-a.5' shows the droplet size increases with time due to the coalescence phenomenon- the collision of small drops giving rise to larger droplets. For instance, the possible interpretation for this distribution observed in Figure 5.7 a.3'' is as a result of the collision of small drops with one large peak denoted as 'e' centred around 2-3 µm diameter, then giving rise to larger droplets of smaller broadband denoted as 'f' around 6-8 µm diameter. The same phenomenon dominates in all cases; however, in some cases, the peaks are smaller and almost insignificant. For example, case a.6 nearly formed a monomodal distribution with one evident narrow peak denoted as 'k' around 3 µm and a tiny peak almost insignificant denoted as 'l' around 5 µm. Overall, the larger the droplets formed due to the collision of small droplets, the more unstable the emulsion is (evident case is as seen in Figure 5.7 a.1'' and 5.7 a.3''). Whilst in cases where smaller droplets are formed from the collision process or when no collision occurs at all, the more stable the emulsion is likely to be. Droplet size distribution data for test case a.1 to a.6 exhibit an unstable emulsion in the order of a.3>a.1>a.4>a.2>a.5>a.6. This result correlates with work done by Noor et al. on the stability of water in diesel fuel emulsions, concluding that the more stable an emulsion is, the narrower the droplet size distribution [135]. Whilst this is based on the result and trend observed, the statistical evidence based on the calculation of the kurtosis and skewness (equations iii and iv) further elucidates the result from the droplet distribution (Table 5.4).

Table 5.4 Kurtosis and skewness data for case a.1 to case a.6

	Case a.1	**Case a.2**	**Case a.3**	**Case a.4**	**Case a.5**	**Case a.6**	**Hexanol**
Kurtosis (after 40 min)	6.6	6.66	6.29	6.58	8.21	7.09	28.4
Skew (after 40 min)	2.63	2.79	2.65	2.75	2.95	2.68	4.6

Kurtosis (after 60 min)	7.4	7.3	7.5	7.8	10.31	9.47	34.90
Skew-(after 60 min)	2.86	2.87	2.87	2.89	3.17	3.01	5.07

The more unstable a solution, the lower the skew value. In contrast, kurtosis relates to a metric indicating the "tailedness" of a real-valued random variable's probability distribution and how the data corresponds to the greater effect of outliers. 1-hexanol (which is likely to form a stable solution) was included to serve as a baseline for comparison between a stable solution and unstable emulsion and has the highest kurtosis and skew value of the fluids investigated.

The skew to the right, seen in the droplet distribution in Figure 5.7 a.1'' to a.6'', shows that all fuels exhibit a positive skewness as the right-hand tail is longer than the left. The droplet size distribution for cases a.5 and a.6 are characterised by their exhibition of a smaller second peak at larger droplets and a slightly higher kurtosis value of 8.21 and 7.09 (Table 5.4). While droplet size distribution for cases a.1 to a.4 is characterised by their almost evident second peak distribution and a lower kurtosis value of 6.6, 6.7, 6.29, and 6.58, respectively (Table 5.4).

5.4 Conclusions and Recommendations

The fundamental variable that influences the characteristics of an emulsion in aviation fuels is the water droplet size distribution. The experimental test data has indicated that water droplet size/count distribution is sensitive to changes in fuel composition; the evaluated synthetic jet fuels, GTL S-8, SASOL and HEFA, exhibited good water separation comparable to conventional jet fuel. This is consistent with previous work conducted on the water settling ability of various jet fuels [4,10,24]. Fuel with a higher water settling rate is beneficial for aviation refuelling purposes. The synthetic fuels had higher droplet counts, lower skew and kurtosis values compared to the biofuels, which means good prospects for faster water separation. In contrast, the bio-jet fuels explored for this work, ATJ and farnesane, exhibited worse water separation.

Further work should be carried out at different blending ratios of sustainable fuels

and temperatures (cold temperatures- to simulate high altitudes). This would assist with development of a mathematical relationship to predict the relationship that exists between the droplet size, droplet count and droplet volume. Finally, experiments should be repeated on a larger scale with the outlet emulsion transferred to a waste container instead of the bottom of the tank/measuring cylinder.

6 Chapter 6 How will sustainable aviation fuels impact ice formation and pump performance in aircraft fuel lines?

Abstract

With the aviation industry facing increasing environmental and energy challenges, there has been a growing demand for sustainable aviation fuel (SAF). Previous studies have shown the role of ice accretion, release and blockage in aviation-related incidents and accidents with conventional Jet A-1 fuel. However, there is no available data that establishes the degree of influence new fuel compositions will pose on ice formation and accretion in aircraft fuel systems. A recirculating fuel test rig capable of cooling fuel from ambient to -30 °C within 4 hours was built by Airbus to simulate conditions in an aircraft wing tank and allow characterisation of ice accretion. The key characteristic was the pressure drop across an inline fuel strainer for the different SAF explored but visual analysis of ice accretion on the strainer mesh was performed for individual experimental runs for comparison. Measurements revealed that 100% conventional fuel exhibited a higher propensity to strainer blockage compared to the SAF tested. However, all SAF blends behaved differently as the blending ratio with Jet A-1 fuel had a diverging impact on the pressure differential at different temperatures. Data from this work is essential to establish confidence in the safe operation of future aircraft fuel systems that will potentially be compatible with 100 % SAF.

Keywords: Sustainable, Aviation fuels, Fuel systems, Icing, Jet fuel, Aircraft

6.1 Background to study

The aviation industry is currently facing increasing environmental and energy challenges regarding its fuel use [2,13,75,183,188]. Research is currently in progress to develop sustainable alternatives. Hence, an understanding of the properties of new SAF is required to understand their impact on aircraft fuel systems (AFS) [15,27,30,199]. Water solubility, water settling and ice formation, amongst others, are some such properties of interest [187][202]. The behaviour of water and ice in Jet A-1 fuel has been studied from different perspectives (like the investigation of ice release in AFS, collection of ice in Jet A-1 fuel pipes, and ice accretion and release in Jet A-1 AFS) [2][18–20,22,44,46,156]. This has resulted in a large number of systems being employed for preventing the build-up of ice in AFS [43][45][205]. Most original equipment manufacturers (OEM) protect their fuel feed pumps using mesh strainers, and pressure relief bypasses on the fine fuel system filters and fuel oil heat exchangers (FOHE). The latter ensure uninterrupted fuel flow to the engine in the event of ice build-up and filter or FOHE blockage [156]. Ice formation will occur when an aircraft is at altitude for a prolonged period. Ice accretion has been shown to be influenced principally by fuel velocity, turbulence, and temperature. Lower flow velocities bring both lesser shear rates as well as less rapid mixing. On the other hand, a higher flow velocity is likely to produce rapid mixing and higher shear rates, potentially leading to reduced ice accretion [44][20]. For some users, an anti-icing additive (Fuel System Icing Inhibitor (FSII)) is mixed with the jet fuel in small quantities to depress the freezing point of free water in the fuel and minimize the risk from hard ice bodies. FSII is mostly required in military aviation fuels but is also specified in jet fuel (Jet A-1 and Jet A) used in certain small turbojet and turboprop aircraft, such as those manufactured by Bombardier Learjet, Cessna Citation, Daher TBM, Mitsubishi and Raytheon. Ice accretion on the surface of filter mesh screens and other parts of the engine fuel system has operational implications as it can cause a significant decrease in fuel flow to the engine [44][17]. As well as impeding fuel flow, any blockage on the inlet of the feed pumps could affect pump output. If inlet feed is reduced significantly, then cavitation within the pump body

may occur, leading to erosion damage of close-fitting parts, such as pump impellers, gear teeth and housings.

The UK Air Accidents Investigation Branch (AAIB) has released safety recommendation statements for research to be conducted to better understand ice accumulation and release within AFS. With the emerging new fuels, it is currently not known whether ice crystals in alternative fuels that conform with ASTM D7566 can cause a measurable pressure difference across a pump strainer and affect pump performance. Therefore, it is necessary to understand the types and amounts of ice that can be produced from these SAF blends. The objective of this work was to demonstrate whether ice formed from SAF, or its blends could lead to ice blockage. The scope of work involved the design, build and commissioning of a test rig at an Airbus facility to simulate conditions seen in flight operations as closely as possible.

6.2 Materials and Method

6.2.1 Rig Overview

A schematic of the test rig is shown in Figure 6.1 and in pictorial form in Figure 6.2. The rig consisted of a storage tank, 1" nominal bore insulated pipework (total length of pipework was approximately 4.4 m), centrifugal pump and ancillary parts to allow controlled circulation of jet fuel around a closed loop. The rig maximum fuel capacity was approximately 50 L and the estimated volume of fuel within the pipework, pump and fittings was 2.5 L; the system could achieve flow velocities of between 0.1 and 1.0 m/s. The tank was situated within a controlled-temperature cabinet so that exposure to different external atmospheric conditions could be simulated. Fuel temperature could be controlled between -30 and +30 °C; the rig was largely intended to simulate steady-state conditions but was capable of cooling 40 L of fuel from ambient to -30 °C within 4 hours. The rig was instrumented, and data acquisition and capture were handled within LabVIEW on an associated laboratory computer.

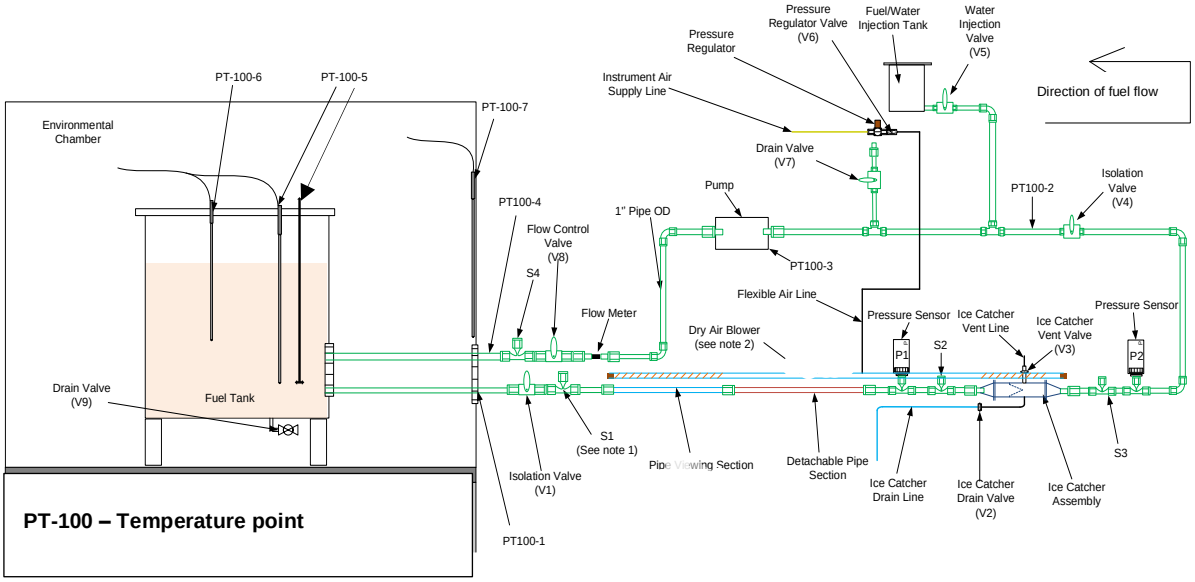

Figure 6.1 Cold fuel test rig schematic

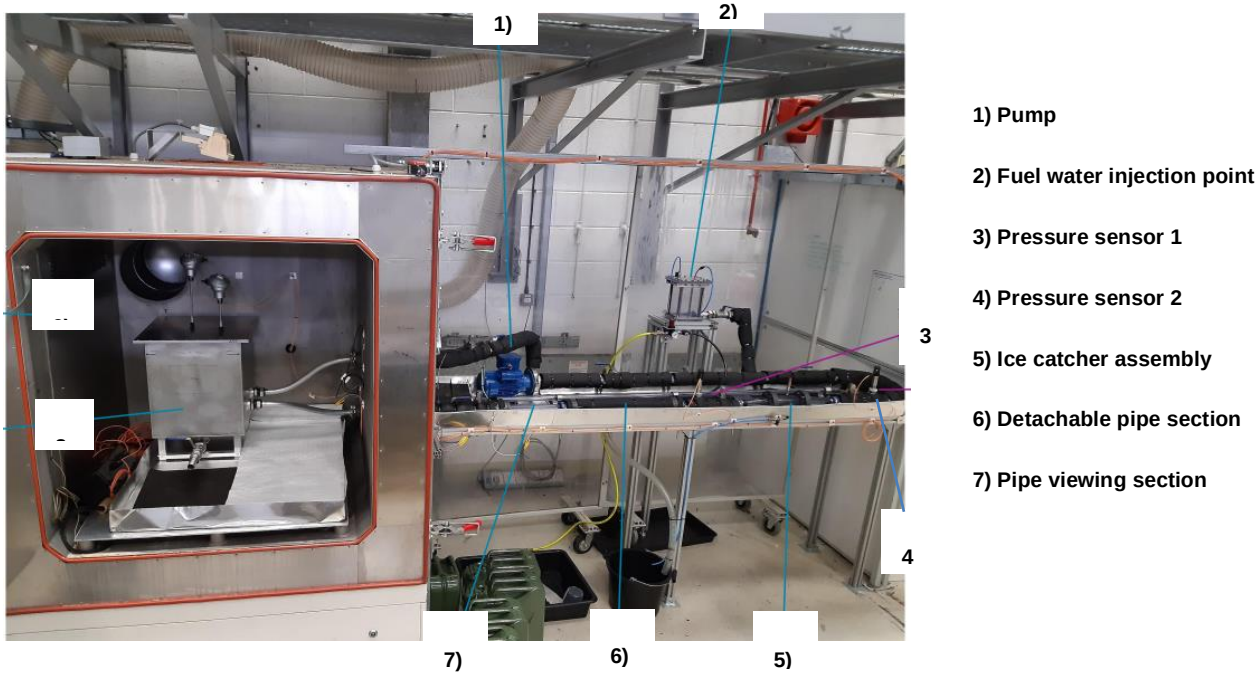

Figure 6.2 Cold fuel test rig with fuel tank in the environmental chamber

The rig was fitted with an ATEX-rated pump motor, protective extra-low voltage (PELV) instrumentation and full bunding. It had no exposed moving parts, and thermal insulation was applied to most cold surfaces to improve thermal performance and minimise atmospheric condensation. The test rig was designed to be compatible with aviation jet fuels, as noted in the materials section.

The test section comprised of two parts. A removable length of aluminium tube that allowed inspection internally for accreted ice and a transparent viewing section to allow assessment of ice accumulation across a strainer mesh. This latter section was also removable, housing a mesh strainer/ice catcher, to investigate the effects of particulate or ice build-up and blockage. The ice catcher assembly is shown in Figure 6.3a and Figure 6.3b. As seen in Figure 6.3d and Figure 6.3e, a conical wire mesh of 20 holes per inch was utilised. The mesh was supported by a perforated metal cone with 3 mm diameter holes.

Figure 6.3 Strainer section in flowing fuel at; a) Room temperature and; b) After an icing experiment; c) Strainer section removed after an icing experiment; d)

After an icing experiment (inside view); e) After an icing experiment, removable mesh and outer support cone; f) Fuel sample point

Pressure transducers were situated before and after the test, section to measure dynamic pressure drop across the strainer. Temperature sensors were located at four points around the test loop (PT100-1 - PT100-4) and within the fuel tank (PT100-5 and PT100-6); the air temperature with the environmental chamber was monitored with PT100-7. 2.5 ml fuel samples were taken at regular intervals to allow total water content determination; one of the sampling points is shown in Figure 6.3f. The sampling points were sealed with Viton A rubber (70 Shore A) septa to allow extraction of fuel samples whilst the rig was operating.

6.2.2 Description of Test Equipment and Instruments

Figure 6.4 shows the Mettler Toledo C30 Coulometric Karl Fischer Titrator used for the total water determination and a Branson 1510 ultrasonic bath that was employed for homogenising fuel samples. The KF titration cell was filled with Honeywell Hydranal Coulomat AG-H from Fischer Chemicals; previous test experience has shown that this is the most appropriate solution for evaluation of water content in kerosene fuels by coulometric KF titration. A high-speed stirrer is used in the vessel for rapid distribution of generated iodine to react with the water present in the test sample. Additionally, a semi micro MS105DU Mettler Toledo balance was employed for accurate measurement of fuel samples before KF water determination. The scale can measure up to a maximum of 120 g with a 0.001 g precision.

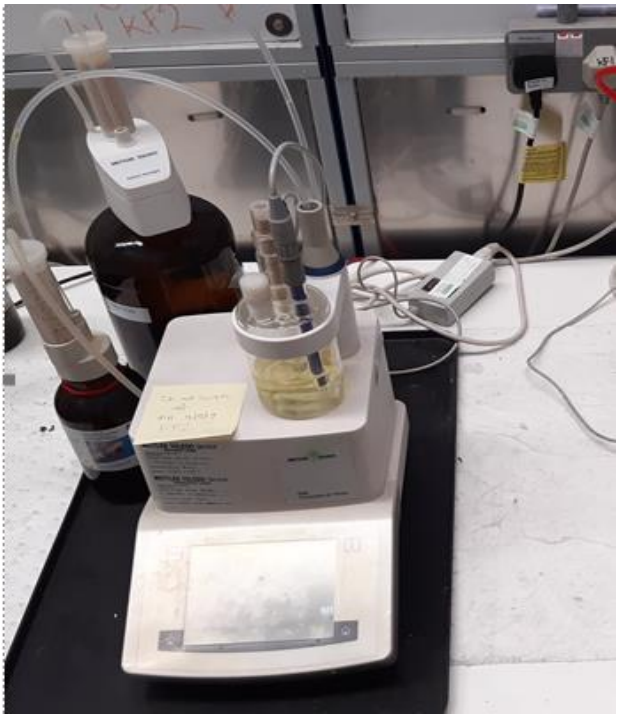

Figure 6.4 a) Mettler Toledo C30 Karl Fischer Titrators with associated solution exchange. coulometer on left; b) Branson 1510 ultrasonic bath used for homogenising fuel/water mixtures

The Weiss environmental chamber shown in Figure 6.2 is a large piece of ATEX approved test apparatus used within a secured segregated area. The chamber has an associated exterior cooling fan outside the building for cooling the chamber to sub-ambient temperatures for chilling test specimens and/or chamber contents. The chamber has the capability to safely house items under tests and may hold flammable liquids at temperatures ranging between -70 ℃ to 100 ℃. Humidity within the chamber can be controlled and a vacuum can also be applied to simulate altitude. The quantity of fuel held within the Weiss chamber, is limited for safety reasons. Therefore, a maximum of 50L of flammable liquids may only be used within the segregated area, without the need to employ additional fire detection and suppression. This quantity includes quantities of flammables stored within secured cabinets hence this limits the test volumes used within the Weiss chamber to a maximum of 40L. The chamber was never heated above 30 ℃ while there is fuel inside, due to risks associated with fuel vapour. A warning light will flash on the rig GUI when the chamber temperature is above the limit.

6.2.3 Rig Materials and Features

Materials used for the rig were the same as those found in a typical aircraft fuel system. Since fuels of markedly different compositions were to be tested, materials compatibility in regard to the fuel aromatic properties was evaluated beforehand. Small-scale laboratory experiments tested three elastomers (silicone rubber, Suba-seal natural red rubber and Viton A rubber) and fuel compatibility. Observations from the small-scale compatibility tests indicated that Viton A rubber would be generally suitable for sealing the sample points but would need replacement when fuel changes were made. Limitations noticed while using the Viton rubber are described in the Discussion section.

Other fuel-wetted components included the main storage tank (5251 aluminium alloy), pipework (5052 aluminium alloy), polycarbonate transparent viewing section, and the fuel sampling points and valves (316 stainless steel). A Finnish Thompson AC4 pump was used to circulate fuel around the test loop; the pump body and impeller were made from 316 stainless steel. Flanged pipe joints were sealed with flat Viton rubber-bonded cork gaskets. Valving facilitated filling, air release, draining and control of flow rate, fuel drainage and general maintenance. Flow was monitored with a Gems FT-110 series turbine flow sensor from RS Components. Some of the limitations of using this transducer are highlighted in the Discussion section. The rig had a 500 mm length of removable 1'' 5052 aluminium tube; this can be used to investigate the effects of materials and surface finish on ice adhesion and build up.

An external vessel (fuel/water addition point) was fitted just upstream of the circulation pump, to allow the introduction of fuel/water mixture into the loop. A low speed (approximately 200 RPM) stirrer was installed in the conditioning tank to mix the fuel and help keep water droplets suspended.

Fuel sampling was achieved with a polypropylene 5 ml luer lock syringe fitted with a 120 mm long x 21 G stainless steel needle and 15 mm thick stop collar to always guide the needle to the same depth (centre of the fuel stream).

6.2.4 Fuels

All fuels employed for this work were provided by Airbus Operations. The fuels employed are (a) SASOL (South African synthetic oil), Fischer-Tropsch synthesised paraffinic kerosene (FT-SPK) is derived from synthesis gas via the FT process using an iron or cobalt catalyst. Sasol synthetic fuels are known to have properties like that of the conventionally refined jet fuels mainly compromising of n-alkanes and iso alkanes, cycloalkanes, and traces of aromatics. (b) HEFA SPK from hydro processed esters and fatty acids is derived from hydrogenation and deoxygenation of fatty esters and free fatty acids. The product of the hydrotreated esters are mainly n-alkanes and iso-alkanes. (c) ATJ-SPK, alcohol to jet synthetic paraffinic kerosene, is derived from ethanol or isobutanol (d) Coryton Jet A-1 is a complex hydrocarbon mixture composed mainly of n-paraffins, iso-paraffins, cycloparaffins and aromatics.

6.2.4.1 Experimental procedure

To define the optimum experimental procedure, some initial tests were performed with Coryton Jet A-1. Checks were carried out to evaluate rig physical parameters such as leak tightness, residual air release, cooling profile, flow rates, data sampling, fuel sampling and water addition. The operating parameters were refined to give the generic procedure described below.

The Weiss altitude chamber was set to 28 °C before introducing any fuel or water into the system. The fuel storage tank was filled with approximately 35 L of test fuel. Valves were gradually opened to allow the flow loop to fill; then, the PC was switched on to begin data logging with LabVIEW. The pump was switched on to displace residual air, stir fuel and recirculate fuel flow back to the conditioning tank. Fuel samples were collected before and after fuel/water introduction into the rig, for coulometric Karl Fischer water content determination using the rig sampling points and a 5 ml syringe fitted with a 120 mm long needle. Thereafter, samples were taken at regular intervals (at the start of the experiment and at 30-minute intervals) Fuel samples were collected before water was introduced to

determine the quantity of de-ionised water required to be added to attain the requisite total water content.

The standard Airbus water introduction method is described by [156] and was adopted with slight modifications for this project. This method requires thorough mixing of calculated volumes of water and fuel at room temperature using an ultrasonic bath, and eventually introducing it into the system before cooling begins; at this stage, the bulk fuel temperature was set to 28 ℃. No water was added after cooling commenced.

The required quantity of water was calculated, and a master fuel/water mix solution was prepared using a Branson 1510 ultrasonic bath. The master fuel/water mix was prepared in a clean and oven dried 300 ml beaker. Typically, 10 mL of water would be mixed with about 200 ml of fuel. Using the ultrasonic bath, the fuel/water solution was mixed for at least 40 minutes. A thermocouple was present in the fuel at all times to monitor the temperature; this was not allowed to exceed the flash point of the test fuel (38 °C for Jet A-1). Immediately after conditioning, the master solution was transferred to the external fill vessel. The fuel/water mixture was added over a 5 minute-period via the fill vessel; when added to the bulk fuel, the aim was to achieve an overall concentration of about 260 ±50 ppm water, based on regulations by EASA [102]. In practice, it was found difficult to achieve exactly the right water concentration due to the dynamic nature of the test rig, and some undershoot, or overshoot occurred with some experimental runs.

The ideal was to create a dispersion of small water droplets (<20 μm) in the fuel stream, without introducing large globules of water (greater than 1 mm diameter). After completing the fuel/water addition, the environmental chamber cooling system was switched on. The temperature was typically set to -70 °C (thermocouple point labelled as PT100-7) to give the desired cooling rate and end temperature of -30 °C after fuel circulation. From Figure 6.5, it can be seen that the rig is capable of cooling 35 L of fuel from ambient to -30 °C within 4 hours while circulating round the flow loop.

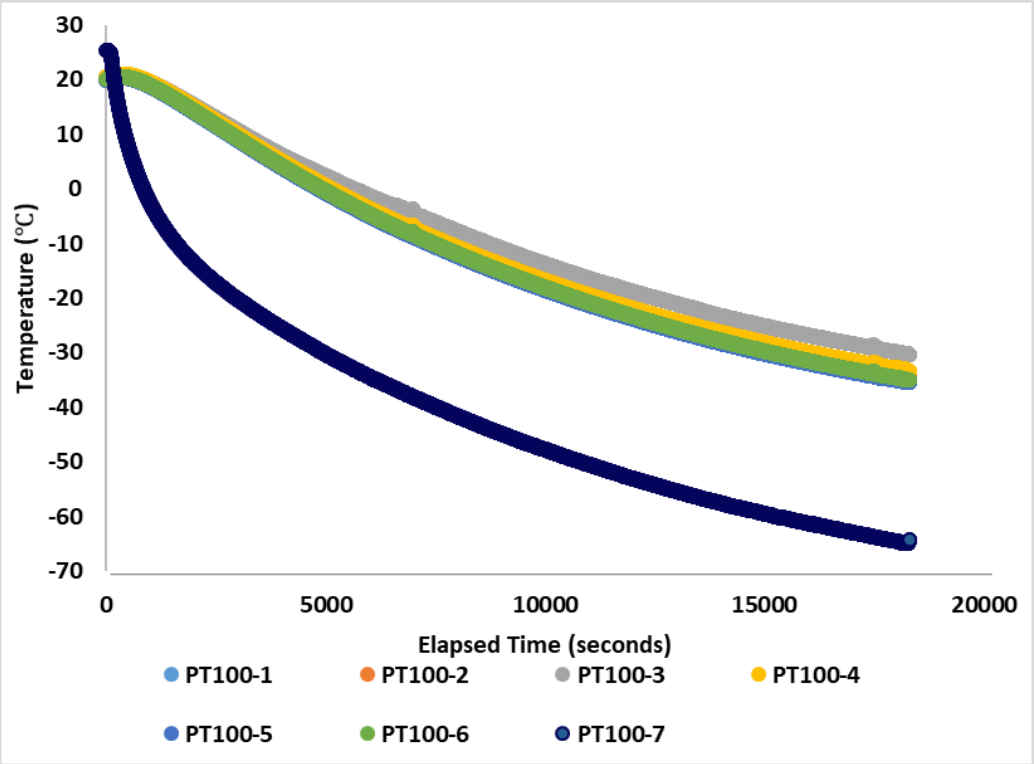

Figure 6.5 Temperature profile for flowing fuel; see Figure 6.1 for temperature points

Fuel samples were taken at intervals for Karl Fischer analysis (adopting the procedure given in ASTM D6304) using a Mettler Toledo C30 coulometer.

Different actions were required on completion of a test run. Typically, the loop was isolated and then drained; the relevant pipe sections were unbolted, so that the mesh strainer and test section of tube could be removed to allow internal inspection and photographs taken of the ice accreted. Since the volumes of ice formed were relatively small, and have low thermal mass, it was important to try to inspect and record observations as quickly as possible.

On completion of testing with one fuel type or mixture, logged data was extracted. Test fuel was drained, and the fuel tank cleaned to prepare for testing the next fuel. This was done to accommodate the limitation of the rig design. It is impossible to drain all the existing fuel unless the rig is completely dismantled to drain and dry. Therefore, the sequence of testing highlighted in 6.2.4.2 was

adopted, so that any old fuel will have less impact on the next fuel/fuel blend to be tested.

6.2.4.2 Systematic set of test conditions

A systematic set of test conditions was proposed and is shown in Table 6.1 and Table 6.2. At least three repeat tests were performed for each test condition. The sequence of testing for sustainable aviation fuels was from 25%, 50% and 100% of the same fuel in a given period. Although the test rig employed for this work is not fully representative of an AFS (fuel tank capacity of 50 L, rig design, and setup), at least it could maintain identical conditions from one test to the next. To maximise ice formation based on the test rig conditions, the flow rate was varied to investigate the effect flow rate has on ice accumulation. The appropriate flow rate for further testing was chosen based on the outcome of the initial test results.

Table 6.1 Phase 1: initial set of test conditions cooling from 20 ℃ to -18 ℃

S/N	Fuel Sample	Fuel type/Category	Blend ratio (CF: SAF)	Flow (m/s)
1	Coryton Jet A-1	Petroleum Derived	100 : 0	1
2	Coryton Jet A-1	Petroleum Derived	100 : 0	0.6
3	Coryton Jet A-1	Petroleum Derived	100 : 0	0.4
4	Coryton Jet A-1	Petroleum Derived	100 : 0	0.2

The primary objective of the phase 2 test campaign was to investigate the effect of fuel type on ice formation. It was also necessary to determine whether ice accumulation may cause a measurable pressure drop across a pump mesh. Cooling rate, flow velocity and pipe surface were all kept constant during these tests.

Table 6.2 Phase 2: influence of fuel composition and flow rate on cooling from 20 ℃ to –18 ℃

s/n	Fuel Sample	Blend ratio (CF : SAF)	Aromatic Content (% v/v)	Density @ +15 °C (kgm^{-3})	Flow (m/s)
1	Coryton Jet A-1	*100 : 0	17.1	796.7	1
2	Coryton Jet A-	*100 : 0	17.1	796.7	0.6
3	Coryton Jet A-1	*100 : 0	17.1	796.7	0.4
4	Coryton Jet A-1	*100 : 0	17.1	796.7	0.2
5	SASOL SPK	***75 : 25	-	761	0.4
6	SASOL SPK	**50 : 50	-	761	0.4
7	SASOL SPK	*0 : 100	2.1	761	0.4
8	HEFA SPK	***75 : 25	-	760	0.4
9	HEFA SPK	**50 : 50	-	760	0.4
10	HEFA SPK	*0 : 100	0.6	760	0.4
11	ATJ	***75 : 25	-	759	0.4
12	ATJ	**50 : 50	-	759	0.4
13	ATJ	*0 : 100	0.5	759	0.4

*Pure fuel to be tested as a baseline
** Additional data to assess any trends between blend ratio and ice formation
***To provide worst-case scenario (max difference in ice formation) for alternative fuels currently approved for use

The pure fuels presented in Table 6.2 are not currently considered satisfactory for aviation service unless blended with conventional fuel or conventional blending components. Aircraft engines are designed to burn only a narrow range of fuels; therefore, using fuels with characteristics that fall outside this range will detract from safety, efficiency, and/or operability. Blending these fuels with conventional Jet A-1 ensures physical fuel properties such as density, volatility, and thermal stability are controlled and conform to detailed requirements; ASTM

D7566 controls the blending limits of these alternative fuels. It is therefore of interest to determine what effect the blending ratio has on ice formation.

6.3 Results

A total of eighty-four individual experiments were carried out to evaluate the effect of various fuel blends on the ice accretion process. The first set of experiments was conducted with Jet A-1, as received, without any water added. The subsequent results were the average of at least three individual experimental runs on a fuel or fuel blend, with a water concentration of approximately 260 ppm. Difficulty was experienced with achieving identical system water concentrations across all tests, and sometimes an individual test exceeded the ±50 ppm tolerance permitted by the EASA test specifications.

Appendix 1 shows unfiltered plots of the pressure differential, across the strainer, against temperature for 100% Jet A-1 with different concentrations of water. The typical form of pressure measurements against temperature are given in Figure 6.6. The plot in Figure 6.6 shows that the pressure upstream of the conical mesh strainer was constant (pressure_1) on cooling from ambient to -35 ℃, but a pressure drop downstream of the strainer was noticed as flow restriction occurred; pressure changes became apparent below -12 ℃ when testing unblended Jet A-1, and at slightly higher temperatures when testing other fuels or fuel blends. However, little impact was noticed on ∆P below approximately -23 °C. The scatter noticed in ΔP of approximately ± 1.5 psi was partly attributed to signal noise from the pressure sensors but also partly due to signal quantization effects related to the resolution of the analogue-to-digital converter. Hence, the results were filtered and fitted to a smoothed curve, as illustrated by the red line in Figure 6.6b below.

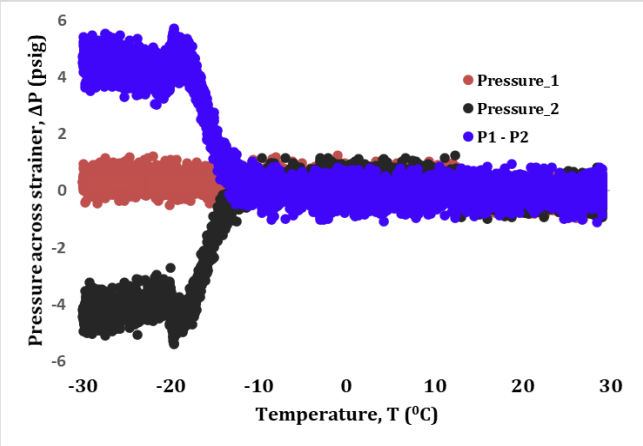

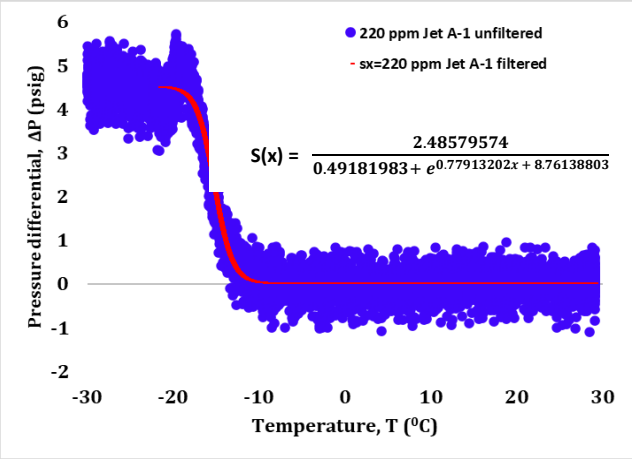

Figure 6.6 a) Typical form of pressure measurement data, showing measurement scatter, for pressures across the strainer with temperature; Pressure_1 was the upstream pressure, Pressure_2 the downstream pressure. Jet A-1 containing 260 ppm water. b) The RH curve illustrates the best fit curve of the pressure difference.

The best fit curve was achieved with the help of the sigmoid activation function using Numerical Python (NumPy). This takes in numbers in any range and returns a positive output. Python is an open-access programming language generally used for data analytics, visualisation, and to solve optimisation problems. For this work, the generalised sigmoid function is given by:

$$s(x) = \frac{a}{b + \exp\ cx + d} \qquad \text{Equation 6-1}$$

To allow for legibility and readability, a generalised sigmoid function was used for all comparative analyses. The sigmoid function helps map the entire number line into a small range (between -1 and +1), as seen in Figure 6.6. The equations for the individual experimental runs are given in Figure D-4.

6.3.1 Influence of stirring effect and fuel flow velocity

Results from some of the experimental runs show that flow restriction due to ice formation increased in the range −6 °C ≥ T ≥ −18 °C. It was difficult to achieve

the same water concentration for every experiment as the measured total water content varied for each experimental run. Figure 6.7a compares the effect of using or not using the stirrer within the fuel tank. In general, bulk fuel stirring led to strainer blockage at higher temperatures, for all fuels tested, compared to tests with no stirring effect.

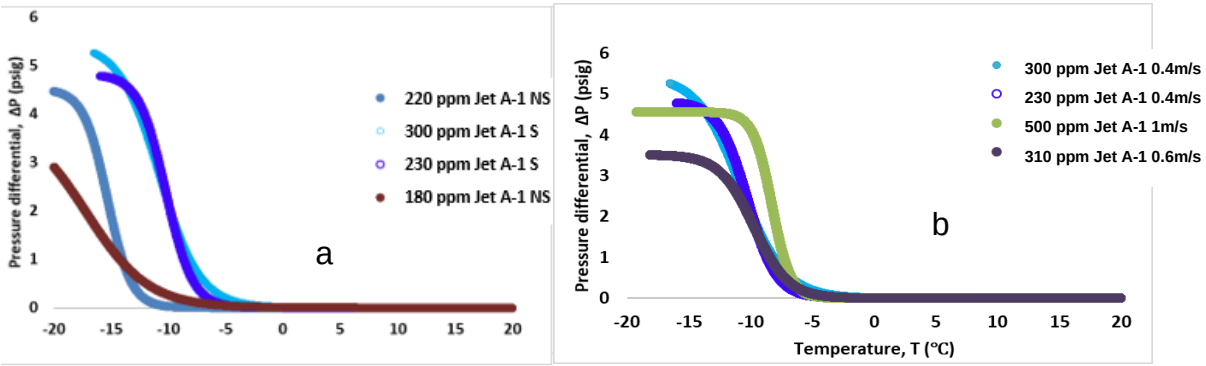

Figure 6.7 a) Jet A-1 containing 260 ppm water. a) ΔP against T with and without stirrer, N and NS respectively; b) ΔP against T for Jet A-1 fuel at different flow velocity

Figure 6.7b shows the effect of velocity on the repeat fuel test. Experiments were conducted at different flow velocities to assess their impact on pump performance, before establishing the ideal test conditions for all other test scenarios. Although AAIB has suggested the flow velocity range to be between 0.2 and 0.6 m/s, testing was conducted at three different flow velocities that are representative of an aircraft in service. The results show that ice accumulation increases at a lower velocity of 0.4 m/s and decreases at high flow velocities of 0.6 m/s and 1 m/s. A flow velocity of 0.4 m/s was therefore adopted for the majority of the rig tests.

6.3.2 Influence of SAF blends

Figures in this section show a repeat set of experiments for the different fuel blends explored in this work. As noted already, it was difficult to achieve the same total water content for individual test runs hence a variation ± 50 ppm water was considered acceptable for this work except for cases that exhibited a lower

blocking potential. Total water content was increased for such cases for comparison purposes. Repeatability was shown to exist with the pressure increase measurement curves shown in Figure 6.8 and Figure 6.9, therefore giving confidence in the data reported. Figure 6.8a and Figure 6.8b show that higher total water content is more likely to create ice rapidly in comparison to lower water contents. Comparing data from 100% Jet A-1 and 100% SPK, it can be seen that the SPK case exhibits a lesser blocking potential even though ice was seen, as illustrated in Figure 6.8a*. The photographs in Figure 6.8a* and b* illustrate that the blocking potential of 100% Jet A-1 at 300 ppm is higher in comparison to that of 100% SPK at 450 ppm. Figure 6.8a shows fuel vapour bubbles forming because of flow restriction, which occurred as a result of pressure differential across the strainer. This can be potentially detrimental as system efficiency has been impaired, which can result in lower fuel flow. In the SPK fuel test, ice was seen to be floating around but without causing any reduction in pressure across the strainer.

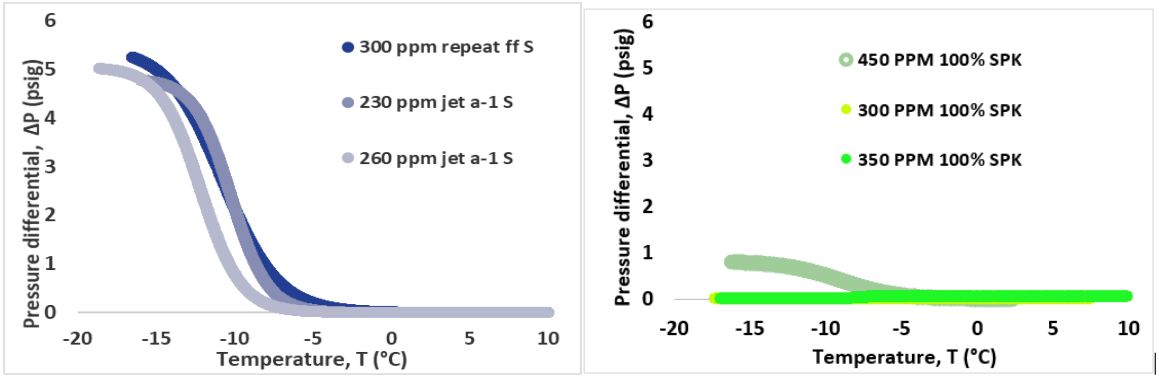

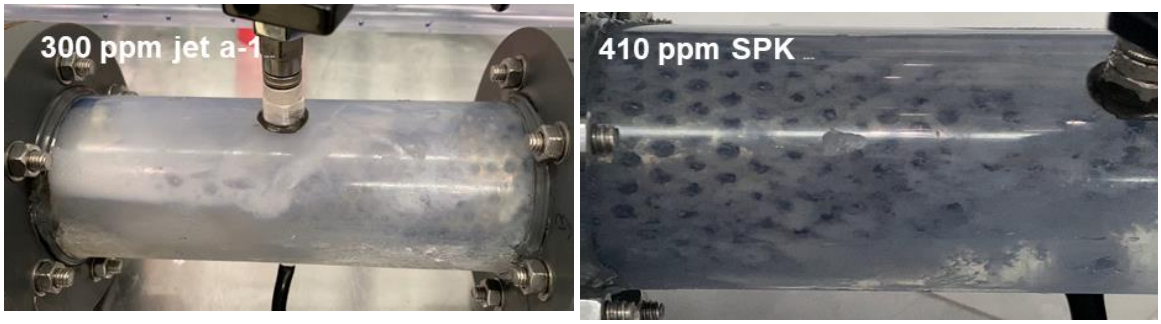

Figure 6.8 Repeat tests of ΔP against T for a) 100% Jet A-1; b) and 100% SPK. Screenshot of mesh section after an icing experiment in; a*) 100% Jet A-1 fuel and b*) 100% SPK fuel

Figure 6.9 shows data from 100% HEFA and ATJ; it can be seen that the HEFA case exhibits a higher blocking potential in comparison to ATJ fuel even though ice is seen as illustrated in Figure 6.9b*. Although ice was seen in the mesh in Figure 6.9b*, it was not enough to cause significant flow restrictions compared to the 100% HEFA and 100% Jet A-1 experimental runs.

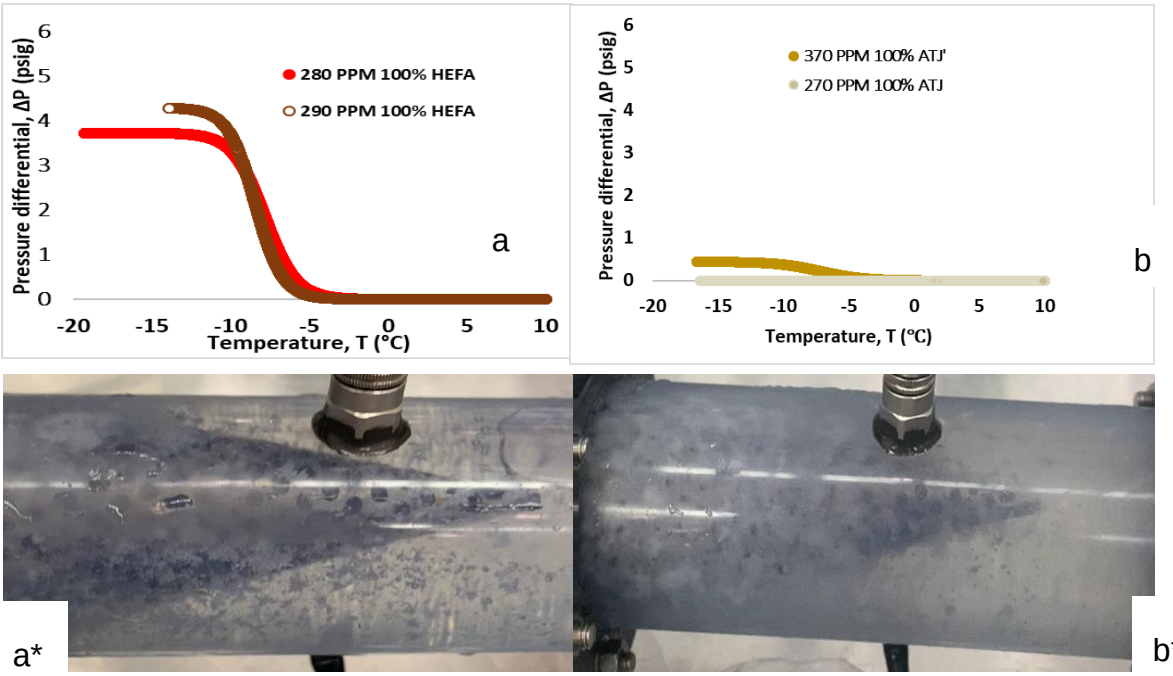

Figure 6.9 Repeat tests of ΔP against T for a) 100% HEFA; and b) 100% ATJ. Screenshot of mesh section after an icing experiment in; a*) 100% HEFA fuel and; b*) 100% ATJ fuel.

Figure 6.10 shows ΔP against T data for all SAF plotted against Jet A-1 fuel in separate plots of 100%, 50% and 25% blends. The comparative plots in Figure 6.10 show that some SAF explored appear to be less problematic from an icing point of view. ATJ shows less propensity towards filter blocking with ice than the other fuels.

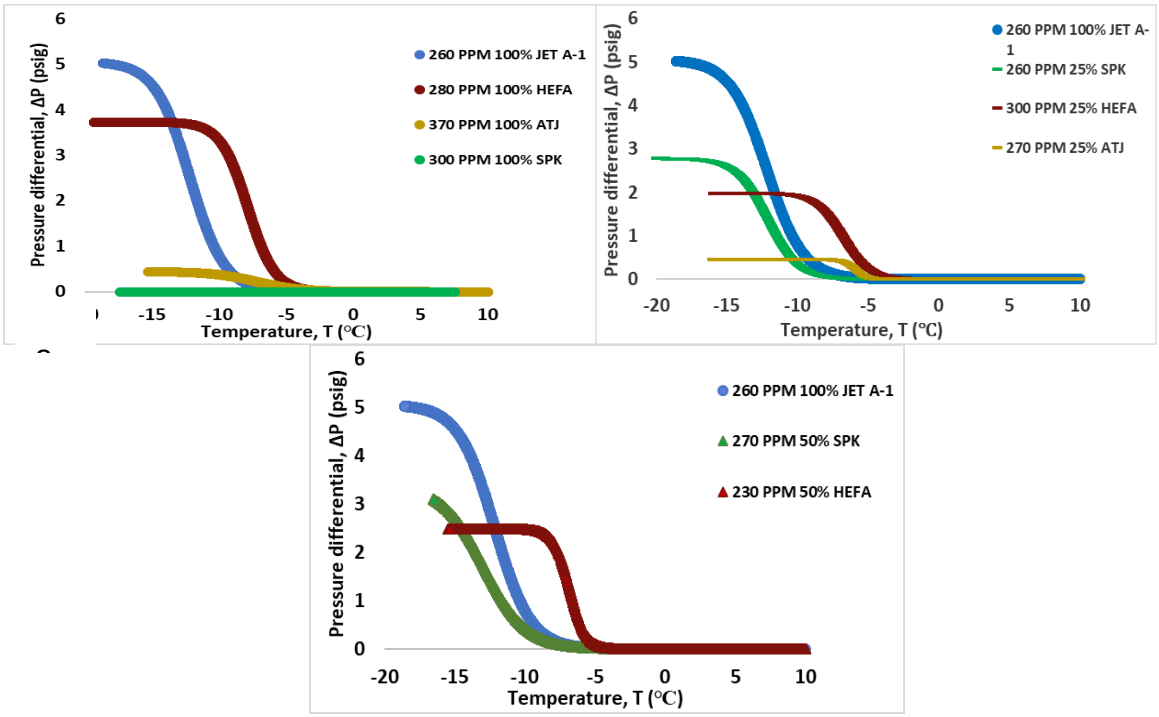

Figure 6.10 Comparative plots of ΔP against T for a) 100% SAF and 100% Jet A-1; and b) 25% SAF and 100% Jet A-1 c) 50% S.AF and 100% Jet A-1

Figure D-2 shows a comparative plot of all blends of a particular fuel type plotted with 100% Jet A-1 fuel. As seen, the ΔP of HEFA reduces on blending with Jet A-1 and increases on blending with SPK.

A bar chart, illustrated by Figure 6.11, helps to shed more light on the ΔP measurements for the different fuels. This chart reveals that all fuels behaved differently as the blending ratio had a different impact on the ΔP at –6 °C and –16 °C. For example, ΔP of HEFA tends to increase on blending with Jet A-1 at a temperature of –6 °C. However, the opposite was the case at –16 °C as ΔP of HEFA was seen to reduce on blending with Jet A-1.

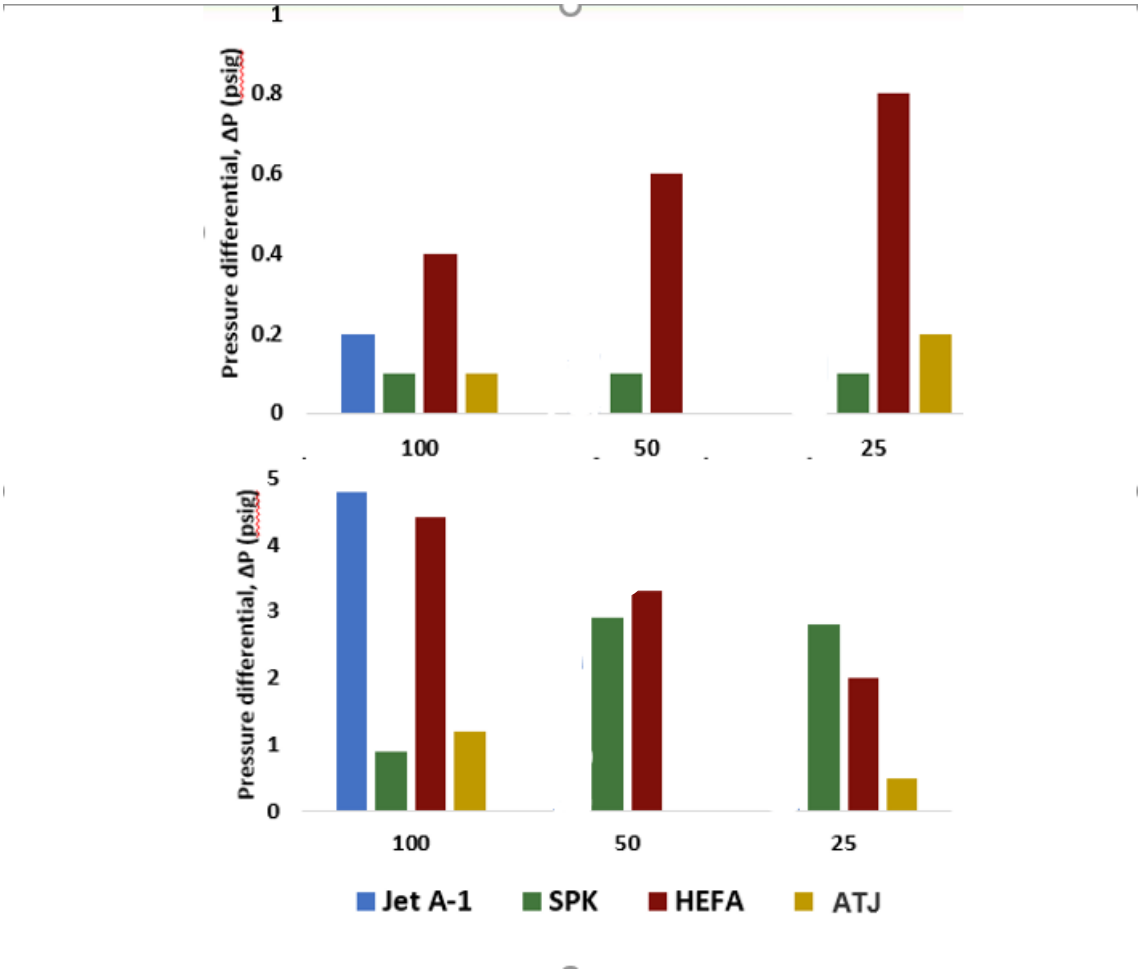

Figure 6.11 a) Average ΔP at -6 °C: SAF and Jet A-1 fuels; b) Average ΔP at -16 °C: for 100%, 75%, 25% blends of SAF and conventional Jet A-1 fuel

Testing does help indicate whether some fuel types pose an increased risk to issues associated with ice formation and blockage of fuel lines. This information is useful as it helps the aerospace industry to predict the temperature ice will start to build up or will potentially lead to blockage in a particular fuel type. Therefore, the availability of this data helps identify potential icing problems in future fuels.

6.4 Discussion

A cold fuel test rig has been developed that attempt to emulate the conditions that might lead to the nucleation of water and ice in an aircraft fuel system. The idea was for these conditions to simulate a worst-case icing scenario and amplify the effect of ice formation so that ice development could be measured and

compared. A typical jet fuel will dissolve around 40 – 70 ppm water at 25° C. At this water concentration, ice crystals will be formed in cold conditions; however, they will be small and hard to detect in an accelerated simulation test and are unlikely to block a filter or strainer. For this reason, the water content for these tests was increased by about six times to 260 ppm, to allow assessment of icing performance within a reasonable timeframe. Stirring of fuel in the bulk tank enhanced the strainer blocking effect as it helps to keep tiny ice crystals in suspension in the fuel. This explains why a greater pressure differential was seen in Figure 6.7a as the mesh collected more floating crystals that had been carried through from the tank to the pipe loop.

Jet fuels are mainly specified to meet certain physical characteristics, but it is known that subtle variations in chemical composition can affect the development and formation of ice in a cold fuel system. It is difficult to isolate the individual contributions from the many constituents in a fuel and, from a practical viewpoint, it is easier to test the overall effect of a new fuel and compare that with a well-characterised benchmark fuel. Apart from chemical composition, factors such as the total water content, distribution of water droplets, thermal gradients and degree of mixing/flow will all play a significant role in ice formation in a cold fuel icing simulation. The tests were designed to evaluate the icing differences between three sustainable aviation fuels and a conventional Jet A-1, and then examine blends of these sustainable fuels with Jet A-1. Other variables that the rig could evaluate included the rate of cooling, the amount of water addition, the effect of bulk fuel stirring and the effect of flow through external pipework. To simplify results evaluation, the cooling profile and nominal water addition were kept constant for all the main tests, but trials were carried out on the effects of bulk fuel stirring and velocity. It should be noted that the rig operates under quasi steady state conditions which means that these results form an internally-consistent data set, but may not be able to predict exactly how and when ice will develop in a particular aircraft fuel system. Novel features of the rig design included a removable pipe section to evaluate the effect of surface finish on

system icing under dynamic conditions and inline test points for fuel sampling by KF analysis.

Observations from the experiments showed that each of the fuels behaved differently after blending with conventional jet fuel. This could be because of the characteristics of the fuel, its molecular structure or level of purity. For instance, Jet A-1 exhibited the greatest potential for ice formation; this is possibly a consequence of its high aromatics content. Whilst the general rule is that oil and water do not mix, nonetheless hydrocarbons and hydrocarbon fuels will absorb small amounts of water from the air, typically in the range 30 – 100 ppm water, until the mixture reaches an equilibrium value depending on the temperature and relative humidity; water uptake is greater at higher temperature and higher relative humidity (relative humidity was not measured for this work). In general terms, the solubility of water in pure hydrocarbons tends to decrease slightly with increasing carbon chain length, but practical experience with commercial fuels has shown that total water content is greater in diesel than in kerosene than in gasoline, i.e., in this case there seems to be a positive correlation with carbon chain length and, indirectly, fuel density. Several studies have emphasised that total aromatics content plays a role in water solubility [2][187][24,83,90,91] in jet fuels, since these species tend to hold about five to eight times more water than equivalent carbon chain length n-alkanes or isoalkanes. However, this is probably not the whole answer since, of the three main hydrocarbon fuel groups, gasoline usually has the highest aromatics content, which implies that fuel density may be a significant factor, particularly in relation to settling rates of tiny water droplets.

Detailed chemical analyses were not undertaken for the fuels used for these tests, but it is possible that water uptake and holdup was influenced by traces of surfactants or polar compounds in the fuel. Some of these materials can be naturally-occurring and are passed through into finished fuel from the crude oil feedstock, but also may be a result of fuel ageing processes or may have been introduced through inadvertent contamination.

Each test condition was performed at least three times to ensure confidence in the data. Various blend ratios of SAF with conventional jet fuel were assessed, as detailed in Table 6.2. Turning to the icing performance of the individual fuels and the blends with Jet A-1, Figure 6.8 and Figure 6.10 show that 100% Jet A-1 seems to precipitate out more ice, hence exhibiting a higher propensity to strainer blockage in comparison to the SPK fuel which shows the lowest. In the SPK fuel test (result illustrated by Figure 6.8b) ice was seen to be floating around the system without causing any flow restriction. This could partly be attributed to its low aromatics content but also partly because of the low free water content to help bond ice crystals. This result agrees with work done by Ugbeh et al assessing the water settling characteristics in SAF [101]. Observations from this study showed that the fully synthetic fuels analysed (SPK and GTL S-8) exhibited the highest water settling rates and also the highest theoretical terminal velocities based on Stokes' law. This implies that the SPK does not hold up water and has a high tendency to shed water quickly. Variations noted in Figure 6.10 could also be attributed to the fact that the quantity of water dissolved in jet fuels is dependent on the hydrocarbon composition of that fuel. This means that the contributing factors by the different chemical characteristics exhibited by each fuel type are all playing a role in the process. These contributing factors could be the chemical composition of the fuel, molecular polarity, purity, aromatics content, or possibly natural surfactants that exists in the fuel.

On the question of bulk fuel velocity in the external pipework, results shown in Figure 6.7 suggest that, at higher flow rates, the soft ice that develops from micron-sized water droplets in cold fuel is being squeezed through the strainer mesh, so that blockage is less likely to occur. Hence, the reason a flow velocity of 0.4 m/s was adopted for the majority of tests, to minimise circulation of small ice crystals.

The peak differential measurements for all fuel types and blends explored is given below in Table 6.3. The peak ΔP of HEFA is noted to reduce with the addition of Jet A-1, whilst the peak ΔP of SPK increased with the addition of Jet A-1 (although it remained below the ΔP of HEFA). The reason for this may be as a result of the

increased aromatics content for the blended SPK fuel; however, it is unclear why a decrease in ∆P was observed for the HEFA case.

Table 6.3 Peak ΔP measurements for all fuel types explored for this work

Fuel type	Blend	Peak ∆P (psi)	T (°C)
1. Jet A-1	100	5.8	-16
2. HEFA	100	5.3	-19
3. SPK : Jet A-1	25 : 75	3.9	-11
4. HEFA : Jet A-1	50 : 50	3.8	-11
5. SPK : Jet A-1	50 : 50	3.5	-15
6. HEFA : Jet A-1	25 : 75	2.9	-13
7. SPK	100	0.9	-20

ATJ data was not included in Table 6.3because the test was conducted with the faulty flow meter and it is unclear why anomalies were noticed hence, repeat experiments are recommended for data validation. For instance, Figure 6.10b* shows a lot of ice formed in the mesh for the synthetic bio-derived fuel (ATJ) test run compared to that of HEFA (as seen in Figure 6.10a*). However, HEFA exhibited a higher ΔP than ATJ as seen in Figure 6.10a and b respectively. From this observation, the authors assumed that finer dissolved water droplets might have formed, yielding a lesser ice accumulation as there is ease of ice passage through the mesh.

Finally, 100% Jet A-1 has the highest ΔP compared to all other fuels as discussed above. Therefore, it is suggested, based on observations from this study, that the SAF will pose less of a safety issue from an icing point of view.

In terms of practical experimentation, the rig performed satisfactorily after some initial minor improvements indicated during the running-in phase. However, some rig design limitations were noticed during the experimental phase:

1) Positioning of the turbine flow meter after the fuel/water introduction point. When the valve of the external fill vessel was opened, air was inadvertently introduced into the system as the fuel/water emulsion level dropped. This caused damage to the blades of the turbine flow sensor due to buffeting from mixed media flow caused by pressure differences and the flow sensor operating outside its specification (unable to handle a two-phase flow of fuel and air bubbles). The flow sensor was replaced with the same model, and a cap (to act as a stopper) was fitted on the flow sensor control valve for calibration purposes; the aim was to achieve approximately the same flow rate for each experimental test run. However, after two experimental runs, similar damage to the turbine blades occurred again. This fault was easily detected as the flow sensor produced a rattling sound and some black debris could be seen in the ice catcher after an icing experiment; also incorrect readings of flow rate were recorded by the data logging system. Typically, when the flow sensor control valve was fully opened, the flow velocity was 1 m/s. The design of a turbine flow sensor is sensitive to turbulence and pressure pulses reflected by the pump; the sensor should be relocated upstream of the fuel/water addition point, to avoid potential damage due to entrained air.

2) Another limitation was the design of the sample points. The concept of using septa-sealed fittings for inline sampling of fuel for KF tests generally worked well and was considered preferable to the previous method used by Airbus which involved draining a small amount of fuel into a beaker and then extracting the sample with a syringe. Viton had been evaluated in lab tests and shown to be generally compatible with jet fuels, for fuel contact periods of a few days. However, one of the limitations of using Viton for the septa seals was that it became much stiffer when the fuel was cold and did not revert to its original shape or size. Also, due to reduced elasticity at low temperatures, the Viton tended not to self-seal when the syringe needle was removed, leading to slight fuel leakage. To overcome this difficulty, a secondary outer septum was fitted, made from silicone

rubber, to form a duplex seal. This permitted reasonably easy insertion of the syringe needle for fuel sampling, whilst maintaining a leak tight joint.

3) The design of the base of the fuel tank was flat which made it difficult to completely drain the system. In addition, it was not possible to quantify the amount of water at the bottom of the fuel tank after each experimental run. Therefore, there is a possibility that some of the water added to the fuel settled out at the bottom of the fuel tank and was not available for ice formation.

6.5 Conclusion and recommendation

A cold fuel test rig was designed to simulate a small-scale aircraft fuel system in service. Ice accretion was characterised by measuring the pressure differential across a conical mesh for the different fuels investigated for this study.

For this work, it was observed that the rate at which ice crystallisation occurs strongly depends on the temperature and type of fuel/fuel blend employed. Results for the fuel combinations tested reveals that 100% conventional fuel, Jet A-1 exhibited the greatest potential for ice formation whilst 100% SPK exhibited the lowest drop in pressure. Furthermore, analysis showed that pressure differential measurements for SAF like HEFA reduced on blending with 75% Jet A-1 whilst the pressure differential measurement of SPK increased after blending with Jet A-1. Thus was attributed to the increased aromatics content for the blended SPK fuel.

This observation could also be attributed to the fact that the quantity of water dissolved in jet fuels is dependent on the hydrocarbon composition of that fuel. However, this may potentially increase the amount of free water to drain in the sump and lead to the need for frequent draining operations. This could lead to an impact on the maintenance policies; therefore, further work is proposed to analyse the bottom of the tank after an individual experimental run. For this work, repeatability was seen to exist quantitatively with experimental runs, hence providing confidence in the data generated. Additionally, data reveals that the

rate at which ice crystallisation occurs strongly depends on the temperature and type of fuel/fuel blend employed. Therefore, to achieve the target of introducing an entirely new sustainable fuel composition, it is significant to understand the effect of icing characteristics on the existing SAF types.

Therefore, experimental results from this work will help the aerospace industry predict the temperature ice will start to build up or potentially lead to blockage in a particular fuel type and help to understand the ice accretion process in various flowing SAF. Further recommendations for future work are investigating the role surfaces and flowrate play on the accretion and release of ice in different SAF blends, then measuring the mass of ice accreted on the strainer mesh at the end of each experiment. Finally, it is recommended to determine and compare the strength of ice to the surface by the different fuel blends.

7 Chapter 7 Overall Discussion: Implementation of the work

The mechanics of how water and ice behave in jet fuel is still extremely problematic; therefore, the aim of this work was to examine jet fuel constituents and the influence of new fuel composition on the behaviour of water and ice in aircraft fuel systems. The following research objectives were set to achieve this aim.

RO 1. A critical review of the key complexities associated with jet fuel and nucleation of water and ice in aircraft fuel systems

RO 2. Investigation of the effects of hygroscopicity/water-shedding and corresponding water droplet size distribution for various fuel blends

RO 3. Critical analysis of the effects of fuel constituents on the water droplet size distribution in different fuel blends

RO 4. Test campaign to investigate ice formation with various fuel blends - create empirical models of ice formation and pressure drops across strainer mesh

Accordingly, based on the knowledge gaps identified in chapter 2, what will be the impact of sustainable jet fuel and its blends on ice formation, size, and frequency distribution of dispersed water droplets in aircraft fuel systems? Does the theoretical assumption about droplet size/frequency distribution in jet fuel being governed by shearing conditions agree with experimental data? How will jet fuel composition influence the rate of water-shedding under realistic and representative test conditions? How will an increased blending portion with conventional jet fuel of the synthesised fuels approved to ASTM D7566 affect this water-shedding rate? All the questions listed in chapter 1 are set out as RO 2, 3 and 4. The contributions highlighted in chapters 3 to 6 have bridged the gap identified.

Contributions from chapter 3 highlighted that the water settling experiment indirectly measures the presence of surfactants in jet fuels. Additionally, some

alternative fuels (GTL S-8, HEFA and ATJ) proved to be good candidates for increased blending portion with Jet A-1 in terms of water droplet rejection from suspension. Research findings from chapter 3 proposed further work to establish the particle size distribution of water droplets in jet fuels and alternative fuels at a given period, leading to chapters 4 and 5. Work described in chapter 4 established the droplet size distribution of an emulsion produced from an ultrasonic bath and high shear mixing. Data in Chapter 4 also helps expand knowledge of improved quantification of measurements of dispersed water droplets in aviation fuel. It also helps identify that the HSM was the best shearing method for producing a worst-case scenario emulsion to help with data quantification. Therefore, findings from work in chapter 4 influenced the decision to opt for the HSM in establishing the DSD of SAF presented in chapter 5. Contributions from chapter 5 provide the aviation industry with vital insight into the behaviour of dispersed water droplets in various commercially available sustainable aviation fuels. The data and statistics presented in chapter 5 also reveal that water droplet size/count distribution can be influenced by fuel composition. Research findings from chapter 5 recommended further work be carried out at different blending ratios of sustainable fuels and temperatures (specifically cold temperatures- to simulate high altitudes as presented in chapter 6).

Contributions from chapter 6 reveal the effect of sustainable aviation fuel and/or its blends on ice formation and pressure drops across strainer mesh in aircraft fuel systems (AFS). The data presented in chapter 6 is essential to establish confidence in the safe operation of future AFS that will potentially be compatible with 100 % SAF. This information is useful as it helps the aerospace industry to predict the temperature ice will start to build up or potentially lead to blockage in a particular fuel type. Hence, considerations for these can help control potential icing problems. Additionally, the data provided establishes whether ice accumulation on a pump mesh may result in a measurable pressure drop across it.

8 Chapter 8 Conclusions and Future Work

8.1 Conclusion

This study presents a detailed account of some of the complexities associated with jet fuel chemistry on the effects of water and ice in aircraft fuel systems. The research findings from this work identified and bridged knowledge gaps in the literature that will improve understanding about conditions that may exacerbate free water drop-out, ice accretion, and ice formation in flowing fuel.

Previous studies have shown that the presence of surfactants can have an adverse effect on filter separators since they may affect the water separation characteristics. Therefore, in chapter 3, it was suggested that an intermolecular factor should be considered in addition to the Stoke's law variables (radius, density, and viscosity), as this is linked to the presence of surfactants. This work deduced that the water settling rate indirectly measures the presence of surfactants in jet fuels. In terms of water droplet rejection from suspension, GTL S-8, HEFA and ATJ have proven to be good candidates for increased blending portion with Jet A-1.

Findings from chapter 4 revealed experimentally that water droplet size/count distribution is influenced by the type of shearing/mechanical agitation. In this case, mild shearing conditions (HSM) could help promote droplet coalescence, leading to a better separation ability. From a higher energy input to medium energy input, DSD changed significantly in terms of mean values and higher skewness and kurtosis values.

The data provided in chapter 5 established that water droplet size/count distribution is sensitive to changes in fuel composition as synthetic jet fuels - GTL S-8, SASOL and HEFA - exhibit good water separation ability like conventional jet fuel. This is consistent with previous work conducted on the water settling ability of various jet fuels [4,10,24]. Fuel with a higher settling rate is beneficial to the industry as this indicates a good separation ability, consequently promoting the settling of water to the sump. Synthetic fuels presented higher droplet counts, and lower skew and kurtosis values compared to the biofuels, which mean they

tend to form unstable emulsions. Bio-jet fuels explored for this work - ATJ and Farnesane - formed stable emulsions and hence exhibited poor water separation. These findings informed design of an ice test rig to simulate an aircraft in service. Ice accretion was characterised by measuring the pressure differential across a conical mesh for the different SAF employed for this study. Observations revealed that 100% Jet A-1 exhibited a higher propensity to strainer blockage whilst 100% SPK exhibited the lowest drop in pressure. This might be attributed to the fact that the quantity of water dissolved in jet fuels is dependent on the hydrocarbon composition of that fuel. However, greater water drop-out may potentially increase the amount of free water to be drained from tank sumps and lead to the need for more frequent draining operations. This could impact aircraft maintenance policies; therefore, further work is proposed to analyse the bottom of the tank after an individual experimental run.

Additionally, data reveals that the rate at which ice crystallisation occurs strongly depends on the temperature and type of fuel/fuel blend employed. It is significant to understand the effect of icing characteristics of the existing SAF types before introduction of an entirely new sustainable fuel composition. Experimental results from this work will help the aerospace industry predict the conditions that ice will start to build up or potentially lead to blockage in a particular fuel type and help gain a better understanding of the ice accretion process in various flowing SAF.

8.2 Future work

- A key recommendation for future work is to investigate the role surfaces and flowrate play on the accretion and release of ice in different SAF blends and compare this with the mass of ice accreted on the strainer mesh at the end of each experiment. It would be beneficial to devise an experiment to determine and compare the strength of ice adhesion to fuel system surfaces for the different fuel blends.
- This study proposes implementing a hydrophobic/superhydrophobic coating strategy alongside a de-icing strategy in future aircraft fuel systems

design. This serves as a basis for design guidelines to minimise ice formation within an aircraft fuel system and formulate possible solutions to prevent future occurrence of fuel system blockage due to ice.

- From an experimental viewpoint, it would be interesting to establish if water droplets in fuel tend to grow after a given period before dropping out. Hence a more representative experiment would be needed to study the particle size distribution of water droplets in jet fuels after a given time. This could be achieved by positioning the test system emulsion outlet to a separate container, measuring particle diameters at a particular time to draw up a settling rate curve and comparing the results for different fuels.

- If the value of n can be established, a hindered settling velocity for water droplets could be formulated using the Richardson and Zaki equation. Further research could be carried out to develop a new empirical model to account for hindered water droplets settling. Also, it is suggested that an independent experimental data set should be collected to validate the model formulated in this study.

- It is recommended that MSEP tests be conducted on the fuels explored for this study for comparison. Additionally, further research should be carried out to calculate the Ostwald ripening coefficient for all fuels explored to establish how extensively it occurs.

- In observational studies reported in the literature, there is still a potential for bias regarding the most widely used water content determination method. Several authors have concluded that Karl Fischer's analysis is not an entirely reliable technique. Due to the low water concentrations being measured, there is a need to benchmark this procedure to see if there is any consistent offset that requires a correction factor.
- Providing sufficient relevant fuel system icing data can be accumulated, development of a computer-based tool for multivariable analysis and modelling is recommended to accurately reflect the randomness and

interdependence of aircraft fuel system icing and make more accurate predictions about icing susceptibility with different fuels or fuel blends.

REFERENCES

[1] CRC, CRC 663 - Handbook Aviation Fuels, Alpharetta, GA 30022, 2014.

[2] S. Baena, S.L. Repetto, C.P. Lawson, .-W Lam, Behaviour of Water in Jet Fuel A Literature Review, Prog. Aerosp. Sci. 60 (2013) 35–44.

[3] E. Stoyanov, C.A.R. Irina V. Stoyanova, The Basicity of Unsaturated Hydrocarbons as probed by H-Bond Acceptor Ability. Bifurcated N–H+···π Hydrogen Bonding, Natl. Inst. Heal. 61 (2008) 515–525. https://doi.org/10.1002/chem.200800337.The.

[4] A.. Crampton, R.. Finn, J.. Kolfenbach, What happens to the dissolved water in Aviation fuel?, SAE Summer Meet. (1953).

[5] Federal Aviation Administration, Aviation Maintenance Technician Handbook-General, U.S. Department of Transportation, Oklahoma City, 2018. https://www.faa.gov/regulations_policies/handbooks_manuals/aircraft/amt_airframe_handbook/media/amt_airframe_vol2.pdf.

[6] K. Libbrecht, Morphogenesis on Ice: The Physics of Snow Crystals, Eng. Sci. 64 (2001) 10–19.

[7] B.J. Murray, S.L. Broadley, T.W. Wilson, S.J. Bull, R.H. Wills, H.K. Christenson, E.J. Murray, Kinetics of the homogeneous freezing of water, Phys. Chem. Chem. Phys. (2010) 10380–10387. https://doi.org/10.1039/C003297B.

[8] B.J. Murray, S.L. Broadley, G.J. Morris, Supercooling of water droplets in jet aviation fuel, Fuel. 90 (2011) 433–435. https://doi.org/10.1016/j.fuel.2010.08.018.

[9] S. Baena, C.P. Lawson, J.K. Lam, Cold Fuel Test Rig To Investigate Ice Accretion on Different Pump Inlet Filter-Mesh Screens, ICAS 2012 28th Int. Congr. Aeronaut. Sci. (2012) 11.

[10] S.J. Cox, S.M. Kathmann, B. Slater, A. Michaelides, Peeling back the layers: a molecular dynamics investigation into heterogeneous ice nucleation, ArXiv:1501.01883v1. 184705 (2015) 1–7.

[11] S.L. Repetto, J.F. Costello, D. Parmenter, Current and Potential Aviation Additives for Higher Biofuel Blends in Jet A-1, in: C.J. Chuck (Ed.), Biofuels Aviat., Elsevier, Bath, 2016: pp. 261–275. https://doi.org/10.1016/B978-0-12-804568-8.00011-1.

[12] A.Q. Clark, A.G. Smith, S. Threadgold, S.E. Taylor, Dispersed Water and Particulates in Jet Fuel: Size Analysis under Operational Conditions and Application to Coalescer Disarming, Ind. Eng. Chem. Res. 50 (2011) 5749–5765. https://doi.org/10.1021/ie102533e.

[13] S. Naya, R. Cao, M. Francisco-Fernández, J. Tarrío-Saavedra, H. Brage, C. Cancelo, Estimating water and solid impurities in jet fuel from ISO codes, Energy and Fuels. (2013). https://doi.org/10.1021/ef401378z.

[14] ASTM D6469, Standard Guide for Microbial Contamination in Fuels and Fuel Systems, (2017).

[15] J. Bwapwa, A. Anandraj, C. Trois, Possibilities for conversion of microalgae oil into aviation fuel: A review, Renew. Sustain. Energy Rev. 80 (2017) 1345–1354. https://doi.org/https://doi.org/10.1016/j.rser.2017.05.224.

[16] L. Lao, C. Ramshaw, H. Yeung, M. Carpenter, J. Lam, S. Barley, Behaviour of Water in Jet Fuel in a Simulated Tank, SAE Int. (2011). https://doi.org/10.4271/2011-0102794.

[17] S. Baena, J. Lam, C. Lawson, Dimensional Analysis to Parameterise Ice Accretion on Mesh Strainers, SAE Int. (2011). https://doi.org/10.4271/2011-012795.

[18] T.C. Maloney, The Collection of Ice in Jet A-1 Fuel Pipes, Rutgers, The State University of New Jersey, 2012.

[19] M. Schmitz, G. Schmitz, Experimental study on the accretion and release

of ice in aviation jet fuel, Aerosp. Sci. Technol. 82–83 (2018) 294–303. https://doi.org/10.1016/j.ast.2018.08.034.

[20] T.C. Maloney, F.J. Diez, T. Rossmann, Ice accretion measurements of Jet A-1 in aircraft fuel lines, Fuel. 254 (2019) 115616. https://doi.org/10.1016/j.fuel.2019.115616.

[21] V.L. Zherebtsov, M.M. Peganova, Water solubility versus temperature in jet aviation fuel, Fuel. (2012). https://doi.org/10.1016/j.fuel.2012.06.070.

[22] J.K.-W. Lam, M.D. Carpenter, C. Williams, J. Hetherington, WAFCOLT – Water in Aviation Fuel Under Cold Temperature Conditions, 2013. https://www.easa.europa.eu/sites/default/files/dfu/EASA_WAFCOLT_Final_Report_v2_signed.pdf.

[23] A. Charro, S. Baena, J.K. Lam, Water Solubility in Different Alternative Jet Fuels : A Comparison with Petroleum-Based Jet Fuel, (2015). https://doi.org/10.4271/2015-01-2563.

[24] Z.J. West, T. Yamada, C.R. Bruening, R.L. Cook, S.S. Mueller, L.M. Shafer, M.J. Dewitt, S. Zabarnick, Investigation of Water Interactions with Petroleum-Derived and Synthetic Aviation Turbine Fuels, Am. Chem. Soc. ACS; Energy Fuels. (2018). https://doi.org/10.1021/acs.energyfuels.7b02844.

[25] C. Marche, C. Ferronato, J.-C. De Hemptinne, J. Jose, Apparatus for the Determination of Water Solubility in Hydrocarbon: Toluene and Alkylcyclohexanes (C 6 to C 8) from 30 °C to 180 °C, J. Chem. Eng. Data. 51 (2006) 355–359. https://doi.org/10.1021/je0502041.

[26] J.I. Hileman, D.S. Ortiz, J.T. Bartis, H.M. Wong, P.E. Donohoo, M.A. Weiss, I.A. Waitz, Near-Term Feasibility of Alternative Jet Fuels, Massachusetts, 2009. http://www.atac.ca/web/images/atac/files/Members_Only/Les_Alders/Technical_Operations_Engineering_Maintenance/Issues/2010_AGM_-

altfuelfeasrpt.pdf.

[27] N. Yilmaz, A. Atmanli, Sustainable alternative fuels in aviation, Energy. (2017). https://doi.org/10.1016/j.energy.2017.07.077.

[28] B. Kärcher, The importance of contrail ice formation for mitigating the climate impact of aviation, J. Geophys. Res. Atmos. 121 (2016) 3497–3505. https://doi.org/10.1002/2015JD024696.

[29] R.H. Moore, M. Shook, A. Beyersdorf, C. Corr, S. Herndon, W.B. Knighton, Miake-Lye, Influence of jet fuel composition on aircraft engine emissions: A synthesis of aerosol emissions data from the NASA APEX, AAFEX, and ACCESS missions., Energy & Fuels. 29 (2015) 2591-2600.

[30] K.T. Hari, Z. Yaakob, N.N. Binitha, Aviation biofuel from renewable resources: Routes, opportunities and challenges, Renew. Sustain. Energy Rev. (2015). https://doi.org/10.1016/j.rser.2014.10.095.

[31] ASTM D7170, Standard Test Method for Determination of Derived Cetane Number (DCN) of Diesel Fuel Oils—Fixed Range Injection Period, Constant Volume Combustion Chamber Method, 2016. https://extranet.cranfield.ac.uk/EDIT/,DanaInfo=compass.astm.org,SSL+html_annot.cgi?D7170+16.

[32] Air BP, Air BP HANDBOOK OF PRODUCTS, Hertfordshire, 2000. https://www.fmv.se/FTP/Drivmedel 2016/datablad/M0754-233000_Avgas_100_LL.pdf.

[33] S. Dooley, S. Hee_Won, M. Chaos, J. Heyne, J. Yiguang, L.D. Frederick, K. Kama, S. Chih-Jen, W. Haowei, M. A.Oehlschlaeger, R. J.Santorod, A.L. Thomas, A jet fuel surrogate formulated by real fuel properties, Combust. Flame. 157 (2010) 2333–2339. https://doi.org/https://doi.org/10.1016/j.combustflame.2010.07.001.

[34] C. Zhang, X. Hui, Y. Lin, C.J. Sung, Recent development in studies of alternative jet fuel combustion: Progress, challenges, and opportunities,

Renew. Sustain. Energy Rev. 54 (2016) 120–138. https://doi.org/10.1016/j.rser.2015.09.056.

[35] W.C. Wang, L. Tao, Bio-jet fuel conversion technologies, Renew. Sustain. Energy Rev. 53 (2016) 801–822. https://doi.org/10.1016/j.rser.2015.09.016.

[36] D.N. K. Lokesh, V. Sethi, T. Nikolaidis, E. Goodger, Life cycle greenhouse gas analysis of biojet fuels with a technical investigation into their impact on jet engine performance, Biomass Bioenergy. (2015) 26–44. https://doi.org/https://doi.org/10.1016/j.biombioe.2015.03.005.

[37] T. Pray, J. Pramanik, D. McPhee, J. Galazzo, K. Reiling, J Cherry, L.N. Renninger, Amyris integrated biorefinery operations for domestic renewable diesel and chemical production, in: Proc. 32nd Symp. Biotechnol. Fuels Chem., Clearwater Beach FL, 2010.

[38] A. Zschocke, S. Scheuermann, J. Ortner, High biofuel blends in aviation (HBBA), Interim Report, ENER C. 2 (2017) 420–421.

[39] K.P. Brooks, L.J. Snowden-Swan, S.B. Jones, M.G. Butcher, G.-S.J. Lee, D.M. Anderson, J.G. Frye, J.E. Holladay, J. Owen, L. Harmon, F. Burton, I. Palou-Rivera, J. Plaza, D. R.Handler, Shonnard., Low-Carbon Aviation Fuel Through the Alcohol to Jet Pathway, in: C.J. Chuck (Ed.), Biofuels Aviat., Elsevier, 2016: pp. 109–150. https://doi.org/10.1016/B978-0-12-804568-8.00006-8.

[40] A. de Klerk, Aviation Turbine Fuels Through the Fischer–Tropsch Process, in: Biofuels Aviat., Elsevier, Edmont on, 2016: pp. 241–259. https://doi.org/10.1016/B978-0-12-804568-8.00010-X.

[41] S. Raikova, C.D. Le, J.L. Wagner, V.P. Ting, C.J. Chuck, Towards an Aviation Fuel Through the Hydrothermal Liquefaction of Algae, in: science direct (Ed.), Biofuels Aviat., Elsevier, Bath, 2016: pp. 217–239. https://doi.org/10.1016/B978-0-12-804568-8.00009-3.

[42] J. Holladay, Z. Abdullah, J. Heyne, Sustainable Aviation Fuel: Review of Technical Pathways, 2020. https://doi.org/10.2172/1660415.

[43] AAIB, Report on the accident to Boeing 777-236ER, G-YMMM, at London Heathrow Airport on 17 January 2008, Technical Report, 2010. https://assets.publishing.service.gov.uk/media/5422f3dbe5274a1314000495/1-2010_G-YMMM.pdf.

[44] S. Baena, J. Lam, C. Lawson, Effects of Ice Accretion in an Aircraft Protective Mesh Strainer of a Fuel Pump, SAE Tech. Pap. (2015). https://doi.org/doi:10.4271/2015-01-2449.

[45] W. Zhang, D.J. Webb, M. Carpenter, C. Williams, Measuring water activity of aviation fuel using a polymer optical fiber Bragg grating, in: 23rd Int. Conf. Opt. Fibre Sensors, 2014: p. 91574. https://doi.org/10.1117/12.2059273.

[46] J.K.W. Lam, L. Lao, D.W. Hammond, J.P. Power, Character and interface shear strength of accreted ice on subcooled surfaces submerged in fuel, Aeronaut. J. 119 (2015) 1377–1396. https://doi.org/10.1017/S0001924000011301.

[47] C. Antonini, M. Innocenti, T. Horn, M. Marengo, A. Amirfazli, Understanding the effect of superhydrophobic coatings on energy reduction in anti-icing systems, Cold Reg. Sci. Technol. 67 (2011) 58–67. https://doi.org/10.1016/j.coldregions.2011.02.006.

[48] R. Zhang, P. Hao, X. Zhang, F. He, Supercooled water droplet impact on superhydrophobic surfaces with various roughness and temperature, Int. J. Heat Mass Transf. 122 (2018) 395–402. https://doi.org/10.1016/j.ijheatmasstransfer.2018.01.076.

[49] J.W. Elliott, F.T. Smith, Ice formation on a smooth or rough cold surface due to the impact of a supercooled water droplet, J. Eng. Math. 102 (2017) 35–64. https://doi.org/10.1007/s10665-015-9784-z.

[50] A. Work, Y. Lian, A critical review of the measurement of ice adhesion to solid substrates, Prog. Aerosp. Sci. 98 (2018) 1–26. https://doi.org/10.1016/j.paerosci.2018.03.001.

[51] Rolls-Royce, The Jet Engine, 5th ed., Rolls-Royce plc, Derby, 1996.

[52] J.E. Shepherd, C.D. Nuyt, J.J. Lee, J.E. Woodrow, Flash Point and Chemical Composition of Aviation Kerosene (Jet A), (2000).

[53] P. Vozka, G. Kilaz, A review of aviation turbine fuel chemical composition-property relations, Fuel. 268 (2020) 117391. https://doi.org/10.1016/j.fuel.2020.117391.

[54] IATA, IATA Sustainable Aviation Fuel Roadmap, 1st Edition, International Air Transport Association, Switzerland, 2015.

[55] M. Samavati, M. Santarelli, A. Martin, V. Nemanova, Production of Synthetic Fischer–Tropsch Diesel from Renewables: Thermoeconomic and Environmental Analysis, Energy & Fuels. 32 (2018) 1744–1753. https://doi.org/10.1021/acs.energyfuels.7b02465.

[56] J.C. Serrano-Ruiz, J.A. Dumesic, Catalytic routes for the conversion of biomass into liquid hydrocarbon transportation fuels, Energy Environ. Sci. 4 (2011) 83–99. https://doi.org/10.1039/C0EE00436G.

[57] L. Brennan, P. Owende, Biofuels from microalgae—A review of technologies for production, processing, and extractions of biofuels and co-products, Renew. Sustain. Energy Rev. 14 (2010) 557–577. https://doi.org/10.1016/j.rser.2009.10.009.

[58] T.J. Lundquist, I.C. Woertz, N.W.T. Quinn, J.R. Benemann, A realistic technology and engineering assessment of algae biofuel production, Energy Biosci. Inst. (2003) 1–178. https://www.scopus.com/record/display.uri?eid=2-s2.0-84870576931&origin=inward&txGid=96091faa5cd3b4892aa433d4df0efd53.

[59] M.A. Clarke, The Evolution of Military Aviation, Natl. Acad. Eng. (2008).

[60] ASTM D7566, Standard Specification for Aviation Turbine Fuel Containing Synthesized Hydrocarbons 1, (2016). https://doi.org/10.1520/D7566-16B.

[61] B. Saynor, A. Bauen, M. Leach, The Potential for Renewable Energy Sources in Aviation, London, 2003. https://www.imperial.ac.uk/media/imperial-college/research-centres-and-groups/icept/7294712.PDF.

[62] ASTM D4175, Standard Terminology Relating to Petroleum, Petroleum Products, and Lubricants, (2014).

[63] J. Solash, R.. Hazlett, J.M. Hall, C.J. Nowack, Relation between fuel properties and chemical composition, Fuel. 57 (1978) 521–528. https://doi.org/10.1016/0016-2361(78)90036-4.

[64] ASTM D6379, Standard Test Method for Determination of Aromatic Hydrocarbon Types in Aviation Fuels and Petroleum Distillates—High Performance Liquid Chromatography Method with Refractive Index Detection, (2011).

[65] R. John, F. Obaid, L. Fernando, I. Lisa, C. Mario, Toxicological profile for Jp-5, Jp-8, AND Jet A Fuels, Atlanta, 2017. https://www.atsdr.cdc.gov/ToxProfiles/tp121.pdf.

[66] ASTM D7039, Standard Test Method for Sulfur in Gasoline, Diesel Fuel, Jet Fuel, Kerosine, Biodiesel, Biodiesel Blends, and Gasoline-Ethanol Blends by Monochromatic Wavelength Dispersive X-ray Fluorescence Spectrometry, (2015).

[67] I. LEE, H. UBANYIONWU, Determination of sulfur contaminants in military jet fuels, Fuel. 87 (2008) 312–318. https://doi.org/10.1016/j.fuel.2007.05.010.

[68] CRC, Handbook of aviation fuel properties, (1983).

[69] H. Tang, F. Chen, G. Li, X. Yang, Y. Hu, A. Wang, Y. Cong, X. Wang, T. Zhang, N. Li, Synthesis of jet fuel additive with cyclopentanone, J. Energy Chem. 29 (2019) 23–30. https://doi.org/10.1016/j.jechem.2018.01.017.

[70] C. Falter, V. Batteiger, A. Sizmann, Climate Impact and Economic Feasibility of Solar Thermochemical Jet Fuel Production, Environ. Sci. Technol. 50 (2016) 470–477. https://doi.org/10.1021/acs.est.5b03515.

[71] B. Gawron, T. Białecki, Impact of a Jet A-1/HEFA blend on the performance and emission characteristics of a miniature turbojet engine, Int. J. Environ. Sci. Technol. 15 (2018) 1501–1508. https://doi.org/10.1007/s13762-017-1528-3.

[72] ASTM D1655, Standard Specification for aviation turbine fuels., 2019. https://doi.org/10.1520/D1655-17A.

[73] (IATA) International Air Transport Association, Annual review 2018, Sydney, 2018. https://www.iata.org/publications/Documents/iata-annual-review-2018.pdf.

[74] J. Hileman, H.M. Wong, D. Ortiz, A.M.R. N. Brown, Lourdes Q. Maurice, The Feasibility and Potential Environmental Benefits of Alternative Fuels for Commercial Aviation, in: the 26th I.C. of the A. Sciences (Ed.), Proc. 26th Int. Congr. Aeronaut. Sci., Alaska, 2008: pp. 5–9.

[75] M.I. ElGalad, K.M. El- Khatib, E. Abdelkader, R. El-Araby, G. ElDiwani, S.I. Hawash, Empirical equations and economical study for blending biofuel with petroleum jet fuel, J. Adv. Res. 9 (2018) 43–50. https://doi.org/10.1016/j.jare.2017.10.005.

[76] A.C. McCoy, M.J. Duran, A.M. Azad, S. Chattopadhyay, M.A. Abraham, Performance of sulfur tolerant reforming catalysts for production of hydrogen from jet fuel simulants, Energy and Fuels. (2007). https://doi.org/10.1021/ef070111k.

[77] E. Nygren, K. Aleklett, M. Höök, Aviation fuel and future oil production

scenarios, Energy Policy. 37 (2009) 4003–4010. https://doi.org/10.1016/j.enpol.2009.04.048.

[78] S. Blakey, R. Lucas, W.W. Christopher, Aviation gas turbine alternative fuels: A review, Proc. Combust. Inst. 33 (2011) 2863–2885. https://doi.org/10.1016/j.proci.2010.09.011.

[79] L.. Maurice, H. Lander, T. Edwards, W.. Harrison, Advanced aviation fuels: A look ahead via a historical perspective, Fuel. 80 (2001) Pages 747-756. 10.1016/S0016-2361(00)00142-3.

[80] S. Leonard, Above & Beyond: Fire and Ice, AIR Sp. Mag. (2010). https://www.airspacemag.com/military-aviation/above-and-beyond-fire-and-ice-58712306/.

[81] AAIB, Bulletin: Field Investigation on Cessna 525 Citation Jet at London Gatwick Airport on 31 October 2013 at 1820 hrs, Berkshire, 2014. https://www.gov.uk/government/uploads/system/uploads/attachment_data/file/391225/AAIB_Bulletin_4-2014.pdf.

[82] W. Zhang, D.J. Webb, M. Carpenter, C. Williams, Measuring water activity of aviation fuel using a polymer optical fiber Bragg grating, in: J.M. López-Higuera, J.D.C. Jones, M. López-Amo, J.L. Santos (Eds.), 23rd Int. Conf. Opt. Fibre Sensors, 2014: p. 91574V. https://doi.org/10.1117/12.2059273.

[83] M.D. Carpenter, J.I. Hetherington, L. Lao, C. Ramshaw, H. Yeung, J. K-W Lam, S. Masters, S. Barley, Behaviour of Water in Aviation Fuels at Low Temperatures, in: Int. Conf. Stability, Handl. Use Liq. Fuels, 2011.

[84] C.G. Tsanaktsidis, E.P. Favvas, G.T. Tzilantonis, S.G. Christidis, E.C. Katsidi, A. V. Scaltsoyiannes, Water removal from biodiesel/diesel blends and jet fuel using natural resin as dehydration agent, Can. J. Chem. Eng. 93 (2015) 1812–1818. https://doi.org/10.1002/cjce.22279.

[85] S. Bucko, P. Havran, J. Lesko, D. Megyesi, Dielectric frequency spectroscopy as potential tool for the designation water content in aviation

fuel, MOSATT 2019 - Mod. Saf. Technol. Transp. Int. Sci. Conf. Proc. (2019) 25–28. https://doi.org/10.1109/MOSATT48908.2019.8944095.

[86] C. Tsonopoulos, Thermodynamic analysis of the mutual solubilities of normal alkanes and water, Fluid Phase Equilib. 156 (1999) 21–33.

[87] S.L. Repetto, J.F. Costello, B. De Lacy Costello, N.M. Ratcliffe, J.K.-W. Lam, The Development of Novel Fuel Dehydrating Icing Inhibitors, SAE Int. J. Fuels Lubr. 6 (2013) 553–563. https://doi.org/10.4271/2013-01-2169.

[88] O. Merkulov, V. Zherebtsov, M. Peganova, E. Kitanin, J.K.-W. Lam, A. Sartori, OBIGGS for Fuel System Water Management - Proof of Concept, SAE Int. J. Aerosp. 4 (2011) 1465–1474. https://doi.org/10.4271/2011-01-2793.

[89] J. Krynitsky, J. Crellin, H. Carhart, The Behaviour of Water in Jet Fuels and the Clogging of Micronic Filters at Low Temperature, Washington, D.C., 1950.

[90] N. Wu, Z. Zong, J. Hu, J. Ma, Mechanism of dissolved water in jet fuel, in: AIP Conf. Proc., 2017: p. 040014. https://doi.org/10.1063/1.4977286.

[91] J.K.W. Lam, M.D. Carpenter, C.A. Williams, J.I. Hetherington, Water solubility characteristics of current aviation jet fuels, Fuel. 133 (2014) 26–33. https://doi.org/10.1016/j.fuel.2014.04.091.

[92] J.I. Hetherington, L Copson, The Combined Effects of Static Dissipator Additive and Fuel Impurities on the Separation of Water from Aviation Fuel, Spain, in: 9th Int. Conf. Stability, Handl. Use Liq. Fuels, Sitges, Spain, 2005.

[93] S.L. Repetto, R. Patel, T. Johnson, J.F. Costello, J.K.W. Lam, C.J. Chuck, Dual Action Additives for Jet A-1: Fuel Dehydrating Icing Inhibitors, Energy & Fuels. 30 (2016) 9080–9088. https://doi.org/10.1021/acs.energyfuels.6b01727.

[94] V.L. Zherebtsov, M.M. Peganova, Oxidation Influence on Water Solubility in Aviation Jet Fuel, OALib. 04 (2017) 1–8.

https://doi.org/10.4236/oalib.1103404.

[95] A. Goebel, K. Lunkenheimer, Interfacial Tension of the Water/ n -Alkane Interface, Langmuir. 13 (1997) 369–372. https://doi.org/10.1021/la960800g.

[96] J.R. Delfino, T.C. Pereira, H.D. Costa Viegas, E.P. Marques, A.A. Pupim Ferreira, L. Zhang, J. Zhang, A.L. Brandes Marques, A simple and fast method to determine water content in biodiesel by electrochemical impedance spectroscopy, Talanta. 179 (2018) 753–759. https://doi.org/10.1016/j.talanta.2017.11.053.

[97] S. Rani, G. Nagasowjanya, V. Ajitha, U. Maheswarrao, Aquametry- The Moisture Content Determination, World J. Pharm. Pharm. Sci. 4 (2015).

[98] L.A. Frink, D.W. Armstrong, Determination of trace water content in petroleum and petroleum products, Anal. Chem. 88 (2016) 8194–8201. https://doi.org/10.1021/acs.analchem.6b02006.

[99] S.A. Margolis, K. Vaishnav, J.R. Sieber, Measurement of water by oven evaporation using a novel oven design. 2. Water in motor oils and motor oil additives, Anal. Bioanal. Chem. (2004). https://doi.org/10.1007/s00216-004-2829-1.

[100] E. Kang, H.R. Park, J. Yoon, H.-Y. Yu, S.-K. Chang, B. Kim, K. Choi, S. Ahn, A simple method to determine the water content in organic solvents using the 1 H NMR chemical shifts differences between water and solvent, Microchem. J. 138 (2018) 395–400. https://doi.org/10.1016/j.microc.2018.01.034.

[101] J. Ugbeh, M. Carpenter, J. Pons, Assessment of HEFA, ATJ, GTL S-8 and farnesane as alternative jet fuels based on their water shedding characteristics, in: Proc. 16th Int. Conf. Stab. Handl. Use Liq. Fuels, 2019. http://iash.conferencespot.org/69070-iash-1.4569809/t001-1.4569870/f0015-1.4569871/a073-1.4569883/ap215-1.4569884?qr=1.

[102] European Union Aviation Safety Agency, Certification specifications & acceptable means of compliance for large aeroplanes, CS-25 (2015).

[103] J. Mitchell, Methods for the determination of water in polymers, Anal. Chim. Acta. 81 (1975) 231–263. https://doi.org/https://doi.org/10.1016/S0003-2670(01)82024-9.

[104] GFS, MOISTUR, 2nd ed., GFS Chemicals, Inc., Ohio, 2001. www.crescentchemical.com.

[105] H.S. Jung, P. Verwilst, W.Y. Kim, J.S. Kim, Fluorescent and colorimetric sensors for the detection of humidity or water content, Chem. Soc. Rev. 45 (2016) 1242–1256. https://doi.org/10.1039/C5CS00494B.

[106] H. Sun, B. Wang, S.G. DiMagno, A Method for Detecting Water in Organic Solvents, Org. Lett. 10 (2008) 4413–4416. https://doi.org/10.1021/ol8015429.

[107] S. Inagaki, N. Morii, M. Numata, Development of a reliable method to determine water content by headspace gas chromatography/mass spectrometry with the standard addition technique, Anal. Methods. (2015). https://doi.org/10.1039/C5AY00832H.

[108] P. Bruttel, R. Schlink, Water determination by Karl Fischer titration, (2006).

[109] C. DECARO, K. RUEGG, A. DEAGOSTINI, Coulometric Karl Fischer titration with a diaphragm-free cell: Cell design and applications, Food Chem. 96 (2006) 431–435. https://doi.org/10.1016/j.foodchem.2005.03.050.

[110] T. Yao, H. Yang, L. Guo, Y. Fei, H. Jiang, S. Bian, T. Wu, The Deterioration Mechanism of Diester Aero Lubricating Oil at High Temperature, J. Spectrosc. 2017 (2017) 1–8. https://doi.org/10.1155/2017/5392864.

[111] ASTM E203, Standard Test Method for Water Using Volumetric Karl Fischer Titration, (2001).

[112] ASTM D6304, Standard Test Method for Determination of Water in Petroleum Products, Lubricating Oils, and Additives by Coulometric Karl Fischer Titration 1, (2016). https://doi.org/10.1520/D6304-16.

[113] I.Y. Mohammed, F.K. Kazi, Y.A. Abakr, S. Yusuf, M.A. Razzaque, Novel Method for the Determination of Water Content and Higher Heating Value of Pyrolysis Oil, BioResources. 10 (2015) 2681–2690.

[114] E. Tavčar, E. Turk, S. Kreft, Simple modification of Karl-Fischer titration method for determination of water content in colored samples, J. Anal. Methods Chem. 2012 (2012) 1–6. https://doi.org/10.1155/2012/379724.

[115] J. Hu, J. Zhang, S. Yang, Y. Xin, L. Guo, T. Yao, Thermometric Titration for Rapid Determination of Trace Water in Jet Fuel, J. Spectrosc. 2017 (2017) 141–148. https://doi.org/10.1155/2017/8429525.

[116] L.S. Bark, S.M. Bark, TITRATIONS IN NON-AQUEOUS MEDIA, in: Thermom. Titrim., Elsevier, 1969: pp. 81–93. https://doi.org/10.1016/B978-0-08-013047-7.50010-1.

[117] P. Phansi, K. Danchana, V. Cerdà, Kinetic thermometric methods in analytical chemistry, TrAC - Trends Anal. Chem. 97 (2017) 316–325. https://doi.org/10.1016/j.trac.2017.09.019.

[118] B. Dacre, J.I. Hetherington, The effects of contaminants on the behaviour of conductivity improvers in hydrocarbons, J. Electrostat. 45 (1998) 53–68. https://doi.org/10.1016/S0304-3886(98)00036-9.

[119] M. Goertz, L. Tull, D. Moravec, Impact of Ice Formation in Diesel Fuel on Tier 4 Off-Road Engine Performance with High Efficiency Fuel Filtration, SAE Int. J. Commer. Veh. 8 (2015) 506–512. https://doi.org/10.4271/2015-01-2817.

[120] J.K.W. Lam, J.I. Hetherington, M.D. Carpenter, Ice growth in aviation jet fuel, Fuel. (2013). https://doi.org/10.1016/j.fuel.2013.05.048.

[121] A. Tascón, P.J. Aguado, Simulations of vented dust explosions in a 5 m3

vessel, Powder Technol. 321 (2017) 409–418. https://doi.org/10.1016/j.powtec.2017.08.047.

[122] M. Fitzner, P. Pedevilla, A. Michaelides, Predicting heterogeneous ice nucleation with a data-driven approach, Nat. Commun. 11 (2020) 1–9. https://doi.org/10.1038/s41467-020-18605-3.

[123] M.A. Clemens Hall, Bastian Rauch, Uwe Bauder, Patrick Le Clercq, MACHINE LEARNING ALGORITHMS FOR FUEL PROPERTY PREDICTION IN COMPARISON WITH STATE OF THE ART PHYSICAL MODELS, in: Proc. 16th Int. Conf. Stab. Handl. Use Liq. Fuels, 2019. http://iash.conferencespot.org/69070-iash-1.4569809/t001-1.4569870/f009-1.4570127/a032-1.4570134/ap091-1.4570137.

[124] M. Alves, M. Fortunato, Laurie Starck Hajiw-Riberaud, M. Creton, Benoit Yanis, F. Ancelle, Jacques Ser, M. Sicard, B. Uwe, B. Rauch, P. Le Clercq, Jetscreen Program Quantitative Assessmentof the Jet Fuel Physical, Chemical and Thermophysical Propertiesand Development of Lowand High Fidelity Models, in: Proc. 16th Int. Conf. Stab. Handl. Use Liq. Fuels, 2019. http://iash.conferencespot.org/69070-iash-1.4569809/t001-1.4569870/f009-1.4570127/a033-1.4570128/ap095-1.4570129.

[125] S.J. Cox, S.M. Kathmann, B. Slater, A. Michaelides, Molecular simulations of heterogeneous ice nucleation. I. Controlling ice nucleation through surface hydrophilicity, J. Chem. Phys. 142 (2015). https://doi.org/10.1063/1.4919714.

[126] Z.J. West, L.M. Shafer, R.C. Striebich, S. Zabarnick, C. Delaney, D. Phelps, M.J. DeWitt, Equilibrium Partitioning of Di-ethylene Glycol Monomethyl Ether (DiEGME) between Fuel and Aqueous Phases at Sub-Ambient Temperatures, Energy & Fuels. 28 (2014) 4501–4510. https://doi.org/10.1021/ef500900p.

[127] C. Moon, H. Seo, S.Y. Yoon, Visual observation of fuel-borne ice crystals, J. Vis. 21 (2018) 835–840. https://doi.org/10.1007/s12650-018-0498-y.

[128] J. Jiao, D.J. Burgess, Ostwald ripening of water-in-hydrocarbon emulsions, J. Colloid Interface Sci. 264 (2003) 509–516. https://doi.org/10.1016/S0021-9797(03)00276-5.

[129] J. Peixinho, V. Ageorges, B. Duchemin, Growth of Clathrate Hydrates from Water Drops in Cyclopentane, Energy & Fuels. 32 (2018) 2693–2698. https://doi.org/10.1021/acs.energyfuels.7b02740.

[130] S. Ariyaprakai, S.R. Dungan, Influence of surfactant structure on the contribution of micelles to Ostwald ripening in oil-in-water emulsions, J. Colloid Interface Sci. 343 (2010) 102–108. https://doi.org/10.1016/j.jcis.2009.11.034.

[131] S. Jung, M.K. Tiwari, N.V. Doan, D. Poulikakos, Mechanism of supercooled droplet freezing on surfaces, Nat. Commun. 3 (2012). https://doi.org/10.1038/ncomms1630.

[132] P.. Wilson, A.. Heneghan, A.D.. Haymet, Ice nucleation in nature: supercooling point (SCP) measurements and the role of heterogeneous nucleation, Cryobiology. 46 (2003) 88–98. https://doi.org/10.1016/S0011-2240(02)00182-7.

[133] G.D. Soria, J.R. Espinosa, J. Ramirez, C. Valeriani, C. Vega, E. Sanz, A simulation study of homogeneous ice nucleation in supercooled salty water, J. Chem. Phys. 148 (2018) 222811. https://doi.org/10.1063/1.5008889.

[134] J.M. Campbell, F.C. Meldrum, H.K. Christenson, Is ice nucleation from supercooled water insensitive to surface roughness?, J. Phys. Chem. C. 119 (2015) 1164–1169. https://doi.org/10.1021/jp5113729.

[135] M.R. Noor El-Din, S.H. El-Hamouly, H.M. Mohamed, M.R. Mishrif, A.M. Ragab, Water-in-diesel fuel nanoemulsions: Preparation, stability and physical properties, Egypt. J. Pet. 22 (2013) 517–530. https://doi.org/10.1016/j.ejpe.2013.11.006.

[136] K.L.K. Cook, R.W. Hartel, Mechanisms of Ice Crystallization in Ice Cream Production, Compr. Rev. Food Sci. Food Saf. 9 (2010) 213–222. https://doi.org/10.1111/j.1541-4337.2009.00101.x.

[137] P. V. Hobbs, S. Chang, J.D. Locatelli, The dimensions and aggregation of ice crystals in natural clouds, J. Geophys. Res. 79 (1974) 2199–2206. https://doi.org/10.1029/JC079i015p02199.

[138] M.J. Gay, J. Latham, The freezing behaviour of supercooled water drops, J. Glaciol. 17 (1976) 99–109.

[139] T. Li, D. Donadio, G. Galli, Ice nucleation at the nanoscale probes no man's land of water, Nat. Commun. 4 (2013) 1–6. https://doi.org/10.1038/ncomms2918.

[140] B.C. Bernstein, C.A. Wolff, F. McDonough, An Inferred Climatology of Icing Conditions Aloft, Including Supercooled Large Drops. Part I: Canada and the Continental United States, J. Appl. Meteorol. Climatol. 46 (2007) 1857–1878. https://doi.org/10.1175/2007JAMC1607.1.

[141] Y. Xu, N.G. Petrik, R.S. Smith, B.D. Kay, G.A. Kimmel, Homogeneous Nucleation of Ice in Transiently-Heated, Supercooled Liquid Water Films, J. Phys. Chem. Lett. 8 (2017) 5736–5743. https://doi.org/10.1021/acs.jpclett.7b02685.

[142] M.E. Earle, T. Kuhn, A.F. Khalizov, J.J. Sloan, Volume nucleation rates for homogeneous freezing in supercooled water microdroplets : results from a combined experimental and modelling approach, Atmos. Chem. Phys. (2010) 7945–7961. https://doi.org/10.5194/acp-10-7945-2010.

[143] H. Laksmono, T.A. McQueen, J.A. Sellberg, N.D. Loh, C. Huang, D. Schlesinger, R.G. Sierra, C.Y. Hampton, D. Nordlund, M. Beye, A. V Martin, A. Barty, M.M. Seibert, M. Messerschmidt, G.J. Williams, S. Boutet, K. Amann-Winkel, T. Loerting, L.G.M. Pettersson, M.J. Bogan, A. Nilsson, Anomalous Behavior of the Homogeneous Ice Nucleation Rate in "No-

Man's Land," J. Phys. Chem. Lett. 6 (2015) 2826–2832. https://doi.org/10.1021/acs.jpclett.5b01164.

[144] S. Zabarnick, N. Widmor, Studies of Jet Fuel Freezing by Differential Scanning Calorimetry, Energy & Fuels. 15 (2001) 1447–1453. https://doi.org/10.1021/ef010074b.

[145] S.E. Taylor, Component Interactions in Jet Fuels: Fuel System Icing Inhibitor Additive, Energy & Fuels. 22 (2008) 2396–2404. https://doi.org/10.1021/ef800090p.

[146] T. Bharathidasan, S.V. Kumar, M.S. Bobji, R.P.S. Chakradhar, B.J. Basu, Effect of wettability and surface roughness on ice-adhesion strength of hydrophilic, hydrophobic and superhydrophobic surfaces, Appl. Surf. Sci. 314 (2014) 241–250. https://doi.org/10.1016/j.apsusc.2014.06.101.

[147] J. Liu, C. Zhu, K. Liu, Y. Jiang, Y. Song, J.S. Francisco, X.C. Zeng, J. Wang, Distinct ice patterns on solid surfaces with various wettabilities, Proc. Natl. Acad. Sci. (2017). https://doi.org/10.1073/pnas.1712829114.

[148] A. Alizadeh, M. Yamada, R. Li, W. Shang, S. Otta, S. Zhong, L. Ge, A. Dhinojwala, K.R. Conway, V. Bahadur, A.J. Vinciquerra, B. Stephens, M.L. Blohm, Dynamics of Ice Nucleation on Water Repellent Surfaces, Langmuir. 28 (2012) 3180–3186. https://doi.org/10.1021/la2045256.

[149] M. Mohammadi, M. Tembely, A. Dolatabadi, Supercooled Water Droplet Impacting Superhydrophobic Surfaces in the Presence of Cold Air Flow, Appl. Sci. 7 (2017) 130. https://doi.org/10.3390/app7020130.

[150] G. Tang, R.L. Panetta, P. Yang, G.W. Kattawar, P.-W. Zhai, Effects of ice crystal surface roughness and air bubble inclusions on cirrus cloud radiative properties from remote sensing perspective, J. Quant. Spectrosc. Radiat. Transf. 195 (2017). https://doi.org/10.1016/j.jqsrt.2017.01.016.

[151] M. Zou, S. Beckford, R. Wei, C. Ellis, G. Hatton, M.A. Miller, Effects of surface roughness and energy on ice adhesion strength, Appl. Surf. Sci.

257 (2011) 3786–3792. https://doi.org/10.1016/j.apsusc.2010.11.149.

[152] M. Susoff, K. Siegmann, C. Pfaffenroth, M. Hirayama, Evaluation of icephobic coatings - Screening of different coatings and influence of roughness, Appl. Surf. Sci. 282 (2013) 870–879. https://doi.org/10.1016/j.apsusc.2013.06.073.

[153] S. Zou, Y. Zhang, W. Xu, Y. Wan, C. He, C. Dong, X. Li, Galvanic Corrosion Behavior of Aluminum Alloy (2219 and ZL205A) Coupled to Carbon Fiber-Reinforced Epoxy Composites, Int. J. Electrochem. Sci. 17 (2016) 9625 – 9633. https://doi.org/10.201964/2016.11.25.

[154] Y. Li, D.J. McGillicuddy, M.S. Dinniman, J.M. Klinck, Processes influencing formation of low-salinity high-biomass lenses near the edge of the Ross Ice Shelf, J. Mar. Syst. 166 (2017) 108–119. https://doi.org/10.1016/j.jmarsys.2016.07.002.

[155] W. Cavage, Studying the Accumulation of Water Ice on Fuel Lines and System Components, (2010). https://www.fire.tc.faa.gov/pdf/systems/May10Meeting/cavage-0510-FreezingFuel.pdf.

[156] J.K.-W. Lam, R.D. Woods, Ice accretion and release in fuel systems, Aeronaut. J. 122 (2018) 1051–1082. https://doi.org/10.1017/aer.2018.50.

[157] M. Fitzner, G.C. Sosso, S.J. Cox, A. Michaelides, Ice is born in low-mobility regions of supercooled liquid water, Proc. Natl. Acad. Sci. 116 (2019) 2009–2014. https://doi.org/10.1073/pnas.1817135116.

[158] A.B. Thompson, J.K.W. Lam, Water run-off in aircraft fuel tanks, IMA J. Appl. Math. (Institute Math. Its Appl. 77 (2012) 72–85. https://doi.org/10.1093/imamat/hxr077.

[159] A.J. Meuler, J.D. Smith, K.K. Varanasi, J.M. Mabry, G.H. McKinley, R.E. Cohen, Relationships between water wettability and ice adhesion, ACS Appl. Mater. Interfaces. 2 (2010) 3100–3110.

https://doi.org/10.1021/am1006035.

[160] S. Tarquini, C. Antonini, A. Amirfazli, M. Marengo, J. Palacios, Investigation of ice shedding properties of superhydrophobic coatings on helicopter blades, Cold Reg. Sci. Technol. 100 (2014) 50–58. https://doi.org/10.1016/j.coldregions.2013.12.009.

[161] K.Y. Chan, J.K.-W. Lam, Water drop runoff in aircraft fuel tank vent systems, Proc. Inst. Mech. Eng. Part C J. Mech. Eng. Sci. 231 (2017) 4548–4563. https://doi.org/10.1177/0954406216669175.

[162] G. Momen, R. Jafari, M. Farzaneh, Ice repellency behaviour of superhydrophobic surfaces: Effects of atmospheric icing conditions and surface roughness, Appl. Surf. Sci. 349 (2015) 211–218. https://doi.org/10.1016/j.apsusc.2015.04.180.

[163] G. Fortin, Considerations on the use of hydrophobic, superhydrophobic or icephobic coatings as a part of the aircraft ice protection system, SAE Tech. Pap. 7 (2013). https://doi.org/10.4271/2013-01-2108.

[164] V. Upadhyay, T. Galhenage, D. Battocchi, D. Webster, Amphiphilic icephobic coatings, Prog. Org. Coatings. 112 (2017) 191–199. https://doi.org/10.1016/j.porgcoat.2017.07.019.

[165] ATA 103, Standards for Jet Fuel Quality Control at Airports, 2019.

[166] CERA, Why the ’ “Peak Oil”’Theory Falls Down: Myths, Legends, and the Future of Oil Resources, (2006).

[167] R. Bentley, R. Miller, S. Wheeler, G. Boyle, Comparison of global oil supply forecasts, UKERC Review of Evidence for Global Oil Depletion, 2009. UKERC/WP/TPA/2009/022.

[168] OPEC, World oil outlook - Organization of the Petroleum Exporting Countries, Organization of the Petroleum Exporting Countries (OPEC), Vienna, 2017. http://www.opec.org/opec_web/en/press_room/4606.htm.

[169] M. Lapuerta, M. Villajos, J.R. Agudelo, A.. Boehman, Key properties and blending strategies of hydrotreated vegetable oil as biofuel for diesel engines, Fuel Process. Technol. 92 (2011) 2406–2411. https://doi.org/10.1016/j.fuproc.2011.09.003.

[170] A.M.N. Renzaho, J.K. Kamara, M. Toole, Biofuel production and its impact on food security in low and middle income countries: Implications for the post-2015 sustainable development goals, Renew. Sustain. Energy Rev. 78 (2017) 503–516. https://doi.org/10.1016/j.rser.2017.04.072.

[171] J. Bosch, S. De Jong, R. Hoefnagels, R. Slade, Aviation biofuels: strategically important, technically achievable, tough to deliver, London, 2017. https://www.imperial.ac.uk/media/imperial-college/grantham-institute/public/publications/briefing-papers/BP-23-Aviation-Biofuels.pdf.

[172] S.N. Naik, V. V. Goud, P.K. Rout, A.K. Dalai, Production of first and second generation biofuels: A comprehensive review, Renew. Sustain. Energy Rev. 14 (2010) 578–597. https://doi.org/10.1016/j.rser.2009.10.003.

[173] A.N. Oumer, M.M. Hasan, A.T. Baheta, R. Mamat, A.A. Abdullah, Bio-based liquid fuels as a source of renewable energy: A review, Renew. Sustain. Energy Rev. 88 (2018) 82–98. https://doi.org/10.1016/j.rser.2018.02.022.

[174] G. Dragone, D. Fernandes, A.V. António, J.A. Teixeira, Third generation biofuels from microalgae, Biotechnol. Bioeng. (2010) 1355–1366. http://repositorium.sdum.uminho.pt/handle/1822/16807.

[175] M. Kousoulidou, L. Lonza, Biofuels in aviation: Fuel demand and CO2 emissions evolution in Europe toward 2030, Transp. Res. Part D Transp. Environ. 46 (2016) 166–181. https://doi.org/10.1016/j.trd.2016.03.018.

[176] D. Hammel, Aviation biofuel sustainability scorecards, in: NRDC (Natural Resour. Def. Counc. Issue Br., NRDC (Natural Resources Defense Council), 2015.

[177] S.. Yang, Bioprocessing – from Biotechnology to Biorefinery, in: Bioprocess. Value-Added Prod. from Renew. Resour., Elsevier, 2007: pp. 1–24. https://doi.org/10.1016/B978-044452114-9/50002-5.

[178] A. Bernardo, R. Howard-Hildige, A. O'Connell, R. Nichol, J. Ryan, B. Rice, E. Roche, J.. Leahy, Camelina oil as a fuel for diesel transport engines, Ind. Crops Prod. 17 (2003) 191–197. https://doi.org/10.1016/S0926-6690(02)00098-5.

[179] D.J. Robichaud, R.W. Jenkins, A.D. Sutton, Pyrolysis of Biomass for Aviation Fuel, in: Science Direct (Ed.), Biofuels Aviat., Elsevier, Los Alamos, 2016: pp. 191–215. https://doi.org/10.1016/B978-0-12-804568-8.00008-1.

[180] F. Goodarzi, S. Zendehboudi, A Comprehensive Review on Emulsions and Emulsion Stability in Chemical and Energy Industries, Can. J. Chem. Eng. 97 (2019) 281–309. https://doi.org/10.1002/cjce.23336.

[181] V.G. Morgan, C.M.S. Sad, A.F. Constantino, R.B.V. Azeredo, V. Lacerda, E.V.R. Castro, L.L. Barbosa, Droplet size distribution in water-crude oil emulsions by low-field NMR, J. Braz. Chem. Soc. 30 (2019) 1587–1597. https://doi.org/10.21577/0103-5053.20190057.

[182] M. Stewart, K. Arnold, Produced Water Treating Systems, in: Prod. Water Treat. F. Man., Elsevier, 2011: pp. 1–134. https://doi.org/10.1016/B978-1-85617-984-3.00001-8.

[183] A.P.P. Pires, Y. Han, J. Kramlich, M. Garcia-Perez, Alternative jet fuel properties, 2018. https://bioresources.cnr.ncsu.edu/wp-content/uploads/2018/02/BioRes_13_2_2632_Pires_HKG_Chem_Compos_Fuel_Props_Aternative_Jet_Fuels_13266-1.pdf.

[184] J.W. Elliott, F.T. Smith, Ice formation on a smooth or rough cold surface due to the impact of a supercooled water droplet, J. Eng. Math. 102 (2017) 35–64. https://doi.org/10.1007/s10665-015-9784-z.

[185] A.J. Miller, K.P. Brennan, C. Mignani, J. Wieder, R.O. David, N. Borduas-Dedekind, Development of the drop Freezing Ice Nuclei Counter (FINC), intercomparison of droplet freezing techniques, and use of soluble lignin as an atmospheric ice nucleation standard, Atmos. Meas. Tech. 14 (2021) 3131–3151. https://doi.org/10.5194/amt-14-3131-2021.

[186] B.C. Bernstein, C. Le Bot, An Inferred Climatology of Icing Conditions Aloft, Including Supercooled Large Drops. Part II: Europe, Asia, and the Globe, J. Appl. Meteorol. Climatol. 48 (2009) 1503–1526. https://doi.org/10.1175/2009JAMC2073.1.

[187] J. Ugbeh Johnson, M. Carpenter, C. Williams, J.-F. Pons, D. McLaren, Complexities associated with nucleation of water and ice from jet fuel in aircraft fuel systems: A critical review, Fuel. 310 (2022) 122329. https://doi.org/10.1016/j.fuel.2021.122329.

[188] K.Y. Chan, J.K.W. Lam, Water drop runoff in aircraft fuel tank vent systems, Proc. Inst. Mech. Eng. Part C J. Mech. Eng. Sci. 231 (2017) 4548–4563. https://doi.org/10.1177/0954406216669175.

[189] C. Zhang, X. Chen, D.J. Webb, G.-D. Peng, Water detection in jet fuel using a polymer optical fibre Bragg grating, in: 20th Int. Conf. Opt. Fibre Sensors, 2009: p. 750380. https://doi.org/10.1117/12.848696.

[190] S.T. McClain, T. Zhang, S. Ahmed, G. Stafford, J.A. Cornejo, D.L. O'Neal, A Climatic Facility and Apparatus for Investigations of Cold Soaked Fuel Frost Evolution, in: AIAA Aviat. 2020 FORUM, American Institute of Aeronautics and Astronautics, Reston, Virginia, 2020. https://doi.org/10.2514/6.2020-2808.

[191] G. Bessee, Determination of water droplet size distributions in diesel and aviation fuels, in: 13th Int. Conf. Stability, Handl. Use Liq. Fuels 2013, 2013: pp. 267–272.

[192] M. Wedd, PARTICLE SIZE ANALYSIS, in: Encycl. Anal. Sci., Elsevier,

2005: pp. 18–29. https://doi.org/10.1016/B0-12-369397-7/00439-8.

[193] I. 9276-2:2014, Representation of results of particle size analysis — Part 2: Calculation of average particle sizes/diameters and moments from particle size distributions, Int. Stand. ISO 9276-2. (2014). https://www.iso.org/standard/57641.html.

[194] P.H. Westfall, Kurtosis as peakedness, 1905–2014. R.I.P., Am. Stat. 68 (2014) 191–195. https://doi.org/10.1080/00031305.2014.917055.

[195] T.E. Baldock, M.R. Tomkins, P. Nielsen, M.G. Hughes, Settling velocity of sediments at high concentrations, Coast. Eng. 51 (2004) 91–100. https://doi.org/10.1016/j.coastaleng.2003.12.004.

[196] J.F. Richardson, W.N. Zaki, The sedimentation of a suspension of uniform spheres under conditions of viscous flow, (1954) 65–73. https://www.sciencedirect.com/science/article/pii/0009250954850159.

[197] J. Garside, M.R. Al-Dibouni, Velocity-voidage relationships for fluidization and sedimentation in solid-liquidsystems., Ind. Eng. Chem. Res. 16 (1977) 206–214.

[198] M.A. Al-Naafa, M.S. Selim, Sedimentation of monodisperse and bidisperse hard-sphere colloidal suspensions, AIChE J. 38 (1992) 1618–1630. https://doi.org/10.1002/aic.690381012.

[199] C. Gutiérrez-Antonio, F.I. Gómez-Castro, J.A. de Lira-Flores, S. Hernández, A review on the production processes of renewable jet fuel, Renew. Sustain. Energy Rev. 79 (2017) 709–729. https://doi.org/10.1016/j.rser.2017.05.108.

[200] Z.J. West, T. Yamada, C.R. Bruening, R.L. Cook, S.S. Mueller, L.M. Shafer, M.J. Dewitt, S. Zabarnick, Investigation of water interactions with petroleum-derived and synthetic aviation turbine fuels, Energy and Fuels. 32 (2018) 1166–1178. https://doi.org/10.1021/acs.energyfuels.7b02844.

[201] F. Wang, R. Liu, M. Li, J. Yao, J. Jin, Kerosene evaporation rate in high

temperature air stationary and convective environment, Fuel. 211 (2018) 582–590. https://doi.org/10.1016/j.fuel.2017.08.062.

[202] J. Ugbeh, M. Carpenter, J. Pons, Assessment of HEFA, ATJ, GTL S-8 and farnesane as alternative jet fuels based on their water shedding characteristics, in: Proc. 16th Int. Conf. Stab. Handl. Use Liq. Fuels, 2019. https://iash.conferencespot.org/69070-iash-1.4569809/t001-1.4569870/f0015-1.4569871/a073-1.4569883/ap214-1.4569886?qr=1.

[203] A.P.P. Pires, Y. Han, J. Kramlich, M. Garcia-Perez, Chemical Composition and Fuel Properties of Alternative Jet Fuels, BioResources. 13 (2018). https://doi.org/10.15376/biores.13.2.2632-2657.

[204] J.M. Leiva, E. Geffroy, Evolution of the size distribution of an emulsion under a simple shear flow, Fluids. 3 (2018). https://doi.org/10.3390/fluids3030046.

[205] E. Marechal, S. Khelladi, F. Ravelet, F. Bakir, O. Delepierre-Massue Snecma, Towards Numerical Simulation of Snow Showers in Jet Engine Fuel Systems, in: Adv. Hydroinformatics, Springer Water (Springer, Singapore), 2016: pp. 613–624. https://doi.org/10.1007/978-981-287-615-7_41.

APPENDICES

Appendix A Assessment of HEFA, ATJ, GTL-S8 & Farnesane as Alternative Jet Fuels Based on their Water Shedding Characteristics

A.1 Results from water settling experiments

Table A-1 KF results for neat fuels with 500 ppm nominal water addition

500 ppm Test 1										
	100% Conv. Jet A-1		**100% GTL S-8**		**100% Farnesane**		**100% ATJ**		**100% HEFA**	
s/n	**Time interval (minutes)**	**Measured water content(ppm)**	**Time interval (minutes)**	**Measured water content(ppm)**	**Time interval (minutes)**	**Measured water content(ppm)**	**Time interval (minutes)**	**Measured water content(ppm)**	**Time interval (minutes)**	**Measured water content(ppm)**
1	0.00	483.9	0.00	475.2	0.00	508.3	0	492.3	0.0	493.7
2	2.00	471.1	2.00	415.8	8.00	528.9	3	471.3	2.0	433.5
3	4.00	527.6	3.00	425.1	10.00	560.2	5	480.4	4.0	475
4	15.00	485.4	7.00	387.2	12.00	490.1	7	423.4	5.0	475.7
5	17.00	491.5	15.00	395.8	14.00	520.9	10	404.4	7.0	489

6	25.00	498.3	16.00	414.4	18.00	517.4	12	402.3	9.0	474.8
7	30.00	487.8	17.00	411.9	20.00	531.1	28	343.3	27.0	464.8
8	32.00	505.0	18.00	395	21.00	526.5	34	376.2	29.0	392.8
9	39.00	496.9	34.00	365.4	27.00	556.8	36	388.3	32.0	458
10	40.00	486.9	37.00	337.3	33.00	516.1	41	375.1	33	494.7
11	50.00	480.2	38.00	296.7	35.00	518.3	45	337.3	35	461.6
12	54.00	490.3	41.00	299.7	36.00	521.1	70	322.7	39.0	461.1
13	57.00	477.5	43.00	320.2	42.00	511.1	72	268.3	40.0	382.2
14	59.00	494.8	55.00	316.3	72.00	519.1	77	265.4	76.0	406.7
15	60.00	478.1	56.00	329.6	73.00	513.6	81	255.7	77.0	411.3
16	92.00	398.6	97.00	248.1	78.00	514.8	87	250.5	78.0	394.6
17	95.00	399.3	100.00	239.2	80.00	505.7	94	180.8	81.0	370.1
18	100.00	393.3	104.00	231.4	104.00	456.5	97	189.7	126.0	341.3
19	102.00	390.6	106.00	229.3	106.00	471.3	125	208.8	129.0	348.8

20	137.00	335.1	109.00	227.5	109.00	479.3	131	233.1	132.0	282.3
21	139.00	314.4	127.00	216.6	148.00	499.2	132	176.8	133	234.2
22	142.00	314.4	145.00	172.5	150.00	500.3	133	191.5	135	299.3
23	144.00	314.4	151.00	193.1	151.00	495.0	136	169.1	157	293.5
24	167.00	311.7	152.00	191.8	154.00	509.1	174	168.6	159	237.5
25	168.00	312.4	154.00	169.6	166.00	515.6	175	177.3	160	167
26	169.00	337.2	155.00	175.8	168.00	519.4		392.3	161	221.4
27	171.00	317.4	172.00	142.7	170.00	446.9		371.3	163	213.9
28	175.00	305.9	177.00	148.6	171.00	481.3		380.4	191	147
29	179.00	215.6	228.00	121.6	191.00	356.6		383.4	193	178.9
30	181.00	183.5	230.00							

Table A-2 KF results for neat fuels with 1,000 ppm nominal water addition

1000 ppm Test 1										
	100% Conv. Jet A-1		100% GTL S-8		100% Farnesane		100% ATJ		100% HEFA	
s/n	Time interval (minutes)	Measured water content(ppm)	Time interval (minutes)	Measured water content(ppm)	Time interval (minutes)	Measured water content(ppm)	Time interval (minutes)	Measured water content(ppm)	Time interval (minutes)	Measured water content(ppm)
1	0	1091.1	0	901.6	0	1196.0	0	1029.9	0	1018.9
2	2	1002.1	2	737.9	5	1175.0	1	883.1	2	728.5
3	5	965.6	4	678.3	7	1100.4	4	987.5	3	753.7
4	7	930.1	5	593.8	8	1051.1	6	908.4	5	658.1
5	25	877.4	8	736.4	20	1050.4	9	856.4	7	789.3
6	27	900.1	11	593.8	0	1039.1	10	847.5	21	783.7

7	29	950.6	14	476.2	3	1047.9	18	880.1	26	740.0
8	32	988.6	41	522.5	5	1003.1	20	800.1	28	644.9
9	72	874.1	47	526.5	7	1010.5	22	845.6	29	849.9
10	77	932.7	71	441.5	9	1019.3	54	531.9	45	850.1
11	79	751.5	74	388.9	11	1002.4	55	532.5	47	844.5
12	81	803.6	78	285.3	14	1012.3	65	367.1	49	653.1
13	102	742.4	80	285.3	21	1036.8	67	314.3	79	785.3
14	103	437.2	82	261.2	23	1021.4	82	260.7	80	708.2
15	104	498.2	84	250.8	25	1019.2	93	227.0	82	560.7
16	106	398.9	92	320.2	31	967.9	95	232.7	90	318.3
17	107	432.9	93	322.8	33	993.6	97	244.6	93	296.7
18	109	389.6	94	228.0	40	1000.2	100	153.7	95	311.2
19	133	381.8	96	291.9	119	1018.1	107	144.2	96	303.3
20	134	482.4	97	318.8	121	994.0	134	236.9	107	249.6

21	135	494.2	98	237.8	129	1035.4	137	259.8	110	253.3
22	137	455.1	112	265.5	132	994.6	149	300	159	244.3
23	140	429.8	129	238.5	135	980.5	151	168.8	162	175.7
24	142	324.8	133	181.4	141	859.0	153	216.7	163	178.2
25	144	439.5	134	158.4	147	844.4	161	212.5	167	181.3
26	146	363.2	135	220.0	149	801.8	164		170	150.3
27	152	337.8	136	255.0	150	751.5			171	177.0
28	167	307.9	151	221.3	152	801.8			173	147
29	168	308.5	152	160.9	189	751.5			175	178.9
30	169	326.2	154	158.8	192	790.7				
31	189	251.8	167	156.1	195	871.1				
32	190	289.6	168	147.9	199	851.9				
33	191	288.9	169	146.7	199	843.5				
34	193	282.7	170	199.0	201	889.6				

35	1059	121.4	176	207.0	1207	376.9		
36	1061	134.6	177	197.4	1210	370.0		

Table A-3 KF results for fuel blends with 1,000 ppm nominal water addition

Blend ratios - 1000 ppm Test 1										
	50% Jet A-1 and 50% GTL S-8		50% Jet A-1 and 50% Farnesane		75% GTL S-8 and 25% Hexanol		50% Jet A-1 and 50% ATJ		50% Jet A-1 and 50% HEFA	
S/n	Time interval (minutes)	Measured water content(ppm)	Time interval (minutes)	Measured water content(ppm)	Time interval (minutes)	Measured water content(ppm)	Time interval (minutes)	Measured water content(ppm)	Time interval (minutes)	Measured water content(ppm)
1	0	1023.3	0	1139.8	0	974.2	0	1000.9	0	979.3
2	2	930.3	1	1147.9	1	942.4	2	1039.1	1	896.0
3	4	1029.0	2	1108.3	2	916.3	4	976.4	4	881.8
4	6	1000.3	4	1183.2	3	963.2	7	942.0	8	1083.3

5	19	1023.1	18	1099.7	4	969.2	11	909.7	12	902.4
6	22	788.0	20	1093.2	24	975.6	12	893.6	32	819.6
7	23	778.3	54	1095.3	26	977.1	13	888.4	35	676.6
8	24	705.9	57	1049.8	27	982.4	15	876.0	37	819.6
9	26	672.2	58	1000.4	36	977.5	27	842.1	40	752.4
10	46	654.8	78	519.9	37	975.1	42	800.5	60	745.6
11	50	650.3	81	554.2	60	881.9	44	808.5	65	740.9
12	52	637.1	82	543.8	62	837.2	47	763.7	66	700.8
13	53	643.1	84	487.9	63	870.2	48	741.0	68	712.3
14	72	717.8	86	480.6	89	799.7	67	658.6	70	692.0
15	73	645.8	89	455.6	90	799.1	69	659.6	90	599.0
16	76	601.0	103	457.8	93	783.2	70	604.7	91	558.2
17	77	582.1	104	467.5	94	759.0	101	434.0	94	597.1
18	102	460.8	105	475.1	95	761.2	102	447.0	96	566.7

19	103	451.7	123	491.5	96	754.3	103	387.6	110	440.9
20	104	419.0	125	489.5	99	784.9	104	312.6	112	470.3
21	111	349.2	129	473.7	103	766.8	109	312.7	124	473.3
22	114	394.0	142	448.3	105	796.6	116	273.9	126	433.3
23	128	350.6	146	341.5	107	762	117	265.6	128	400.1

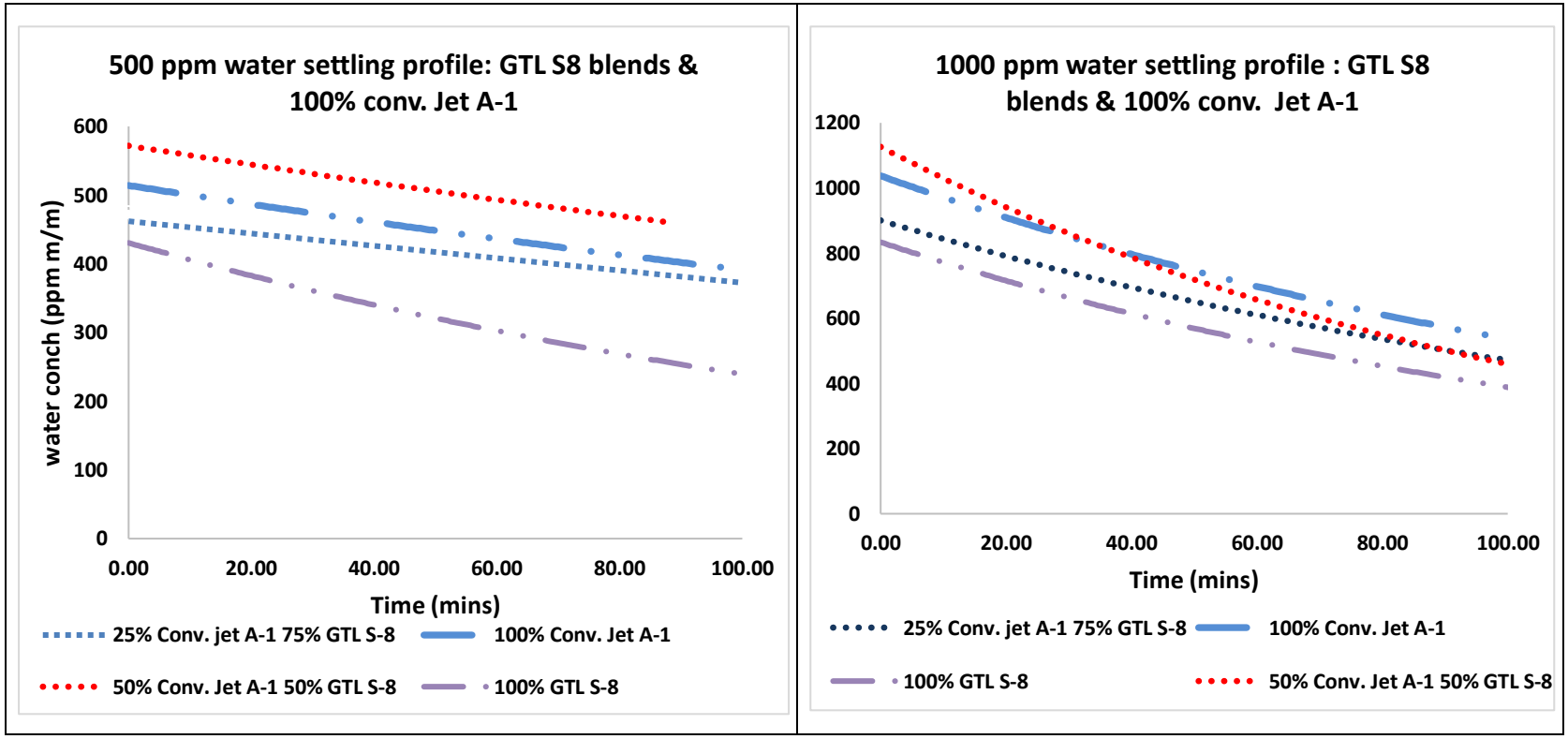

- There is more driving force for the water to come out of the suspension at a higher nominal water level hence the steeper curve in the 1000 ppm nominal water level

Figure A-1 Settling profile at 1000 ppm and 500 ppm nominal water cases

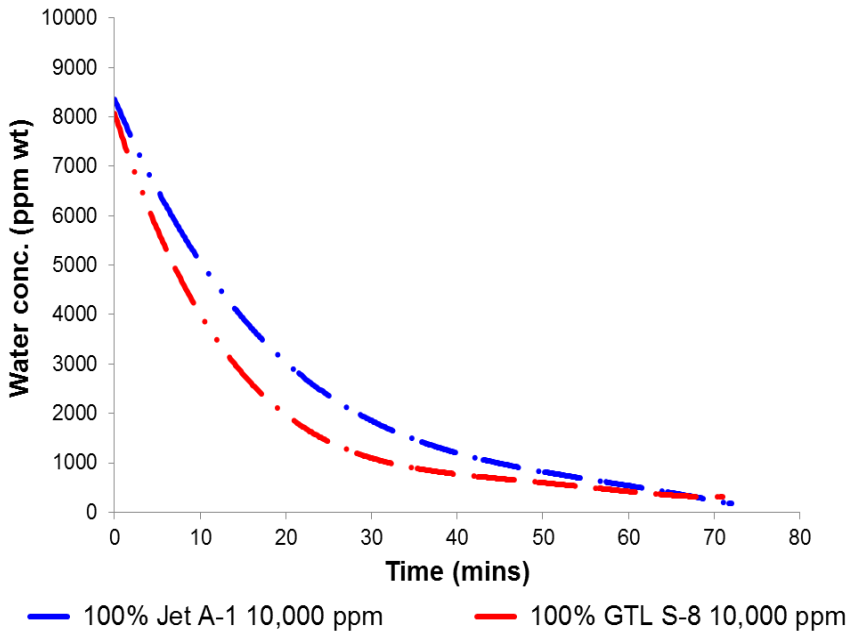

Figure A-2 Water settling rate for GTL S-8 & Conv. Jet A-1 (10,000 ppm nominal water addition)

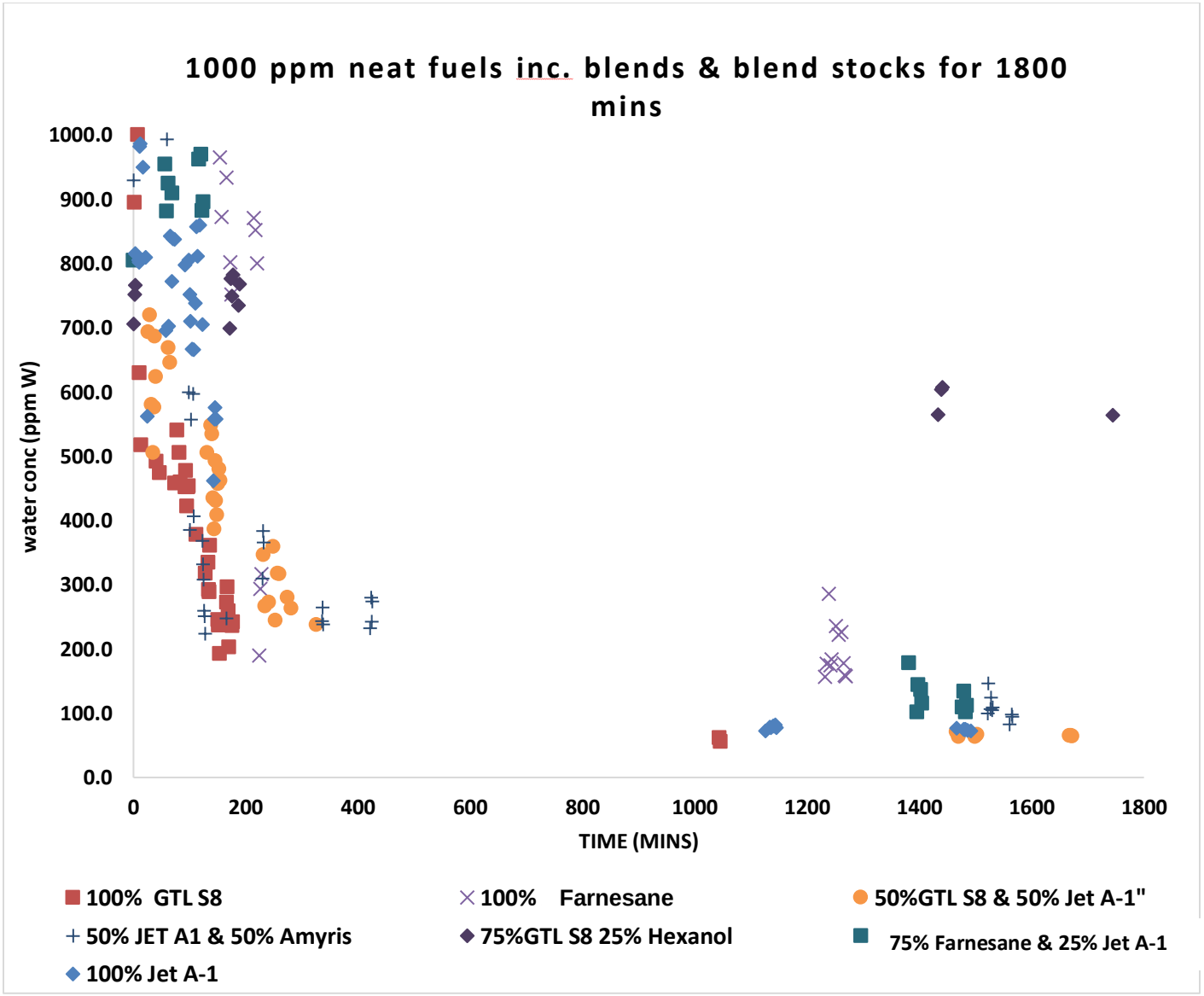
1000 ppm neat fuels inc. blends & blend stocks for 1800 mins
water conc (ppm W)
1000.0
900.0
800.0
700.0
600.0
500.0
400.0
300.0
200.0
100.0
0.0
0
200
400
600
800
1000
1200
1400
1600
1800
TIME (MINS)
100% GTL S8
100% Farnesane
50%GTL S8 & 50% Jet A-1"
50% JET A1 & 50% Amyris
75%GTL S8 25% Hexanol
75% Farnesane & 25% Jet A-1
100% Jet A-1

Figure A-3 Water settling rate with data points for neat fuels/fuel blends

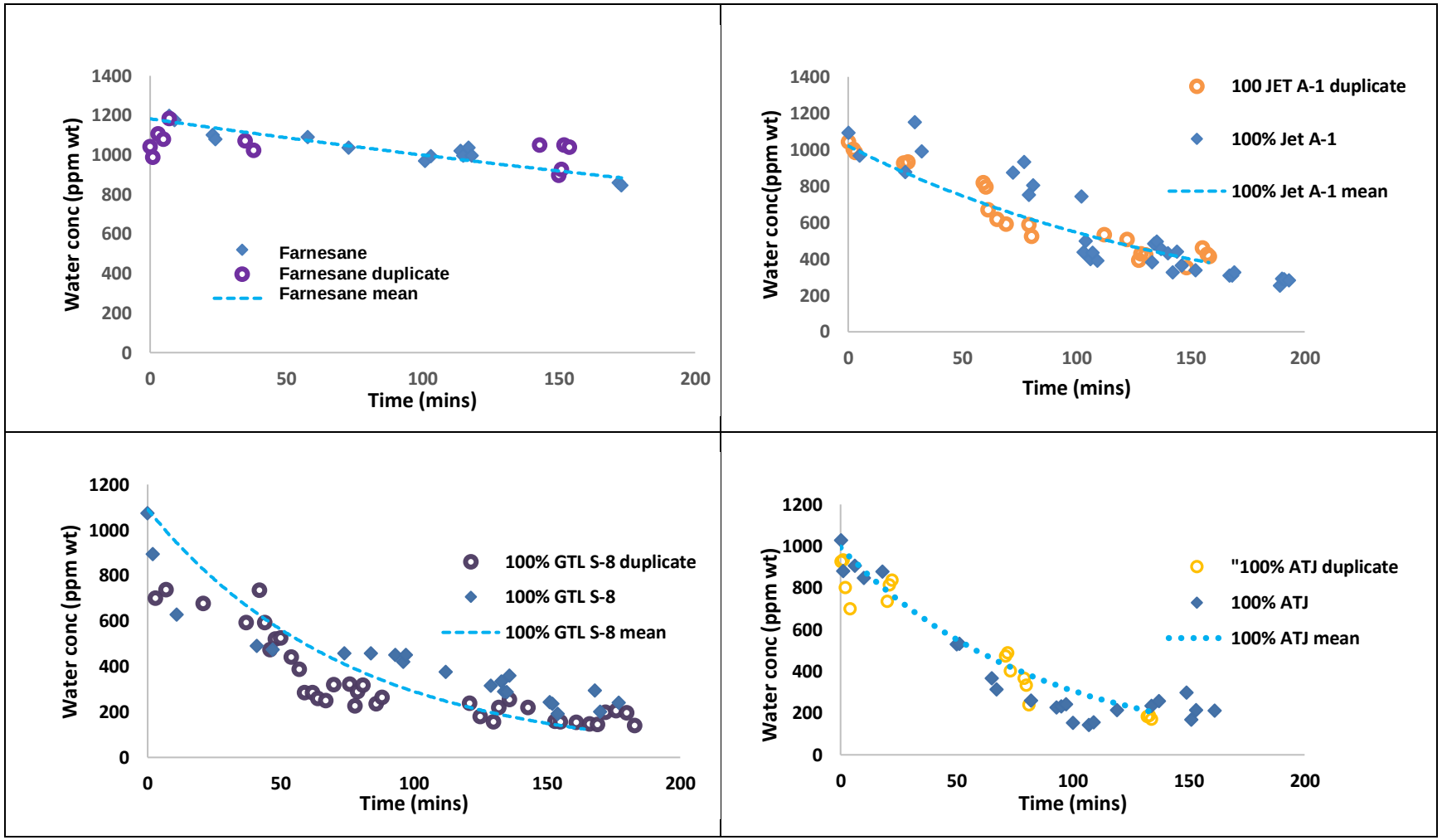

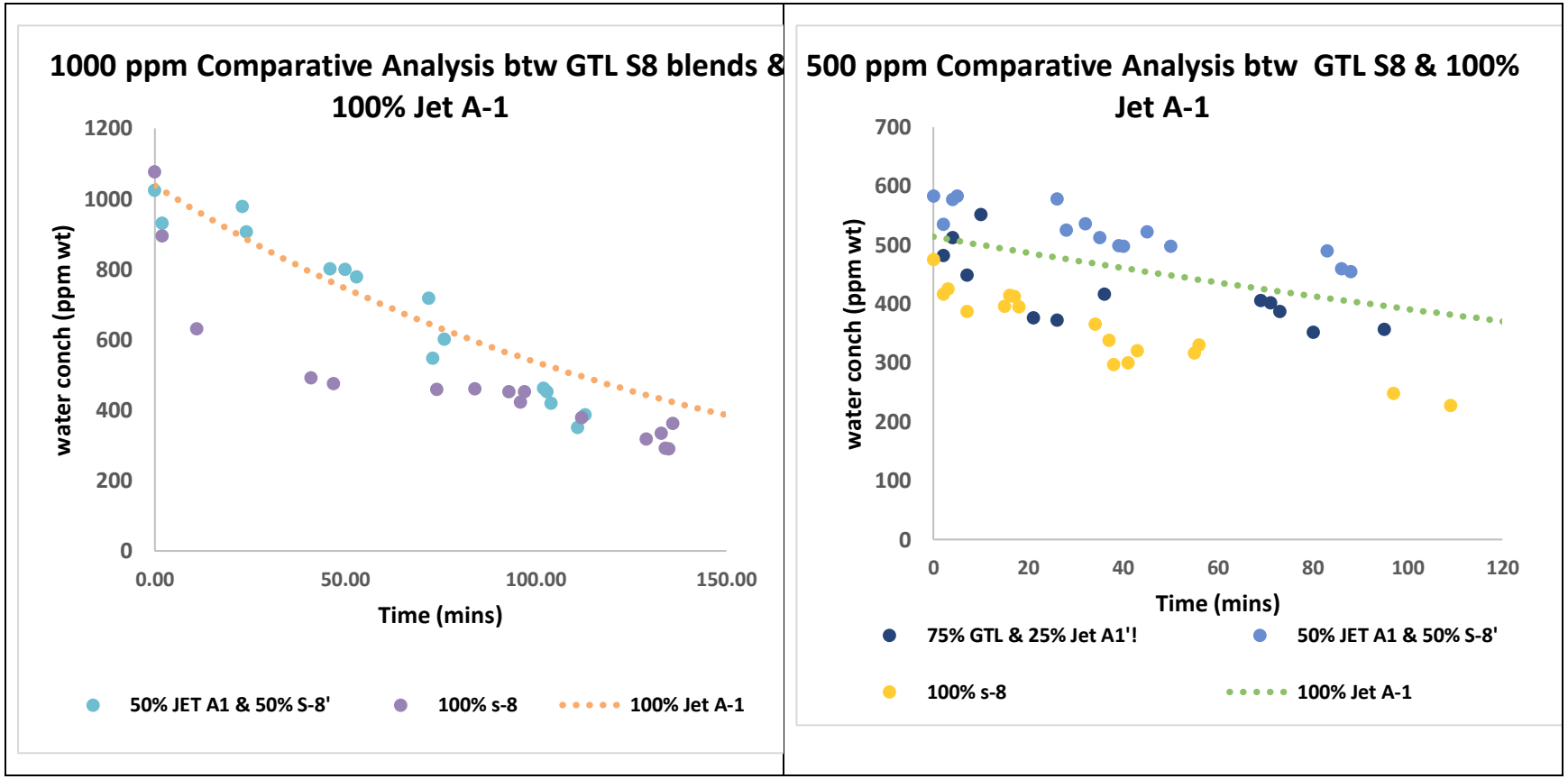

Figure A-4 Average of duplicate tests conducted for 1000 ppm nominal water level

Appendix B Characterization of water droplets size distribution in aviation turbine fuel: Ultrasonic homogeniser vs High shear speed mixer

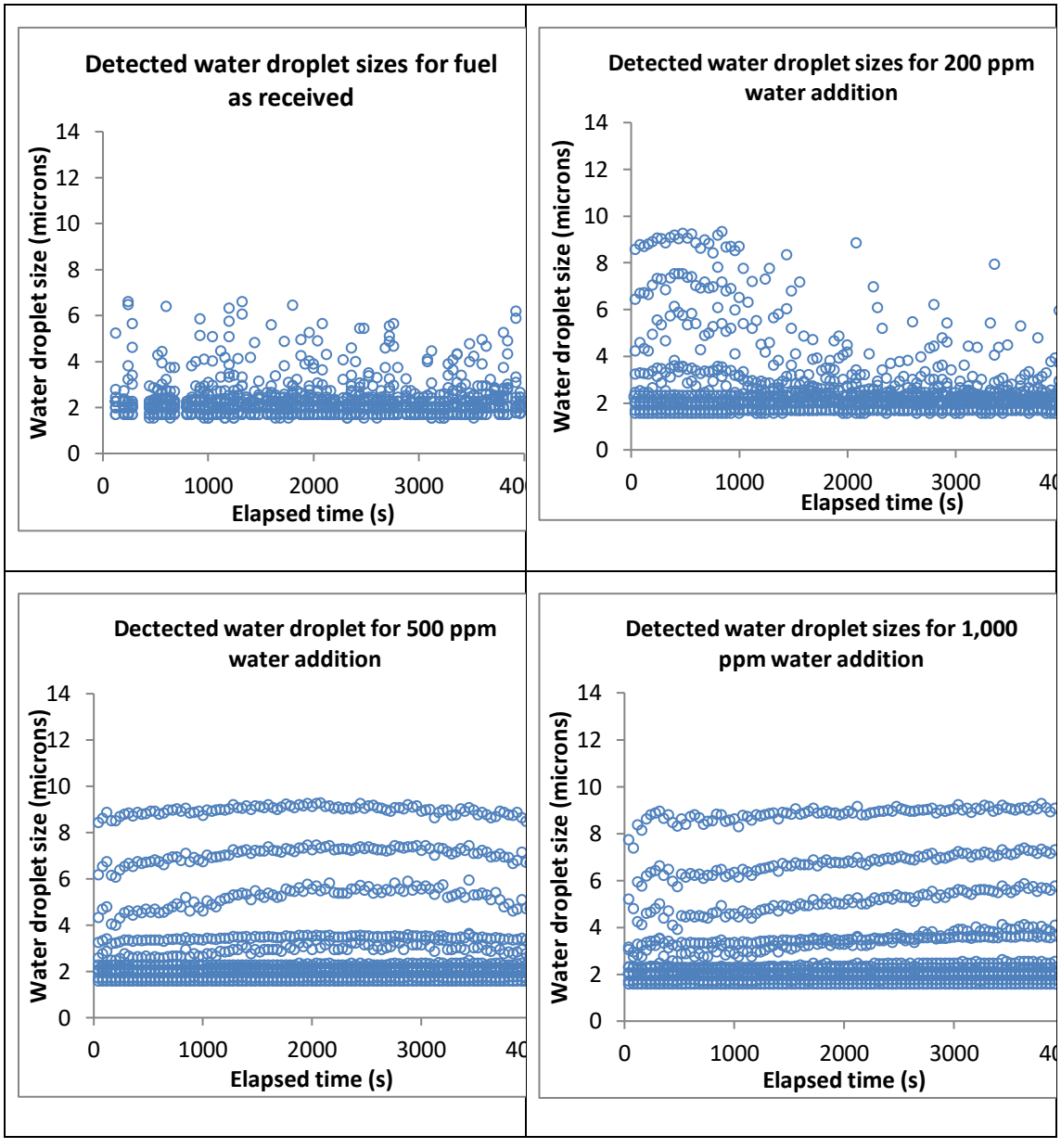

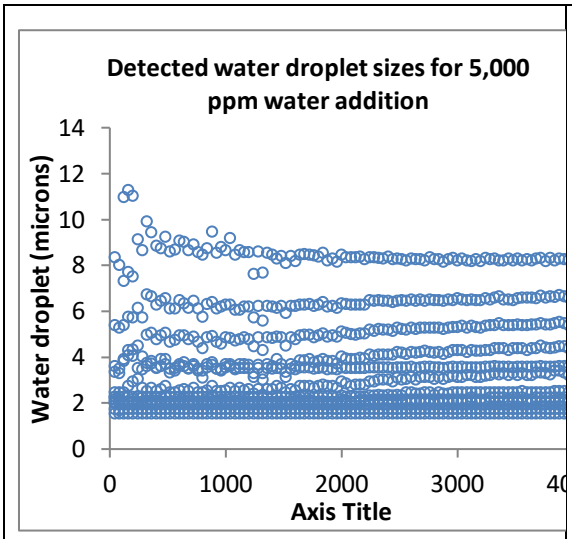

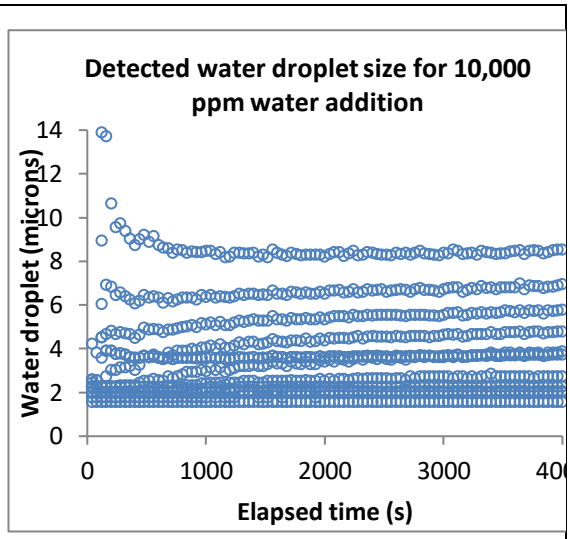

INCLUDING MAX VALUE (D10)

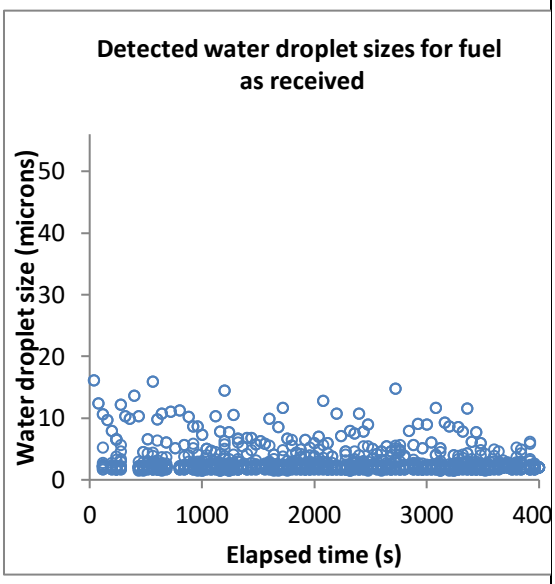

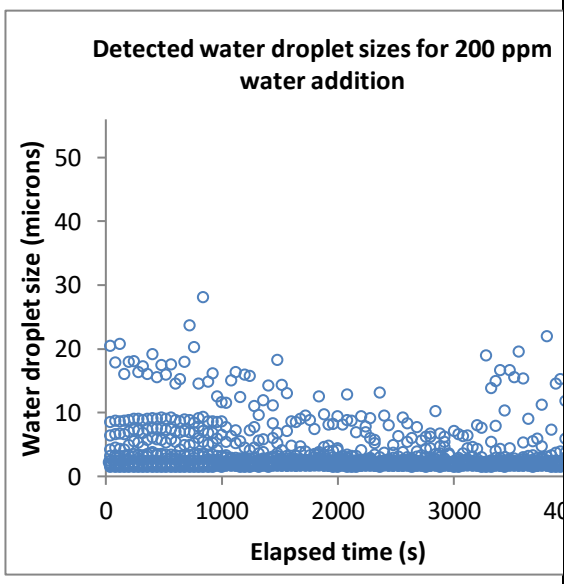

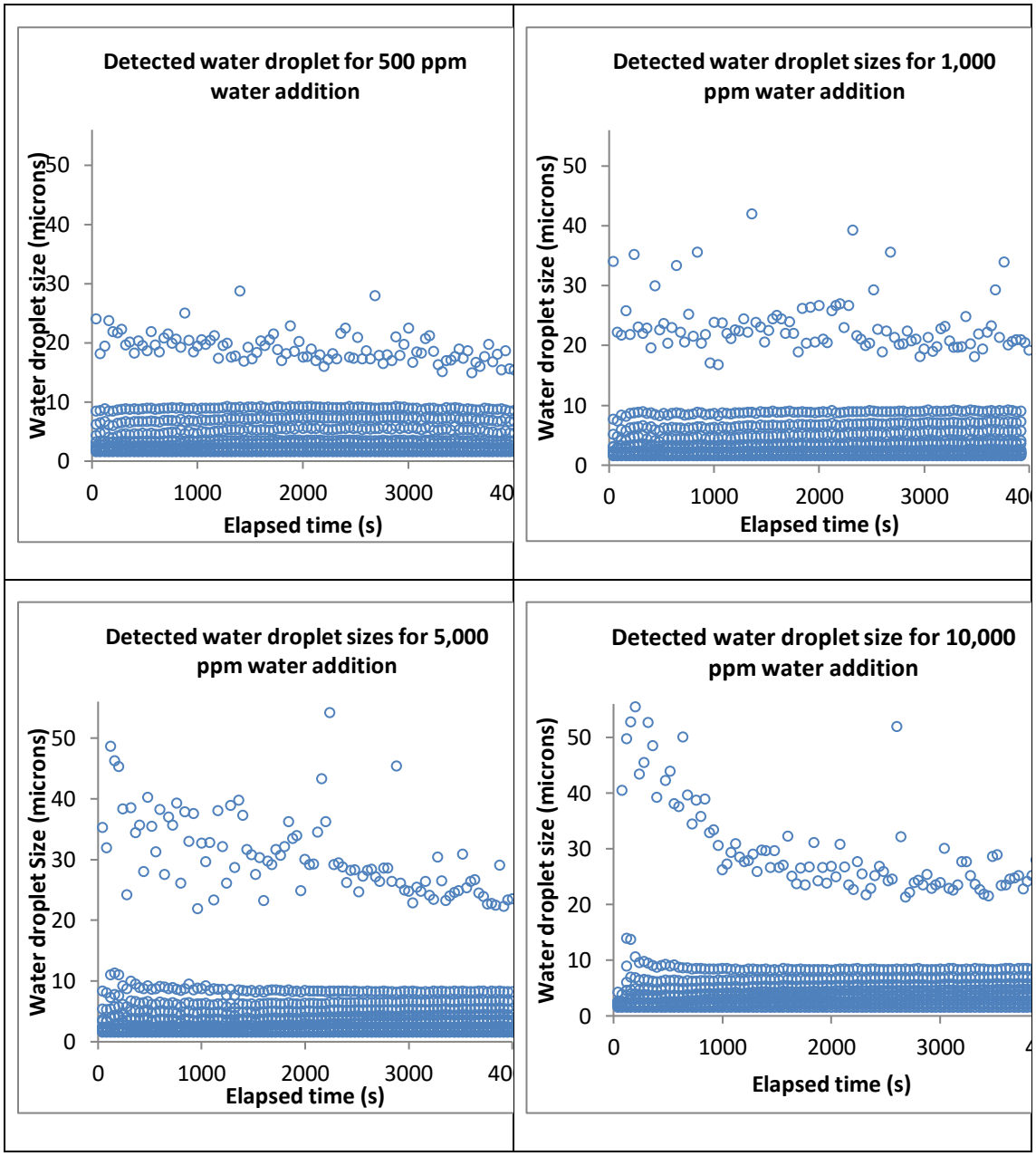

Figure B-1 KF experimental data for neat fuels with 1,000 ppm nominal water addition

Appendix C Investigation of Water Droplet Size Distribution in Conventional and Sustainable Aviation Turbine Fuels

Table C-1 KF experimental data for neat fuels with 1,000 ppm nominal water addition

Conv. Jet A-1		100% SASOL		100% GTL	
*TI (mins)	KF water content(ppm)	TI (mins)	KF water content(ppm)	TI (mins)	KF water content(ppm)
1	1078	1	991	1	996
2	1009	2	767	2	798
5	975.6	5	678	5	729
32	889	32	522	32	559
34	884	34	525	34	581
60	782	60	529	60	544
62	789	62	522	62	531

100% HEFA		100% ATJ		100% Farnesane	
TI (mins)	KF water content(ppm)	TI (mins)	KF water content(ppm)	TI (mins)	KF water content(ppm)
1	1029	1	1019	1	1199
2	829	2	995	2	1186
5	837	5	931	5	1119
32	859	32	855	32	1001
34	849	34	856	34	1015
60	767	60	427	60	991
62	777	62	439	62	989

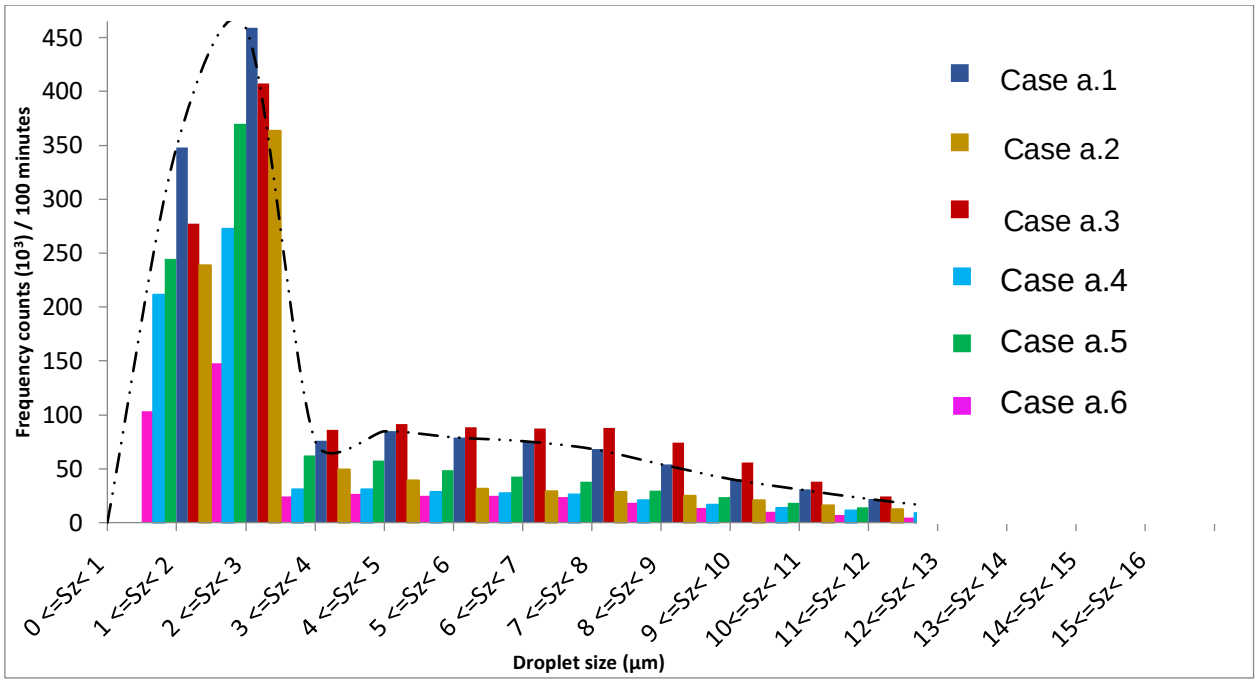

Figure C-1 Frequency distribution of the different size water droplets after 100 minutes settling for the six aviation fuels explored in this work

The droplet frequency distribution for all cases a.1 to a.6 is given in Figure C-1. This reveals that the droplet counts separated into discrete size intervals between Jet A-1 fuel and sustainable aviation fuels explored for this work. The height of the rectangular bar/peak indicates the total count of water droplets in each range. If the magnitudes of the rectangular bars for the different size intervals are summed, it will give the total droplet count of the selected fuel.

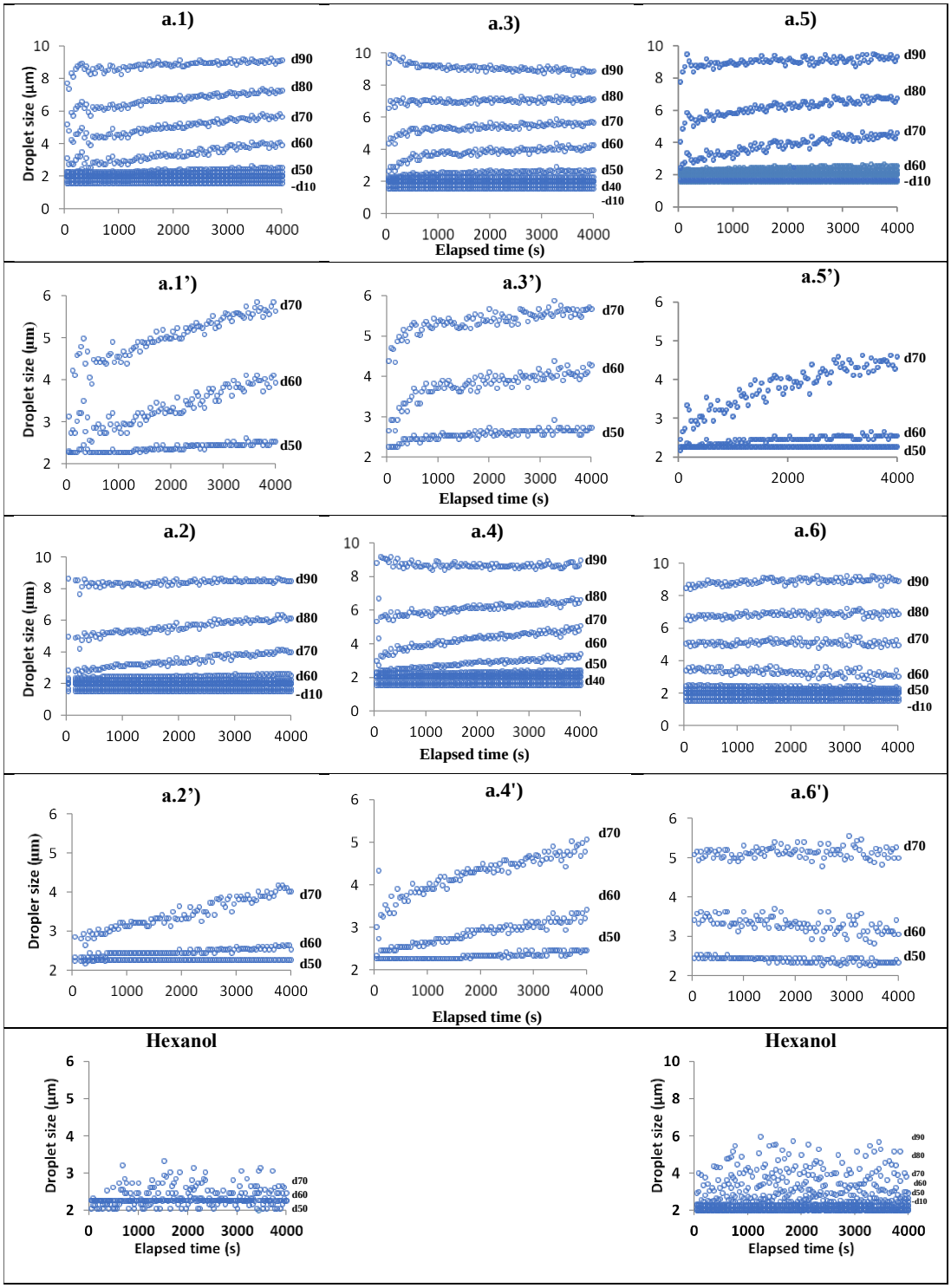

Figure C-2 Water droplet size population represented against time for test cases a.1 to a.6; a.1' to a.6'shows an indication that coalescence occurred

Figure C-2 shows the corresponding water droplet size population against time for all cases a.1 to a.6 tests and hexanol. The droplet size population for hexanol was also included to serve as the baseline for extreme comparison between a stable solution and unstable solution for data clarity, as hexanol is likely to form a very stable solution.

The minimal change seen for hexanol, and case a.6 can be attributed to the fact that a highly stable solution was formed. This means there exist a good mix between the water fuel mixture. The noticeable gap from d90-d50 water droplets compared to the d40-d10 droplets can be attributed to a lesser frequency/count distribution of the larger droplets in comparison to that of the smaller droplets (d40-d10).

Appendix D How will sustainable aviation fuels impact ice formation and pump performance in aircraft fuel lines?

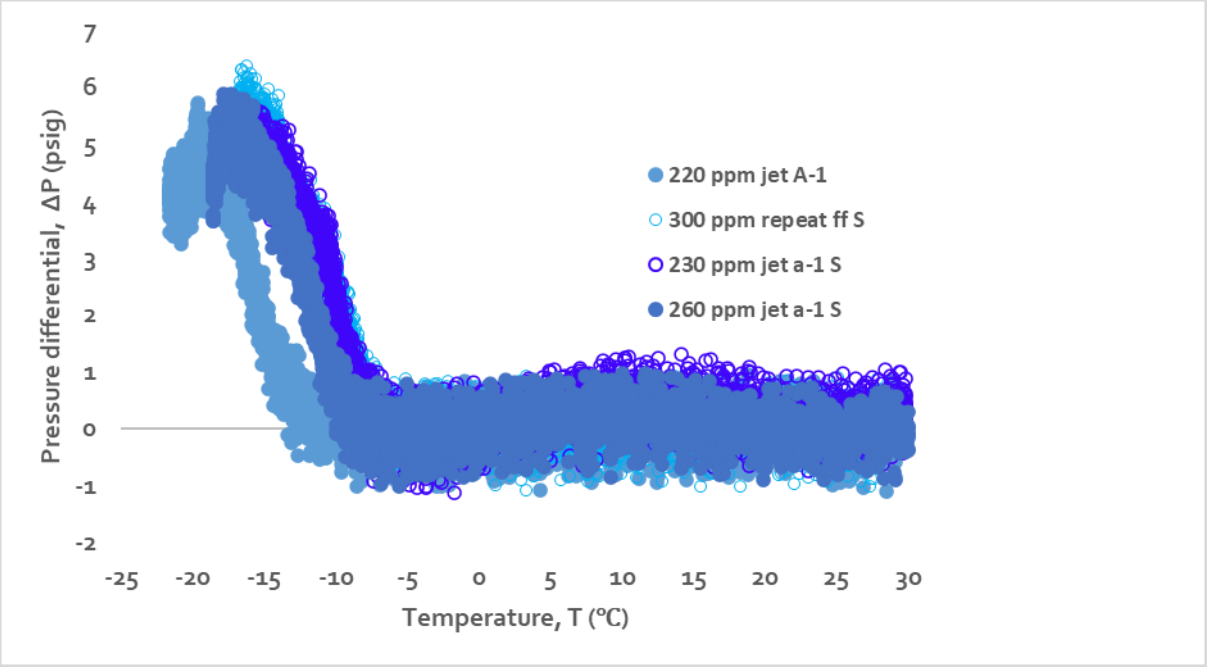

Figure D-1 Unfiltered data for conventional Jet A-1 fuel

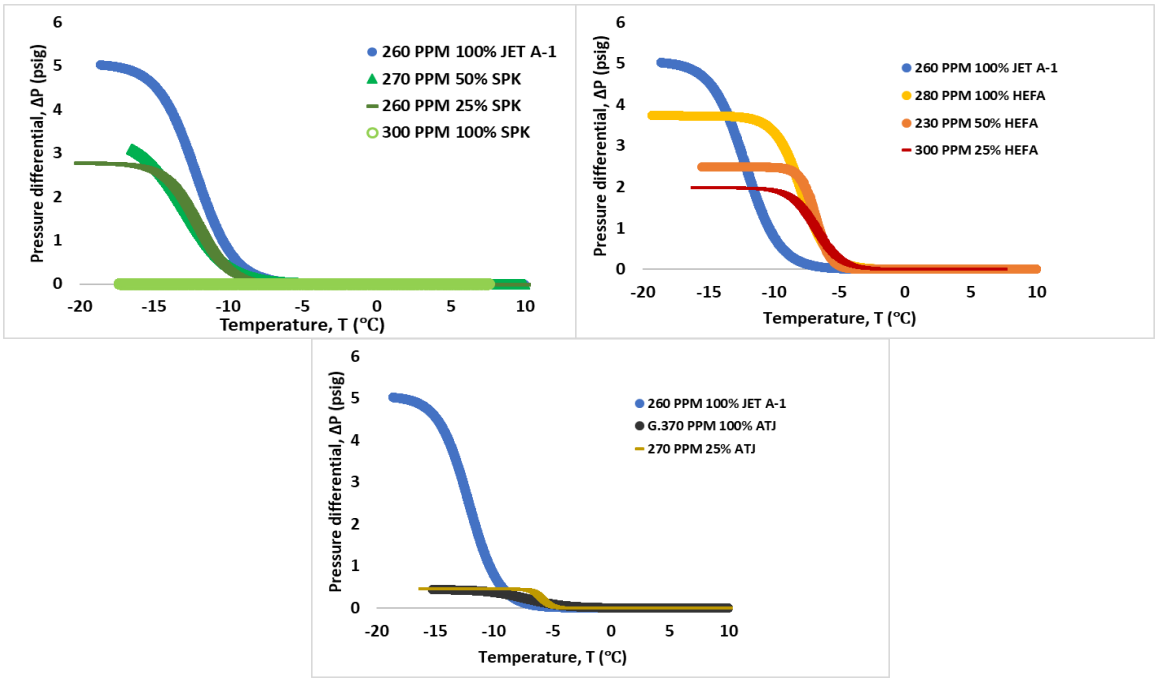

Figure D-2 Comparative analysis: Separate plots of SPK blends, HEFA blends and ATJ blends with 100% Jet A-1

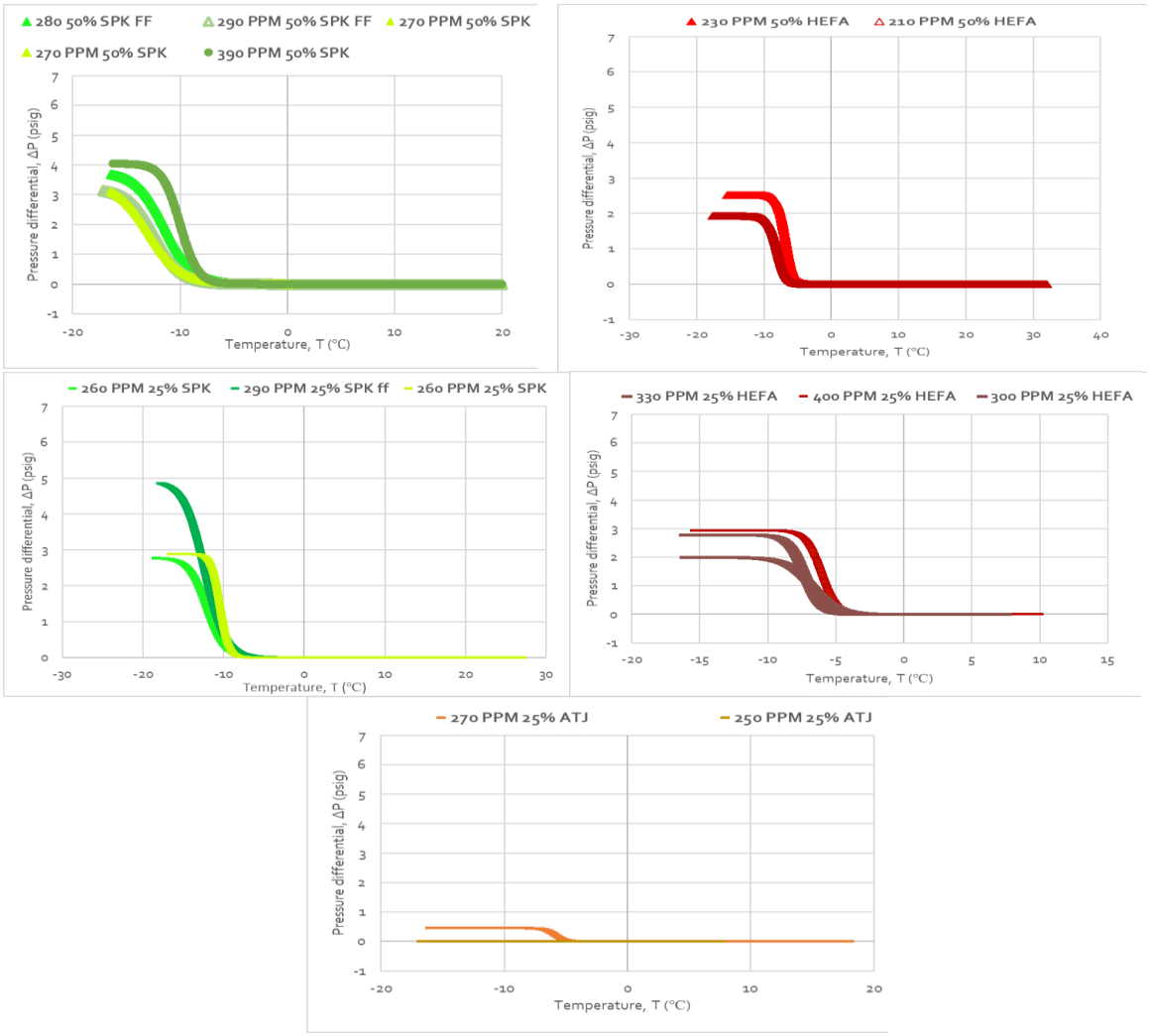

Figure D-3 Repeat tests for SAF blends explored

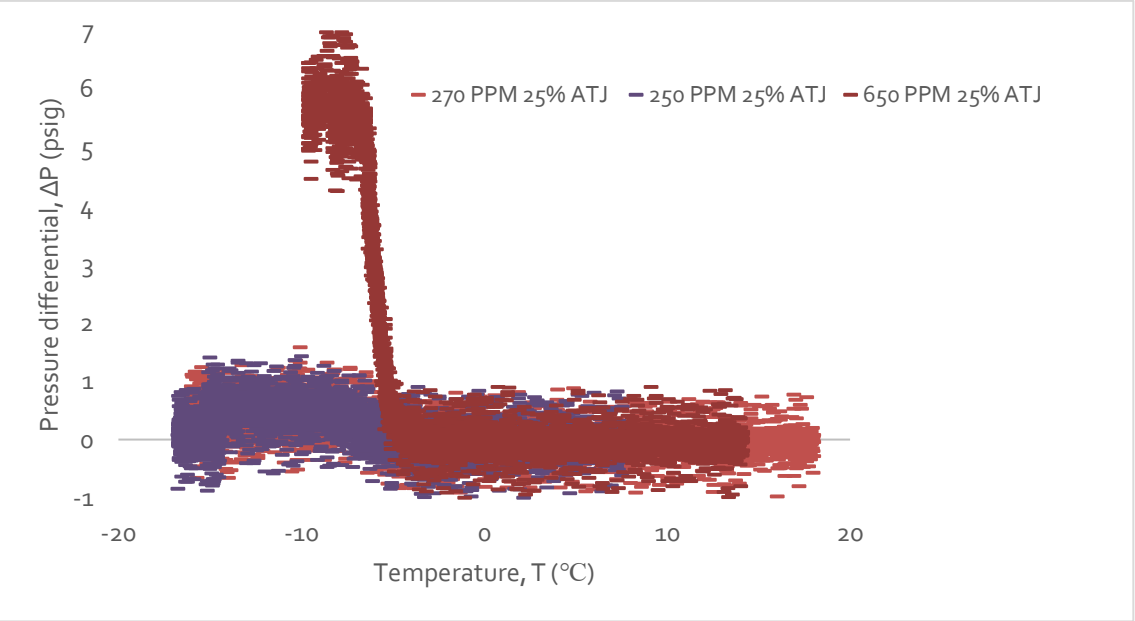

Figure D-4 Fitted curve formula for individual experimental runs

D.1 Fitted curve formula for individual experimental runs

100% Jet A-1

$$220\ \text{ppm} = \frac{2.48579574}{(0.49181983 + \text{EXP}(0.77913202\,x + 8.76138803)}$$

$$230\ \text{ppm} = \frac{3.64265541}{0.75576262 + \text{EXP}(0.85261935\,x + 8.45124828)}$$

$$260\ \text{ppm} = \frac{3.45322305}{0.76533775 + \text{EXP}(0.96036099\,x + 14.45881803)}$$

$$300\ \text{ppm} = \frac{3.95410129}{(0.72460812 + \text{EXP}(0.56578875\,x + 5.76146086)}$$

100% SASOL SPK

$$300\ \text{ppm} = \frac{100.90201011}{101.91206135 + \text{EXP}(1.01660055x + 102.133976)}$$

$$450\ \text{ppm} = \frac{0.19297303}{0.2351481 + \text{EXP}(0.5248066\,\text{x} + 3.26363154)}$$

$$390\ \text{ppm} = \frac{2.61577996}{0.64725828 + \text{EXP}(1.21591539\,\text{x} + 11.73935283)}$$

$$480\ \text{ppm} = \frac{-0.02853329}{0.54603541 + \text{EXP}(-2.04445388\,\text{x} + (-17.07465259))}$$

50% SASOL SPK

$$240\ \text{ppm} = \frac{1.32467904}{0.62871816 + \text{EXP}(0.98738553\,\text{x} + 10.44840386)}$$

$$270\ \text{ppm} = \frac{0.59518124}{0.17701145 + \text{EXP}(0.67186849\,\text{x} + 6.91378875)}$$

$$270\ \text{ppm} = \frac{0.56681363}{0.19139291 + \text{EXP}(0.67368238\,\text{x} + 6.79922827)}$$

$$280\ \text{ppm} = \frac{2.01968238}{0.53777306 + \text{EXP}(0.760078\,\text{x} + 8.01721123)}$$

$$290\ \text{ppm} = \frac{3.509685}{1.09590569 + \text{EXP}(0.79684747\,\text{x} + 9.90448006)}$$

$$390\ \text{ppm} = \frac{2.61577996}{0.64725828 + \text{EXP}(1.21591539\,\text{x} + 11.73935283)}$$

25% SASOL SPK

$$230\ \text{ppm} = \frac{1.88211023}{0.75988313 + \text{EXP}(0.47991129 * \text{D2} + 7.22091864))}$$

$$260\ \text{ppm} = \frac{1.00290258}{0..36084819 + \text{EXP}(0.91836156 + 10.0748744)}$$

$$290\ \text{ppm} = \frac{0.87470933}{0.17764703 + \text{EXP}(0.78492266\,\text{x} + 7.98080159)}$$

100% HEFA

$$280\ \text{ppm} = \frac{0.24124325}{0.06465329 + \text{EXP}(0.99611877\,\text{x} + 5.0817563)}$$

$$290\ \text{ppm} = \frac{1.35556289}{(0.31555691 + \text{EXP}(1.15961877\,\text{x} + 8.62047587)}$$

50% HEFA

$$210\ \text{ppm} = \frac{8.00095682}{4.15779675 + \text{EXP}(1.5276104\,\text{x} + 13.71556389)}$$

$$230\ \text{ppm} = \frac{1.6733463}{(0.6632973 + \text{EXP}(1.72767347\,\text{x} + 11.36816688)}$$

25% HEFA

$$330\ \text{ppm} = \frac{5.57260589}{1.99776172 + \text{EXP}(1.68128084\,\text{x} + 13.01468707)}$$

$$400\ \text{ppm} = \frac{2.74861539}{0.93417159 + \text{EXP}(1.76251704\,\text{x} + 10.62188658)}$$

$$300\ \text{ppm} = \frac{4.51510494}{(2.25542043 + \text{EXP}(1.03553559\,\text{x} + 7.8484447)}$$

100% ATJ

$$260\ \text{ppm} = \frac{2.02402647\text{e} - 01}{1.48873734\text{e} + 00\ +\ \text{EXP}\ (3.70334129\text{e} + 02\text{x}\ + (-8.65282592\text{e} + 01))}$$

$$270\ \text{ppm} = \frac{101.13947769}{101.93436134 +\ \text{EXP}\ (0.51201546\ \text{x}\ +\ 100.59670169)}$$

$$370\ \text{ppm} = \frac{0.79485713}{1.80130534\ +\ \text{EXP}\ (0.60445893\ \text{x}\ +\ 4.93471799)}$$

25% ATJ

$$250\ \text{ppm}\ = \frac{101.12667578}{101.77355829 +\ \text{EXP}\ (0.13410694\text{x}\ +\ 102.17694364)}$$

$$270\ \text{ppm} = \frac{0.83958275}{1.85762286\ +\ \text{EXP}\ (2.45395435\ \text{x}\ +\ 15.07627439)}$$

$$270\ \text{ppm} = \frac{0.23371081}{0.04142296\ +\ \text{EXP}\ (3.08930349\text{x}\ +\ 15.15451367)}$$